Mathematical Modeling of Social Insect Colonies as Complex Adaptive Systems

by

Jun Chen

A Dissertation Presented in Partial Fulfillment
of the Requirements for the Degree
Doctor of Philosophy

Approved October 2023 by the
Graduate Supervisory Committee:

Yun Kang, Chair
Gloria DeGrandi-Hoffman
Jeniffer Fewell
Jon Harrison
Sherry Towers

ARIZONA STATE UNIVERSITY

December 2023

ABSTRACT

This research focuses on the intricate dynamical systems of eusocial insects, particularly ants and honey bees, known for their highly organized colonies and cooperative behaviors. Research on eusocial insects contributes to understanding of animal and social behavior and promises to help agriculture and have huge economic impacts. Collaborating closely with ecologists, I construct diverse mathematical models tailored to different environmental contexts. These models encompass individual stochastic (Agent-based model), Ordinary Differential Equation (ODE), non-autonomous, and Delay Differential Equation (DDE) models, rigorously validated with experimental data and statistical methods.

Employing dynamical theory, bifurcation analysis, and numerical simulations, I gain deeper insights into the adaptive behaviors exhibited by these insects at both colony and individual levels. Our investigation addresses pivotal questions:

1) What mechanisms underlie spatial heterogeneity within social insect colonies, influencing the spread of information and pathogens through their intricate social networks? 2) How can I develop accurate mathematical models incorporating age structures, particularly for species like honeybees, utilizing delayed differential equations? 3) What is the influence of seasonality on honeybee population dynamics in the presence of parasites, as explored through non-autonomous equations? 4) How do pesticides impact honeybee population dynamics, considering delayed equations and seasonality?

Key findings highlight: 1) The spatial distribution within colonies significantly shapes contact dynamics, thereby influencing the dissemination of information and the allocation of tasks. 2) Accurate modeling of honeybee populations necessitates the incorporation of age structure, as well as careful consideration of seasonal variations. 3) Seasonal fluctuations in egg-laying rates exert varying effects on the survival of

honeybee colonies. 4) Pesticides wield a substantial influence on adult bee mortality rates and the consumption ratios of pollen.

This research not only unveils the intricate interplay between intrinsic and environmental factors affecting social insects but also provides broader insights into social behavior and the potential ramifications of climate change.

DEDICATION

I would like to dedicate this dissertation to my beloved husband, Junmin Zhong, and precious daughter, Lydia Li Zhong, their love and support mean the world to me as I pursue my Ph.D.. To my incredible mom, Jiawen Li, she has shown me that women can be strong and achieve anything they set their minds to, and support my life. To my lovely grandparents, Chuanzhao Li and Shengchang Duan, their wisdom and love continue to inspire me every step of the way. To my dear father-in-law, Hangui Zhong, his support has been invaluable in shaping our lives.

ACKNOWLEDGMENTS

I would like to express my deepest gratitude to my precious advisor, Dr. Yun Kang. Her wholehearted dedication, invaluable guidance, and insightful feedback have been instrumental in shaping my research. I am truly fortunate to have had her as my mentor throughout my academic journey. I sincerely appreciate her consistent efforts in providing me with opportunities for growth in various areas and enhancing my resume. When I faced the highest levels of pressure in life and study, her support and help made me out of dilemmas. Her unwavering support was the cornerstone of my degree completion. I am immensely grateful for her never-ending belief in me.

I would like to thank and recognize the other members of my thesis committee. I extend my gratitude to Dr. Jon Harrison. He always supported my work and offered unlimited help when I encountered difficulties. His understanding of bees is unparalleled, and he always brings me new ideas when discussing mathematics and bees. Dr. Jennifer Fewell led me through the captivating realm of biology, imparting knowledge and the invaluable skill of effective writing through her patient guidance. I appreciate Dr. Gloria DeGrandi-Hoffman's boundless enthusiasm, unwavering support, and ever-present readiness to offer guidance whenever I seek it in all fields. I appreciate Dr. Sherry Towers for her invaluable support and the practical skills I gained from her outstanding class and excellent website.

I want to acknowledge my collaborators: Dr. Adiran Fisher, he taught me a lot about bee experiments and helped me with my paper. Dr. Xiaohui Guo, he is the one who sparked my fascination with social insects, and our collaboration was consistently delightful. Dr. Asma Azizi, Dr. Vadayani Ratt, and Dr. Dingyong Bai, they always help my work. Dr. Komi Messan, his previous works gave me lots of inspiration.

The excellent research environment fostered by Dr. Kang's Lab has been in-

valuable. I thank Dr. Gabriela Zuloaga, Dr. Marisabel Messan, Lucero Rodriguez Rodriguez, Carlos Orellana, Jordy Rodriguez, and Tamantha Pizarro for the fruitful discussions and collaborations. I also thank the people at the SAL MCMSC, Dr. Victor Moreno and Dr. Baltazar Espinoza for always answering my questions. The journey wasn't easy, but you all made it enjoyable, and for that, I am truly grateful.

I want to thank Arizona State University for providing me with the research and study environment and SAL MCMSC for providing me with support for my program. This accomplishment was made possible only through the following fundings: ASU Graduate Completion Fellowship, James S. McDonnell Foundation 21st Century Science Initiative in Studying Complex Systems Scholar Award, NSF-DMS, NSF-IOS/DMS, NSF-MathBio, NSF-CN, Agricultural Research Service.

Last but not least, I would like to thank my family: To my husband, he unfailingly supports all my decisions and ensures I have nourishing meals every day, providing me with the strength to persevere. To my daughter, she always gives me a warm hug when I feel depressed, giving me the strength to get back to fighting. To my mother, she stood by me wholeheartedly, emphasizing that there is no distinction between girls and boys. To in memory of my late grandparents, their wisdom emphasized the value of knowledge, and their support propelled me onward. I miss them and hoped they can see me earn my Ph.D. degree. To my uncle and father-in-law, they support my life and and let me fulfill my dreams without any worries.

TABLE OF CONTENTS

CHAPTER Page

CHAPTER Page

LIST OF TABLES

LIST OF FIGURES

Figure Page

Figure Page

Figure Page

Figure Page

Figure Page

Chapter 1

INTRODUCTION

1.1 Overview

A complex adaptive system works in a dynamic network [Miller and Page, 2009]. They interact in interdependent ways to produce system-wide patterns. Complex adaptive systems can be used in different fields like the economy, the internet, a social insect colony, or the brain [Johnson, 2009b]. These are several important characteristics of the complex adaptive system [De Ridder *et al.*, 2017]: 1) the system consists of many heterogeneous agents, and each agent has its behavior which can evolve; 2) agents interact with each other; 3) the system shows emergence, where *"the whole is more than the sum of the components and the very specific connectivity creates a new property" [De Ridder* et al.*, 2017]*; 4) the system is self-organizing, which means we cannot understand the whole system from individuals. A typical example of a complex adaptive system is an ant colony. Each ant has its task behavior, such as forager or nurse, and each ant also interacts with others. They have lots of local interactions. Similar to honey bees and wasps, their behaviors emerge in a colony. The complex adaptive system is one method that can dissect complex organizations in nature, such as insect communities.

Eusocial colonies display high levels of organization without leadership and strategic planning in the Animal Kingdom [Messan, 2018], and there are three main characteristics in the colonies: social interaction, division of labor, and overlapping of

generations [Holbrook *et al.*, 2011]. Social interaction occurs in multi-scale interactions among members of the colony and between the colony and the environment [Wilson, 1978]. Division of labor refers to the notion that individuals are specialized to perform particular tasks [Wilson, 2000]. Overlapping of generations refers to mating systems where more than one breeding generation is present at any one time [Olsen, 2009]. With the emergence of task groups in social insect communities, the division of labor regulates the colony's homeostasis and helps to achieve effective information transfer, rapid response to nest defense, and minimizing disease exposure at the colony level [Gordon and Mehdiabadi, 1999; Robinson *et al.*, 2009a]. Therefore, task specialization establishes individual rules [Chen *et al.*, 2020b], such as age-dependency (temporal polyethism) and size/shape-dependency (morphological polyethism) [Beshers and Fewell, 2001].

In addition to task allocation, reproduction within Eusocial colonies is directly connected with the success of the colonies. One good example is the honey bee. Why should we pay attention to the reduction of the honey bee population? Honey bees play an important role in the pollination of crops, such that pollinating behavior is worth $215 billion [Smith *et al.*, 2013]. In addition, the main bee products in human life are honey, pollen, propolis, royal jelly, and venom. However, as the yield of honey bees' products reduces, their prices increase; for example, honey prices were up 2% in 2017 from the USDA report [USDA, 2017]. Current research found three main reasons threaten the survival of honey bees [Oldroyd, 2007]: 1) environmental stressors, such as pesticide and deforestation [Perry *et al.*, 2015; Fisher II *et al.*, 2021; Campbell *et al.*, 2016]; 2) parasites and pathogens, such as Varroa mites and virus [Smith *et al.*,

2013; DeGrandi-Hoffman *et al.*, 2017; Guzmán-Novoa *et al.*, 2010; Martin, 2001b]; and 3) genetic variation and vitality [Meixner *et al.*, 2014, 2010]. Therefore, analyzing the impact of these three aspects on the dynamics of honey bee colonies can help us learn how to better manage ecology, economy [Degrandi-Hoffman *et al.*, 2019], and human life.

The study of social insect behavior and colony dynamics, particularly adaptive and underlying mechanisms, can help us better understand behavioral ecology and human social behavior, such as processes of information transmission and disease spreading, social networks, and spatial influences. Mathematicians and biologists have collaborated to build different models with realistic biological backgrounds to help solve or reveal problems, such as computational models, compartmental models, or partial differential models [Chen *et al.*, 2021]. The agent-based model can be used to simulate biological experiments, which can better quantify the relationship between parameters and allow the researchers to draw better conclusions [Guo *et al.*, 2020]. Also, combine equations to simulate the species in the environment, like temperature and food, to predict the fate of the species, and also can explore key reasons for the different outcomes [DeGrandi-Hoffman *et al.*, 1989]. Compartmental modeling can be used to describe the system to reveal the dynamics [Chen *et al.*, 2020a], and partial differential equations can be used to describe the dynamics of colony and contaminated food sources [Magal *et al.*, 2020a] with spatial factors.

Social division of labor, colony dynamics, and existential threats interact. The age-dependent work assignment will change when the colony population declines ab-

normally because of external threats. For example, when the number of old foragers in the hive is insufficient, younger bees will become foragers [Leoncini *et al.*, 2004; Beshers and Fewell, 2001]. This dissertation is consequently concerned with understanding the complex adaptive systems in eusocial colonies by multi-scale modeling. The motivations presented in this dissertation fall into two categories. First, I analyze and visualize information spread and task allocation in the colony to expose that spatial heterogeneity plays an important role in contact dynamics, from individual to group level. The second portion of this research focuses on applications to honey bee population dynamics and the reduction reasons: parasites and pesticides. Experimental data verifies the practical significance of these works.(See Figure 1.1).

1.2 Research Questions

The central question of this dissertation is how to create multi-scale models at the individual, group, and colony levels to understand the complex adaptive systems in social insects.

The following sub-questions can help answer the preceding question:

- How do spatial interactions and task switching impact task allocation and information spread?
- How can honeybee population dynamics be modeled by age structure and seasonality?
- How does seasonality affect the parasitism colony dynamics?

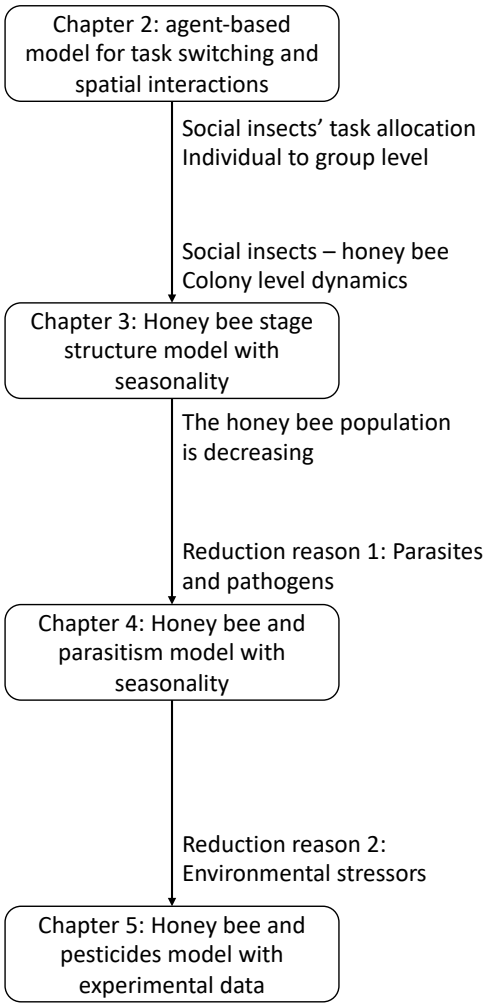

Figure 1.1: Chapters in the dissertation

- How does pesticide influence colony dynamics? How does the seasonality of queen egg-laying contribute to colony dynamics with pesticide exposures?

1.3 Division of Labour & Task Allocation

In social insect colonies, workers have particular tasks. Division of labor occurs when different workers in the colony perform specialized subsets of tasks. It is one of the most notable characteristics of group behavior of social insects [Beshers and

Fewell, 2001]. From simple to complex groups, various social classifications describe this basic attribute. Therefore, the division of labor is related to colony size. With the expansion of the group size, the division of labor in social groups increases. Workforce allocation is flexible, responding to current needs [Bourke, 1999; Anderson and McShea, 2001; Mersch *et al.*, 2013]. The whole process is self-organized, so how do they distribute the division of labor? One method is that ants contact each other to switch their tasks. After that, they decide whether to switch tasks depending on the physical state of the environment and social cues from interaction with other ants [Robinson *et al.*, 2009b].

In order to understand the division of labor, task allocation is the key to achieving collective plasticity [Chen *et al.*, 2018]. [Gordon, 1996] defined, *"Task allocation is the process that results in specific workers being engaged in specific tasks, in numbers appropriate to the current situation."* Three things can influence task allocation: genetics [Oldroyd and Fewell, 2007], stimuli from environment [Page Jr and Mitchell, 1998], and hormones [Robinson, 1987]. For example, singly-mated and multiple-mated queens impact task allocation [Oldroyd and Fewell, 2007]. Individuals share information (a stimulus) to operate a self-organized complex system [Page Jr and Mitchell, 1998]. Juvenile hormones influence four important age-relative tasks (nursing, food storage, nest maintenance, and foraging) [Robinson, 1987].

These hormones result in Age polyethism, which plays an important role in the social insects' division of labor. [Beshers and Fewell, 2001]. In the colony, young adults always assume the nursery role to take care of brood and queen, and older

adults always assume the foraging role to scout the food and collect nectar, water, and propolis [Coffey, 2007]. Thus, for social insect groups with age polyethics, the tasks performed by individuals within the group change with maturity [Capinera, 2008].

1.4 Honey Bees

The honey bee is a social insect that is very important to humans. American beekeepers generally carry western honey bees, named *Apis Mellifera*. Honey bees have various products, such as honey, royal jelly, beeswax, and propolis. They also are responsible for pollinating crops such as blueberries, cherries, and almonds, resulting in many more objective economic benefits. But right now, the population of honey bees has noticeably decreased in the long-term and annually [Smith *et al.*, 2013].

The population of honey bees in winter is less than in the summer because pollen and nectar are the food of honey bees, and they lack food in the winter. Additionally, the queen bee's fertility also declines. Then, due to pollen availability in the spring, the birth rate of honey bees increases. The peak of the population is achieved in late June, until the middle of summer, as it starts to decline [Research and Extension Consortium, 2004]. However, beekeepers discovered a strange phenomenon in the winters of 2006-2007 and 2007-2008. They found the hive abandoned by the residents, with only a small amount of honey and almost no honeycombs or worker bees. This phenomenon is called Colony Collapse Disorder (CCD) [Evans *et al.*, 2009], resulting in a 40% to 50% reduction in the total number of honey bee colonies in the United States.

In contrast, the total number of colonies worldwide is reduced by 5% to 10% [Paula María Montoya-Pfeiffer and Parra., 2016]. Considering our dependence on honey bee pollination, many problems are caused by the declining number of bees.

The colony comprises a queen, who breeds offspring, a few hundred male drones, who provide sperm, and thousands of female workers who maintain colony operation [Fredrick *et al.*, 2017]. It takes 16 days for a queen to mature, and a strong mature queen can lay 1500-2000 eggs daily, but after two years, only lays a few eggs [Coffey, 2007]. Drones are bigger than workers and develop from unfertilized eggs; their main job is to mate with the queen. They need 24 days to mature [Fredrick *et al.*, 2017; Coffey, 2007]. Most bees in the colony are workers, and it takes 21 days for a worker to mature.

1.5 Parasitism in Honey Bees

Many problems plague the colony survival of bees. One of them is parasites and pathogens. Beginning in 2006, many honeybee colonies collapsed for no observed reasons [Cox-Foster *et al.*, 2007]. [Hayes Jr *et al.*, 2008] published a survey of honey bees that revealed around 30% colonies losses from 2007 to 2008. Until now, the cause of CCD has not been fully understood, but some scientists believe parasites, like Varroa and Nosima, and viral disease are some reasons for CCD [Johnson, 2010]. In the United States, Varroa mite is one reason for the losses of honey bee colonies [Neumann and Carreck, 2010]. Varroa mites seriously threaten the survival of honeybee colonies, especially in winter [Koleoglu *et al.*, 2017]. Due to lack of food in winter and

to keep the temperature in the hive, bees will choose to stay in the colony, and the queen will reduce or stop laying egg [Johnson, 2002; Coffey, 2007; DeGrandi-Hoffman *et al.*, 1989; SEELEY and Visscher, 1985]. An adult female varroa mite enters an uncapped pupa and begins parasitism. They live on brood, and the first egg laid will be male and will mate with females that are laid later [Donze *et al.*, 1996; DeGrandi-Hoffman *et al.*, 2017].

Varroa mites reduce the lifespan of bees [Genersch *et al.*, 2010] and spread viral diseases to the colony, causing collapse. They are also one of the main factors affecting colony overwinter [Guzmán-Novoa *et al.*, 2010; Degrandi-Hoffman *et al.*, 2019]. At least 14 viruses can be found in the bee community. Among them, deformed wing virus (DWV) can cause wing malformations, and acute bee paralysis virus (ABPV) can prevent bees from growing up and dying [bai, 1991]. When adult bees are infected with DWV, they are the same as healthy bees, but their life span will be reduced. Therefore, during this time, adult bees and their mites carry the virus and spread it from colony to colony by moving [Martin, 2001a]. Adult bees infected with the ABPV are paralyzed, shivered, unable to fly, and gradually blacken and lose hair from the chest and abdomen [Martin, 2001b]. If the colony is mite-free, then the ABPV will be latent, and Varroa can provoke the disease [Chen and Siede, 2007]. Therefore, social interaction between colonies and environments will infect and spread diseases and parasites. Studying social interaction between them is important for protecting honey bee colonies and helping them to overwinter effectively.

1.6 Pesticides in Honey Bees

One more factor threatening the survival of bee colonies is environmental stressors, including habitat destruction and the use of pesticides [Oldroyd, 2007; Fisher *et al.*, 2023]. Pesticides are integral to modern agriculture, providing vital functions like crop protection, economic benefits, and enhancing efficiency in food production. Hence, pesticides are extensively applied to crops, and in the course of pollination and nectar collection, bees, being the primary pollinators, may inadvertently transport residual pesticides or pollen containing these chemicals back to their hives [Devillers *et al.*, 2002]. The nurse bees will subsequently consume or provide the food to their larvae [Haydak, 1970; Owens and Farrar, 1967], then these residues can impact bee health, potentially resulting in colony collapse [Tosi *et al.*, 2017; Fisher II *et al.*, 2021].

Therefore, pesticides can adversely affect bee populations, some of which may not be directly lethal [Fisher *et al.*, 2023; Mullin *et al.*, 2010; Sánchez-Bayo *et al.*, 2016]. A diverse range of pesticides is used within safe limits, but their residues in bees can produce synergistic effects, rendering them sub-lethal or threatened [Fisher *et al.*, 2023; Mullin *et al.*, 2010; Tosi *et al.*, 2022]. Research indicates that exposure to pesticides can result in various detrimental effects, including compromised foraging behavior [VanEngelsdorp *et al.*, 2012], impaired navigation [Chmiel *et al.*, 2020; Tosi *et al.*, 2017], and weakened immune systems [DeGrandi-Hoffman *et al.*, 2013]. Moreover, specific classes of pesticides, such as neonicotinoids and Pristine, have been closely associated with declines in bee populations [Tosi *et al.*, 2017; Fisher II *et al.*, 2021], including higher death rate of adults and reduced worker lifespan [Fisher II *et al.*, 2021]. These chemicals can induce hyperresponsiveness in bees, disrupting

their ability to forage effectively and ultimately contributing to colony collapse.

Therefore, studying how pesticides affect honey bees is crucial. I constructed an age-structured delay differential equation to describe the experiment [Fisher II *et al.*, 2021]. By integrating theoretical analysis, simulations, and data fitting, the study to explore the effects of pesticides on honey bee dynamics.

1.7 Contribution and Significance

This research analyzes and visualizes complex adaptive systems using a multi-scale modeling approach to describe social insects' behavior, interaction, or life span. Due to the complexity of systems of social insects, analyzing the mechanisms in these systems is complicated. I provide three models to study their mechanisms and novel solutions to generate by dispersal through theoretical analysis and computational simulations. My work continues existing work on agent-based and compartmental models, making the models more biologically relevant. My work combines real experimental data and uses dynamical system models to more accurately reveal biological systems' internal relationships and importance.

In the remaining chapters, I will present four projects. The first is an agent-based model to explore an ant colony's task-switching and information-spreading systems. The second project is a compartmental model with age structure to explore the colony dynamic of honey bee colony by delay differential and seasonality equations. The last project is a compartmental model to explore the parasitism and seasonality effects in

honey bee colonies.

Chapter 2

DYNAMICS OF INFORMATION FLOW AND TASK ALLOCATION OF SOCIAL INSECT COLONIES: IMPACTS OF SPATIAL INTERACTIONS AND TASK SWITCHING

Abstract

Models of social interaction dynamics have been powerful tools for understanding the efficiency of information spread and the robustness of task allocation in social insect colonies. How workers spatially distribute within the colony, or spatial heterogeneity degree (SHD), plays a vital role in contact dynamics, influencing information spread and task allocation. We used Agent-Based Models (ABM) to explore factors affecting spatial heterogeneity and information flow, including the number of task groups, variation in spatial arrangements, and levels of task switching, to study: 1) the impact of multiple task groups on SHD, contact dynamics, and information spread, and 2) the impact of task switching on SHD and contact dynamics. Both models show a strong linear relationship between the dynamics of SHD and contact dynamics, which exists for different initial conditions. The multiple-task-group model without task switching reveals the impacts of the number and spatial arrangements of task locations on information transmission. The task-switching model allows task-switching with a probability through contact between individuals. The model indicates that the task-switching mechanism enables a dynamical state of task-related spatial fidelity at the individual level. This spatial fidelity can assist the colony in redistributing their workforce, with consequent effects on the dynamics of spatial het-

erogeneity degree. The spatial fidelity of a task group is the proportion of workers who perform that task and have preferential walking styles toward their task location. Our analysis shows that the task switching rate between two tasks is an exponentially decreasing function of the spatial fidelity and contact rate. Higher spatial fidelity leads to more agents aggregating to task location, reducing contact between groups, thus making task switching more difficult. Our results provide important insights into the mechanisms that generate spatial heterogeneity and deepen our understanding of how spatial heterogeneity impacts task allocation, social interaction, and information spread.

2.1 Introduction

Eusocial insects live in highly cooperative and cohesive societies with complex organizational structures Class [2000]. These societies are organized around the work of raising new individuals for colony growth and reproduction and maintaining conditions for colony function. These goals involve a series of differentiable tasks. Their systems of task allocation and division of labor allow the diverse members of these societies to perform multiple different tasks in parallel. At the same time, the colony as a whole regulates the allocation of effort to different tasks as needs and opportunities change. In fact, task allocation is a problem across most complex systems, such as multicellular organisms Navlakha and Bar-Joseph [2014]; Yanni *et al.* [2020], collective robotics Gerkey and Matarić [2004]. The distributed information systems provided by their social networks allow colonies to regulate work homeostatically and dynamically around current needs Robinson *et al.* [2009c]; Charbonneau *et al.* [2017]; Leitner and Dornhaus [2019]; Beshers and Fewell [2001]; Gordon [1996].

Many, although not all, tasks take place in specific locations in the nest of social insects, and workers performing the same task tend to aggregate around those locations, which are described as spatial fidelity zones (SFZ)Mersch *et al.* [2013]. Spatial fidelity adds an important spatial component to task regulation that likely influences task communication networks. The locations in which workers perform tasks, or spatial fidelity zones (SFZ), can reinforce communication among individuals within the corresponding task group and, in so doing, potentially enhance communication efficiency for elongating their fidelities toward that task location Sendova-Franks and Franks [1994, 1995]. Conversely, communication between task groups across SFZs may be less frequent, potentially limiting coordinating tasks across the colony. Cross-colony communication is necessary for the function of these distributed systems. Thus, we would expect more flexibility in task choice, spatial preferences, and communication strategies than would be provided with strictly delineated task zones. Flexible spatial strategies can provide multiple functionalities beyond task regulation, including facilitating information transmission or inhibiting the spread of pathogens Sendova-Franks *et al.* [2010]; Feigenbaum and Naug [2010]; Naug [2008]; Feigenbaum and Naug [2010]; Quevillon *et al.* [2015]; Regnier and Wilson [1968]; Wilson and Regnier Jr [1971]. These make it critical to understand the inter-dependency between social communication among individuals in the same or different task groups and the formulation or decomposition of task groups.

As decentralized distributed systems, social insect colonies rely heavily on the capability of individual workers to acquire information from the environment inde-

pendently and on the ability to receive or send information via local inter-individual communications Feinerman and Korman [2017]. The specific information and resources acquired by workers can, in turn, influence individual spatial preferences and, in doing so, assist the whole colony to re-establish the spatial distribution of workers to cope with various challenges Theraulaz *et al.* [2003]. This interplay between information acquisition and worker spatial movement patterns has been widely studied in various ant species, for example, nest-site choice and famine relief of *T. albipennis* Pratt *et al.* [2002a]; Sendova-Franks *et al.* [2010], alarm propagation of *P. californicus* Guo *et al.* [2022], social immunity of *L. niger* Stroeymeyt *et al.* [2018] and nutritional balance of *C. sanctus* Baltiansky *et al.* [2021]. Although an ideal model for studying this interplay, the processes and mechanisms by which task-related information and social contact mediate workforce re-allocation within colonies are still understudied.

One way to study the dynamics of task regulation within a colony is to examine how internal factors, such as genotype Oldroyd and Fewell [2007], physiological states Robinson [1987], and environmental stimulus Page Jr and Mitchell [1998], induce workers to switch their tasks from one to another. Alternatively, it is worth considering the task allocation as a product of task recruitment via social interactions Pacala *et al.* [1996]. The task-related cuticular hydrocarbons of red harvester ant (*Pogonomyrmex barbatus*) have been found to assist workers' decision on task performances Gordon [1989], and their encounter rate informs the possibility of task switching Gordon and Mehdiabadi [1999]. Models incorporating components of tasks, social interactions, and spatial behavior of individual workers are needed to better understand the dynamic task allocation in social insect colonies.

Previous models incorporating subsets of these components have revealed several potential mechanisms of how individuals acquire local information by spatial coincidence Richardson and Gorochowski [2015], how task allocation is mediated by individual movement Johnson [2009a], and how the encounter rate of individuals contributes to collective patterns of task allocation Pacala *et al.* [1996]; Chen *et al.* [2020b]. However, these models do not provide an integrative view of task re-allocation as individual spatial behavior associated with task-related interactions changes dynamically. For example, the algorithm proposed by Johnson *et al.* (2009)Johnson [2009a] relying on a self-organizing model of task-quitting, patrolling, task-searching, and task-working, serves the random location of individuals throughout the colony without considering task demand. This model showed the dynamics of workers switching between tasks and locations. Pacala *et al.*Pacala *et al.* [1996] demonstrated that responses to demand a task could arise from the interactions among individuals, environmental stimuli, and local densities. Therefore, a model that simultaneously integrates task fidelity, the spatial distribution of individuals, and task-related interactions would facilitate our understanding of relations among those three components in social insect colonies and further our understanding of mechanisms of adaptive task allocations.

In recent modeling work Guo *et al.* [2020], we investigated the information transmission through physical contact in several realistic scenarios involving three task groups of ants. We assumed that the performance of each task group is tied to predefined spatial fidelities, which reflect the proportion of ants that prefer to drift back to the task location compared to those that move randomly. With this assumption

in place, we revealed the contributions of ants with different spatial fidelities, e.g., random-walking and drifted-walking, to the information transmission. To explore further, in this study, we focused on how the number of task groups (ranging from 2 to 5) and the spatial distribution of task locations impact information transmission. Additionally, we investigate how the task switching associated with the spatial coincidence of ants is formulated by ants' spatial distribution and, in turn, affects task allocations, physical contact, and information transmission. Therefore, we propose two discrete-time Markov chain models: 1. Multiple-task-group model, which assumes that each task group (consisting of 2-5 tasks) has a fixed and pre-defined spatial fidelity (i.e., the proportion of drifted-walker within each task group); 2. The task-switching model assumes that individuals can be recruited to another task that is different from their original tasks by their neighboring ants via physical interactions, and after switching the task, they may change their task spatial fidelities with a certain probability. Our models address the following: (1) How do multiple task groups and related spatial distribution of workers affect social contact dynamics and information transmission; (2) How may task-switching lead to changes in spatial fidelity and therefore impact task allocation.; and (3) How may spatial fidelity dynamics affect contact and information dynamics after task switching.

The models and discussion are organized as follows. In Section 2, we derive our agent-based model with associated information and task-switching scenarios. We introduce two different modeling approaches: The multiple-task-group model, which includes various task groups while keeping spatial fidelity constant, and the Task-switching model, which provides for only a two-task group but dynamic spatial fi-

delity. In Section 3, we perform our simulations and analysis for those two models and compare their dynamics. In Section 4, we discuss the findings and conclude our study.

2.2 Model derivation

Our model extends the agent-based discrete-time Markov chain model developed in Guo *et al.* [2020] by including various task groups and task-switching procedures. Unlike conducting experiments in such contexts that can be very challenging, our model is an easy and effective tool that can shed some light on dynamics in real social insect colonies.

We assume that the colony has N workers living on $X = K \times K = \{(i,j) : 1 \leq i \leq K, 1 \leq j \leq K\}$ grids for some $K \in \mathbb{Z}$. We also assume that $N \leq K^2$. At any given time t, a worker $\mathbf{A}$ is characterized by $\eta_{\mathbf{A}}(t) = (l_{\mathbf{A}}(t), p_{\mathbf{A}}(t), w_{\mathbf{A}}(t), f_{\mathbf{A}}(t))$ with four attributes explained below. The $l_{\mathbf{A}} \in X$ is the location of worker, and $p_{\mathbf{A}} \in \{1, 2, ..., P\}$ is its task group. The walking style of the worker is represented by $w_{\mathbf{A}} \in \{\text{Random (R), Drifted (D)}\}$. Based on previous work and literature Charbonneau and Dornhaus [2015b]; Mersch *et al.* [2013]; Guo *et al.* [2020], we set two walking styles for Worker $\mathbf{A}$: Some workers do not wander inside during each task; they randomly select one of the neighboring cells and moves toward that Charbonneau and Dornhaus [2015b]. We set the walking style of such an ant to be $w_A = R$. This random walking behavior provides the chance of task switching. In the drifted walking style, when $w_A = D$, the worker has a preferential direction toward its task location (S_p) Mersch *et al.* [2013]. Finally,

$f_{\mathbf{A}} \in \{0 \text{ (not informed)}, 1 \text{ (informed)}\}$ represents its information state. Informed workers have the ability to disseminate information to their uninformed workers.

Let $N_p(t)$ be the number of workers performing task p at time t, then we have $N = \sum_{p=1}^{P} N_p(t) \leq K^2$. The notation $SF_p(t)$ is dynamical spatial fidelity (SF) of task p at time t, and it is calculated by the fraction of workers performing task p at time t who have drifted walking style (D). That is,

$$SF_p(t) = \frac{|\{\mathbf{A} : p_{\mathbf{A}}(t) = p \& w_{\mathbf{A}} = D\}|}{N_p(t)}. \tag{2.1}$$

We adopt notations in Guo *et al.* [2020]. Each worker A with $l_{\mathbf{A}}(t) = (i, j)$ has up to four neighbors that are located at $\{(i \pm 1, j), (i, j \pm 1)\}$. If workers are on the edge or in the corner of the colony, the size of these neighboring cells will reduce to three and two, respectively. For convenience, we use $NC_{\mathbf{A}}(t)$ to denote its neighbor sites which could have four, three, or two depending on its location $l_{\mathbf{A}}(t) = (i, j)$. We define $|N_A(t)|$ as the number of nonempty neighbors of worker A.

We develop models to address two questions: (1) How do multiple task groups with associated spatial fidelity affect social contact dynamics and information spread through a colony when tasks are located in different zones? and (2) How does task switching affect dynamical spatial fidelity and social interactions? We use a multiple-task model to explore the first question by allowing information to spread over the whole colony with different numbers of tasks, and we use the task-switching model to explore the second question.

Initially, workers are located randomly in the colony, and the population of task

groups and initial spatial fidelity are the same (i.e., $N_1(0) = N_2(0) = \ldots = N_P(0)$ & $SF_1(0) = SF_2(0) = \ldots = SF_P(0)$). We set the population of drifted walking workers in each task group by $N_p(0) * SF_p(0)$, and other workers are random walking. Then, we randomly choose one worker $\mathbf{A}$ in the multiple-task-group model, make it informed ant, $f_{\mathbf{A}}(0) = 1$, and set its location at the center of the colony, $l_A(0) = (\frac{K-1}{2}, \frac{K-1}{2})$ with K is an odd number.

For each update $\Delta t = 1$ (each update corresponding to 0.001s in real colonies)Guo *et al.* [2020]; Hurlbert *et al.* [2008], we randomly select a worker $\mathbf{A}$ to do the following steps:

1. Based on the neighbors of worker $\mathbf{A}$, it has a probability of $\frac{|N_{\mathbf{A}}(t)|}{|NC_{\mathbf{A}}(t)|}$ to make a contact with one of its neighbors and then switch its location with the neighbor. And it has a probability of $1 - \frac{|N_{\mathbf{A}}(t)|}{|NC_{\mathbf{A}}(t)|}$ to move into its neighborhood sites in next step 2 based on its walking style:

2. (a) If the walking style of $\mathbf{A}$ is random ($w_{\mathbf{A}}(t) = R$), $\mathbf{A}$ randomly selects an empty neighboring cell $l_{\bar{\mathbf{A}}} \in NC_{\mathbf{A}}(t)$ to move in the new location $l_{\bar{\mathbf{A}}}$: $l_{\mathbf{A}}(t+1) = l_{\bar{\mathbf{A}}}$,

   (b) If the walking style of $\mathbf{A}$ is drifted ($w_{\mathbf{A}}(t) = D$), $\mathbf{A}$ selects an empty neighboring cell $l_{\bar{\mathbf{A}}} \in NC_{\mathbf{A}}(t)$ closest to SFZ (S_p) to move in new location $l_{\bar{\mathbf{A}}}$: $l_{\mathbf{A}}(t+1) = l_{\bar{\mathbf{A}}}$. To determine the distance between task SFZ and all neighboring empty lattices, we utilized Euclidean distance. In the event that two empty lattices are equidistant from SFZ, the worker will randomly select one to move to.

   We repeat the process for the next randomly selected worker.

3. Makes contact with one of its neighbors by randomly selecting a neighbor worker $\mathbf{B} \in N_{\mathbf{A}}(t)$ and switches its location with this neighbor worker $\mathbf{B}$, and $l_{\mathbf{A}}(t+1) = l_{\mathbf{B}}(t)$ and $l_{\mathbf{B}}(t+1) = l_{\mathbf{A}}(t)$.

   Workers can sense and communicate with neighbors located in adjacent grids within the length of the antenna (2mm) Guo *et al.* [2020]. Each grid can occupy at most one worker; therefore, the physical contact of two workers results in their movement. Because of their proximity, these motions cause them to switch locations, which is biologically and mathematically reasonable. Now we have the following two scenarios:

   (a) In multiple-task-group model: if two contact agents have different statuses in information, i.e., $f_{\mathbf{A}}(t) \neq f_{\mathbf{B}}(t)$, we define $f_{\mathbf{A}}(t+1) = f_{\mathbf{B}}(t+1) = 1$,

   (b) In the task-switching model: worker $\mathbf{A}$ is randomly chosen from population, without loss of generality, we assume that neighbor $\mathbf{B}$ will switch its task to worker $\mathbf{A}$'s with probability β_A when worker $\mathbf{A}$ and $\mathbf{B}$ have different tasks (i.e., $p_{\mathbf{A}}(t) \neq p_{\mathbf{B}}(t)$), thus the task of $\mathbf{B}$ at time $t+1$ is $p_{\mathbf{B}}(t+1) = p_{\mathbf{A}}(t)$. Based on task-switching mechanisms in ant colonies (Wilson [1985]; Robinson [1992]), individuals in our model are assumed to update their walking style in a negative feedback manner via sensing the demand/supply of task activities. After task switching, the worker $\mathbf{B}$ updates its walking style ($w_{\mathbf{B}}$) to be drifted (D), i.e., $w_{\mathbf{B}}(t+1) = D$, with probability $1 - SF_{p_A}(t)$; and to be random with probability $SF_{p_A}(t)$. The assumptions of how the worker $\mathbf{B}$ updating its walking style follow from the "balancing," which means if more workers stay at the task location, then the new workers who join this task group will be more inclined to do

a random walk.

We repeat the process for the next randomly selected worker.

The model flowchart for a single time-step is shown in Figure (2.1), and the left of Figure (2.2) shows the walking style of a typical worker, and the right of the Figure (2.2) shows the location of the different number of groups, and the right bottom of the Figure (2.2) shows different spatial arrangement of four task-groups.

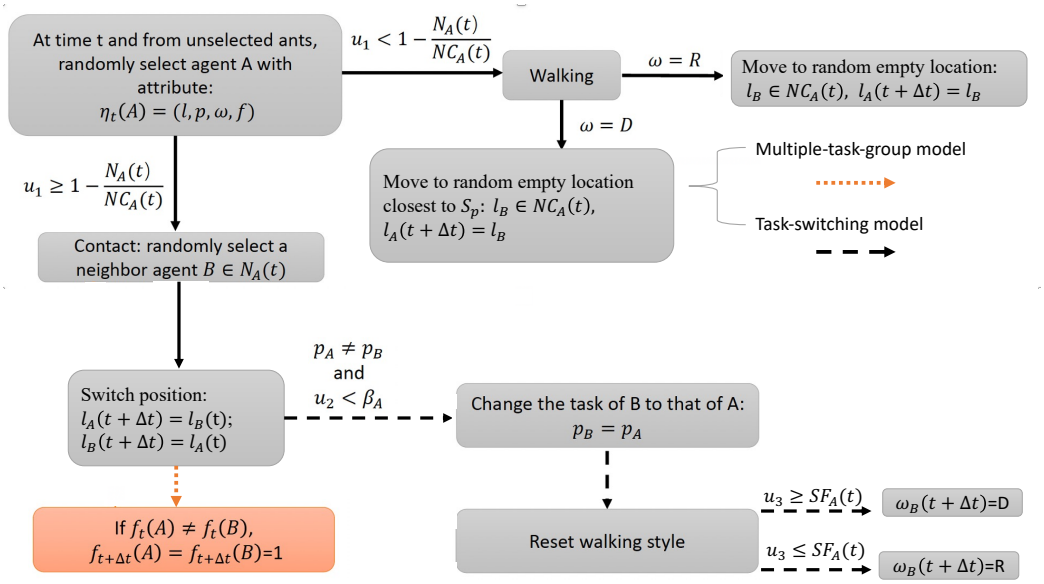

Figure 2.1: The dynamics process for each update Δt. u_i indicates random numbers in $(0, 1)$, $i = 1, 2, 3$

.

To continue our study, we define the following measurements. Spatial Heterogeneity Degree (SHD) measures the distribution of workers in the colony Myers [1978] and is defined as

$$SHD(t) = \frac{\sum_{l=1}^{K^2} \left(P_l(t) - \frac{N}{K^2}\right)^2}{K^2}, \tag{2.2}$$

where $P_l(t)$ indicates the probability that location l is occupied by a worker at time t, $\frac{N}{K^2}$ is the probability of location occupation when all workers do symmetric random walks. The function $SHD(t)$ is bounded from the above by its maximum $SHD_{max} = \frac{N(K^2-N)}{K^4}$. We assume one lattice has 1 or 0 workers at any given time t, and we calculate the approximation of SHD following the method in Guo *et al.* [2020].

Let $C_{pq}(t)$ be the total number of contacts that occurred between two different tasks workers of social insects colony in the time interval $(0, t)$. If $p = q$, then $C_{pp}(t)$ is the total number of contacts within a task group p and R_{pp} is the contact rate within a task group p; if $p \neq q$ then $C_{pq}(t)$ is the total number of contacts between different task groups and R_{pq} is the contact rate between different task group p and q. Therefore,

$$R_{pq}(i) = \frac{C_{pq}(im) - C_{pq}(1 + (i-1)m)}{m}, i \in \mathbb{Z} \cap [1, \frac{\text{total time}}{m}] \tag{2.3}$$

Similarly, we define $R_{pp}(i)$ to be intact rates within the task groups p. Then we set total contact rate within group (R_w) as $\sum_{p=1}^{P} R_{pp}(i)$ and total contact rate between groups (R_{bt}) is $\sum_{p=1}^{P} \sum_{q=1}^{P} R_{pq}(i)$, where $p \neq q$.

The task switching rate per m updates shown by TS_{pq} is the total number of workers that change their task from task p to task q through contacts over $m - 1$ updates divided by m updates Guo *et al.* [2020]:

$$TS_{pq}(i) = \frac{\text{The total number of workers who switch task p to q from time 1+(i-1)m to time im}}{m}. \tag{2.4}$$

Finally, let $I(t)$ as the total number of informed workers ($f_{\mathbf{A}}(t) = 1$) in the time

interval $(0, t)$. We denote $I_{trans}(i)$ as the information transfer rate per m updates. This implies the following formulation:

$$I_{trans}(i) = \frac{I(im) - I(1 + (i-1)m)}{m}, \tag{2.5}$$

Those definitions above allow us to ask the following questions:

1. What are the main differences between the two models, multiple-task-group and task-switching, in effects on spatial heterogeneity degree (SHD) and contact dynamics?

2. How does the presence of multiple task groups with their associated spatial arrangement influence the dynamics of spatial heterogeneity degree (SHD) and contact dynamics, and how does this consequently impact information spread and/or task switching rates?

3. What are the relationships between spatial fidelity (SF), spatial heterogeneity degree (SHD), and contact dynamics in the task-switching model, and how do they affect the dynamics of task population for a task group of p workers $(N_p(t))$?

In the following section, we implemented 2-5 groups in our simulations, given that social insects exhibit various task allocations in response to their environment Guo *et al.* [2020]; O'Donnell and Bulova [2007]; Pinter-Wollman *et al.* [2012] with associated SFZs as shown in Figure (2.2), because Charbonneau *et al.* (2015) Charbonneau *et al.* [2015] observed that workers' tasks and associated movement areas are not fixed, to answer these three questions.

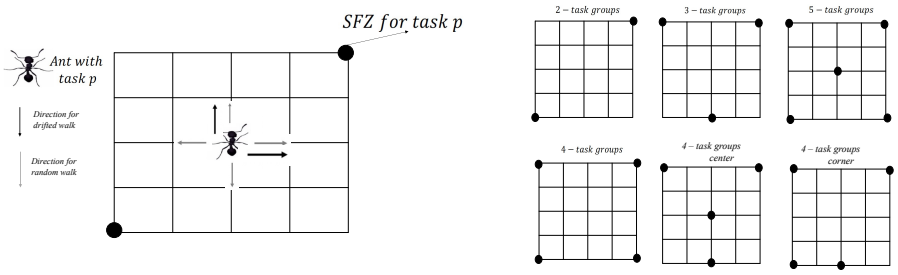

(a) (b)

Figure 2.2: Schematic illustrations of walking style and the SFZ geometry when the colony has two, three, four, and five task groups: A worker performing task p moves to its random adjacent neighboring cell if its walking style is random ($w = R$) or moves to its adjacent neighboring cell that is the closest to its SFZ S_p if its walking style is drifted ($w = D$). The SFZ for two, three, four, and five task groups are shown as the big solid dark dots in the right panel of the figure. Especially for the four task groups, we set different positions of SFZ, which are four groups at the corners (4-task groups), one at the center and three in a triangle (4-task groups center), and one at the corner and three be the triangle (4-task groups corner).

Agent-based model simulations, based on three major tasks (brood-caring, food-processing, and trash-maintaining) observed in *P. californicus* ant colonies Holbrook *et al.* [2011], revealed the relation between individual spatial distribution and spreading agents transmission Guo *et al.* [2020]. To incorporate more possible scenarios, such as more than 3 tasks in the nest Charbonneau and Dornhaus [2015b], and spatial arrangements of tasks beyond the triangular structure of task locations described in other species of social insects Richardson *et al.* [2022], we simulate scenarios where colonies consist of 2-5 task groups in 6 different spatial arrangement of task locations.

2.3 Results

In this Section, we perform our simulations and analyses on the two models provided in Section 2.2. Spatial fidelity (SF) of task group p denoted by $SF_p(t)$ is the fraction of workers performing task p that does preferential walking to their own task

location at time t. Spatial heterogeneity degree ($SHD(t)$) defined as in Eqt. (2.2) measures how workers are distributed in the colony at time t. Our recent work Guo *et al.* [2020] indicates that $SHD(t)$ can be affected by task-associated spatial fidelity SF_p in a significant way, as shown in Figure 2.3a. We aim to use a multiple-task-group model to explore how the number of task groups may impact their related spatial distribution and thus influence social contact dynamics and information spread through a colony (see mechanisms diagram shown in Figure 2.3a). Moreover, we use the task-switching model to study how the task-switching dynamics may impact spatial heterogeneity degree (SHD) and therefore impact social contact dynamics and task allocation (see mechanisms diagram shown in Figure 2.3b).

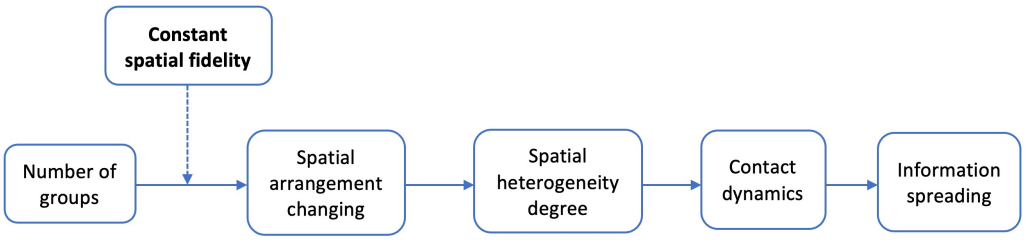

(a) multiple-task-group model

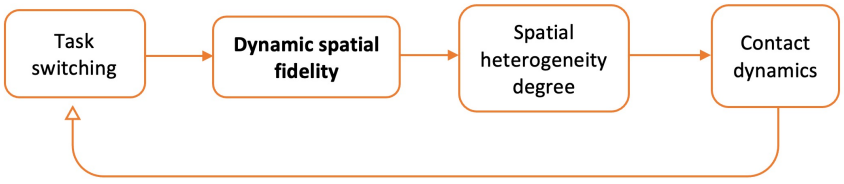

(b) task-switching model

Figure 2.3: Mechanisms for generating spatial heterogeneity degree for multiple-task-group model versus task-switching Model.

Figure 2.3, a flowchart, visually illustrates the relationships between the elements, clearly depicting how they are interconnected. It helps in understanding the results

presented in the following section.

In the multi-task-group model, we set different numbers of groups. Because there is no task switching in this model, spatial fidelity remains constant. Due to the different number of groups, the model has different spatial arrangements of these groups (see Figure 2.2). After these settings, we aim to explore how the number of task groups may impact their related spatial distribution (SHD) and thus influence social contact dynamics and information spread through a colony (Figure 2.3a).

In the task-switching model, workers can switch tasks. Due to task switching, spatial fidelity has changed. After these settings, we aim to study how the task-switching dynamics may impact spatial heterogeneity degree (SHD) and therefore impact social contact dynamics and task allocation (Figure 2.3b).

All simulations start with the same initial condition and use the same baseline parameters listed in Table (2.1) unless stated otherwise. Our initial setting values are from previous work Guo *et al.* [2020]. We can also roughly calculate the colony size and population of workers by some information from Waters *et al.* [2017] to be equivalent to our settings. However, our model is not only for this species. Our model serves more general species. The purpose of our model is to learn the dynamic changes of the internal space and information of the system. In this study, we did not incorporate the influence of the external environment into our model. To ensure the competition of two task switching is equal, we assigned an equal and unbiased probability of 50% for task switching between the two tasks we have set.

Parameter	Description	Baseline
$K \times K$	Colony size	69×69
N	Total number of workers	180
p	Workers task	$p \in \{1, 2, 3, 4, 5\}$
β_p	Task switching probability	0.5
$SF_p(0)$	The initial spatial fidelity in task groups	$0.4 \sim 0.8$
m	per m updates	1000
I	initial informed workers	1

Table 2.1: Parameters used in the simulations for the multiple-task-group and task-switching models

.

2.3.1 Dynamics of the Multiple-Task-Group Model

We adopted the modeling approach of Guo *et al.* [2020] to inform our multiple-task-group model. The number of task groups in our previous model Guo *et al.* [2020] is three. This model expands to scenarios of 2, 3, 4, and 5 task groups while keeping the same worker density. For convenience, we assume that the size of each task group is the same; each task group has 90 agents for two task groups, 60 agents for three task groups, 45 agents for four task groups, and 36 agents for five task groups. We also assume that spatial fidelity (SF) for each task is the same for all cases, i.e., $SF_p(t) = SF_p(0) = SF$.

Dynamics of Spatial Heterogeneity Degree (SHD): Figure 2.4 and Figure 2.5

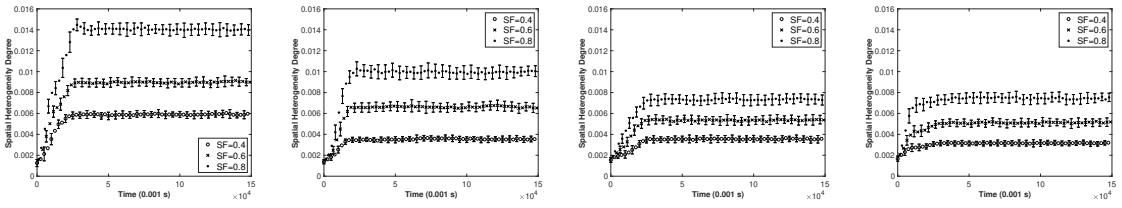

(a) Two groups (b) Three groups (c) Four groups (d) Five groups

Figure 2.4: The impact of spatial fidelity (SF) on spatial heterogeneity degree (SHD) across 2, 3, 4, 5 task groups: $SF = 0.4(circle), 0.6(cross), 0.8(dot)$. 4-task groups are four groups at the corner shown in the bottom left corner of Fig.2.2b. The plateau of SHD increases with its fixed SF $SF = SF_p(0)$. The curves represent the dynamic of the average of 40 replicates, and the error bars show the standard deviation of the data.

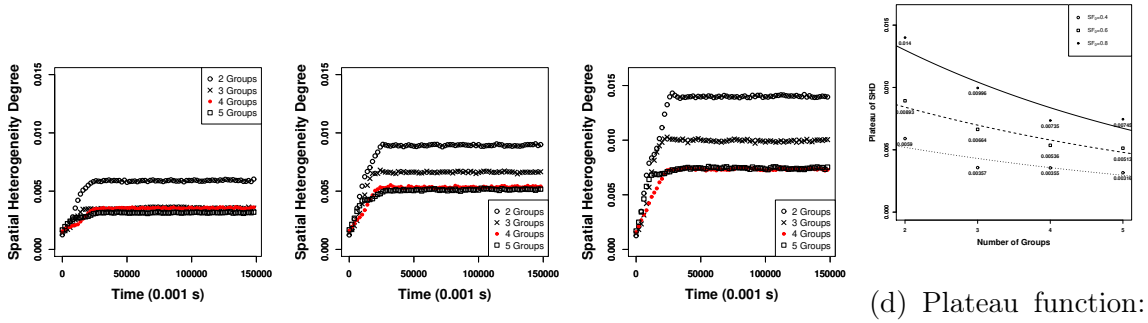

(a) $SF = 0.4$ (b) $SF = 0.6$ (c) $SF = 0.8$ (d) Plateau function: $y = e^{a+bx}$

Figure 2.5: The impact of multiple task groups on spatial heterogeneity degree (SHD): Different numbers of task groups (2, 3, 4, and 5 task groups) for $SF = 0.4, 0.6, 0.8$ respectively. 4-task groups are four groups at the corner shown in the bottom left corner of Fig.2.2b. The plateau of SHD seems to be non-linearly decreasing with multiple task groups. 2.5d) the plateau of SHD (y) has exponential decay: $y = e^{a+b*x}$ by different numbers of task groups (x). Dot line is for $SF = 0.4$, $a = -4.88$, $b = -0.1879$; dash line is for $SF = 0.6$, $a = -4.40$, $b = -0.1880$; solid line is for $SF = 0.8$, $a = -3.90$, $b = -0.22$. The curves represent the dynamic of the average of 40 replicates.

provide us insights on how the number of task groups and spatial fidelity affect SHD. In Figure 2.4, we varied spatial fidelity (SF) $SF = 0.4$ (circle), 0.6 (cross), and 0.8 (dot) for colonies with 2 task groups (see Figure 2.4a), 3 task groups (see Figure 2.4b), 4 task groups (see Figure 2.4c), and 5 task groups (see Figure 2.4d). Our results show

that SHD increases with its SF for all number of task groups. This observation is in line with results observed in Guo *et al.* [2020]; Lloyd [1967]. The potential explanations are that with larger SF, more workers aggregate to their task location after large enough time, thus larger SHD, which measures the spatial distribution of workers in the colony. However, the increasing rate of SHD with respect to SF varies with multiple task groups.

Figure 2.5 reorganizes the presentation of results in Figure 2.4, comparing how the number of task groups impacts spatial heterogeneity degree (SHD) when the spatial fidelity (SF) is $SF = 0.4, 0.6, 0.8$ respectively. After analyzing the data (see Figure 2.5d), we performed both linear and exponential fitting. Based on the mean square error and positivity, it was determined that the exponential fit yielded superior results. The dynamics shown in Figure 2.5 suggest that (1) the plateau of SHD decreases as the number of task groups increases; and (2) The plateau of SHD drops faster as SF increases (see Figure 2.5d and the value of b in Table 2.2). For example, the SHD dynamics of task group 4 (shown as red dots in Figure 2.5) is very close to the task group 5. To determine the quantified relationship between SF, SHD, and multiple task groups, The best fit outcomes are provided in Table 2.2.

Effects of the number of task groups on the contact dynamics: Figure 2.6 shows the contact dynamics within groups (Figure 2.6a) and between groups (Figure 2.6b) for a colony with two, three, four, and five task groups when the spatial fidelity (SF) is 0.6. The dynamics shown in Figure 2.6a suggest that with a higher number of task groups within the colony, the plateau of the contact dynamics within task

	$SHD = e^{a+b*x}$	
SF	a	b
0.4	-4.88	-0.1879
0.6	-4.4	-0.1880
0.8	-3.9	-0.22

Table 2.2: The first equation shows the plateau of SHD has exponential decay with the number of task groups (x): $SHD = e^{a+b*x}$ (see Figure 2.5d).

groups is lower. Through the Welch ANOVA test (Table B.1 in Appendix), Figure 2.6b and Table 2.3 observe the number of task groups impacts on the plateau of the contact dynamics between groups. Among them, the t-test shows that 2-group, 3-group, and 5-group have significant differences; the plateau of the contact dynamics between groups increases as the number of task groups increases. However, the t-test shows 3-group compared with the 4-group and the 4-group compared with the 5-group have no significant difference. In other words, when the number of groups increases, the difference between adjacent cases is not significant and shrinks as the number of groups increases.

From Figure 2.4, we find that higher spatial fidelity (SF) leads to a higher spatial heterogeneity degree (SHD) because of more agent clustering. We find the contact dynamics ($R = R_1 + R_2$) have a strong positive linear relationship with SHD, i.e., the more agents gathering, the more contact that occurs. For example, $R(t) = 63.46 \times SHD(t) - 0.06$ when $SF = 0.6$ with two task groups in the colony. The contact dynamics includes contact rate between groups ($R_{12} + R_{21}$) and within group ($R_{11}+R_{22}$). Figure 2.4 shows that the colony with more task groups has smaller

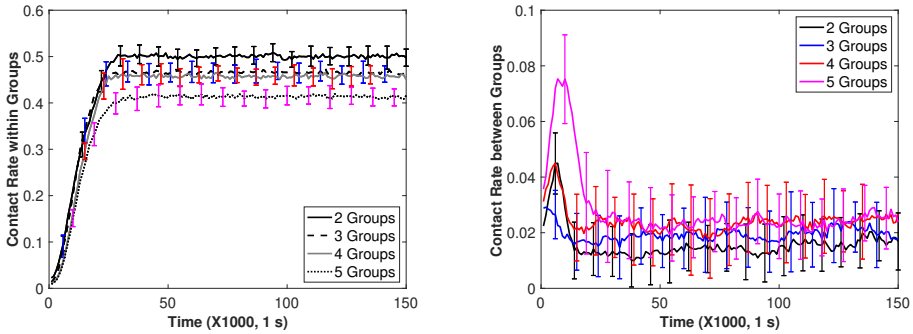

(a) Contact dynamics with-in task groups

(b) Contact dynamics between task groups

Figure 2.6: Impacts of multiple task groups on the contact dynamics: Colony has two, three, four, and five task groups when the spatial fidelity (SF) is 0.6. 4-task groups are four groups at the corner shown in the bottom left corner of Fig.2.2b. a) The plateau of contact dynamics within task groups seems to decrease with multiple task groups increasing. b) The plateau of contact dynamics between task groups is increasing with multiple task groups increasing. The curves represent the dynamic of the average of 40 replicates.

SHD; then it leads to lower contact dynamics.

Effects of different *SF* on contact dynamics: Figure 2.7 shows that (1) the plateau of contact dynamics within the group increases with spatial fidelity (SF), (2) the plateau of contact dynamics between groups decreases as SF increases, and (3) the highest value of contact rate between groups is higher as SF increases.

When SF increases, more agents prefer walking to their task location. After a specific time, more agents aggregated in their task location, which led to the increased density for increased contacts within their task group. When SF reduces, more agents would prefer doing the random walk, and then they will move out of the task fidelity zone, which increases the density of the contact between task groups (higher contact

Groups	between groups	with-in group
2	0.0155	0.500
3	0.0230	0.463
4	0.0234	0.457
5	0.0237	0.414

Table 2.3: The mean of plateaus of the contact dynamics between groups and with-in group for colonies having two, three, four, and five task groups when the spatial fidelity is 0.6, i.e., $SF = 0.6$. The plateau of contact dynamics within task groups decreases with the number of task groups, and the plateau of contact dynamics between task groups increases with the number of task groups, same with Figure 2.12.

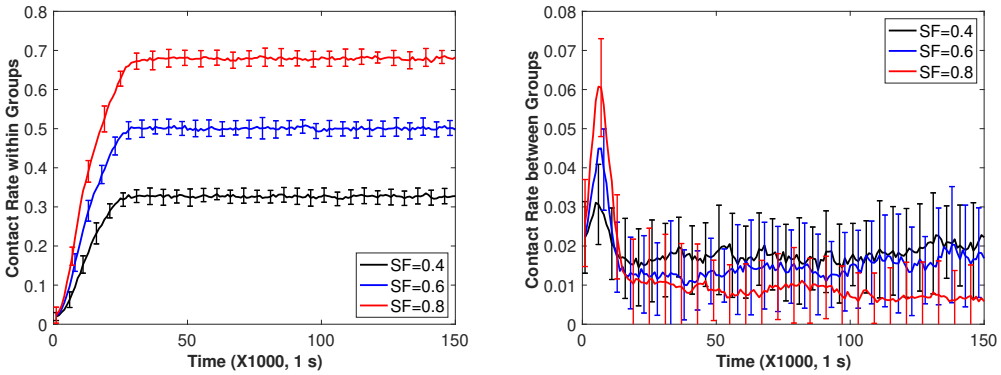

(a) Contact rate within a task, 2 task groups with different SF

(b) Contact rate between tasks, 2 task groups with different SF

Figure 2.7: Spatial fidelity affects the plateau of contact dynamics. The error bar shows the standard deviation. The curves represent the dynamic of the average of 40 replicates.

between groups). In the beginning, a larger SF will cause more agents to walk toward their task zone location, and this movement will inevitably lead to more contact dynamics between and within groups during this process.

	$y = c * time + d$	
SF	c	d
0.4	$2.806 * 10^{-5}$	$5.933 * 10^{-2}$
0.6	$3.644 * 10^{-5}$	$7.13 * 10^{-2}$
0.8	$4.77 * 10^{-5}$	$8.602 * 10^{-2}$

Table 2.4: The equation shows the proportion of informed workers (y) has a positive linear relationship with time: $y = c * time + d$ (see Figure 2.8 yellow lines).

Effects of the number of task groups and task location on spreading information: Our model focuses on the case when information spreads through physical contact between workers, with higher contact rates leading to faster information spread. Figure 2.8 shows the dynamics of information spread in the colony for different values of spatial fidelity (SF) and the number of task groups. From this Figure, we observe that: 1) In Figures 2.8a to 2.8f, there exists some special time (horizontal red line) before which all cases have similar trends. 2) Our fitting (equation in Table 2.4) explores that information spread speed rises when SF increases. 3) After the special time (horizontal red line), information continues to be transmitted at a slower speed. 4) In Figures 2.8a-2.8c, the 3-group (asymmetric) information transfer process is slower than the 2-group and 5-group. We defined the spatial arrangement of the 2 and 5 groups case as "Symmetric". Therefore, symmetry may be a positive influence on information spreading. The greater number of groups may take less time to make

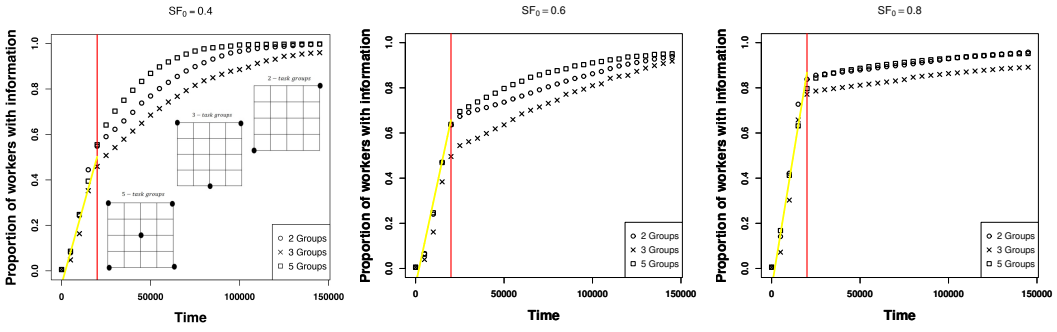

(a) $SF = 0.4$ (b) $SF = 0.6$ (c) $SF = 0.8$

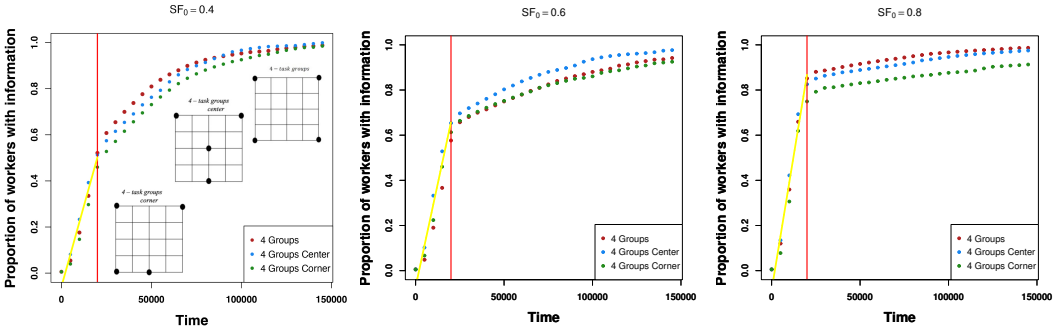

(d) $SF = 0.4$ with 4 groups (e) $SF = 0.6$ with 4 groups (f) $SF = 0.8$ with 4 groups

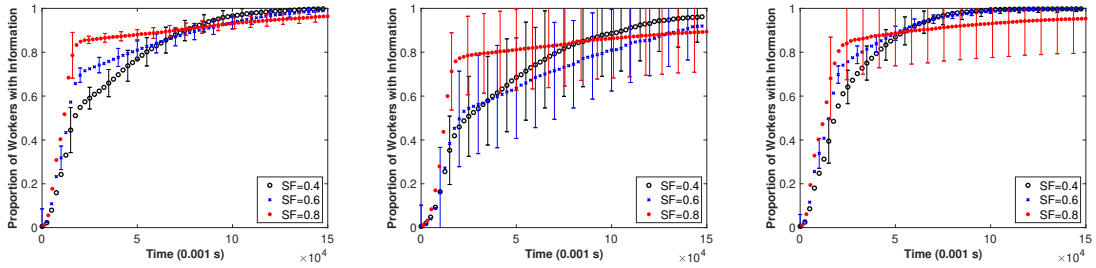

(g) 2 task groups (h) 3 task groups (i) 5 task groups

Figure 2.8: Impacts of multiple task groups and task location on information spread with varied fixed spatial fidelity (SF): Figure (2.8a) - (2.8f) are different numbers of task groups (2, 3, 4 and 5 task groups) for $SF = 0.4, 0.6, 0.8$. Horizontal red lines (all lines are t=20,000) are the special time value for speed change of information spreading. Before this time, the spatial arrangement of task location does not affect the information spread in the same SF case. The yellow lines are linear regression of the proportion of informed workers (y) with time before critical values. Figure (2.8g)-(2.8i) are the same data from Figure (2.8a) - (2.8c) and show same numbers of task groups with varied SF. The points represent the dynamic of the average of 40 replicates.

all workers get the information. 5) Figures 2.8d-2.8f are all four groups of information transmission, and the difference is that the task locations are different (see Figure 2.2). The corner case (green dots) has the largest average distance between locations, and information spreading is slowest, and the center case (blue dots) has the lowest average distance, then information spreading is fastest. Therefore, the lower average distance between locations may lead to the information spreading faster. And the larger the SF, the more significant the result. 6) In Figures 2.8g to 2.8i, SF=0.8 is always lower than others, and 2 task groups case and 3 task groups case show that the number of task groups is the same but with lower SF, information is faster delivered to all workers. Therefore, the symmetrical distribution of task locations may help information transfer faster.

2.3.2 Dynamics of task-switching model

The task-switching model has dynamical spatial fidelity (SF) shown by $SF_p(t)$. In this model, we assume that our simulations have only any two task groups that differ in the population and focus on task switching, in which the selected agent contacts its neighbor with a different task, and then this neighbor switches its task to that of the selected agent via some probability.

Spatial dynamics: Figure 2.9 shows the time-series of spatial heterogeneity degree (SHD) and spatial fidelity (SF) with varied initial SF. Figure 2.9 suggests that (1) dynamic SF and SHD are not affected by initial spatial value, and 2) SF with varied initial values has a similar shape; the shapes of SHD are similar as well.

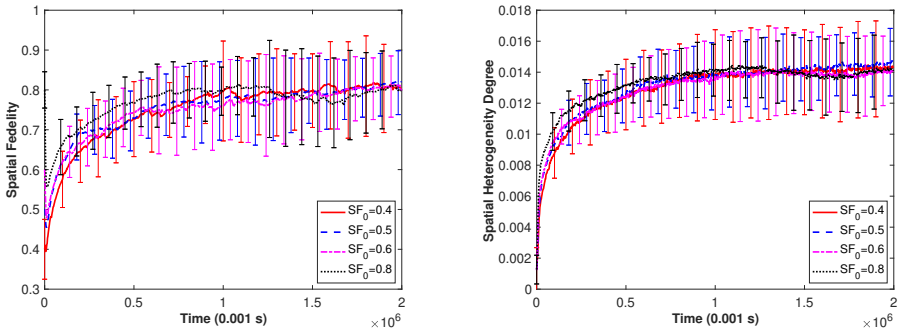

(a) Dynamics of Spatial Fidelity (b) Spatial Heterogeneity Degree

Figure 2.9: Dynamics of spatial fidelity (SF) and spatial heterogeneity degree (SHD) with varied initial spatial fidelity values: The curves represent the average of 40 replicates, and error bars are the standard deviation. In the task-switching model and independent from its initial value $SF_p(0)$, both $SHD(t)$ and $SF_p(t)$ seem to reach a fixed quasi-stationary state.

Comparison of contacts between the multiple-task-group model and task-switching model: Figure 2.12 compares the time-series of contacts when the colony has two task groups in multiple-task-group model and task-switching model. Notice that spatial fidelity (SF) in the multiple-task-group model is constant while SF in the task-switching model changes over time (see Figure 2.9a). Figure 2.12 in the task-switching model suggests that (1) the plateau of contacts within and between groups are similar with different initial SF, (2) the initial increase in speed is faster with higher initial SF (see Figure 2.12a-2.12c), and (3) the largest value of contacts between groups is higher when initial SF is higher (see Figure 2.12d-2.12f). On the other hand, Figure 2.12 suggests that (1)the plateau of within-group contacts group in the task-switching model is always higher than that of the multiple-task-group model, and (2) the plateau of contact between groups in the task-switching model is always lower than that of the multiple-task-group model when the final result stabilized.

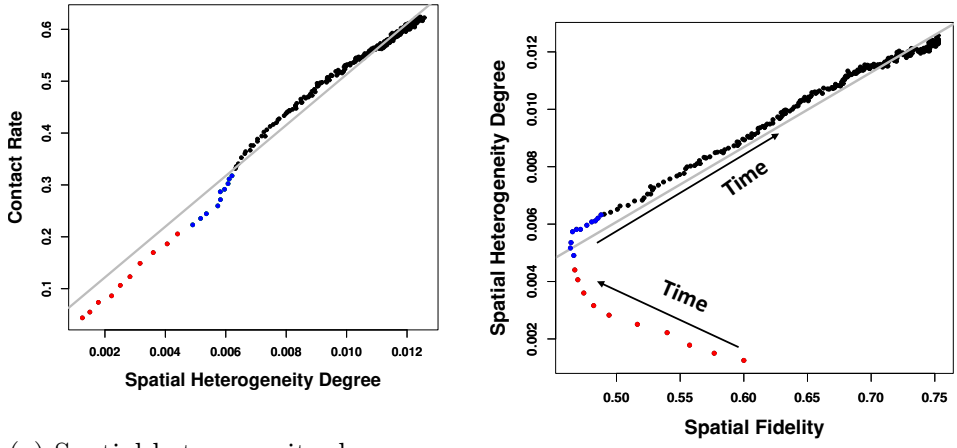

(a) Spatial heterogeneity degree versus contact rate: task-switching model with initial spatial fidelity being 0.6 $SF_p(0) = 0.6$. Contact rate ($R = R_1 + R_2$) is the inclusion of between groups ($R_{12} + R_{21}$) and within groups ($R_{11} + R_{22}$). These two metrics have an strong positive linear relationship: $R(T) = 48.92SHD(T) + 0.02$.

(b) Spatial heterogeneity degree versus task 1 spatial fidelity (SF): task-switching model with initial spatial fidelity being 0.6 $SF_p(0) = 0.6$. These two metrics have a strong positive linear relationship: $SHD(t) = 0.026SF_1(t) - 0.007$ (gray line). Figure 2.9a shows SF decreases with time series, in the beginning, these data are red dots in this figure.

Figure 2.10: Strong linear relationship in the task-switching model: Spatial heterogeneity degree has a linear relationship with contact rates and spatial fidelity (SF) in the task-switching model. Thus, it can be deduced that contact rates and SF also have a linear relationship. Both figures use the same simulations. Blue dots are the data under the line except for the red dots part in Figure 2.10a. The red dots are the negative correlation between SF and SHD in Figure 2.10b. We keep colors for both figures. The curves represent the dynamic of the average of 40 replicates.

Figure 2.10a shows that contact rate positively correlates with spatial heterogeneity degree (SHD). In the multiple-task-group model, $SF = 0.8$ has the highest plateau

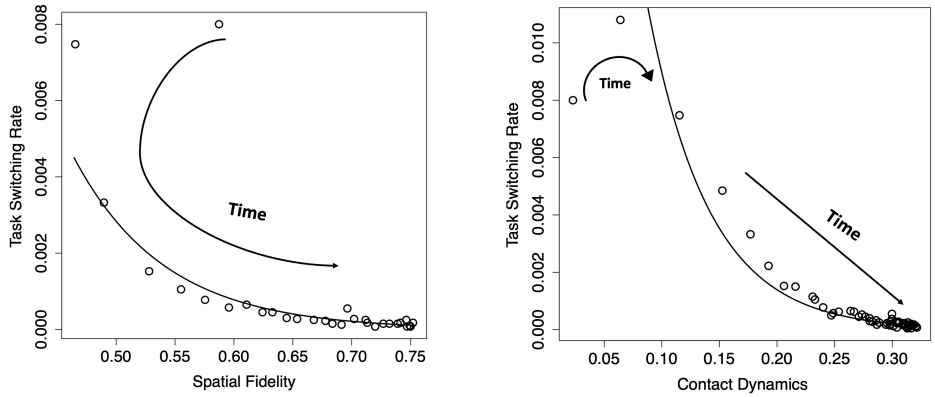

(a) Task switching rate versus spatial fidelity

(b) Task switching rate versus contact rate

Figure 2.11: The relationship between contact rates and spatial fidelity: The task switching rate is a non-linear decay with spatial fidelity (SF) and contact rate. Among them, contact rate (R_1) is the inclusion of between groups (R_{12}) and within groups (R_{11}), task switching rate is the rate of task 2 agents switch to task 1 (TS_{21}), and SF is SF in task 1 ($SF_1(t)$). a) the function of the curve is $TS_{21}(t) = e^{0.60-12.94SF_1(t)}$; b) the function of the curve is $TS_{21}(t) = e^{-2.85-18.64SR_1(t)}$. The curves represent the dynamic of the average of 40 replicates.

of SHD, and the plateau of SHD achieves a similar value in the task-switching model. We compared the initial SF of 0.8 with two task groups, and the plateau of SHD in the task-switching model is higher than in the multiple-task-group model (see Figure 2.13). Physical contact between groups leads to agents switching their tasks. As spatial fidelity (SF) increases, more agents aggregate at their task locations. Therefore, when spatial fidelity (SF) is higher, they will have more chance for within-group contact and less chance to contact other groups' agents with an increased probability of switching their tasks. The data fitting shows that the task switching rate has an exponential decay by SF (see Figure 2.11a). Due to the positive linear relationship between contact rate and SF (see Figure 2.10), task switching rate also has an exponential decay in relation to contact dynamics (see Figure 2.11b). Figure 2.10b shows

that red points are under the gray line of $SHD(t) = 0.026SF_1(t) - 0.007$. Those points occur at the initial time frame of $[0, 10000]$ and suggest the negative correlation between spatial fidelity and the spatial heterogeneity degree.

Task groups: Figure 2.14 presents three different dynamics of task populations from our simulations. The replicate runs of the model with the same parameter values. We set two task groups with the same population at proportion values of 0.5 for each task (red baseline) initially. The black curves are the proportion of the task 1 population size in the colony. We use a histogram to show the frequency of population switching, which is the major task change. The histogram of Figure 2.14d shows the proportion of the major task changing less or equal to 6 is 49.47%, including 11 cases is no-changing. We used geometric distribution to fit the histogram (red curve) with a probability value of 0.1136. The median of the fitting distribution is 4.7. Half of the simulations changed the major task 5 times. For example, Figure 2.14a has no switching (0 bar), which means one task is always a major task and needs more agents. Figure 2.14b has fewer switching (less than 5 times), which means the major task can switch to another one but not often. Figure 2.14c has fewer switching (more than 5 times), which means the major task often switches to another one, and both tasks have equal demand. The simulations can be classified into those categories that align with the observation of experiments in the lab and literature Leighton *et al.* [2017].

2.4 Discussion

We used an agent-based model to explore the factors that generate spatial heterogeneity and explore how spatial heterogeneity affects contact dynamics, information spread, and task switching. We focused on two models based on the consequences of social contact inside the colony: (1) The first consequence of social contact is that contact leads to potential information spread. We developed the multiple-task-group model to understand how the number of task groups and associated constant SFZs and spatial distributions would affect contact dynamics and information spread. (2) The task-switching model studies the second consequence of social contacts; the contact between two workers can lead to a change in behavior by increasing the chance that one worker may decide to switch tasks with associated changes in walking style. These behavioral changes can generate spatial heterogeneity and dynamical changes in spatial fidelity and can affect the size of the task group if this leads to task switching.

When few workers are engaged in a task (low spatial fidelity), positive feedback draws more workers toward their task locations, while a disproportionately high density of workers at a task results in negative feedback that increases the likelihood of workers leaving to search for a new task Page Jr and Mitchell [1990]; Gordon *et al.* [1992]. Thus, spatial fidelity allows the colony to balance workers among tasks regardless of the initial spatial heterogeneity (see Figure 2.9). Spatial fidelity influences physical interactions among ants, affecting task switching. The findings of this study should be considered with the following caveats: First, our results are simulation-based, and there are no experimental data to support the findings. Second, the model is a general case only. In the future, we could set specific tasks for each group

relevant to colony task organization, for example, by introducing a food source to increase demand for the task of foraging. This would allow us to further study the impact of space on task switching in a more specific context. Below we review how insights gained from the models may be applied to the case of social insect task organizations by discussing the interaction between spatial effects and mechanisms of task allocation and the role of interactions in information transfer.

2.4.1 Group effects

In the multiple-task-group model, we explored how the different numbers of groups in the colony influence information spread. We tested 2,3,4, and 5 groups in one colony with varied spatial fidelity (SF). Varied SF and task group location both affect the information spread speed. Different SF and task group locations influence the spatial heterogeneity (Figure 2.5). When space is more heterogeneous, task-related information can be more quickly communicated within a task group Naug [2009] (Figure 2.3a). In contrast, with lower spatial fidelity, information transmission speed may be slower locally, but information spreads through the colony more quickly. Spreading information or transmission elements (i.e., food) is easier between individuals within a colony Naug [2008], and information spreads faster at beginning Sendova-Franks *et al.* [2010]. We observed from Figure 2.8 that the number of task groups could affect information transmission speed and process. This suggests that geometry is a key to information transmission speed and process. This may also be why the organizational layout of tasks within social insect colonies is often similar. Although the specific locations and substrates for tasks vary considerably, the organizational relationships

among tasks often follow similar rules Mersch *et al.* [2013]. Therefore, further exploring the task-switching model, we focus on the dynamics of spatial fidelity rather than on different numbers of tasks. Additionally, the plateau of within-group contact rates decreases as the number of task groups increases; there will be more contact between groups conversely. Therefore, more task groups will disperse the population, reduce the social interaction within the group, but increase the social interaction between the groups and create more opportunities for task switching.

2.4.2 Spatial effects on task switching and task allocation

In the task-switching model, individuals use both social (shared task information) and contextual (density of workers at task location) cues to make decisions about task allocation. In contrast, in the multiple-task-group model, only contextual cues are used. Furthermore, the contextual cues in the task-switching model are dynamic, adjusting to the relative density of workers actively engaged in a task. As such, the task-switching model more closely resembles cases of flexible task allocation, such as the role of response thresholds in bee fanning behavior Weidenmuller [2004]; Jones *et al.* [2004]. The multiple-task-group model better mimics cases in which tasks are more fixed, such as morphologically specialized workers (e.g., soldiers) or more intrinsically directed temporal polytheism (as in honey bee nursing vs. foraging) (See Charbonneau and Dornhaus [2015a]; Johnson [2003] for a discussion on fixed vs. flexible task allocation mechanisms).

In Figure 2.3, these two models have different spatial fidelity (SF) settings, one

changes by time and one is constant. Comparison of the model's performance in SHD to explore how SF infects spatial heterogeneity. SHD shows faster reaching steady state in the multiple-task-group model than in the task-switching model, suggesting that fixed task allocation mechanisms may be more efficient (i.e., workers allocated to their tasks more quickly) than flexible task allocation mechanisms. On the other hand, SHD plateaus in the task-switching model converge on similar numbers regardless of the initial value of $SF_p(0)$. In contrast, the level of the SHD plateaus in the multiple-task-group model directly depends on the $SF_p(0)$ value. This suggests that flexible task allocation mechanisms may take longer to reach equilibrium but are more robust to perturbation. Indeed, if these systems suffered large losses of individuals in one task group, thereby changing the value of spatial fidelity ($SF_p(t)$), the task-switching model would return to the distribution of workers among tasks (i.e., SHD) comparable to pre-disturbance levels, while multiple-task-group model would be irreversibly changed and be unable to return to pre-disturbance SHD levels.

2.4.3 Social interaction

From Figure 2.3, we discuss how these elements influence contacts, including the information, in the following paragraphs. In both models, there are two main processes that influence behavior: allocation of workers among spatially segregated tasks and information transfer among workers. In the multiple-task-group model, task allocation, i.e. task group in which the population of each group is fixed, affects the contact rate among workers, which in turn affects the speed with which information is propagated among workers. However, information in the multiple-task-group model

does not affect task allocation. For the task-switching model, task allocation affects information transfer via the same process as in the multiple-task-group model (task switching rates and likelihoods of information transfer), but in the task-switching model, information also affects task allocation. The result is an exponential growth of informed individuals (vs. uninformed) in the multiple-task-group model, where propagation speed is determined by constant SF. In the task-switching model, both bits of information compete with each other, and no single task can eliminate the other within a certain time, though they may go through phases of fluctuation over time (Fig. 2.14). In our algorithm, we set the task switching rate (β_p) to 50%, which is $\beta_A = \beta_B$. Although this is not our purpose in this study, we tried different values of β_A and β_B during some test simulations. We found that the results were influenced by the comparing value of β_p. If $\beta_A = \beta_B$, the dynamics of SF and task switching rate have no significant difference, but if $\beta_A \neq \beta_B$, the situation becomes different. Therefore, task-switching probabilities will have different effects to some extent, as larger β_p leads to a higher number of this task (Figure B.1 in Appendix). Therefore, we believe that the random selection of the worker and our setting of task switching is a process without losing generality.

Interestingly, regardless of the mode of the consequence of social contact (i.e., task switching or information transfer), the contact dynamics are very similar. This suggests that the mechanisms allowing increased robustness in task allocation to disturbance (discussed above) are not necessarily dependent on transmission rate, but rather the dynamic nature of task allocation in the task-switching model, i.e., feedback between spatial fidelity and task information. This is particularly interesting

because several behaviors in social insects have been shown to be dependent on interaction rate (e.g., foraging Gordon and Mehdiabadi [1999]; Greene and Gordon [2007], emigration consensus (Pratt *et al.* [2002b]; Mallon *et al.* [2001])). However, our model shows that spatially dependent individual feedback mechanisms, as opposed to interactions rates *per se*, can also result in collective flexibility.

In both models, contact rates between task groups initially peak at approximately the same moment, then decrease and stabilize. Their simultaneous peaking is likely caused by the initial random location of individuals. Though this may be an artifact of the initial model setup, it can provide insight into how colonies may react to disturbances that would relocate individuals (e.g., emigration or nest destruction) Pratt *et al.* [2002b]. The fact that the same pattern seems to occur in both models suggests that, regardless of whether task allocation mechanisms are flexible or rigid, both models are capable of adjusting to disturbances.

After the initial peak in contact rate during which the colony reorganizes, contact rates between task groups are lower in the task-switching model than in the multiple-task-group model. Additionally, contact rates within groups rise more slowly in the task-switching model than in the multiple-task-group model and reach a plateau more slowly (Fig. 2.12). This suggests that in the multiple-task-group model, workers can resume their set distribution among tasks more rapidly after disturbance than in the task-switching model. However, in the event of a disturbance where workers are lost (e.g., forager loss or nest defense) Tschinkel and Hanley [2017], the task-switching model should be more robust, and with the colony re-equilibrating according to the

relative densities of workers per tasks (i.e., reach similar plateaus of SHD), In contrast, in the multiple-task-group model, workers will attempt to reach there and thus may not reach optimal task allocation.

2.4.4 Future works

Our previous models Guo *et al.* [2020] have studied information transmission with three task groups and fixed spatial fidelity to indicate that information spreads faster within groups and slower between task groups, while our study provides important insights into the number of task groups and task switching. We build the network model constructed by social insect behavior to analyze the spatial heterogeneity, the number of task groups, and the process of information spreading and task switching from individual-level effects to group-level process. However, our proposed model does have its limitations that we should work with. In an actual social insect colony, there are more complex reasons for workers to change their tasks, such as environmental stimulus Page Jr and Mitchell [1998] and task performances Gordon [1989], not as straightforward as designed in our model, contact and switch with a fixed probability. In addition, the location of our task group zone is simply defined from geometry and is not combined with the task distribution of the social insect colony in reality. In our future work, we should include setting particular tasks and task-related response thresholds in our model. As a basis for future work, our current research is of great help to the understanding of social contact processes with spatial distribution.

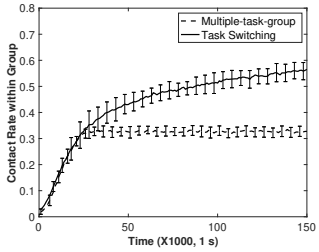

(a) The contact rates within group R_{pp} when the initial spatial fidelity (SF) is 0.4 $SF = SF_p(0) = 0.4$

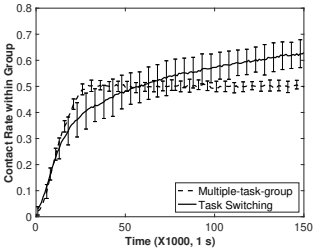

(b) The contact rates within group R_{pp} when the initial spatial fidelity (SF) is 0.6 $SF = SF_p(0) = 0.6$

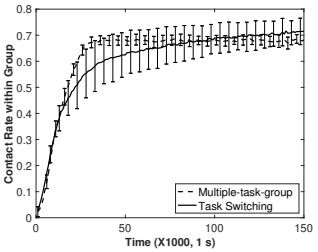

(c) The contact rates within group R_{pp} when the initial spatial fidelity (SF) is 0.8 $SF = SF_p(0) = 0.8$

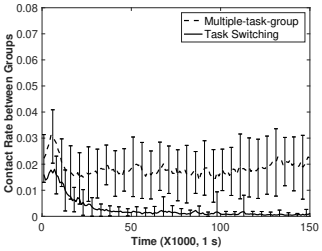

(d) The contact rates between groups R_{pq} when the initial spatial fidelity (SF) is 0.4 $SF = SF_p(0) = 0.4$

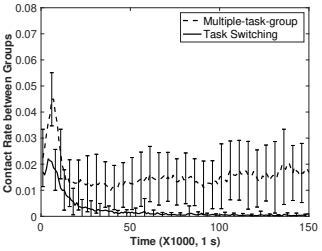

(e) The contact rates between groups R_{pq} when the initial spatial fidelity (SF) is 0.6 $SF = SF_p(0) = 0.6$

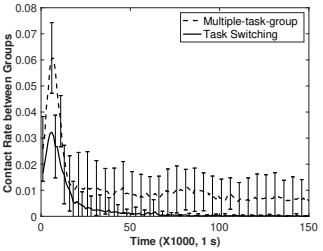

(f) The contact rates between groups R_{pq} when the initial spatial fidelity (SF) is 0.8 $SF = SF_p(0) = 0.8$

Figure 2.12: Task switching leads to dynamic spatial fidelity. Impacts of task switching on contact rates for two task groups with varied initial spatial fidelity (SF) and fixed SF on contact dynamics for two task groups: For the model of multiple task groups, spatial fidelity is constant while task switching changes by time. a) - c) The plateau of the contact within group R_{pp} in the multiple-task-group model (dash curve) is increasing as SF increases, while in the task-switching model, they (solid curves) are similar. d)-f) The plateau of the contact between groups R_{pq} in the multiple-task-group model (dash curve) decreases as SF increases, while in the task-switching model, they (solid curves) are similar; and the peak of R_{pq} is higher as SF increasing in both model. The curves represent the dynamic of the average of 40 replicates.

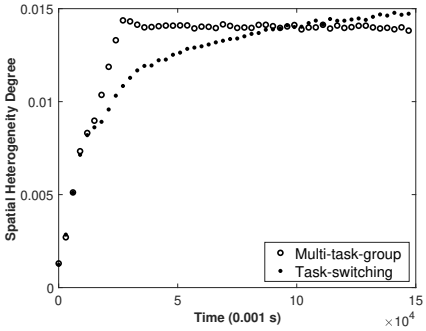

Figure 2.13: Spatial heterogeneity degree in multi-task-group model and task-switching model. Two task groups in $SF_0 = 0.8$.

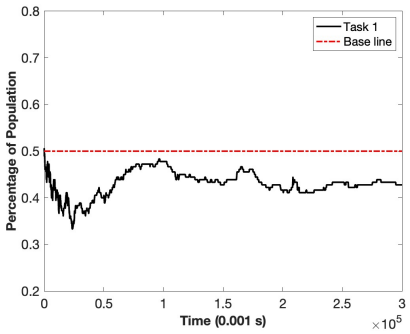

(a) One group always be major task

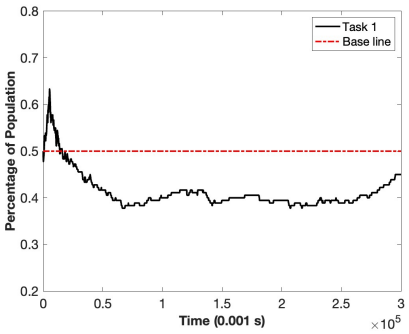

(b) Major task switching

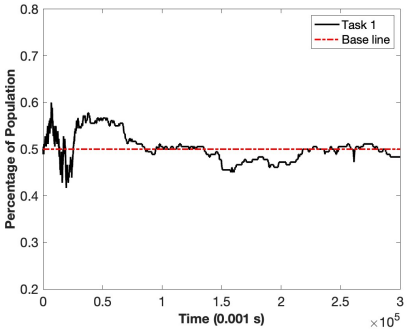

(c) Major task switching frequently

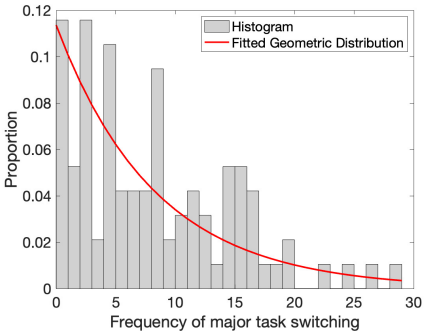

(d) Histogram for frequency major task switching

Figure 2.14: Different dynamics of two task group populations. Figure 2.14a-2.14c: Individual case for population changing in task 1 with initial spatial fidelity (SF) being 0.5 ($SF_p(0) = 0.5$). The baseline (red line) is set at 0.5 because both groups start with the same number of agents, with an associated proportion of task 1 and task 2 groups of 0.5 ($N_1(0) = N_2(0)$). Figure 2.14d: Histogram for frequency of major task switching. There are 11 cases (11.58%) where one task has been the leading task. The total is 95 replications in $SF_0 = 0.5$. The geometrical distribution fitting probability is 0.1136, mean of the distribution is 7.8, and the median is 4.7.

Chapter 3

HOW TO MODEL HONEY BEE POPULATION DYNAMICS: STAGE STRUCTURE AND SEASONALITY

Abstract

Western honey bees (*Apis Mellifera*) serve extremely important roles in our ecosystem and economics as they are responsible for pollinating $ 215 billion dollars annually over the world. Unfortunately, the honey bee population and their colonies have declined dramatically. The purpose of this article is to explore how I should model the honey bee population with age structure and validate the model using empirical data so that I can identify different factors that lead to the survival and health of the honey bee colony. Our theoretical study, combined with simulations and data validation, suggests that the proper age structure incorporated in the model and seasonality are important for modeling the honey bee population. Specifically, our work implies that the model assumes that (1) the adult bees survive from the egg population rather than the brood population; and (2) seasonality in the queen egg laying rate gives a better fit than other honey bee models. The related theoretical and numerical analysis of the fittest model indicates that (a) the survival of honey bee colonies requires a large queen egg-laying rate and smaller values of the other life-history parameter values in addition to proper initial condition; (b) both brood and adult bee populations are increasing with respect to the increase in the egg-laying rate and the decreasing in other parameter values; and (c) seasonality may promote/suppress the survival of the honey bee colony.

3.1 Introduction

Western honey bee (*Apis Mellifera*) is a eusocial insect that has an advanced level of social organization. In the honey bee colony, the queen produces the offspring, and non-reproductive individuals cooperate in caring for the young ones, which forms complex colonies [Winston, 1991]. honey bees play indispensable and important roles in human life, economy, and agriculture. For example, honey bees not only produce valuable products, such as honey, royal jelly, bee wax, and propolis in the market but also are responsible for pollinating crops such as blueberries, cherries, and almonds, which is worth $215 billion annually worldwide [Smith *et al.*, 2013]. If there is no honey bee, it likely leads to changes in human diets and a disproportionate expansion of agricultural land in order to fill this shortfall in crop production by volume [Potts *et al.*, 2016]. Unfortunately, the honey bee population has been decreasing globally [Smith *et al.*, 2013]. In the United States, the total number of honey bee colonies has been reduced by approximately 40% to 50%, while in the rest of the world, the total number of colonies is reduced by 5% to 10% [Paula María Montoya-Pfeiffer and Parra., 2016]. The important and critical causes for honey bee colony mortalities include diseases, land-use change, pesticides, pathogens and parasites, and poor bee-keeping management [Smith *et al.*, 2013; DeGrandi-Hoffman *et al.*, 2013; Perry *et al.*, 2015; Oldroyd, 2007; Degrandi-Hoffman *et al.*, 2019]. The purpose of this article is to explore how I could better model colony population dynamics to help us understand the honey bee colony mortalities.

honey bee colony itself is a complex adaptive system with its own resilience to disturbances, whose survival depends on its individual quality, its adaptive capacity,

and its threshold of resilience to pressures [Fredrick *et al.*, 2017]. On average, a colony has about 10,000 to 60,000 bees, which consists of a queen (fertile female) who produces all offspring, a few hundred drones (males), and thousands of workers (sterile females). Generally, a queen may lay approximately 1000-2000 eggs per day in the peak period [Coffey, 2007]. Due to aging or disability of the queen bee, beekeepers will replace the queen every 1-2 years [Coffey, 2007]. Each honey bee goes through four stages of development: egg, larva, pupa, and adult [Coffey, 2007]. For worker bees, they need 21 days to eclosion to adult bees [Winston, 1991; Harris, 1980; DeGrandi-Hoffman *et al.*, 1989], and drones need 24 days to mature [DeGrandi-Hoffman *et al.*, 1989]. Population size at each stage and the related maturation time have huge influences on the colony development and its population dynamics [Fredrick *et al.*, 2017]. Needless to say, age is linked to the division of labor in honey bees [Robinson *et al.*, 1992]. Young workers In the colony, young workers prefer to perform nursing tasks, while older workers prefer foraging activities. However, colonies can accelerate, delay, or even reverse their recruitment behavior as the internal or external environment changes [Huang and Robinson, 1996].

Not only the age structure will affect the honey bees colony, but the change of season, temperature, Weather, etc., also will influence the honey bees [Johnson, 2002; Coffey, 2007; DeGrandi-Hoffman *et al.*, 1989; SEELEY and Visscher, 1985]. Through experiments and observations, the honey bee population presents periodic fluctuations due to different reasons. For instance, I observe great foraging activity during spring, summer, and fall but the highest activity during the summer [Coffey, 2007]. During spring and summer, pollen and nectar from diverse floras are in great abundance,

giving rise to an increased honey bee population. Therefore, given that temperature is one of the main factors in honey bee food availability and thus brood production, honey bee population size is smaller during the winter [SEELEY and Visscher, 1985; DeGrandi-Hoffman *et al.*, 1989]. Thus, the peak of the population is achieved in late June until the middle of summer as it starts to decline [Research and Extension Consortium, 2004]. The temperature in the colony also will influence honey bees, middle-aged honey bees will respond to the heat stress in order to perform [Johnson, 2002]. Thus, it is very important to include age structure and seasonality in studying of honey bee population dynamics and the factors that affect the health of honey bee colonies. Research has shown that the major problems threatening the survival of honey bee colonies could link to: 1) environmental stressors, such as habitat destruction (urbanization, deforestation, forest fires); 2) parasites and pathogens, such as varroa and viruses; 3) genetic variation and vitality, like limited importation [Perry *et al.*, 2015; Oldroyd, 2007; Smith *et al.*, 2013]. In order to quantify the problems and consider the difficulty of directly observing the dynamics of bee populations, mathematical models can be a powerful tool to help us understand how the bee population changes and predict the fate of the colony.

Mathematical models indeed have been developed to study bee populations dynamics and the related stressors, particularly the effects of pathogens, parasites and nutrient stress factors [Russell *et al.*, 2013; Kribs-Zaleta and Mitchell, 2014; Khoury *et al.*, 2011, 2013; Perry *et al.*, 2015; Betti *et al.*, 2014; Camazine *et al.*, 1990; Kang *et al.*, 2015; Eberl *et al.*, 2010; Aronstein *et al.*, 2012; Smith *et al.*, 2013]. DeGrandi-Hoffman [DeGrandi-Hoffman *et al.*, 1989] proposed a first simulation model for honey

bee colony dynamics that includes many important factors such weather, egg-laying rate, the age of queen, foraging and brood life cycles. There are some previous works focusing on how the death rate of foragers impacts colony viability [Khoury *et al.*, 2011, 2013]. Khoury [Khoury *et al.*, 2011] published a compartmental model based on these circumstances. The model includes three states, brood, hive, and foragers, and incorporates the recruitment process to study the forager death rate. There is a work [Russell *et al.*, 2013] that investigated seasonal food availability and the transition of hives to foragers. The most recent recent works [Messan *et al.*, 2018; Ratti *et al.*, 2015] consider the seasonality in the queen egg-laying rate. Messan et al [Messan *et al.*, 2018] applied seasonality effects to the pollen collection rate that has annual periodicity by the first order harmonic. Ratti et al [Ratti *et al.*, 2015] also agree that seasonality affects the dynamics of honey bees and its parasitic virus. This article [Ratti *et al.*, 2015] incorporated seasonality in varroa treatment control as the treatment is applied with four seasons: spring, summer, fall, and winter [Ratti *et al.*, 2015].

Motivated by the previous work on honey bee population models with age structure [Khoury *et al.*, 2011, 2013; Kang *et al.*, 2015] and seasonality [Russell *et al.*, 2013; Messan *et al.*, 2018; Ratti *et al.*, 2015], I propose and study honey bee population models with different delay terms to include age structure. I use data to validate our models and explore which model would be more appreciated and the importance of incorporating seasonality in the honey bee population model. More specifically, the objective of our paper is to develop a proper honey bee population dynamical model with age structure to understand important factors for colony survival and to explore how seasonality may affect the colony dynamics and its survival.

The remainder of the article is shown as follows: In Section 2, I derive two honey bee colony dynamics models that incorporate varied delay terms. In Section 3, I perform a rigorous mathematical analysis of those two models and compare their dynamics. In Section 4, I validate our two models with real honey bee data. Our study shows the importance of seasonality and suggests that one of those two proposed models would be more appropriate for studying honey bee population dynamics. In Section 5, I conclude our study. In the last section, I provide detailed proof of our theoretical results.

3.2 Model Derivations

In this section, I focus on modeling of honey bee colony dynamics with age structure. For convenience, I divide the population of the honey bee colony into brood and adult bees. Let $B(t)$, $H(t)$ be the population of brood and adult bees in a given hive at time t, respectively. I assume that:

A1: The daily egg-laying rate of honey bee queen is r with the survival rate of $\frac{H^2}{K+H^2+\alpha B}$ where the parameter K is the population of adult bee needed for half of the maximum brood survival rate, and α represents the regulation effects from brood population B. The term $\frac{H^2}{K+H^2+\alpha B}$ reflects (1) the cooperative brood care from adult bees that perform nursing and collecting food for brood; and (2) the queen and workers that regulate the actual egg laying/survival rate based on the current available brood population B, which has been supported by the literature work [Messan *et al.*, 2018; Schmickl and Crailsheim, 2007;

Kang *et al.*, 2016; Eischen *et al.*, 1984].

A2: I assume that both brood and adult bees have constant mortality, d_b and d_h, respectively. The maturation time from brood B to adult bee H is denoted by τ ($\tau = 16$ for queen, $\tau = 21$ for workers, and $\tau = 24$ for drones [Coffey, 2007; Khoury *et al.*, 2013]), thus the maturation rate is termed as follows:

$$\underbrace{e^{-d_b\tau}}_{\text{survival rate of brood during time } \tau} \underbrace{\frac{rH(t-\tau)^2}{K+H(t-\tau)^2+\alpha B(t-\tau)}}_{\text{new brood at } t-\tau}$$

The two assumptions above lead to the following non-linear delayed differential equations of honey bee population dynamics (Model (3.1)):

$$\begin{aligned} \frac{dB}{dt} &= \frac{rH(t)^2}{K+H(t)^2+\alpha B} - d_b B - e^{-d_b\tau}\frac{rH(t-\tau)^2}{K+H(t-\tau)^2+\alpha B(t-\tau)} \\ \frac{dH}{dt} &= e^{-d_b\tau}\frac{rH(t-\tau)^2}{K+H(t-\tau)^2+\alpha B(t-\tau)} - d_h H \end{aligned} \tag{3.1}$$

where I assume that the initial condition for $H(t)$ is a non-negative continuous function when $t \in [-\tau, 0]$ and $B(0) = \int_{-\tau}^{0} \frac{rH^2(s)e^{d_b s}}{K+H^2(s)+\alpha B(s)} ds$. The biological meaning of each parameter of the proposed model (3.1) is listed in Table 3.1. In the case $\alpha = 0$, the model (3.1) reduces to the following Model (3.2)

$$\begin{aligned} \frac{dB}{dt} &= \frac{rH(t)^2}{K+H(t)^2} - d_b B - e^{-d_b\tau}\frac{rH(t-\tau)^2}{K+H(t-\tau)^2} \\ \frac{dH}{dt} &= e^{-d_b\tau}\frac{rH(t-\tau)^2}{K+H(t-\tau)^2} - d_h H(t) \end{aligned} \tag{3.2}$$

Notes: Our proposed model (3.2) (when $\alpha = 0$ in the model (3.1)) is a single specie model with brood B and adult H stage where these two stages seem to be decoupled.

Thus, I could study the dynamics of Model (3.2) by exploring the dynamics of H first, then the dynamics of B is totally determined by H. I will see the analytical results in the next section.

Table 3.1: Biological meanings and references of parameters of models (3.1 & 3.3) with and without seasonality.

Parameter	Description	Estimate/Units	Reference
r	Daily egg-laying rate of Queen	[500 10,000] bees/day	Estimated
α	the regulation effects of brood	[0 20]	Estimated
d_b	Death rate of the brood	[0, 0.3] day^{-1}	Estimated
d_h	Death rate of the adult bees	[0, 0.3] day^{-1}	Estimated
γ	The length of seasonality	[170, 365] days	Estimated
$\sqrt{K}$	Colony size at which brood survival rate is half maximum	for K [50,000, 1,300,000](model 3.3) $[1*(10^7), 1*(10^8)]$(model 3.1) bees/day	Estimated
τ	Time spent in brood	21 days	Khoury 2013
ψ	the time of the maximum laying rate	12 days	Harris 1980

In literature (e.g., see [Tang and Chen, 2002]), researchers have been using the compartmental models through ODEs to model population dynamics with age and/or stage structure. Motivated by this, I have the following delay model.

$$\begin{aligned} \frac{dB}{dt} &= \frac{rH(t)^2}{K+H(t)^2} - d_b B - e^{-d_b\tau} B(t-\tau) \\ \frac{dH}{dt} &= e^{-d_b\tau} B(t-\tau) - d_h H(t) \end{aligned} \tag{3.3}$$

where the term $e^{-d_b\tau}B(t-\tau)$ describes the maturation entry rate coming from the juvenile stage with a survival rate $e^{-d_b\tau}$ during the juvenile period τ.

More specifically, the model (3.3) above assumes that the adult $H(t)$ matures

from the survived brood population at time $t - \tau$. In the following two sessions, I will compare the population dynamics of Model (3.3) and the proposed model (3.1) to address the importance of deriving proper delay population models due to the outcomes of dynamics and model validations.

3.3 Mathematical Analysis

The state space of the proposed model (3.1) is $\mathbb{X} = C([-\tau, 0], \mathbb{R}_+) \times C([-\tau, 0], \mathbb{R}_+)$. I first show that the proposed model (3.1) is positive invariant and bounded in $\mathbb{X}$ as the following theorem:

Theorem 3.3.1. *Assume that the initial condition $H(t)$ is a non-negative continuous function defined in $t \in [-\tau, 0]$ with $B(0) = \int_{-\tau}^{0} \frac{rH^2(s)e^{d_b s}}{K+H^2(s)+\alpha B(s)} ds$, then the proposed model* (3.1) *is positive invariant and bounded in* $\mathbb{X}$.

Notes: The detailed proof of Theorem 3.3.1 is in the last section. Theorem 3.3.1 implies that our proposed model is biologically well-defined. The model (3.1) always has the extinction equilibrium $E_e = (0, 0)$, which would be locally or globally stable as stated in the next theorem:

Theorem 3.3.2. *[Stability of Extinction Equilibrium] The extinction equilibrium E_e of Model* (3.1) *is always locally asymptotically stable. If the inequality $d_h > \frac{re^{-d_b\tau}}{2\sqrt{K}}$ holds, the extinction equilibrium E_e is globally stable.*

Notes: The detailed proof of Theorem 3.3.2 is in the last section. Theorem 3.3.2 indicates that the large maturation time τ or the mortality at different stages d_h, d_b

can lead to the collapsing of the colony.

Now I focus on the condition of the colony's survival. Let (B, H) be an interior equilibrium of Model (3.1). Then it satisfies the following equations:

$$0 = \frac{rH(t)^2}{K + H(t)^2 + \alpha B(t)} - d_b B - e^{-d_b\tau}\frac{rH(t)^2}{K + H(t)^2 + \alpha B(t)} \Rightarrow d_b B = \frac{[1 - e^{-d_b\tau}]rH^2}{K + H^2 + \alpha B} \quad (3.4)$$

$$0 = e^{-d_b\tau}\frac{rH(t)^2}{K + H(t)^2 + \alpha B(t)} - d_h H(t) \Rightarrow d_h H = \frac{e^{-d_b\tau}rH^2}{K + H^2 + \alpha B} \quad (3.5)$$

which gives

$$B = \frac{d_h[e^{d_b\tau} - 1]}{d_b} \quad (3.6)$$

and

$$0 = \frac{e^{-d_b\tau}rHd_b}{d_b(K + H^2) + \alpha d_h(e^{d_b\tau} - 1)H} - d_h. \quad (3.7)$$

Solving the equation (3.7) gives

$$H_1^* = \frac{e^{-d_b\tau}\left(d_b r - \alpha d_h^2 e^{d_b\tau}\left[e^{d_b\tau} - 1\right] - \sqrt{\left(d_b r - \alpha d_h^2 e^{d_b\tau}\left[e^{d_b\tau} - 1\right]\right)^2 - 4d_b^2 d_h^2 K e^{2d_b\tau}}\right)}{2d_b d_h}$$

and

$$H_2^* = \frac{e^{-d_b\tau}\left(d_b r - \alpha d_h^2 e^{d_b\tau}\left[e^{d_b\tau} - 1\right] + \sqrt{\left(d_b r - \alpha d_h^2 e^{d_b\tau}\left[e^{d_b\tau} - 1\right]\right)^2 - 4d_b^2 d_h^2 K e^{2d_b\tau}}\right)}{2d_b d_h}$$

with $H_1^* \leq H_2^*$. Now I have the following proposition:

Proposition 3.3.1. *[Existence of Interior Equilibria] If* $\frac{d_b r - d_h^2 e^{d_b\tau}[e^{d_b\tau}-1]\alpha}{2d_h d_b e^{d_b\tau}\sqrt{K}} > 1$, *then Model* (3.1) *has two interior equilibria* $E_i, i = 1, 2$*:*

$$E_i = (B_i^*, H_i^*) = \left(\frac{d_h[e^{d_b\tau}-1]}{d_b}H_i^*, H_i^*\right)$$

where H_1^* *is an increasing function of* α, K, d_b *and* d_h, *and* H_2^* *is a decreasing function of* α, K, d_b *and* d_h; *whereas,* H_1^* *is a decreasing function of* r, *and* H_2^* *is an increasing function of* r. *In the case that* $\frac{d_b r - d_h^2 e^{d_b\tau}[e^{d_b\tau}-1]\alpha}{2d_h d_b e^{d_b\tau}\sqrt{K}} = 1$, *then Model* (3.1) *has an unique interior equilibrium*

$$E_i = (B^*, H^*) = \left(\frac{d_h[e^{d_b\tau}-1]}{d_b}H^*, H^*\right) \text{ with } H^* = H_1^* = H_2^* = \frac{e^{-d_b\tau}\left(d_b r - \alpha d_h^2 e^{d_b\tau}\left[e^{d_b\tau}-1\right]\right)}{2d_b d_h}.$$

Notes: Proposition 3.3.1 implies that one of the necessary conditions for the honey bee colony survival is $\frac{d_b r - d_h^2 e^{d_b\tau}[e^{d_b\tau}-1]\alpha}{2d_h d_b e^{d_b\tau}\sqrt{K}} > 1$ which requires large values of the queen egg laying rate r, and the smaller values of the maturation time τ and the brood regulation effect α. In addition, Proposition 3.3.1 indicates that at the interior equilibrium, the ratio of brood B to adult population H is determined by their mortality and maturation time through the equation $\frac{d_h\left[e^{d_b\tau}-1\right]}{d_b}$. Based on simulations and analytical results, the interior equilibrium H_2^* is always locally stable if it exists, while H_1^* is locally unstable. If $\frac{d_b r - d_h^2 e^{d_b\tau}[e^{d_b\tau}-1]\alpha}{2d_h d_b e^{d_b\tau}\sqrt{K}} > 1$, then by simple calculations, I have $\frac{dH_1^*}{d\alpha} > 0$ and $\frac{dH_2^*}{d\alpha} < 0$. This implies that the brood regulation coefficient α has negative effects on brood and adult population sizes. In the case that $\alpha = 0$, then if $\frac{d_b r}{2d_h d_b e^{d_b\tau}\sqrt{K}} > 1$ holds, the interior equilibria $H_i^*, i = 1, 2$ have the following expressions:

$$H_1^* = \frac{e^{-d_b\tau}\left(d_b r - \sqrt{(d_b r)^2 - 4d_b^2 d_h^2 K e^{2d_b\tau}}\right)}{2d_b d_h}$$

$$H_2^* = \frac{e^{-d_b\tau}\left(d_b r + \sqrt{(d_b r)^2 - 4d_b^2 d_h^2 K e^{2d_b\tau}}\right)}{2d_b d_h}$$

In order to study the stability of the interior equilibrium $E_i = (B^*, H^*)$, I start with the characteristic equation of the interior equilibrium $E_i = B_i^*, H_i^*$ as follows by letting $A = \frac{Hr}{(\alpha B+H^2+K)^2}$

$$
\begin{aligned}
C(\lambda) &= det\left(\left[\begin{array}{cc} -\frac{\alpha H^2 r}{(\alpha B+H^2+K)^2} - d_b & \frac{2Hr(\alpha B+K)}{(\alpha B+H^2+K)^2} \\ 0 & -d_h \end{array}\right] + \left[\begin{array}{cc} -\frac{\alpha H^2 r e^{-d_b\tau}}{(\alpha B+H^2+K)^2} & -\frac{2Hre^{-d_b\tau}(\alpha B+K)}{(\alpha B+H^2+K)^2} \\ \frac{\alpha H^2 r e^{-d_b\tau}}{(\alpha B+H^2+K)^2} & \frac{2Hre^{-d_b\tau}(\alpha B+K)}{(\alpha B+H^2+K)^2} \end{array}\right] * e^{-\lambda\tau} - \lambda\mathscr{I}\right) \\
&= det\left(\left[\begin{array}{cc} -\alpha AH - d_b & 2A(\alpha B+K) \\ 0 & -d_h \end{array}\right] + \left[\begin{array}{cc} -\alpha AHe^{-d_b\tau} & -2A(\alpha B+K)e^{-d_b\tau} \\ \alpha AHe^{-d_b\tau} & 2A(\alpha B+K)e^{-d_b\tau} \end{array}\right] * e^{-\lambda\tau} - \lambda\mathscr{I}\right) \\
&= det(\left[\begin{array}{cc} -\alpha AH(1+e^{-(\lambda+d_b)\tau}) - d_b - \lambda & 2A(\alpha B+K)(1-e^{-(\lambda+d_b)\tau}) \\ \alpha AHe^{-d_b\tau} & -d_h + 2A(\alpha B+K)e^{-(\lambda+d_b)\tau} - \lambda \end{array}\right] \\
&= (-\alpha AH(1+e^{-(\lambda+d_b)\tau}) - d_b - \lambda)(-d_h + 2A(\alpha B+K)e^{-(\lambda+d_b)\tau} - \lambda) \\
&- 2A(\alpha B+K)(1-e^{-(\lambda+d_b)\tau})\alpha AHe^{-d_b\tau}
\end{aligned}
\tag{3.8}
$$

I can see the characteristic equation (3.8) of the interior equilibrium $E_i = (B_i^*, H_I^*)$ is very complicated and difficult to analyze. Thus, for convenience, I start with the simpler case by setting $\alpha = 0$, which is our model (3.2).

Theorem 3.3.3. *[Stability of Interior Equilibria] If* $\frac{r}{2d_h e^{d_b\tau}\sqrt{K}} > 1$, *then Model* (3.2) *has two interior equilibria* E_i *where* E_1 *is always unstable and* E_2 *is always locally asymptotically stable.*

Notes: Theorem 3.3.3 indicates that the value of the maturation time τ has no effects on the stability of its interior equilibria $E_i, i = 1, 2$ for Model (3.2). In the case that $\frac{r}{2d_h e^{d_b\tau}\sqrt{K}} = 1$, i.e., $d_h = \frac{re^{-d_b\tau}}{2\sqrt{K}}$, then Model (3.2) has an unique interior $E = (B^*, H^*) = \left(\frac{r\left[1-e^{-d_b\tau}\right]}{2d_b}, \sqrt{K}\right)$. The following theorem provides results on the interior equilibrium stability of this critical case:

Theorem 3.3.4. *[Unique Interior Equilibrium] If* $d_h = \frac{re^{-d_b\tau}}{2\sqrt{K}}$, *Model* (3.2) *has a unique interior equilibrium* $E = (B^*, H^*) = \left(\frac{r\left(1-e^{-d_b\tau}\right)}{2d_b}, \sqrt{K}\right)$ *which is always locally asymptotically stable for any delay* $\tau > 0$.

Notes: The detailed proof of Theorem 3.3.4 uses normal form theory in [Faria and Magalhaes, 1995], and is provided in the last section. Both Theorem 3.3.3 and Theorem 3.3.4 implies that when $\alpha = 0$, i.e., Model (3.2), the colony can survive at $E_2 = (B_2^*, H_2^*)$ if $\frac{r}{2d_h e^{d_b\tau}\sqrt{K}} \geq 1$ and initial conditions are in a proper range.

What if $\alpha > 0$? Our simulations suggest that E_1 is still unstable and E_2 is locally stable. Based on our analytical results and simulations, I summarize the general dynamics of Model (3.1) as follows:

1. The extinction equilibrium E_e of Model (3.2) always exists and is always locally asymptotically stable.

2. If $\frac{r}{d_h} < 2e^{d_b\tau}\sqrt{K}$, Model (3.1) has its global stability at the extinction equilibrium E_e.

3. If $\frac{d_b r - d_h^2 e^{d_b\tau}[e^{d_b\tau}-1]\alpha}{2d_h d_b e^{d_b\tau}\sqrt{K}} \geq 1$, Model (3.1) has two locally asymptotically stable equilibria: the extinction equilibrium E_e and the interior equilibrium $E_2 = (B_2^*, H_2^*)$.

Figure 3.1 shows bifurcation diagrams of Model (3.1) regarding (a) the queen egg-laying rate (r) (see Figure 3.1a&3.1b); (b) the brood regulation effects on reproduction α (see Figure 3.1c&3.1d); (c) the half-saturation coefficient K (see Figure

3.1e&3.1d) (d) the mortality of brood d_b (see Figure 3.1g&3.1h); and (e) the mortality of adult d_h (see Figure 3.1i&3.1j). Those bifurcation diagrams indicate that (1) the colony survival requires the large value of the queen egg-laying rate (r), which leads to the increased brood and adult population as it increases; (2) the large values of α, the half-saturation coefficient K, or any mortality rate d_b or d_h can lead to the colony collapsing, and both brood and adult population are decreasing with respect to these parameter values; and (3) increasing the value of the adult population mortality can lead to the dramatic decreasing of the adult population.

The another modeling approach with age structure for the honey bee colony: In our model derivation section, I proposed the model (3.3) below, assuming that the adult $H(t)$ matures from the survived brood population at time $t-\tau$.

$$\begin{aligned} \frac{dB}{dt} &= \frac{rH(t)^2}{K+H(t)^2} - d_b B - e^{-d_b\tau} B(t-\tau) \\ \frac{dH}{dt} &= e^{-d_b\tau} B(t-\tau) - d_h H(t) \end{aligned}$$

The model above is motivated by the compartmental ODE model in the literature [Tang and Chen, 2002]. I aim to compare the dynamics of Model (3.3) to the model (3.1) to address the importance of deriving a proper biological model with age structure.

First, I notice that the extinction equilibrium $E_e = (0,0)$ always exists as for the model (3.1). However, E_e can go through stability switching that leads to an oscillatory solution around E_e for Model (3.3)

Theorem 3.3.5. *[Extinction equilibria dynamics] Model* (3.3) *always has the extinction equilibrium* $E_e = (0,0)$.

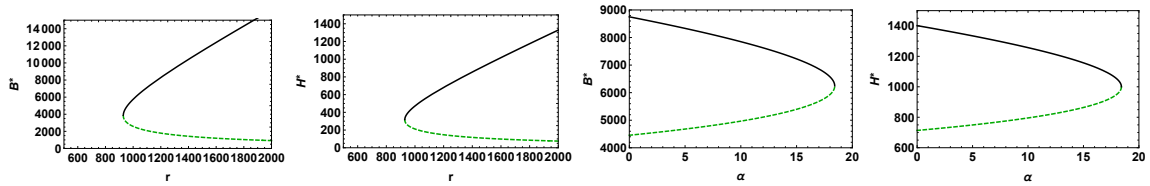

(a) Brood population and the queen egg-laying rate r (b) Adult population and the queen egg-laying rate r (c) Brood population and the brood regulation effect α (d) Adult population and the brood regulation effect α

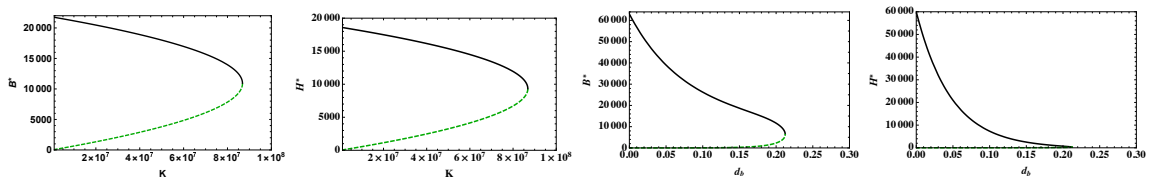

(e) Brood population and the square of half max of colony size K (f) Adult population and the square of half max of colony size K (g) Brood population and the death rate of the brood d_b (h) Adult population and the death rate of the brood d_b

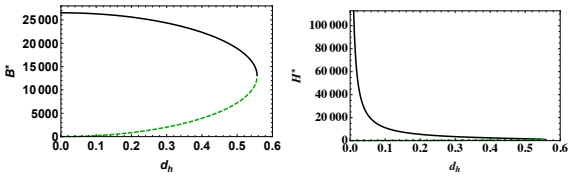

(i) Brood population and the death rate of the adult d_h (j) Adult population and the death rate of the adult d_h when .

Figure 3.1: Bifurcation diagrams of Model (3.1) with the interior equilibrium $E_1 = (B_1^*, H_1^*)$ in black and $E_2 = (B_2^*, H_2^*)$ in green where the solid curve indicates stable, and the dashed curve indicates saddle. All figures have $r = 1400, \alpha = 3, \tau = 21$. Figure 3.1a&3.1b: $K = 10^5, d_b = 0.1, d_h = 0.17$. Figure 3.1c&3.1d: $K = 10^6, d_b = 0.09, d_h = 0.1$. Figure 3.1e&3.1f: $d_b = 0.03, d_h = 0.04$,. Figure 3.1g&3.1h: $K = 10^5, d_h = 0.05$. Figure 3.1i&3.1j: $K = 1 * 10^4, d_b = 0.01$.

1. *If* $d_b \geq \frac{\sqrt{2}}{2}$, *then* $E_e = (0, 0)$ *is asymptotically stable for all* $\tau \geq 0$.

2. *If* $0 < d_b < \frac{\sqrt{2}}{2}$, *then* $E_e = (0, 0)$ *is asymptotically stable for* $\tau \in (0, \tau_0)$ *or* $\tau \geq \tau_1$,

while unstable for $\tau \in (\tau_0, \tau_1)$*, where* $\tau_k = \frac{\theta + k\pi}{w}, k = 0, 1$*,* $\theta = \pi - \arctan\left(\frac{w}{d_b}\right)$ *and* $w = (e^{-2d_b\tau} - d_b^2)^{\frac{1}{2}}$*.*

Notes: Theorem 3.3.5 suggests that the smaller value of the brood mortality can destabilize the colony dynamics. In addition, it implies that Model (3.3) is not positive invariant as the extinction equilibrium $E_e = (0, 0)$ could have stability switches that lead to an oscillatory solution around E_e. See Figure 3.2 when Model (3.3) exists a limit cycle of population around $E_e = (0, 0)$.

Figure 3.2: Phase plane of honey bee brood and adult population of with $r = 1000, K = 1 * 10^6, d_b = 0.1, d_h = 0.17, \tau = 18$ when Model (3.3) has an unstable E_e (the black dot).

Let (B, H) be an interior equilibrium of Model (3.3), then it satisfies that the following two equations:

$$\begin{aligned} 0 &= \frac{rH^2}{K + H^2} - d_b B - e^{-d_b\tau} B \\ 0 &= e^{-d_b\tau} B - d_h H \end{aligned}$$

which gives the brood population at the equilibrium $B^* = d_h e^{d_b \tau} H^*$ and by solving $\frac{rH}{K+H^2} - d_b d_h e^{d_b \tau} - d_h = 0$ I could solve

$$H_i^* = \frac{r \pm \sqrt{r^2 - 4K\left(d_b d_h e^{d_b \tau} + d_h\right)^2}}{2\left(d_b d_h e^{d_b \tau} + d_h\right)}, \; i = 1, 2.$$

Now define the characteristic equation of the interior equilibrium (B^*, H^*) of Model (3.3) as follows:

$$C(\lambda, \tau) = (-d_h - \lambda)(-d_b - e^{-d_b \tau} e^{\lambda \tau} - \lambda) - \frac{2rKH^*}{(K + (H^*)^2)^2} e^{-(d_b + \lambda)\tau} \tag{3.9}$$

$$= \lambda^2 + (d_b + d_h)\lambda + (\lambda + d_h - \frac{2rKH^*}{(K + (H^*)^2)^2}) e^{-(\lambda + d_b)\tau} + d_h d_b = 0 \tag{3.10}$$

Theorem 3.3.6. *[Interior Equilibrium Dynamics] Let* $r > 2d_h\sqrt{K}(1 + d_b)$ *and* $\tau^* = \frac{1}{d_b} \ln\left(\frac{1}{d_b}\left(\frac{r}{2d_h\sqrt{K}} - 1\right)\right)$. *If* $\tau \in [0, \tau^*)$, *Model (3.3) has two positive interior equilibrium*

$$E_i = (B_i^*, H_i^*) = (d_h e^{d_b \tau} H_i^*, H_i^*), i = 1, 2$$

which $H_1^* < H_2^*$. *And* $E_1 = (B_1^*, H_1^*)$ *is always unstable in* $[0, \tau^*)$, $E_2 = (B_2^*, H_2^*)$ *is always stable or occurs stability switching by following cases:*

Case 1. *If* $d_b \geq 1$ *or* $0 < d_b < 1$, $d_b^2 + d_h^2 \geq 1$ *and* $2d_h\sqrt{K}(1 + d_b) < r \leq \frac{2d_h\sqrt{K}(1+d_b)^2}{\sqrt{(1+d_b)^2 - 4d_b^2}}$, E_2 *is locally asymptotically stable for all* $\tau \in [0, \tau^*)$.

Case 2. *If* $0 < d_b < 1$, $d_b^2 + d_h^2 \geq 1$ *and* $r > \frac{2d_h\sqrt{K}(1+d_b)^2}{\sqrt{(1+d_b)^2 - 4d_b^2}}$, *then the stability of* E_2 *switches just once from stable to unstable as* τ *increases in* $[0, \tau^*)$.

Case 3. *If* $d_b^2 + d_h^2 < 1$ *and* $2d_h\sqrt{K}(1 + d_b) < r \leq \frac{2d_h\sqrt{K}(1+d_b)^2}{\sqrt{(1+d_b)^2 - 4d_b^2}}$, *the stability of* E_2 *can change a finite number of times at most as* τ *is increased* $\tau \in [0, \tau^*)$, *and eventually it becomes unstable.*

Case 4. *If* $d_b^2 + d_h^2 < 1$ *and* $r > \frac{2d_h\sqrt{K}(1+d_b)^2}{\sqrt{(1+d_b)^2-4d_b^2}}$, *the stability of* E_2 *switches at least once in* $[0, \tau^*)$ *from stable to unstable.*

Notes: Theorem 3.3.6 indicates that: (1) The large value of mortality in brood and/or adult bees with the intermediate value of the egg laying rate r can have the simple equilibrium dynamics; and (2) The relatively small values of mortality in brood and/or adult bees with the large value of the egg laying rate r can destabilize the colony dynamics that lead to stability switching in the interior equilibrium E_2. For example, Figure 3.3 provides an example of when Model (3.3) can have stability switches at its interior attractor E_2 as τ changes: Model (3.3) has local stability when $\tau = 21$ while it has an oscillatory solution when $\tau = 16$. Figure 3.4 also indicates the importance of the initial conditions that may lead to the survival or collapse of the colony.

Comparisons between Model (3.1) **and Model** (3.3)**:** Both models can have up to three equilibria with always the existence of the extinction equilibrium E_e. However, the maturation time τ has no effects on the stability of the equilibrium of Model (3.1) while it could lead to stability switches for Model (3.3). The consequence is that Model (3.3) is not positive invariant and could have an oscillatory solution around the extinction equilibrium E_e and the interior equilibrium E_2.

To continue exploring how I should model population dynamics of honey bees with the proper age structure so that I could have a better understanding of important factors contributing to colony survival, I perform bifurcation diagrams on both Model (3.1) and Model (3.3). Figure 3.1 shows bifurcation diagrams of Model (3.1)

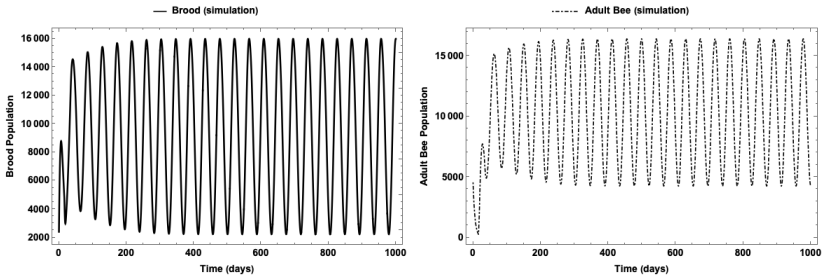

(a) Brood population in $\tau = 16$ (b) Adult population in $\tau = 16$

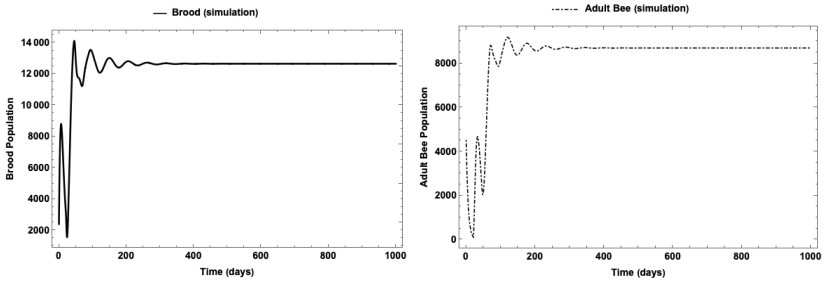

(c) Brood population in $\tau = 21$ (d) Adult population in $\tau = 21$

Figure 3.3: Time series of the brood (solid) and adult (dot-dashed) bee when $r = 3000; d_h = 0.178; d_b = 0.1; K = 5,000,000;\ B(\theta) = 2400; H(\theta) = 4500, \theta \in [-\tau, 0]$.

regarding (a) the queen egg-laying rate (r) (see Figure 3.1a & 3.1b); (b) the brood regulation effects on reproduction α (see Figure 3.1c & 3.1d); (c) the half-saturation coefficient K (see Figure 3.1e & 3.1f) (d) the mortality of brood d_b (see Figure 3.1g & 3.1h); and (e) the mortality of adult d_h (see Figure 3.1i & 3.1j).

Figure 3.5 shows bifurcation diagrams of Model (3.3) regarding (a) the queen egg-laying rate (r) (see Figure 3.5a & 3.5d); (b) the half-saturation coefficient K (see Figure 3.5e & 3.5h) (c) the mortality of brood d_b (see Figure 3.5i & 3.5j); and (d) the mortality of adult d_h (see Figure 3.5k & 3.5l). The biggest differences of those bifurcation diagrams between Model (3.1) and Model (3.3) are: (1) The survival equilibrium (E_2) can become destabilized if I decrease the value of the brood mortality d_b

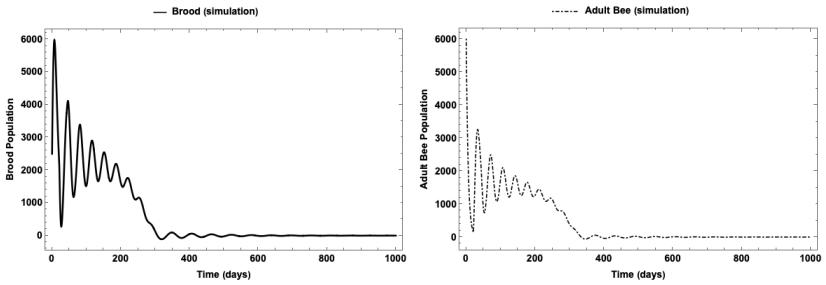

(a) Brood population for $B(0) = 2500; H(0) = 6000$

(b) Adult population for $B(0) = 2500; H(0) = 6000$

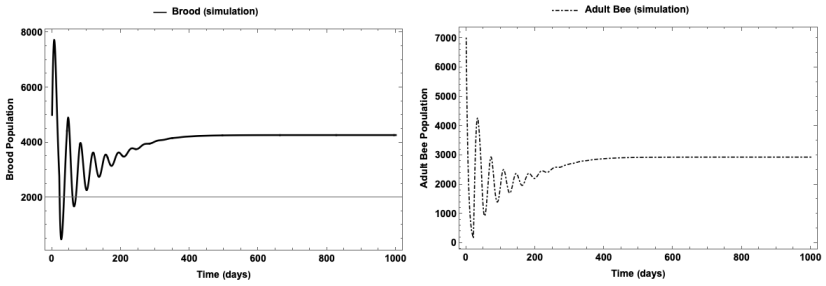

(c) Brood population for $B(0) = 5000; H(0) = 7,000$

(d) Adult population for $B(0) = 5000; H(0) = 7,000$

Figure 3.4: Time series of the brood (solid) and adult (dot-dashed) bee using $r = 1500; d_h = 0.178; d_b = 0.1; K = 5,000,000; \tau = 21.$; $B(\theta) = B(0)$ and $H(\theta) = H(0)$, $\theta \in [-\tau, 0]$.

and/or increase the adult mortality; (2) the brood population may have its maximum point when the mortality of the brood d_b is in a proper range: In Figure 3.5i, it shows that the interesting pattern on how the brood population changes with its mortality rate; and (3) Model (3.1) has only equilibrium dynamics either at the extinction E_e or the interior equilibrium E_2. honey bee population data shown in Figure 3.6 seems to exhibit seasonality. By comparing the dynamics of Model (3.1) with Model (3.3), I know that only Model (3.3) has oscillatory solutions. Does it mean that Model (3.3) is better than Model (3.1) as it has oscillatory solutions?

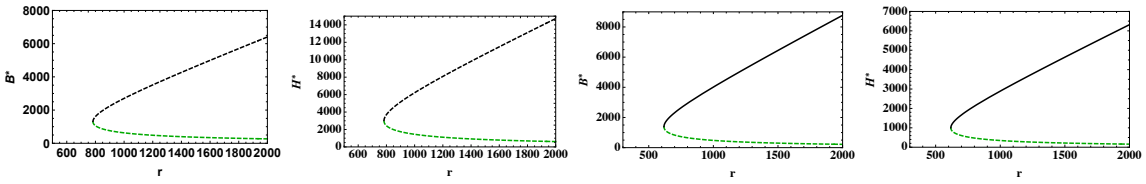

(a) Brood population and the egg-laying rate r (b) Adult population and the egg-laying rate r (c) Brood population and the egg-laying rate r (d) Adult population and the egg-laying rate r

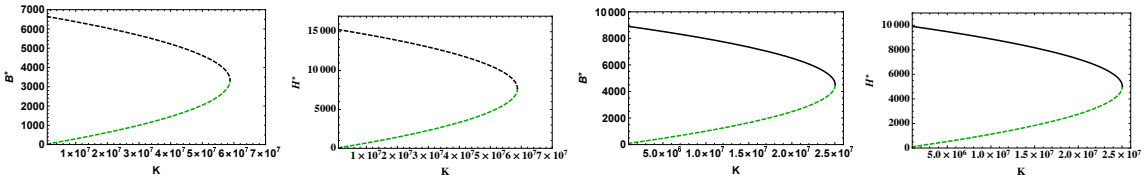

(e) Brood population and the square of half max of colony size K (f) Adult population and the square of half max of colony size K (g) Brood population and the square of half max of colony size K (h) Adult population and the square of half max of colony size K

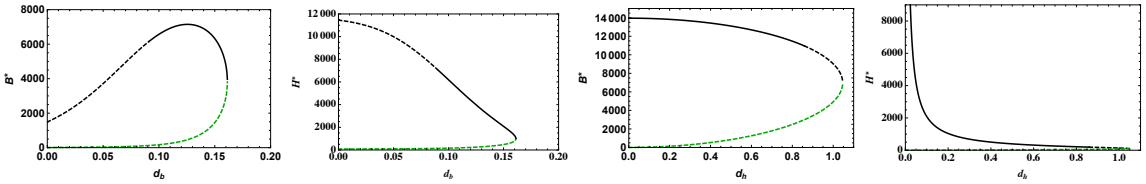

(i) Brood population and the death rate of the brood d_b (j) Adult population and the death rate of the brood d_b (k) Brood population and the death rate of the adult d_h (l) Adult population and the death rate of the adult d_h

Figure 3.5: Bifurcation diagrams of interior equilibrium $E_1 = (B_1^*, H_1^*)$ (black) and $E_2 = (B_2^*, H_2^*)$ (green) for Model (3.3): solid curve indicates stable, and dash curve indicates unstable. All figures have $\tau = 21$. Figure 3.5a & 3.5b: $K = 9 * 10^6, d_b = 0.07, d_h = 0.1$. Figure 3.5c & 3.5d: $K = 10^6, d_b = 0.1, d_h = 0.17$. Figure 3.5e & 3.5f: $r = 2000, d_b = 0.07, d_h = 0.1$. Figure 3.5g & 3.5h: $r = 2000, d_b = 0.1, d_h = 0.11$. Figure 3.5i & 3.5j: $K = 10^6, r = 1500, d_h = 0.13$. Figure 3.5k & 3.5l: $K = 10^4, r = 3000, d_b = 0.2$.

3.4 Data and Seasonality

In this section, I use the honey bee population data collected by James Harris (1980) [Harris, 1980] to do parameter estimations and model validations. The honey

bee population data of two colonies: May 5, 1975 to Oct 22, 1975 and May 3, 1976 to Dec 5, 1976, is shown in Figure 3.6 in the left (1975) and right (1976) side, respectively: The brood B (the sum of egg, larvae, and pupa) population is shown by triangle dots while the adult H population is represented by point dots. Based on Figure 3.6, the initial population of brood is $B_0 = 6125$ and adult $H_0 = 5362$ for 1975 while $B_0 = 5982$ and $H_0 = 5362$ for 1976. Figure 3.6 shows seasonality. The mathematical analysis provided in our previous section indicates that Model (3.3) can have oscillatory solutions under certain conditions while Model (3.1) only exhibits simple equilibrium dynamics.

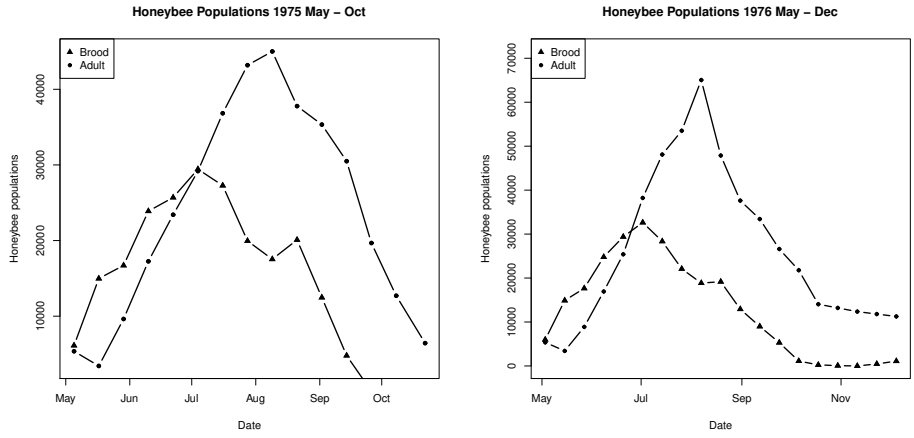

(a) honey bee population in 1975 (b) honey bee population in 1976

Figure 3.6: The observed population data for honey bee colonies in 1975 (left) and 1976 (right), respectively. The triangle line corresponds to the brood population (eggs, larvae, and pupa), while the circle line corresponds to adults.

The questions are: (1) Is Model (3.3) better than Model (3.1) because it shows oscillatory solutions? Or (2) Is seasonality shown in honey bee population data (see Figure 3.6) caused by external factors such as resources?

To address the questions above, I first assume that the queen-laying eggs are seasonal due to resource constraints. The literature work suggests that food, temperature, weather, and oviposition place would affect the queen [Bodenheimer, 1937; Khoury *et al.*, 2011; DeGrandi-Hoffman *et al.*, 1989], thence her egg-laying rate is not constant, and assumed to have the following expression:

$$r(t) = r_0 * (1 + \cos(\frac{2\pi(t-\psi)}{\gamma})); \tag{3.11}$$

$$r(t-\tau) = r_0 * (1 + \cos(\frac{2\pi(t-\tau-\psi)}{\gamma})). \tag{3.12}$$

where γ indicates the length of seasonality; τ indicates the time length of the juvenile period; ψ indicates the time of the maximum laying rate; and r_0 indicates the baseline egg-laying rate. The literature work suggests that climate/temperature may affect winter mortality indirectly, but the location, elevations, and humidity are more likely directly affecting factors, especially the link between temperature and mortality is not particularly prominent [Switanek *et al.*, 2017]. Therefore, our model only considers the egg-laying rate to be seasonal as it has more direct impacts from external internal factors such as temperature/resource, and it is reasonable to set the mortality rates of brood and adults constant. However, it would be interesting to explore how the seasonal mortality of brood and adults affects dynamics in future work.

Then I perform parameter estimations and model validations based on data shown in Figure 3.6: I implement the Monte Carlo parameter sweep method as our fitting method to the honey bee population data to attain parameter estimates [Cowan, 1998]. Essentially, I randomly sample hypotheses for the parameters following negative binomial regression with appropriate ranges (see Table.3.1). For each observed

value, I defined the negative binomial probability density function. The mean (μ) is set by the corresponding predictive value, and the variance is $\mu + \alpha * \mu^2$, which is $\alpha = k^{-1}$. k indicates dispersion parameter, which I set range [0.5,2] [Piegorsch, 1990; Lloyd-Smith, 2007]. Then I calculate the likelihood for a negative binomial regression model to get a better estimate for parameters [Lawless, 1987; Ismail and Jemain, 2007]. Afterward, I performed data fitting on the above model (model number) and compared the results.

I first assume that the egg-laying rate r is constant. All fittings are set by constant history functions with $B(\theta) = 6125$ and $H(\theta) = 5362$ for 1975, and $B(\theta) = 5982$ and $H(\theta) = 5362$ for 1976, for all $\theta \in [-\tau, 0]$.

1. Fitting Model (3.1): the best fit is shown in Figure (3.7a & 3.7b). If I use the estimated parameters: $r = 1237; d_h = 0.033; d_b = 0.001; K = 20,574,000; \alpha = 16.9$, then $E_2 = (25299, 36124.5)$ in 1975; and $r = 1149; d_h = 0.03; d_b = 0.001; K = 10,653,000; \alpha = 4$, then $E_2 = (23693.5, 37215.3)$ in 1976. Model (3.1) approaches to its plateau under those two fittings.

2. Fitting Model (3.2): the best fit is shown in Figure (3.7c & 3.7d). If I use the estimated parameters: $r = 1573; d_h = 0.04; d_b = 0.0001; K = 15,716,000$, then $E_2 = (32658.1, 38837.8)$ in 1975; and $r = 1065; d_h = 0.03; d_b = 0.0001; K = 19,600,000$, then $E_2 = (21987, 34863.3)$ in 1976. Model (3.2) approaches to its plateau under those two fittings.

3. Fitting Model (3.3): the best fit is shown in Figure (3.7e & 3.7f). If I use the estimated parameters: $r = 5333; d_h = 0.12; d_b = 0.11; K = 867,000$, then $E_2 =$

$(25435.1, 21039.3)$ in 1975; and $r = 5333; d_h = 0.12; d_b = 0.11; K = 1,088,000$, then $E_2 = (25422.3, 21028.8)$ in 1976. Model (3.3) approaches to its steady state through damping oscillations.

The fittings shown in Figure 3.7 suggest that the assumption of the queen egg laying being constant is not realistic enough. Thus I assume that the egg-laying rate is a periodic function $r(t) = r_0 * (1 + \cos(\frac{2\pi(t-\psi)}{\gamma}))$. All fittings are set by constant history functions, i.e., $B(\theta) = 6125$ and $H(\theta) = 5362$ for 1975, and $B(\theta) = 5982$ and $H(\theta) = 5362$ for 1976, for all $\theta \in [-\tau, 0]$

1. Fitting Model (3.1): the best fit is shown in Figure (3.8a & 3.8b). If I use the estimated parameters: $r_0 = 1193; d_h = 0.03; d_b = 0.02; K = 56,963,000; \alpha = 4; \gamma = 273; \psi = 12$ in 1975; and $r_0 = 1319; d_h = 0.023; d_b = 0.02; K = 84,933,000; \alpha = 3.2; \gamma = 338; \psi = 12$ in 1976. Both data fittings of Model (3.1) have periodic solutions.

2. Fitting Model (3.2): the best fit is shown in Figure (3.8c & 3.8d). If I use the estimated parameters: $r_0 = 1644; d_h = 0.03; d_b = 0.02; K = 139,137,000; \gamma = 277; \psi = 12$ in 1975; and $r_0 = 1477; d_h = 0.04; d_b = 0.02; K = 81,048,000; \gamma = 261; \psi = 12$ in 1976. Both data fittings of Model (3.2) have periodic solutions.

3. Fitting Model (3.3): the best fit is shown in Figure (3.8e & 3.8f). If I use the estimated parameters: $r_0 = 5333; d_h = 0.12; d_b = 0.11; K = 867,000; \gamma = 350; \psi = 12$ in 1975; and $r_0 = 9171; d_h = 0.19; d_b = 0.12; K = 20,000; \gamma = 261; \psi = 12$ in 1976. Both data fittings of Model (3.3) have periodic solutions that would lead to negative solutions as Model (3.3) is not positively invariant.

The data fittings assuming that $r(t) = r_0 * (1 + \cos(\frac{2\pi(t-\psi)}{\gamma}))$ have better outcomes than the previous ones (Figure 3.7) by assuming r being constant. By comparison through the negative log-likelihood method [Ismail and Jemain, 2007], I could deduce that Model (3.1) has the best fittings in both scenarios: r being constant in Figure (3.7) and r being periodic in Figure 3.8. Thus, based on both theoretical work and model validation, I could conclude that even though Model (3.3) could have oscillations in its solution, Model (3.1) with the egg laying rate r being periodic (supported by the best fitting based on data, see Figure 3.8) should be a better model for us to explore the important factors contributing to the healthy of honey bee colonies.

Effects of seasonality: Here I perform two scenarios that seasonality may promote (see Figure 3.9) or suppress (see Figure 3.10) the survival of honey bee colony, respectively. Figure 3.9a & 3.9b are simulations without seasonality by taking $r = 1200, K = 5.4 * 10^6, d_b = 0.01, d_h = 0.05, \alpha = 10$ with a constant history function $B(\theta) = 300; H(\theta) = 200$ for all $\theta \in [-\tau, 0]$, which show that honey bee colony collapses. Figure 3.9c & 3.9d has seasonality by taking $r = r_0 * (1 + \cos(\frac{2\pi(t-45)}{365}))$ whose average is $r_0 = 1200$, which show that honey bee colony survives.

On the other hand, Figure 3.10 shows that seasonability can make honey bee colony collapse. Figures 3.10a & 3.10b has no seasonality by taking $r = 1200, K = 1 * 10^6, d_b = 0.06, d_h = 0.11, \alpha = 10$ with a constant history function $B(\theta) = 6125; H(\theta) = 5362$ for all $\theta \in [-\tau, 0]$, which shows that honey bee colony could survive. While Figure 3.10c & 3.10d has seasonality by taking $r = r_0 * (1 + \cos(\frac{2\pi(t-45)}{365}))$ with $r_0 = 1200$. In this case, I can see that seasonality may suppress the survival of

the honey bee colony.

3.5 Conclusions

honey bees have dramatically decreased population over the long-term and each year [Smith *et al.*, 2013]. As a result, great economic losses and the increase in the price of bee products have adversely affected the market [Smith *et al.*, 2013; USDA, 2017]. The causes of the decline in the number of honey bees have been of great interest, whether they may directly link to human, environmental, or disease [Perry *et al.*, 2015; Oldroyd, 2007; Smith *et al.*, 2013]. Some previous work always focuses on foragers or recruitment, while other works investigated external causes [Khoury *et al.*, 2011, 2013; Russell *et al.*, 2013; Perry *et al.*, 2015; Kang *et al.*, 2015; Aronstein *et al.*, 2012]. In this study, I focus on modeling proper honey bee population age structure model with model validation using empirical data to obtain better biological understanding of the critical factors that could maintain healthy of honey bee colonies.

I propose two different models with age structure to explore the importance of proper modeling. The first model (3.1) has an assumption that the adult bees survive from eggs, while the second model (3.3) assumes that adult bees survive from the brood stage rather than the egg stage. Our theoretical work (see Theorem 3.3.2, 3.3.3, 3.3.5 & 3.3.6) implies that Model (3.1) and Model (3.3) have huge differences in their dynamics. Specifically, Model (3.1) has only equilibrium dynamics and the maturation time doesn't affect its dynamics (see Theorem 3.3.3) while Model (3.3) can be destabilized by the maturation time along with its life history parameter values

(see Theorem 3.3.6) and Model (3.3) is not positively invariant. Also, our bifurcation diagrams (see Figure 3.1 & 3.5) confirmed such different dynamical outcomes. Both theoretical and bifurcation results indicate that the different assumptions can lead to different age structure models with dramatic dynamical outcomes. So which model would be more appealing and biologically relevant? Can I say the second model (3.3) is better as it has oscillatory dynamics that could be supported by seasonality observed in data?

Given that the queen reproduction depends on seasonality [Research and Extension Consortium, 2004; Bodenheimer, 1937; Khoury *et al.*, 2011], this suggests that it is paramount to include seasonality when modeling honey bee population dynamics. To address whether the seasonal pattern observed from data is due to the internal factor such as the maturation time and/or other life history parameters (for example, Model (3.3) could be a better model for generating seasonal patterns from the internal factors) or the external factor such as the queen egg laying rate that is regulated by the temperature and the resource [DeGrandi-Hoffman *et al.*, 1989; Bodenheimer, 1937; Coffey, 2007]. I use data to validate Model (3.1) and Model (3.3) by assuming that the queen egg laying rate is constant and seasonal. Our validations on models without seasonality did not have a good fit by compared to the corresponding models with seasonality. Among all models with seasonality, Model (3.1) has the best fit (see Figure 3.8). Our model validations with data suggest that the seasonal pattern observed from data is very likely due to the external factors, such as the temperature or available resources that may generate periodic dynamics in the queen egg laying rate, while the internal factors, such as the maturation time doesn't seem to be responsible

seasonal pattern observed from data.

Both theoretical and numerical results, including model validations, suggest that Model (3.1) with seasonality in the queen egg laying rate seems to be the fittest model for studying honey bee population dynamics with age structure. Theoretical results (Theorem 3.3.3) and bifurcation diagrams (Figure 3.1) imply that (1) the survival of honey bee colonies requires a large value of the queen egg-laying rate (r) and smaller values of the other life-history parameter values in addition to the proper initial condition; (2) both brood and adult bee population is increasing with respect to the egg-laying rate r and is decreasing with respect to the regulation effects of brood α, the square of half maximum of colony size at which brood survival rate K, and the mortality rates d_b, d_h; and (3) seasonality may promote the survival of the honey bee colony (see Figure 3.9) but also may lead to the colony collapsing (see Figure 3.10c&3.10d). In summary, our work suggests that Model (3.1) with seasonality could be used for our future model that includes more external factors, such as diseases, parasites, food, and human activities [Perry *et al.*, 2015; Oldroyd, 2007; Smith *et al.*, 2013; Khoury *et al.*, 2013]. Our ongoing work has extended the current model (3.1) to include parasites.

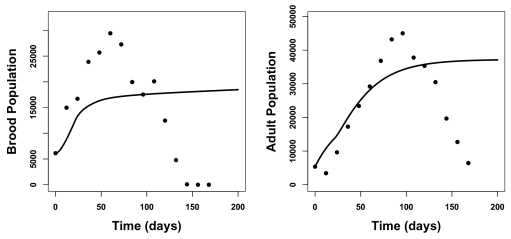

(a) Model (3.1) (1975), $r = 1237; d_h = 0.033; d_b = 0.001; K = 20,574,000; \alpha = 16.9$.

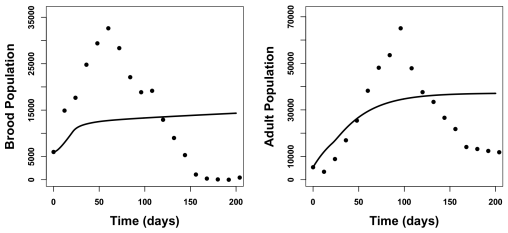

(b) Model (3.1) (1976), $r = 1149; d_h = 0.03; d_b = 0.001; K = 10,653,000; \alpha = 4$.

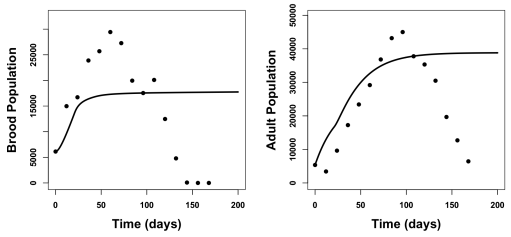

(c) Model (3.2) (1975), $r = 1573; d_h = 0.04; d_b = 0.0001; K = 15,716,000$.

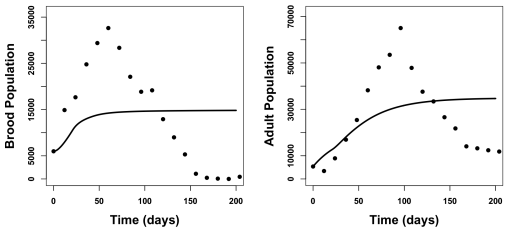

(d) Model (3.2) (1976), $r = 1065; d_h = 0.03; d_b = 0.0001; K = 19,600,000$.

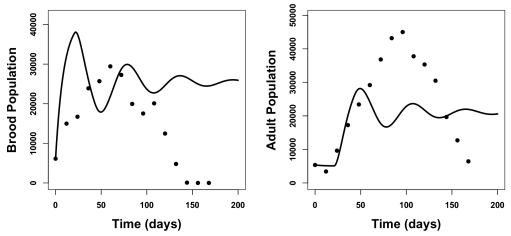

(e) Model (3.3) (1975), $r = 5333; d_h = 0.12; d_b = 0.11; K = 867,000$.

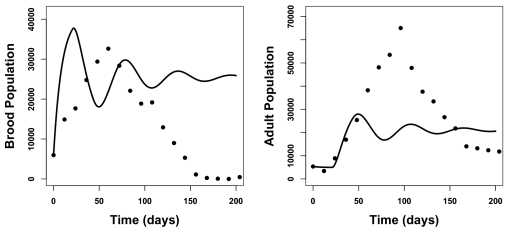

(f) Model (3.3) (1976), $r = 5333; d_h = 0.12; d_b = 0.11; K = 1,088,000$.

Figure 3.7: Data fitting without seasonality for Harris honey bees data in 1975 (a, c, e) and 1976 (b, d, f) with $\tau = 21$. Black dots indicate Harris data, and the black curve indicates our model.

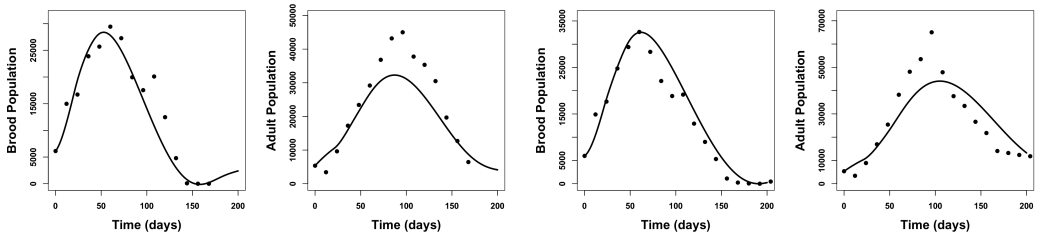

(a) Model (3.1) (1975), $r_0 = 1193; d_h = 0.03; d_b = 0.02; K = 56,963,000; \alpha = 4; \gamma = 273; \psi = 12.$

(b) Model (3.1) (1976), $r_0 = 1319; d_h = 0.023; d_b = 0.02; K = 84,933,000; \alpha = 3.2; \gamma = 338; \psi = 12.$

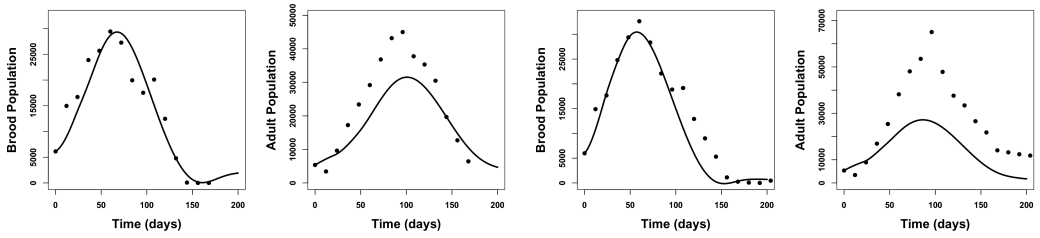

(c) Model 3.2 (1975), $r_0 = 1644; d_h = 0.03; d_b = 0.02; K = 139,137,000; \gamma = 277; \psi = 12.$

(d) Model (3.2) (1976), $r_0 = 1477; d_h = 0.04; d_b = 0.02; K = 81,048,000; \gamma = 261; \psi = 12.$

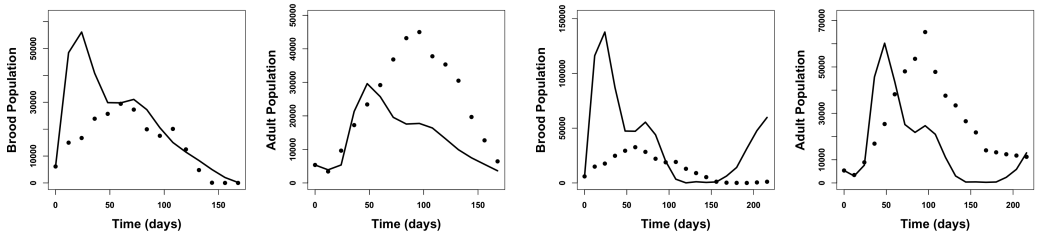

(e) Model (3.3) (1975), $r_0 = 4024; d_h = 0.13; d_b = 0.12; K = 89,000; \gamma = 350; \psi = 12.$

(f) Model (3.3) (1976), $r_0 = 9171; d_h = 0.19; d_b = 0.12; K = 20,000; \gamma = 261; \psi = 12.$

Figure 3.8: Data fitting with the seasonality equation in r for Harris honey bees data in 1975 (a, c, e) and 1976 (b, d, f) with $\tau = 21$. Black dots indicate Harris data, and the black curve indicates our model.

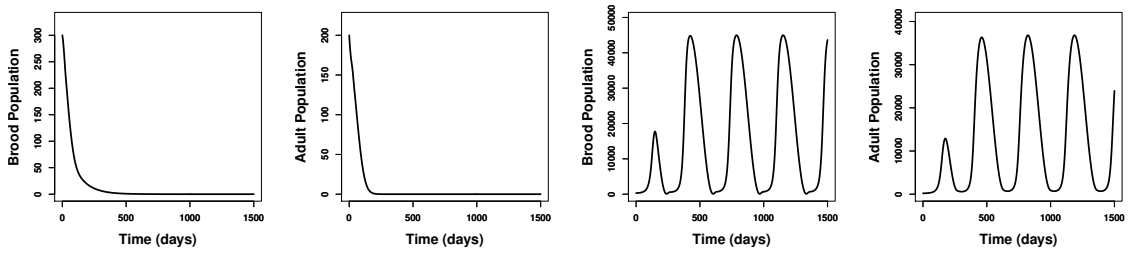

(a) Brood population of Model (3.1) without seasonality

(b) Adult population of Model (3.1) without seasonality

(c) Brood population of Model (3.1) with seasonality

(d) Adult population of Model (3.1) with seasonality

Figure 3.9: Colony dynamic of simulation for Model (3.1) collapses without seasonality while survives with seasonality: $r = 1200, K = 5.4 * 10^6, d_b = 0.01, d_h = 0.05, \alpha = 10, \gamma = 365, \psi = 45$; $B(\theta) = 300$ and $H(\theta) = 200$, $\theta \in [-\tau, 0]$.

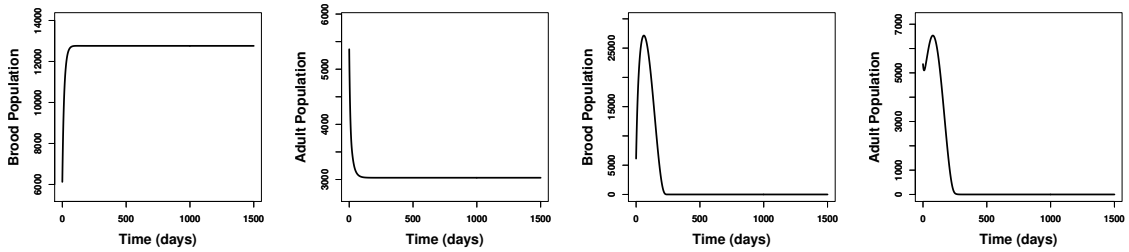

(a) Brood population of Model (3.1) without seasonality

(b) Adult population of Model (3.1) without seasonality

(c) Brood population of Model (3.1) with seasonality

(d) Adult population of Model (3.1) with seasonality

Figure 3.10: Simulations for Model (3.1) survives without seasonality while collapse with seasonality: $r = 1200, K = 1 * 10^6, d_b = 0.06, d_h = 0.11, \alpha = 10, \gamma = 365, \psi = 45$; $B(\theta) = 300$ and $H(\theta) = 200$, $\theta \in [-\tau, 0]$.

Chapter 4

IMPACTS OF SEASONALITY AND PARASITISM ON HONEY BEE POPULATION DYNAMICS

Abstract

The honeybee plays an extremely important role in ecosystem stability and diversity and in the production of bee-pollinated crops. Honey bees and other pollinators are under threat from the combined effects of nutritional stress, parasitism, pesticides, and climate change that impact the timing, duration, and variability of seasonal events. To understand how parasitism and seasonality influence honey bee colonies separately and interactively, I developed a non-autonomous nonlinear honeybee-parasite interaction differential equation model that incorporates seasonality into the egg-laying rate of the queen. Our theoretical results show that parasitism negatively impacts the honey bee population either by decreasing colony size or destabilizing population dynamics through supercritical or subcritical Hopf-bifurcations, depending on conditions. Our bifurcation analysis and simulations suggest that seasonality alone may have positive or negative impacts on the survival of honey bee colonies. More specifically, our study indicates that (1) the timing of the maximum egg-laying rate seems to determine when seasonality has positive or negative impacts; and (2) when the period of seasonality is large it can lead to the colony collapsing. Our study further suggests that the synergistic influences of parasitism and seasonality can lead to complicated dynamics that may positively and negatively impact the honey bee colony's survival. Our work partially uncovers the intrinsic effects of

climate change and parasites, which potentially provide essential insights into how best to maintain or improve a honey bee colony's health.

4.1 Introduction

Honey bee, *Apis mellifera*, the colony is not only an excellent example of a complex adaptive system [Wilson, 2000], but also has great value to our ecosystem and economic development. Per USDA statistics, 80% of crops benefit from pollination by honey bees, including more than 130 types of fruits and vegetables [Randall, 2020], worth $215 billion annually worldwide [Smith *et al.*, 2013]. Additionally, honey bees produce honey and other hive products that are beneficial to human health. For example, the average American consumed 1.0 pounds of honey per person in 2019, which has increased from 0.5 pounds in 1990 [USDA, 2023]. Unfortunately, honey bee colonies are collapsing at an alarming rate, especially during winter [Neumann *et al.*, 2010], causing unsustainable losses to commercial beekeepers and colony shortages to growers.

Research [Perry *et al.*, 2015; Oldroyd, 2007; Smith *et al.*, 2013] suggests that there are many factors contributing to the global decline of the honey bee population. Those factors include nutritional stress from lack of flowering plants, environmental stressors such as global warming, lack of genetic variation, and vitality, parasites such as Varroa mites and Nosema, and diseases such as acute bee paralysis virus and deformed wing virus. Most notably, Varroa mites pose a huge threat to the health of honey bees [Peng *et al.*, 1987; Vetharaniam and Barlow, 2006; DeGrandi-Hoffman and Curry, 2004; Messan *et al.*, 2017, 2021; Kang *et al.*, 2016]. They can parasitize honey

bees, transmit viruses, and also make honey bees more susceptible to viral outbreaks [Koleoglu *et al.*, 2017]. Mites parasitize workers and drones (male bees), larvae, and adults, but not the queen [DeGrandi-Hoffman *et al.*, 2017]. Parasitized honey bees have shortened lifespans, lower weight, and weakened immune systems [Peng *et al.*, 1987]. Foragers that have been parasitized during development are more easily disoriented during foraging as adults [Koleoglu *et al.*, 2017]. Infected colonies also are more prone to viral diseases and struggle to survive in the winter [Degrandi-Hoffman *et al.*, 2019; DeGrandi-Hoffman and Curry, 2004; Martin *et al.*, 2012; Chen and Siede, 2007].

Seasonality has important effects on honey bee foraging behaviors. For example, in temperate areas during in fall and winter, food can become unavailable as temperatures drop below freezing. During this time, honey bees remain in their hives and form a thermoregulated cluster of bees [Stabentheiner *et al.*, 2003], but if the bees fail to maintain cluster warmth, the colony will perish [Simpson, 1961]. Moreover, the queen bee stops or reduces egg laying [SEELEY and Visscher, 1985; DeGrandi-Hoffman *et al.*, 1989; Research and Extension Consortium, 2004] in preparation for overwintering [Martin, 2001a]. Overwintering is stressful to colonies and losses may exceed 30% [Doeke *et al.*, 2015].

Both experimental and simulated bee population data show seasonal patterns in colony population dynamics [DeGrandi-Hoffman *et al.*, 1989; Harris, 1980]. Seasonality also plays a role in the dynamics of parasites and viruses in colonies [DeGrandi-Hoffman and Curry, 2004; Martin, 2001a; Smoliński *et al.*, 2021]. Thus, there is increased attention to including seasonality in honey bee population models. For

example, [Ratti *et al.*, 2015; Eberl *et al.*, 2010; Sumpter and Martin, 2004] adding seasonality equations using four sets of parameter values to differentiate seasons revealed that seasonal dynamics can lead to colonies with persistent Varroa infestations to suddenly collapse in late fall or spring because of the compounding effects of parasitism and viruses transmitted by Varroa [Ratti *et al.*, 2015]. The seasonal models also generated recommendations that controls for Varroa should occur in summer to reduce the colony losses [Sumpter and Martin, 2004]. The work of [Betti *et al.*, 2016, 2014] directly used two sets of models to represent the dynamics of non-winter and winter, respectively. The model [Betti *et al.*, 2014] has no egg laying in the winter system and considering the age structure of the colony during its yearly cycle. The model [Betti *et al.*, 2016] added 21-day transition equations for colonies to wake up between the end of winter and a new active season. This model captured the sharp decline in colony size often seen in the spring (spring dwindling) and showed that the timing of the onset of disease in a colony could impact its severity and persistence in the population.

Here, motivated by the experimental work shown in [DeGrandi-Hoffman *et al.*, 1989; Harris, 1980], I describe a model where seasonality has been incorporated into the queen's egg-laying rate through cosine functions. An age-structure model of honey bees' population dynamics Chen et al. (2020) [Chen *et al.*, 2020a] showed that seasonality may reduce colony survival but may also prevent colony collapse. Messan et al. (2021) [Messan *et al.*, 2021] focused on the colonies with parasites and found seasonality can help colonies recover under certain conditions. Messan et al. (2018) [Messan *et al.*, 2018] focused on the nutrition of colonies and found that seasonality

can be affected by stress and cause colony death.

Based on the data [Kang *et al.*, 2016; DeGrandi-Hoffman *et al.*, 1989] and previously reported models [Chen *et al.*, 2020a; Messan *et al.*, 2018, 2021], I formulate a mathematical modeling framework describing honeybee-mite interactions with seasonality in the queen's egg-laying rate to address the following questions:

- How may seasonality impact honey bee populations in the absence of parasitism?
- How may parasitism impact the honey bee population?
- What are the synergistic impacts of seasonality and parasitism on the honey bee population?

The remaining parts of this article are structured as follows: In Section 2, I provide details of how I modeled seasonality in the egg-laying rate and a general modeling framework for the interactions of parasitism and honey bees. In Section 3, I address how seasonality impacts the survival of honey bee colonies and their population dynamics. I theoretically demonstrate the impacts of parasitism on the honey bee populations without seasonality. In Section 4, I explore how parasites and seasonality might influence colony survival and population dynamics. In the last section, I conclude our theoretical and bifurcation analysis results regarding the effects of seasonality and parasites on colony dynamics and propose future studies needed to understand how climate-related factors may threaten honey bee colonies.

4.2 Model Derivation

In this section, I focus on modeling the honeybee-parasite colony dynamics with seasonality. Let $H(t)$ be the population of the honey bee and $M(t)$ be the population of the mites in a given colony at time t. I assume that:

A1: The term $\frac{H^2}{K+H^2}$ reflects the cooperative brood care from adult bees that perform nursing and collecting food for brood [Chen *et al.*, 2020a; Messan *et al.*, 2021, 2018; Schmickl and Crailsheim, 2007; Kang *et al.*, 2016; Eischen *et al.*, 1984], where $\sqrt{K}$ indicates the colony size at which brood survival rate is half maximum.

A2: I assume that the queen egg-laying rate is seasonal ($r(t)$) due to resource constraints. The literature work suggests that food, temperature, weather, and oviposition place would affect the queen [Bodenheimer, 1937; Khoury *et al.*, 2011; DeGrandi-Hoffman *et al.*, 1989]. Motivated by literature [Chen *et al.*, 2020a; Messan *et al.*, 2021; Chen *et al.*, 2021] and analysis of recent experimental data [Fisher II *et al.*, 2021], I model the egg-laying rate with seasonality as follows:

$$r(t) = r_0(1 + \epsilon \cos(\frac{2\pi(t-\psi)}{\gamma})) \tag{4.1}$$

with $\epsilon \in (0, 1)$ measuring the intensity of seasonal impacts, r_0 representing the average of egg-laying rate, γ representing the length of seasonality, and ψ being the time of the maximum laying rate.

A3: Female mites breed offspring in the cell and complete the mating in the cell. In the phoretic phase, female mites feed on adult bees and immigrate to other colonies [Vetharaniam and Barlow, 2006]. In the reproductive phase, mites attach to foraging bees and then reproduce offspring in the cell [Ramsey *et al.*, 2019]. Based on the biological background and literature work [Messan *et al.*, 2021; Betti *et al.*, 2014; Sumpter and Martin, 2004], I model the honeybee-parasite interaction as follows:

$$\frac{aH}{b+cH}$$

where a is the mite parasitism rate to the honey bee, c is parasite attachment effects, and b is the size of honey bee population at which rate of attachment is half maximal.

A4: Female mites need nutrition from honey bees to produce the next generation. The parameter σ indicates the conversion rate of nutrient consumption obtained from bees into nutrients needed by mites to reproduce.

The four assumptions above lead to the following nonautonomous and non-linear ordinary differential equations of the honeybee-parasite interaction model with seasonality (Model (4.2)):

$$\begin{aligned} H' &= \tfrac{r(t)H^2}{K+H^2} - d_h H - \tfrac{aH}{b+cH} M, \\ M' &= \tfrac{\sigma aH}{b+cH} M - d_m M, \end{aligned} \tag{4.2}$$

with $r(t) = r_0(1 + \epsilon \cos(\frac{2\pi(t-\psi)}{\gamma}))$.

Parameter	Definition (Units)	Parameter	Definition (Units)
H	Honey bee population (bees)	M	Parasite (mites) population (bees)
a	The parasitism rate to honey bee (per day)	b	The size of honey bee population at which the rate of attachment is half-maximal (bees)
c	Parasite attachment effects	r_0	The average of egg-laying rate (bees/day)
$\sqrt{K}$	The colony size at which brood survival rate is half-maximum (bees)	σ	The conversion rate of nutrient consumption obtained from bees to sustenance for mites' reproduction
d_h & d_m	The death rate of honey bee and parasite (mites) (per day)	γ	the length of seasonality (days)
ψ	The time of the maximum laying rate (days)	ϵ	the strength of seasonality

Table 4.1: The biological meanings of parameters.

Note: If $b = 1$ and $c = 0$, Model (4.2) reduces to the previous work of Kang et al. (2016) [Kang *et al.*, 2016] disease free model; and if $c = 1$, Model (4.2) reduces to our previous works of Messan et al. (2017 & 2021) [Messan *et al.*, 2017, 2021]. Thus the current model (4.2) processes the general interaction properties of honey bees and parasitism.

In the following two sections, I will provide our detailed study to obtain insights regarding how seasonality and/or parasitism alone or combined impact honey bee population dynamics.

4.3 Mathematics Analysis

To facilitate our analysis of the proposed system, I start with re-scaling our system (4.2). Assume that $b \neq 0$, $c \neq 0$ and $\sigma \neq 0$, let $u = \frac{c}{b}H$, $v = \frac{c}{b\sigma}M$, $\hat{K} = \frac{Kc^2}{b^2}$, $\omega = \frac{a\sigma}{c}$, $\bar{r}(t) = \frac{r(t)c}{b}$, $\bar{d}_h = d_h$ and $\bar{d}_m = d_m$, then system (4.2) can scaled by following:

$$\begin{aligned} u' &= \frac{\bar{r}(t)u^2}{\hat{K}+u^2} - \bar{d}_h u - \frac{\omega u}{1+u}v \\ v' &= \frac{\omega u}{1+u}v - \bar{d}_m v \end{aligned} \tag{4.3}$$

I first show that the proposed model (4.3) is positive invariant and bounded in $\mathbb{R}^2_+$ as the following theorem:

Theorem 4.3.1. *Assume that all parameters are non-negative. Model* (4.3) *with initial value* $u(0) = u_0$, $v(0) = v_0$, *and* $(u_0, v_0) \in \mathbb{X}$ *possesses a unique solution, and the space* $\mathbb{X}$ *is positively invariant and bounded in* $\mathbb{R}^2_+$.

Remark 4.3.2. *Theorem 4.3.1 provides us reassurances that the proposed model* (4.3) *is well defined biologically and provides bases for our carefully designed numerical studies.*

4.3.1 Impact of Seasonality on Honeybee-Only Population Dynamics

If there is no mites, i.e., $v(0) = 0$, the model (4.2) reduces to the following bee-only population model with seasonality:

$$u' = \frac{\bar{r}(t)u^2}{\hat{K}+u^2} - \bar{d}_h u \tag{4.4}$$

with $\bar{r} = r_0(1+\epsilon\cos(\frac{2\pi(t-\psi)}{\gamma}))$ which satisfies a Lipschitz condition for all $u \geq 0$. Thus according to Theorem 4.3.1, the initial value problem with $u(0) \geq 0$ has a unique non-negative and bounded solution.

In order to study the effects of the strength of seasonality (ϵ) and the length of seasonality (γ) on bee populations, I start with the dynamics of the Honeybee-only model (4.4) when $\bar{r}(t) = r_0$ is a constant. The honeybee-only system without seasonality (4.4) has two equilibria $u_i^*, i = 1, 2$ shown as below provided $r_0 > 2\bar{d}_h\sqrt{\hat{K}}$:

$$u_1^* = \frac{r_0 - \sqrt{r_0^2 - 4\bar{d}_h^2\hat{K}}}{2\bar{d}_h}, \quad u_2^* = \frac{r_0 + \sqrt{r_0^2 - 4\bar{d}_h^2\hat{K}}}{2\bar{d}_h}.$$

The global dynamics of (4.4) when $\bar{r}(t) = r_0$ can be summaries as the following proposition:

Proposition 4.3.1. *If $r_0 < 2\bar{d}_h\sqrt{\hat{K}}$, then the population of $u(t)$ converges to 0 for any initial condition $u(0) \geq 0$. In the case that $r_0 > 2\bar{d}_h\sqrt{\hat{K}}$, $u(t)$ converges to 0 for any initial condition $u(0) < u_1^*$ while $u(t)$ converges to u_2^* for any initial condition $u(0) > u_1^*$.*

Notes: Proposition 4.3.1 indicates that the relationship among the constant egg-laying rate r_0, the honey bee mortality, and the half-maximum rate $\hat{K}$, as well as initial conditions, determine whether the honey bee colony can survive. With the larger egg-laying rate r_0 with the larger initial condition u_0, the honey bee colony is more likely to survive. In the case that the egg-laying rate is seasonal, $\bar{r}(t) = r_0(1+\epsilon\cos(\frac{2\pi(t-\psi)}{\gamma}))$ with its average value over each seasonal length γ being r_0, the consequence of honey bee population dynamics can be complicated. Examples shown in Figure 4.1 suggest that the seasonality in the egg-laying rate can promote the survival of honey bees

when the intensity of seasonality is not too high, and it can also make the honey bee colony prone to collapsing when the intensity of seasonality is high.

In Figure 4.1, without seasonality $\epsilon = 0$, the honey bee colony with $r_0 = 1$, $\bar{d}_h = 0.5$, $\hat{K} = 1/4$, $\psi = 0$ and $\gamma = 100$ can survive under its initial condition $u(0) = 1$ (red curve in Figure 4.1a) while it collapses under its initial condition $u(0) = 0.1$ (red curve in Figure 4.1b). When the intensity of seasonality is not too high, i.e., $\epsilon = 0.2$ or 0.5, the honey bee colony can survive under its initial condition $u(0) = 0.1$ (black and green curves in Figure 4.1b). This is an example showing that seasonality can promote the survival of a honey bee colony. On the other hand, When the intensity of seasonality is high, i.e., $\epsilon = 0.8$ (blue curve in Figure 4.1a), the honey bee colony collapses with the initial condition of $u(0) = 1$ when the honey bee colony can survive without seasonality. This is an example showing that seasonality can make honey bee colony collapse under certain conditions.

In order to explore the impact of the intensity of seasonality ϵ, I first define the minimum and maximum value of the egg-laying rate function: $r_m = \min \bar{r}(t) = r_0(1-\epsilon)$ and $r_M = \max \bar{r}(t) = r_0(1+\epsilon)$. Motivated by Proposition 4.3.1, the intensity of seasonality can be classified into the following three cases:

1. The low egg-laying rate if $r_M = r_0(1+\epsilon) \leq 2\bar{d}_h\sqrt{\hat{K}}$. This case is equivalent to
$$0 \leq \epsilon \leq 1 - \frac{2\bar{d}_h\sqrt{\hat{K}}}{r_0}$$
2. The high egg-laying rate if $r_m = r_0(1-\epsilon) \geq 2\bar{d}_h\sqrt{\hat{K}}$. This case is equivalent to
$$0 \leq \epsilon \leq \frac{2\bar{d}_h\sqrt{\hat{K}}}{r_0} - 1$$

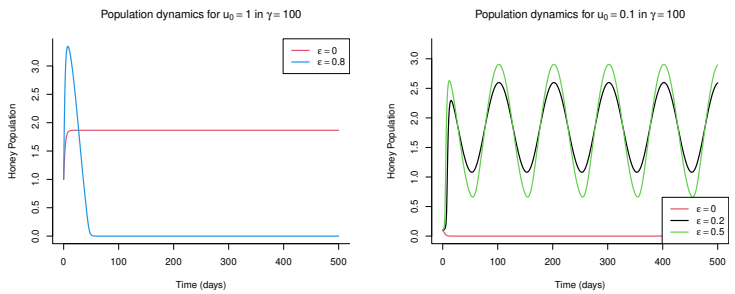

(a) Seasonality leads to the collapsing of the colony when the survival of the colony $u_0 = 1$

(b) Seasonality can promote the colony when $u_0 = 0.1$

Figure 4.1: Population dynamics of honeybee-only model (4.4) with or without seasonality by setting $r_0 = 1$, $\bar{d}_h = 0.5$, $\hat{K} = 1/4$, $\psi = 0$ and $\gamma = 100$ with $u_0 = 0.1$ or 1 as its initial population.

3. The intermediate egg-laying rate if $r_m = \min \bar{r}(t) = r_0(1-\epsilon) < 2\bar{d}_h\sqrt{\hat{K}} \leq r_M = \max \bar{r}(t) = r_0(1+\epsilon)$. This is the case when

$$\max\{1 - \frac{2\bar{d}_h\sqrt{\hat{K}}}{r_0}, \frac{2\bar{d}_h\sqrt{\hat{K}}}{r_0} - 1\} \leq \epsilon \leq 1.$$

Now I have the following theorem:

Theorem 4.3.3. *Let $r_M = r_0(1+\epsilon)$ and $r_m = r_0(1-\epsilon)$. If the egg-laying rate $\bar{r}(t) = r_0(1+\epsilon\cos(\frac{2\pi(t-\psi)}{\gamma}))$ is low, i.e., $r_M = r_0(1+\epsilon) \leq 2\bar{d}_h\sqrt{\hat{K}}$, the honey bee population $u(t)$ converges to zero for any initial condition $u(0) \geq 0$. In the case that the egg-laying rate $\bar{r}(t)$ is high, i.e., $r_m = r_0(1-\epsilon) \geq 2\bar{d}_h\sqrt{\hat{K}}$, honey bee population $u(t)$ can survive if the initial condition $u(0) > \frac{r_m - \sqrt{r_m^2 - 4\bar{d}_h^2\hat{K}}}{2\bar{d}_h}$. More specifically, I have*

$$\frac{r_m - \sqrt{r_m^2 - 4\bar{d}_h^2\hat{K}}}{2\bar{d}_h} < \liminf_{t\to\infty} u(t) \leq \limsup_{t\to\infty} u(t) < \frac{r_M + \sqrt{r_M^2 - 4\bar{d}_h^2\hat{K}}}{2\bar{d}_h}$$

if $r_m \geq 2\bar{d}_h\sqrt{\hat{K}}$ and $u(0) > \frac{r_m - \sqrt{r_m^2 - 4\bar{d}_h^2\hat{K}}}{2\bar{d}_h}$.

Notes: Theorem 4.3.3 implies that I can focus on how seasonality impacts honey bee population when the egg-laying rate $\bar{r}(t)$ is not low, i.e.,$r_M = r_0(1+\epsilon) \geq 2\bar{d}_h\sqrt{\hat{K}}$ which includes the case 2 and 3. Because the low egg-laying rate leads the colony to collapse. Thus, I can reduce the three cases above to the following two cases by introducing the critical intensity of seasonality $\epsilon_c = \frac{2\bar{d}_h\sqrt{\hat{K}}}{r_0} - 1$

1. The low intensity of seasonality, i.e.,

$$0 \leq \epsilon \leq \epsilon_c$$

2. The high intensity of seasonality, i.e.,

$$0 < \epsilon_c \leq \epsilon \leq 1.$$

By applying Proposition 3.1 and the method used in Ratti et al.(2015) [Ratti *et al.*, 2015], I obtain the stability condition when Model 4.4 processes a periodic solution u^* as the following theorem:

Theorem 4.3.4. *Suppose $u(t) = u^*$ are periodic solutions of the Model 4.4, and $f(u) = \frac{u^2}{\hat{K}+u^2}$. Then $u(t) = u^*$ is stable if $\lambda = \int_0^t \left[\bar{r}(z) * f'(u^*) - \bar{d}_h\right] dz < 0$, or is unstable if $\lambda > 0$, where $f'(u^*) = \frac{2\hat{K}u^*}{\left(\hat{K}+(u^*)^2\right)^2}$.*

Notes: Theorem 4.3.4 shows that the stability of the periodic solution of Model 4.4 requires $\int_0^t \left[\bar{r}(z) * f'(u^*) - \bar{d}_h\right] dz < 0$, thus $u = 0$ is always locally stable as the case without seasonality.

To further address the impacts of seasonality on honey bee population dynamics, I provide basins of attractions for Model (4.4) in Figure 4.2 and Figure 4.3 by setting $\bar{d}_h = 0.5, \hat{K} = 1/4, r_0 = 1$. I set $\psi = 0$ in Figure 4.2. The x-axis is the initial honey

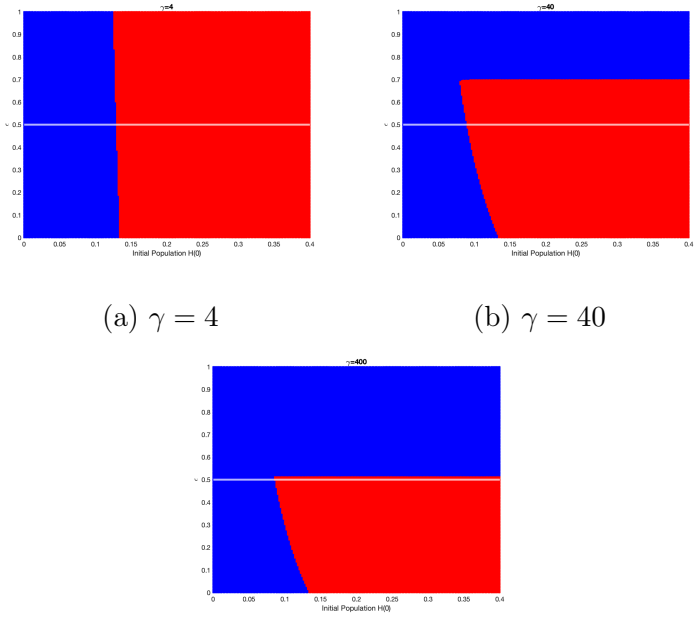

(a) $\gamma = 4$ (b) $\gamma = 40$

(c) $\gamma = 400$

Figure 4.2: Impacts of the strength of seasonality (ϵ) and the length of seasonality (γ). The blue area is colony collapse and red area is colony survive. $r_0 = 1$, $\bar{d}_h = 0.5$, $\hat{K} = 1/4$ and $\psi = 0$. Honey bee initial population is $u_0 \in [0, 0.4]$

bee population $u(0)$, and the y-axis is the intensity of seasonality measured by ϵ. Those parameter values give $\epsilon_c = 0.5$, which is a white horizontal line in Figure 4.2 and Figure 4.3. The blue region in Figures is the value of the strength of seasonality (ϵ) and the corresponding initial conditions that lead the colony to collapse, while the red region is the value of ϵ and $u(0)$ that lead to the colony survival.

Figure 4.2 and Figure 4.3 suggest that the strength of seasonality (ϵ), the length of seasonality (γ), and the time of the maximum laying rate (ψ) impact the survival of honey bee colony in the synergistic ways:

1. The length of seasonality (γ) is small, e.g., $\gamma = 4$:

- If the time of the maximum laying rate (ψ) is less than the half period γ, the seasonality seems to promote the survival of the colony in the sense that the initial bee population that originally leads to collapsing but it leads to colony survival with seasonality.
- If the time of the maximum laying rate (ψ) is larger than the half period γ, the seasonality seems to suppress the survival of the colony in the sense that the initial bee population that originally leads to survival but it leads to colony collapsing with seasonality.

2. When the length of seasonality (γ) is larger, e.g., $\gamma = 40, 400$, the large intensity of seasonality ϵ can lead to the collapsing of the colony while the impacts of the smaller intensity of seasonality ϵ depends on the timing of the maximum laying rate (ψ) as follows:
   - If the time of the maximum laying rate (ψ) is less than the half period γ, the seasonality seems to promote the survival of the colony.
   - If the time of the maximum laying rate (ψ) is larger than the half period γ, the seasonality seems to suppress the survival of the colony.

4.3.2 Impact of Parasitism on Honey Bee Population without Seasonality

In this subsection, I focus on the dynamics of the honeybee-parasite interaction model (4.3) in the absence of seasonality, i.e., $\bar{r}(t) = \bar{r}$. Thus, I have the following

rescaled model (4.5):

$$\begin{aligned} u' &= \frac{\bar{r}u^2}{\hat{K}+u^2} - \bar{d}_h u - \frac{\omega u}{1+u} v \\ v' &= \frac{\omega u}{1+u} v - \bar{d}_m v \end{aligned} \tag{4.5}$$

that would allow us to obtain biological insights on how parasitism impacts the honey bee population by comparing the dynamics of $v(0) = 0$ versus $v(0) > 0$. In the case that $v(0) = 0$, the model (4.3) reduces to the honey bee only model in the constant environment (4.4) whose dynamics are summarized in Proposition 4.3.1.

Let (u^*, v^*) be an equilibrium of Model (4.3), then it satisfies the following equations:

$$\frac{\bar{r}(u^*)^2}{\hat{K} + (u^*)^2} - \bar{d}_h u^* - \frac{\omega u^*}{1+u^*} v^* = 0, \tag{4.6}$$

$$\frac{\omega u^*}{1+u^*} v^* - \bar{d}_m v^* = 0 \Rightarrow (\frac{\omega u^*}{1+u^*} - \bar{d}_m) v^* = 0 \tag{4.7}$$

Solving Eqt.4.7 gives $v^* = 0$ or $u^* = \frac{\bar{d}_m}{\omega - \bar{d}_m}$. And if $v^* = 0$, then Eqt.4.6 is

$$\frac{\bar{r}(u^*)^2}{\hat{K} + (u^*)^2} - \bar{d}_h u^* = 0,$$

which gives the following two positive solutions provided that $\bar{r} > 2\bar{d}_h\sqrt{\hat{K}}$,

$$u_1^* = \frac{\bar{r} - \sqrt{\bar{r}^2 - 4\hat{K}\bar{d}_h^2}}{2\bar{d}_h}$$

or

$$u_2^* = \frac{\bar{r} + \sqrt{\bar{r}^2 - 4\hat{K}\bar{d}_h^2}}{2\bar{d}_h}.$$

In the case that $\omega > \bar{d}_m$, I have $u^* = \frac{\bar{d}_m}{\omega - \bar{d}_m}$ and $v^* = \frac{\left[\bar{r}u^* - \bar{d}_h\left((u^*)^2 + \hat{K}\right)\right](1+u^*)}{\omega((u^*)^2+\hat{K})}$ as the unique interior equilibrium of Model 4.3. The stability of the equilibrium point can be evaluated through the following Jacobean matrix of Model 4.3 is

$$J = \begin{Bmatrix} -\bar{d}_h + \frac{2\hat{K}\bar{r}u}{\left(\hat{K}+u^2\right)^2} - \frac{\omega v}{(1+u)^2} & -\frac{\omega u}{1+u} \\ \frac{\omega v}{(u+1)^2} & \frac{\omega u}{u+1} - \bar{d}_m \end{Bmatrix}$$

Now I are the following on the dynamics of the Honeybee-Parasite system (4.3):

Theorem 4.3.5. *[Dynamics of Honeybee-Parasite system* (4.3)*] The system* (4.3) *can have one, three, or four equilibria whose existence and stability conditions are listed in Table 4.2. The global dynamics of Model* (4.3) *can be summarized as follows:*

1. *The system* (4.3) *converges to extinction* $(0, 0)$ *for almost all initial conditions if one the three conditions holds (1)*$\frac{\bar{r}}{2\sqrt{\hat{K}}} < d_h$*; (2)* $\omega > \bar{d}_m$*; or (3)*$\bar{N}_h^c > u^*$.

2. *If* $\omega < \bar{d}_m$ *or* $\bar{N}_h^* < u^*$*, depending on initial condition, the trajectory of system* (4.3) *converges to either* $(0, 0)$ *or* $(\bar{N}_h^*, 0)$.

3. *If* $\bar{N}_h^c < u^* < \bar{N}_h^*$*, then system* (4.3) *has a unique interior equilibrium* (u^*, v^*) *which is locally asymptotically stable when* $\hat{K} < \hat{K}_1$ *and is a source when* $\hat{K} > \hat{K}_1$.

Notes: Theorem 4.3.5 provides us a global picture of the dynamics of the system (4.3) and the related biological implications of the impact of parasitism on honey bee population dynamics in constant conditions. Theorem 4.3.5 suggests that parasitism can have negative impacts on the honey bee population in three ways: (1) May lead to the collapsing of the colony; (2) May lead to the coexistence of both honey bee

Equilibria	Existence condition	Stability condition
$(0,0)$	Always exists	Always locally stable
$(\bar{N}_h^c, 0)$	$\frac{\bar{r}}{2\sqrt{\hat{K}}} > d_h$	Saddle if $\bar{N}_h^c < u^*$; Source if $\omega < \bar{d}_m$ or $\bar{N}_h^c > u^*$
$(\bar{N}_h^*, 0)$	$\frac{\bar{r}}{2\sqrt{\hat{K}}} > \bar{d}_h$	Sink if $\bar{N}_h^* < u^*$ or $\omega < \bar{d}_m$; Saddle if $\bar{N}_h^* > u^*$
(u^*, v^*)	$\omega > \bar{d}_m$ & $\frac{\bar{r}u^*}{\hat{K}+(u^*)^2} > \bar{d}_h$	Sink if $\hat{K} < \hat{K}_1$; Source if $\hat{K} > \hat{K}_1$

Table 4.2: The existence and stability of equilibrium for Model 4.3, where $\bar{N}_h^c = \frac{\bar{r}-\sqrt{\bar{r}^2-4\hat{K}\bar{d}_h^2}}{2\bar{d}_h}$, $\bar{N}_h^* = \frac{\sqrt{\bar{r}^2-4\hat{K}\bar{d}_h^2}+\bar{r}}{2\bar{d}_h}$, $u^* = \frac{\bar{d}_m}{\omega-\bar{d}_m}$, $v^* = \frac{\left[\bar{r}u^*-\bar{d}_h\left((u^*)^2+\hat{K}\right)\right](1+u^*)}{\omega((u^*)^2+\hat{K})}$, $\hat{K}_1 = \frac{-\sqrt{\bar{r}}\sqrt{\bar{r}(2u^*+1)^2-8\bar{d}_h(u^*)^2(u^*+1)}+2\bar{r}u^*+\bar{r}-2\bar{d}_h(u^*)^2}{2\bar{d}_h}$.

and parasitism but the honey bee population decreases compared to the case without parasitism, or (3) May destabilize the honey bee population.

Item (3) needs further theoretical exploration regarding how parasitism may destabilize the colony dynamics. For example, the colony destabilizes to show fluctuating dynamics through supercritical Hopf-bifurcation; or to collapse supercritical Hopf-bifurcation.

By applying the results in [Wang *et al.*, 2011], our system 4.3 undergoes a Hopf-bifurcation. To study further, I re-scaled the system 4.3 to the following model:

$$\begin{aligned} u' &= g(u)(f(u)-v) \\ v' &= v(g(u)-\bar{d}_m), \end{aligned} \tag{4.8}$$

where $g(u) = \frac{\omega u}{1+u}$ and $f(u) = \frac{\bar{r}}{g(u)} \cdot \frac{u^2}{\hat{K}+u^2} - \frac{\bar{d}_h}{g(u)} \cdot u$. I can verify that our system 4.8

satisfies the following conditions:

(a1) $f \in C^1(\bar{\mathbb{R}}), f(a) = f(b) = 0$, where $0 < a < b$; $f(u)$ is positive for $a < u < b$, and $f(u)$ is negative otherwise; there exists $\bar{\lambda} \in (a, b)$ such that $f'(u) > 0$ on $[a, \bar{\lambda})$, $f'(u) < 0$ on $(\bar{\lambda}, b]$;

(a2) $g \in C^1(\bar{\mathbb{R}}), g(0) = 0$; $g(u) > 0$ for $u > 0$ and $g'(u) > 0$ for $u > 0$, and there exists $\lambda > 0$ such that $g(\lambda) = d$.

(a3) $f(u)$ and $g(u)$ are C^3 near $\lambda = \bar{\lambda}$ and $f''(\bar{\lambda}) < 0$.

Then according to Theorem 3.1 in Wei et al. (2011) [Wang *et al.*, 2011], I can conclude that our system 4.8 exists the first Lyapunov coefficient

$$\begin{aligned} a(\bar{\lambda}) &= \frac{f'''(\bar{\lambda})g(\bar{\lambda})g'(\bar{\lambda}) + 2f''(\bar{\lambda})[g'(\bar{\lambda})]^2 - f''(\bar{\lambda})g(\bar{\lambda})g''(\bar{\lambda})}{16g'(\bar{\lambda})} \\ &= \frac{\omega}{16(1+\bar{\lambda})}(2f''(\bar{\lambda}) + \bar{\lambda}f'''(\bar{\lambda})) \end{aligned}$$

where

$$2f''(\bar{\lambda}) + \bar{\lambda}f'''(\bar{\lambda}) = \frac{2\bar{r}\left(2\hat{K}^3 - \hat{K}^2(2\bar{\lambda}(2\bar{\lambda}+9)+3) + 2\hat{K}(\bar{\lambda}(4-3\bar{\lambda})+9)\bar{\lambda}^2 + (2\bar{\lambda}-3)\bar{\lambda}^4\right)}{\omega\left(\hat{K} + \bar{\lambda}^2\right)^4} \quad (4.9)$$

Thus, I have the following results on Hopf-bifurcations:

Theorem 4.3.6. *The system 4.3 undergoes a supercritical Hopf-bifurcation at $\hat{K} = \hat{K}_1$ with $a(\bar{\lambda}) < 0$, and a subcritical Hopf-bifurcation at $\hat{K} = \hat{K}_1$ with $a(\bar{\lambda}) > 0$.*

Note: Theorem 4.3.6 implies that the system 4.3 can undergo a supercritical or subcritical Hopf-bifurcation depending on the relationship between $\hat{K}$ and $\bar{\lambda}$. If the system goes supercritical bifurcation at $\hat{K}_1$, then it has a stable limit cycle surrounding a source equilibrium when $\hat{K} > \hat{K}_1$. When the system 4.3 undergoes a subcritical Hopf-bifurcation, then both the population of honey bees and the parasitic mites go to zero through the unstable limit cycle. Biologically, it implies that parasitism in the constant environment can destabilize the dynamics and even lead to colony collapse, thus, parasitism has negative impacts on honey bee population dynamics.

4.4 Synergistic Impacts of Parasitism and Seasonality

In the previous two sections, I explore the impacts of seasonality on the honey bee population and the impacts of parasitism on the honey bee population in a constant environment, respectively. Our study shows that seasonality can have positive or negative effects on the survival of honey bee colonies depending on the values of the strength of seasonality ϵ, the period γ, and the timing of the maximum egg-laying rate ψ. Our theoretical work shows that parasitism, in general has negative impacts on the survival of honey bee colonies in a constant environment.

In this section, I will explore how seasonality combined with parasitism affects honey bee population dynamics. I start with the following theorem regarding the stability condition when Model 4.3 processes a periodic solution of $(u^*, 0)$ by applying Floquet theory theorem and the approach in Ratti et al.(2015) [Ratti *et al.*, 2015].

Theorem 4.4.1. *Suppose $u^*(t)$ is a periodic positive solution of the Model 4.4, and $f(u) = \frac{u^2}{\hat{K}+u^2}$. Then, $(u^*, 0)$ is a periodic solution of Model 4.3, and $f'(u) = \frac{2\hat{K}u}{\left(\hat{K}+u^2\right)^2}$.*

It is stable if $\int_0^T \left[\bar{r}(t) * f'(u^*) - \bar{d}_h\right] dt < 0$ *and* $\int_0^T \left[\frac{\omega u^*}{1+u^*} - \bar{d}_m\right] dt < 0$.

Note: Theorem 4.4.1 implies that $(0, 0)$ is always locally stable, thus, initial conditions play important roles in the survival of honeybee colonies.

By comparing the results of Theorem 4.3.5 and Theorem 4.4.1, I can see that the impact of seasonality: the seasonality in the egg laying rate $r(t)$ generates the periodic solution $u^*(t)$ whose stability requires
$\int_0^T \left[\bar{r}(t) * f'(u^*) - \bar{d}_h\right] dt < 0$ and $\int_0^T \left[\frac{\omega u^*}{1+u^*} - \bar{d}_m\right] dt < 0$. Those conditions reduce to $rf'(u^*) < \bar{d}_h$ and $\frac{\omega u^*}{1+u^*} < \bar{d}_m$ when $r(t) = r$ being a constant.

By comparing the results of Theorem 4.3.4 and Theorem 4.4.1, I can see the impact of parasitism. Specifically, the stability of nontrial periodic boundary solution $(u^*, 0)$ requires $\int_0^T \left[\frac{\omega u^*}{1+u^*} - \bar{d}_m\right] dt < 0$.

Note that our honeybee-parasite model (4.4) exhibits strong Allee effects in honey bees due to collaborative behavior in the colony. There is limited theoretical work on exploring the impacts of both parasitism and seasonality. Ratti et al.(2015)[Ratti *et al.*, 2015] developed a honeybee-mite-virus model with seasonality. Their model also exhibits strong Allee effects in honey bees, while their mite-free solution is always unstable due to their formulation of the mite population. They discussed the existence of periodic solution and its stability in the bee-only model and discussed the stability of the disease-free solution and mite-free solution through linearization and the method of Floquet theory in the bee-mite model and bee-mite-virus model, respectively. The most recent work that can be related to our topic is the paper

by Rebelo and Soresina (2020) [Rebelo and Soresina, 2020]. Their paper proposed and studied a prey-predator model with weak or strong Allee effects in a periodic environment. They discussed the stability conditions of trivial, nontrivial solutions, and periodic solutions. They also showed that different initial conditions might lead to the extinction of both species or the coexistence of two species that converge to a stable periodic orbit.

To further our understanding of the impacts of seasonality and parasitism, I perform simple time series simulations and observe the following by setting

$$\bar{r}_0 = 1,\ \bar{d}_h = 0.2,\ \bar{d}_m = 0.21,\ \omega = 0.3,\ \hat{K} = 4.49,\ \psi = 0$$

1. In the absence of seasonality and parasitism, a honey bee colony can establish its population when its initial condition is greater than 1.173; otherwise, it collapses.

2. With seasonality but without parasitism, Figure 4.4a suggests that seasonality can promote the survival of a honey bee colony when its initial condition is 1 (< 1.173) and it can also make a honey bee colony prone to collapse when its initial condition is above 1.173 (see the black curve in Figure 4.4b).

3. With parasitism but without seasonality, a honey bee colony can survive through the stable limit cycle around the interior equilibrium $(2.33, 0.3875)$ for the right initial conditions. For example, a honey bee colony survives when $u_0 = 1.2$ and $v_0 = 0.02$ (see the red curve in Figure 4.5a) while it collapses when the initial parasite population grows up to 0.05 (see the red curve in 4.5b).

4. With both seasonality and parasitism, Figure 4.5b suggests that seasonality can promote the survival of a honey bee colony when the parasite's initial population is 0.05 and the seasonality can also make the honey bee colony prone to collapse when the parasite initial population is 0.02 (see Figure 4.5a).

The observations above suggest that seasonality combined with parasitism may have positive or negative impacts on the honey bee colony survival depending on varied conditions. To explore further, I will perform a bifurcation analysis to understand how may the strength of seasonality ϵ, the length of seasonal period γ, the timing of the maximum egg-laying rate ψ, and the severity of parasitism measured by ω in the following two scenarios of honeybee-parasitism dynamics in the absence of seasonality:

- **Honey bee and parasitism Coexists at a stable equilibrium**
- **Honey bee and parasitism Coexists as a stable limit cycle**

4.4.1 Impacts of Seasonality on the Stable Equilibrium Coexistence

I choose a typical example of our honeybee-parasite interaction model (4.3) by setting

$$\bar{r}_0 = 2.86, \bar{d}_h = \bar{d}_m = 0.25, \omega = 0.3, \hat{K} = 2.04$$

which has a bistability between the colony collapsing state $(0, 0)$ and the survival equilibrium at the locally stable equilibrium point $(5, 5.5769)$ whose basins of attractions are red area shown in Figure 4.6a.

To further explore the impacts of the seasonality strength ϵ and the period of

seasonality γ on the colony survival and population dynamics, without loss of generosity, I set the queen laying her maximum number of eggs at time $\psi = 0$, and I perform the following simulations (Figure 4.6, 4.7, 4.8) on basin's attractions of our honeybee-parasite model (4.3).

1. When the period of the seasonality γ is small, e.g., $\gamma = 4$, comparisons of areas of basin attractions for the colony survival among Figure 4.6a (no seasonality), 4.6c (the seasonality strength $\epsilon = 0.2$), and 4.6d (the seasonality strength $\epsilon = 0.8$), suggest that seasonality strength ϵ may not impact the basin attractions of the colony survival but it impacts the population dynamics as shown in Figure 4.6b. Simulations suggest that the larger value of the strength of seasonality ϵ, the larger amplitude of the population.

2. When the period of the seasonality γ is in the intermediate range, e.g., $\gamma = 80$, the impacts from the strength seasonality ϵ can be very complicated. For example, Figure 4.7d shows that basins of attractions for the colony survival are splitted into two red areas, and Figure 4.7b shows larger ϵ gives larger population amplitude.

3. When the period of seasonality γ is large, e.g., $\gamma = 100, 250$, comparisons of the basin attractions for the colony survival suggest that the small strength seasonality ϵ may not impact the basin attractions of the colony survival while its large value may cause the colony collapsing (see Figure 4.8c & 4.8d). In some cases, the large strength of seasonality ϵ may have a positive influence on the colony

survival by increasing the area of basin attractions of the colony survival (see the comparison of Figure 4.8a & 4.8f). From the population dynamics point of view, Figure 4.8b suggests that the population has a larger amplitude when ϵ is larger.

Next, I explore the impacts of the timing of the maximum egg-laying rate (ψ) on colony survival and population dynamics in Figure 4.9 by fixing

$$\bar{r}_0 = 2.86, \bar{d}_h = \bar{d}_m = 0.25, \omega = 0.3, \hat{K} = 2.04, \gamma = 70, \epsilon \in \{0.2, 0.35\}.$$

$\gamma = 70 : 1)$ $\epsilon = 0.2$ (the order from large to small): $\psi = 10$ is largest, then $\psi = 0$, $\psi = 60 = 30$ these two cases have same survival area, $\psi = 35$, and $\psi = 40$ is the smallest.

2) $\epsilon = 0.35$ (the order from large to small): $\psi = 60$ is largest, then $\psi = 0$, $\psi = 40$, $\psi = 10$, $\psi = 35$, and $\psi = 30$ is the smallest.

Notice that the seasonality period is $\gamma = 70$ and $\epsilon = 0.35$. I choose the timing of the maximum egg-laying rate $\psi \in \{0, 10, 30, 35, 40 \text{ and } 60\}$ and observe that the red area of the basin attractions for the colony survival is largest when the timing of the maximum laying rate (ψ) is $\psi = 60$ (Figure 4.9l), then the second largest in the case when $\psi = 0$ (Figure 4.9g), the smallest one is $\psi = 30$ (Figure 4.9i), and the second smallest in the case when $\psi = 35$ (Figure 4.9j). These observations from Figure 4.9 regarding the impacts of the maximum laying rate (ψ) of our honeybee-parasite model 4.3 seem to show similar trends of our honey bee-only model 4.4 (see Figure 4.3): as the ψ increases, the seasonality can suppress the survival of the colony; and after the minimum survival area, the ψ can promote the survival of the colony. But the significant difference with the bee-only model is the smallest area is not $\psi = \frac{\gamma}{2}$.

Figure 4.9m and 4.9n show how different timing of the maximum egg-laying rate ψ can lead to different colony dynamics.

To further understand the impacts of the timing of the maximum laying rate (ψ) of our honeybee-parasite model 4.3, I set the strength of the seasonality being $\epsilon = 0.2$, and choose the timing of the maximum egg-laying rate $\psi \in \{0, 10, 30, 35, 40 \text{ and } 60\}$, respectively. The basin attractions for the colony survival is largest when the timing of the maximum laying rate (ψ) is $\psi = 10$(Figure 4.9b), the second largest in the case when $\psi = 0$ (Figure 4.9a), the smallest one is $\psi = 40$ (Figure 4.9e), and the second smallest in the case when $\psi = 35$ (Figure 4.9d). These observations are different than the case of $\epsilon = 0.35$ shown in Figure 4.9 and the case of the honey bee only model 4.4 (see Figure 4.3). The significant difference is that ψ can promote the survival of the colony at the very beginning of ψ growth ($\psi = 10$ in our simulation). These comparisons and our further simulations suggest that the impacts of the timing of the maximum laying rate (ψ) on the honey bee colony survival in the presence of parasitism are very complicated. The area of the basin attractions for the colony survival may be increasing or decreasing with respect to the value of ψ and ϵ without clear patterns.

By comparing the basins of attractions of the honeybee-mite system without seasonality in Figure 4.7a to the honeybee-mite system with seasonality in Figure 4.7d, 4.9e & 4.9g, I observe that seasonality can split the basins of attractions into disconnected regions. This may lead to two scenarios after adding seasonality: (1) the colony may survive from collapsing (see Point A in Figure 4.10c versus Figure

4.10d), and (2) the colony may be prone to collapsing (see Point B in Figure 4.10c versus Figure 4.10d). This suggests that seasonality may generate varied outcomes depending on initial conditions. For instance, while an initial rise in the parasite population is generally perceived as detrimental, it can enhance colony survival under specific circumstances, particularly when considering seasonal factors (compare points A and B in Figure 4.10d). This phenomenon has been observed in experimental data [DeGrandi-Hoffman *et al.*, 2020]. To illustrate those observations, I use Figure 4.7d as an example, where I list four cases. Among them, the initial bee populations of Colony 1 (Case 1, blue) and Colony 3 (Case 3, gray) are similar, and Colony 2 (Case 2, red) and Colony 4 (Case 4, black) are close. While the initial mite population is increasing in the order of Case 1, Case 2, Case 3, and Case 4. Figure 4.10a shows the colony of Case 1 and Case 3 survived while Case 2 and Case 4 collapsed, especially Colony 3 has fewer bees and more mites than Colony 2, but survives.

The potential biological explanation for this phenomenon lies in the heart of seasonality impacts on the egg-laying rate incorporated in the model, and the mite population is impacted through the bee population. For the mite population to grow, colonies must have enough bees. If the system doesn't consider the impacts of seasonality (Model 4.5), then a higher parasite level (v_0: Point A > Point B) leads to colony collapse (see red curves in Figure 4.11b & 4.11d), because parasitism reduces colony population growth by shortening the lifespan of adult workers, then the population of bees is reduced and so will Varroa population growth. However, the system with seasonality (Model 4.3) leads to a switch in the outcomes of these two colonies, which is that the survival colony collapses because of seasonality, whereas the collapsing

colony becomes survival. The point is that the egg-laying rate of bees is periodic due to seasonal effects, then the number of bees will increase at some time intervals (the green curve in Figure 4.11a). At a higher parasite level, fewer bees will bring the mite population down ($\frac{\omega u}{1+u}v$) to a manageable level, and the seasonality egg-laying rate helps the colony grow up periodically (seasonality in Point A). At a lower parasite level, seasonality also leads mites to grow more than without seasonality effects (Figure 4.11d). Seasonality and high numbers of bees may lead to excessive mite growth beyond the colony's sustainable threshold and colony collapse. This principle is similar to one method of controlling Varroa mites: removing the brood from the hive and interrupting the brood reproductive cycle. With no brood present, mites are compelled to feed on adult bees, which can limit the mites' ability to reproduce, helping to control their populations [Jack and Ellis, 2021]. Nevertheless, this method will be affected by seasonality. Removing lots of broods in the fall may have strong negative impacts on overwintering survival [Jack *et al.*, 2020].

Now I explore the impacts of parasitism ω on honey bee population dynamics and its colony's survival in Figure 4.12. Comparison of black areas (which are the basins of attractions of only honey bee survival) in Figure 4.12d & 4.12a suggest that small parasitism (e.g., $\omega = 0.18$) with seasonality is more likely to lead to the colony survival than the case without seasonality. When parasitism is not small (e.g., $\omega = 0.30$) (see Figure 4.12b), seasonality can destabilize the system and decrease the average population of the honey bee. When ω is large (e.g., $\omega = 0.5$), parasitism has negative impacts on the honey bee colony that lead the colony to collapse (see all blue areas in Figure 4.12c). Figure 4.12e shows increasing parasitism, colonies may

still survive, but the average population of honey bees decreases (see black and green curves). These observations are in line with our theorem 4.3.5 for the case without seasonality.

4.4.2 Impacts of Seasonality on Stable Limit Cycle Coexistence

I choose a stable limit cycle example of our honeybee-parasite interaction model 4.3 by setting

$$\bar{r}_0 = 1,\ \bar{d}_h = 0.2,\ \bar{d}_m = 0.21,\ \omega = 0.3,\ \hat{K} = 4.49,\ \psi = 0$$

which has a stable collapsing state $(0, 0)$ for the colony, and a stable limit cycle around the source interior equilibrium $(2.33, 0.3875)$ whose basins of attractions are red area shown in Figure 4.13e.

I explore the impacts of the seasonality strength ϵ, the period of seasonality γ, the queen laying her maximum number of eggs at time ψ, and the parasitism effects ω on the colony survival and population dynamics. I perform the following simulation in Figure 4.13 on the basin's attractions of our honeybee-parasite model 4.3. I set the queen laying her maximum number of eggs at time $\psi = 0$ to observe the impacts of γ and ϵ.

1. When the period of the seasonality is small, i.e., $\gamma = 4$, comparisons of areas of basin attractions for the colony survival among Figure 4.13e (no seasonality), 4.13a (the seasonality strength $\epsilon = 0.2$) suggest that small seasonality strength ϵ may not significantly impact the survival of the colony much but larger seasonality strength ϵ can generate larger population amplitude (see Figure 4.13f).

2. When the period of the seasonality is in the intermediate range, e.g., $\gamma = 40$, comparisons of areas of basin attractions for the colony survival among Figure 4.13e (no seasonality), 4.13c (the seasonality strength $\epsilon = 0.2$) and 4.13d (the seasonality strength $\epsilon = 0.5$) suggest that seasonality strength ϵ seems to suppress the survival of the colony.

3. When the seasonality strength ϵ is fixed, increasing the period of the seasonality γ seems to suppress the survival of the colony (See Figures 4.13a & 4.13c and Figures 4.13b & 4.13d).

4. The large γ and ϵ would lead to the colony collapsing as I observe that the colony collapses when $\gamma > 60$.

Let the period of the seasonality be $\gamma = 40$, and the strength of the seasonality be $\epsilon = 0.2$. I explore the impacts of the timing of the maximum egg-laying rate ψ by varying ψ=0, 15($< \frac{\gamma}{2} = 20$), 35($> \frac{\gamma}{2} = 20$) in Figure 4.14. I observe that the basin attractions for the colony survival seem to have similar shapes: the largest area is $\psi = 0$ (Figure 4.14a), the second largest being $\psi = 35$ (Figure 4.14c), and the smallest one is $\psi = 15$ (Figure 4.14b). The observation under this particular parameter set regarding the impacts of ψ of our honeybee-parasite model 4.3 seems to show similar trends as our honey bee only model 4.4 (see Figure4.3). Figure 4.14d provides some visual insights on how γ and ϵ impact population dynamics.

Let the period of the seasonality be $\gamma = 40$, and the strength of the seasonality be $\epsilon = 0.2$. I explore the impacts of the parasitism by varying $\omega \in [0.1, 0.35]$ in Figure 4.15. I observed the following:

1. When the parasitism ω is small (e.g., $\omega = 0.1$), the honey bee can survive while the parasite dies out (see Figure 4.15a).

2. When parasitism is increased to $\omega = 0.292$, colonies can survive with parasitism, but the area of basins of attractions for survival decreases as parasitism increases (see Figure 4.15a, 4.15b & 4.15c). Thus parasitism has a negative influence on the colonies' survival.

3. When the parasitism is large (e.g., $\omega > 0.3$ when $u_0 = 5, v_0 = 0.04$), colonies collapse.

I observe that (1) If the colony can survive, increasing the parasitism attack degree can decrease the average population of honey bees. (2) Large parasitism can lead to a colony collapsing. In general, Seasonality with parasitism can have negative impacts in terms of either decreasing the average honey bee population or the colony collapsing.

Without seasonality, the value of parasitism rate ω can lead to destability through hopf-bifurcation (see Theorem 4.3.6). To further explore how parasitism may impact the honeybee population dynamics with or without seasonality, I perform bifurcation on the impacts of parasitism $\omega = [0.2, 0.33]$ with (see Figure 4.15e) or without (see Figure 4.15f) seasonality by setting $\bar{r}_0 = 1$, $\bar{d}_h = 0.2$, $\bar{d}_m = 0.21$, $\psi = 0$, $\gamma = 40$, $\epsilon = 0.2$, $\hat{K} = 4.49$, $u(0) = 5$ and $v(0) = 0.04$.

In the absence of seasonality (Model 4.3), the ω_3 is the bifurcation value where the mite-free equilibrium $((\bar{N}_h^*, 0))$ changes from being locally stable to unstable (see The-

orem 4.3.5 item (2)), and the coexistence of bee and mite population emerges as the locally stable interior equilibrium, and the interior equilibrium become unstable (see Theorem 4.3.5 item (3)) through supercritical Hopf-bifurcation at ω_4, where exists the stable limit cycle (see Theorem 4.3.6). After the value of ω_5, the colony collapses. Therefore, the bifurcation diagram in Figure 4.15f) suggests that: (1) when the severity of parasitism (ω) is small, the colony survives with non-parasites; (2) when the value of ω rises, bees and parasites coexist in the colony and gradually decreases the population of bees; (3) under the conditions of supercritical Hopf-bifurcation, bees and parasites coexist in a periodic state; (4) when ω is large enough, the parasites leads to the colony collapse.

In the seasonality model (Model 4.4 and see Figure 4.15e), before the value of ω_1, the system is locally stable around mite-free solutions (see Theorem 4.4.1); after this bifurcation point, bees and parasites coexist as the periodic interior solutions. The ω_2 is the critical value when the colony collapses.

I observe that seasonality can delay the impact of parasitism in two bifurcation points: (1) $\omega_1 > \omega_3$: parasite needs larger attacking rates to survive in the periodic environment. And (2) $\omega_2 > \omega_5 > \omega_4$: colony can still survive with the larger attacking rates from parasites in the periodic environment.

4.5 Conclusion

Studies [Chen *et al.*, 2021; Ullah *et al.*, 2021; Vanbergen, 2021; Vercelli *et al.*, 2021] suggest that pollinators like honey bees are facing a crisis of dwindling numbers due to combinations of stressors. In this paper, I proposed and studied a non-autonomous, nonlinear differential equations model that describes the interactions between honey bees and parasites while including seasonality in the queen's egg-laying rate. The seasonality logistics are adopted from the literature [Chen *et al.*, 2020a; Messan *et al.*, 2021, 2018]. The proposed model with related theoretical and bifurcation analysis aims to address how 1) seasonality can influence honey bee colony dynamics? 2) parasitism impact honey bee colonies? and 3) seasonality and parasitism jointly influence honey bee colonies?

I first explored the seasonality impacts on the honey bee colony. Our theoretical results (Theorem 4.3.3) imply that the egg-laying rate plays an important role in determining the colony's survival. If the egg-laying rate is low, the colony is expected to die. When egg laying is not low, the colony's fate depends on the initial population size in varied seasonal conditions. Our mathematical analysis of the honeybee-parasite model (4.3) in a constant environment shows that parasitism most likely has negative impacts on honeybee population dynamics and the survival of the colony. Our theoretical work on Model (4.3) indicates that parasites decrease the honeybee population (Theorem 4.3.5) and destabilize the dynamics through subcritical or supercritical Hopf-bifurcation (see Theorem 4.3.6). The Hopf-bifurcation is determined by the queen egg-laying rate r_0, death rates of both honeybee d_h and parasite d_m and parasitism ω. More specifically, the colony collapses through supercritical Hopf-

bifurcation, and the colony has fluctuating population dynamics through supercritical Hopf-bifurcation.

Seasonality in this paper is defined by its strength of seasonality $\epsilon \in [0, 1]$, period γ, and timing of the maximum queen egg-laying rate ψ. These three factors are intertwined and generate complicated impacts on honeybee population dynamics with or without parasitism. Our study shows that seasonality can have both negative and positive influences on honeybee colony survival, depending on conditions. The colony is more likely to collapse when the period of seasonality (γ) is limited, and the strength of seasonality (ϵ) is large (see Figure 4.2). In the absence of parasitism, the colony may benefit from the seasonality when the timing of the maximum egg-laying (ψ) is larger than half of the period of seasonality (γ), i.e. $\psi > \frac{\gamma}{2}$ (see Figure 4.3). In the presence of parasites, the impacts of the timing of the maximum egg-laying (ψ) are much more complicated. Depending on other parameters' values, in some cases, the smaller timing of the maximum egg-laying (ψ) or closer to the γ may benefit the colony survival (see Figure 4.9& 4.14). There are also situations that are beneficial to the colony when growing ψ in the beginning ($\epsilon = 0.2$ in Figure 4.9).

As shown by our model and results, seasonality plays a significant role in honey bee colony dynamics. Seasonality can affect bees' behavior and resources. Bees tend to visit flowers more frequently and forage more actively in warm and favorable weather rather than in cold and harsh weather [Tuell and Isaacs, 2010]. Ogilvie and Forrest (2017) [Ogilvie and Forrest, 2017] have also highlighted the crucial role of floral resources in determining bee community growth rates and foraging decisions,

suggesting that periodic seasonal changes can help bee communities recover. However, because of climate change, there are seasonality changes, such as a longer period of low flowering abundance in mid-summer, which negatively affects bees [Aldridge *et al.*, 2011]. Moreover, studies have shown that Africanized bees are better adapted to low-shade habitats than native bees in Mexico, indicating that hotter or longer summers because of seasonality or climate change is unfriendly for native bees [Jha and Vandermeer, 2009]. Bees can adapt to seasonal changes by altering their brood production and lifespan throughout the year [Jha and Vandermeer, 2009; Feliciano-Cardona *et al.*, 2020]. These phenomena all reflect that the impact of seasonality on bee populations is complex and tied to factors both within the colony and in the environment.

Seasonality also affects the reproduction and spread of parasites. Jack et al. (2023) [Jack *et al.*, 2023] pointed out that reducing the Varroa mites' population in the spring is important for long-term mite control. Winter also can be an effective time for treating Varroa because there is no brood, and all mites are feeding on adult bees and therefore exposed to the miticide. However, interrupting brood rearing in the fall may not be an effective strategy for mite control by [Jack *et al.*, 2020], as mite populations increase after treatment [Jack *et al.*, 2023]. These findings are consistent with the conclusion of our model, which underscores the complex impacts of seasonality on bee-parasite dynamics. At present, seasonal temperatures are rising due to climate change, and will affect resource availability, bee abundance, and varroa parasitism especially in the fall [Smoliński *et al.*, 2021]. Our model can predict the different fates of bee colonies by changing the seasonal parameters of the egg-laying

rate. Such research underscores the importance of studying the effects of seasonality, and our research further highlights the need for investigation to quantify these impacts mathematically.

Bifurcations and simulations (see Figure 4.8b) suggest that a larger strength of seasonality ϵ leads to a larger amplitude in population oscillating dynamics. Large strength of seasonality ϵ alone can cause colony collapse, especially when the colony exhibits oscillations due to parasitism (see Figure 4.13). Both our theoretical and bifurcation (see Figures 4.15e & 4.15f) results show that parasitism with or without seasonality can lead to the colony collapsing and decrease the average population dynamics of honey bees.

As bee numbers continue to decline, it is crucial to understand the factors that can help honeybees face these threats and/or help them mitigate these ecological disturbances. Strong evidence suggests that climate changes contribute greatly to pollinators' population decline. Seasonality is one aspect of climate change. Our current work and literature [Chen *et al.*, 2020a; Messan *et al.*, 2021, 2018] provide useful insights into how seasonality in the queen egg-laying rate and parasites impact honeybee colonies. Our study suggests that these impacts can be positive or negative depending on the environment. Based on our results, it is possible to develop specific strategies to take advantage of the positive impacts and avoid situations when certain attributes of seasonality lead to colony collapsing or population decreasing. For example, beekeepers may regulate the honeybee population by altering the timing and amount of the egg-laying rate through the amount of food such as sugar and

pollen fed to the colonies. Seasonality affects parasite reproduction, maturation, and transmission rates of the viruses they carry. Colony losses might be reduced if the beekeeper can actively respond to the colonies' needs by observing the colonies' situation, she/he can help the colony to reduce or even eliminate the impacts of seasonality with well-timed treatments [Piot *et al.*, 2022; Vercelli *et al.*, 2021].

Climate change has been considered one of the current significant threats to honey bees and beekeeping [Flores *et al.*, 2019]. As beekeepers have observed in the past ten years, climate impacts on honeybees include scarcity of floral resources and greater spread of disease [Vercelli *et al.*, 2021]. Climate change affects the flowering period, directly affecting foraging and resource gathering through weather conditions, extreme heat, and shifts in the timing and duration of bloom. Available nectar and pollen affect brood rearing and colony growth impacting both colony survival and pollination services [Vercelli *et al.*, 2021; Reddy *et al.*, 2012], potentially affecting societal risk and prolonging exposure to more extreme events within a season [Agency, 2021]. Including seasonality in our model is the first step towards studying the impacts of climate changes on honeybee colonies. To better understand how climate change affects the seasonality of bee behavior, including brood rearing, colony growth, and foraging. There is a need for further field studies that provide data to validate our models and direct our future work.

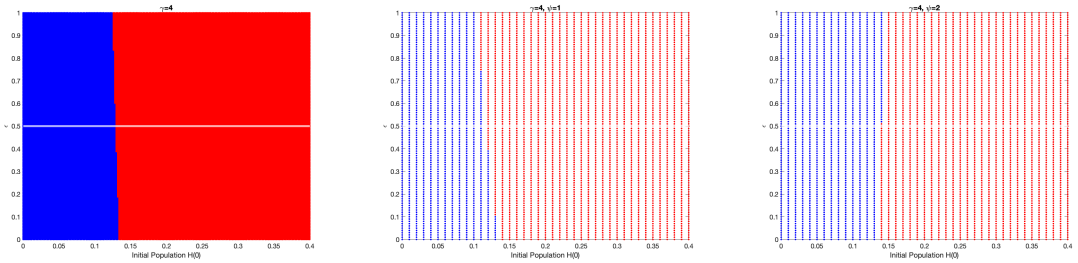

(a) $\gamma = 4, \psi = 0$ (b) $\gamma = 4, \psi = 1$ (c) $\gamma = 4, \psi = 2$

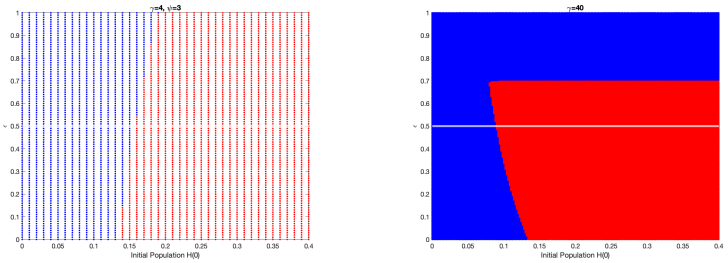

(d) $\gamma = 4, \psi = 3$ (e) $\gamma = 40, \psi = 0$

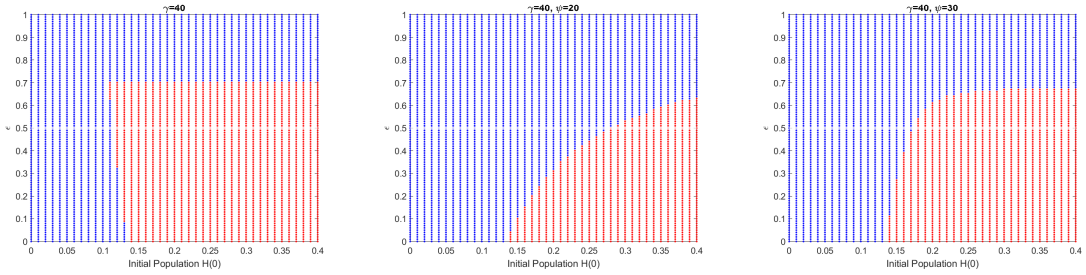

(f) $\gamma = 40, \psi = 10$ (g) $\gamma = 40, \psi = 20$ (h) $\gamma = 40, \psi = 30$

Figure 4.3: Impacts of the maximum laying rate (ψ). The blue area is colony collapse and the red area is colony survival. The horizontal line is the dividing line between ϵ in results 1 and 3. $r_0 = 1$, $\bar{d}_h = 0.5$ and $\hat{K} = 1/4$. Honey bee initial population is $u_0 \in [0, 0.4]$

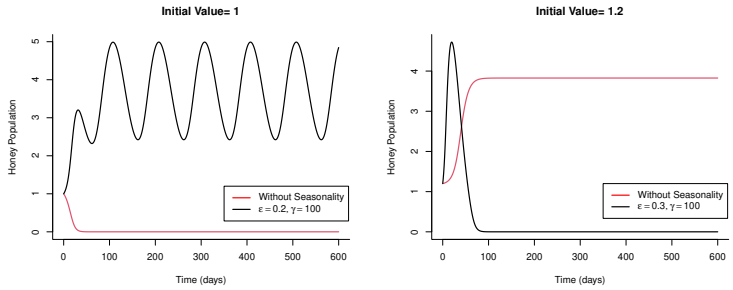

(a) Seasonality promotes honey bee survival

(b) Seasonality leads to the colony collapsing

Figure 4.4: Comparison examples of seasonality having positive or negative effects in the honey bee colony survival without parasitism. Red curves are honey bee populations without seasonality and black curves are honey bee populations with seasonality.

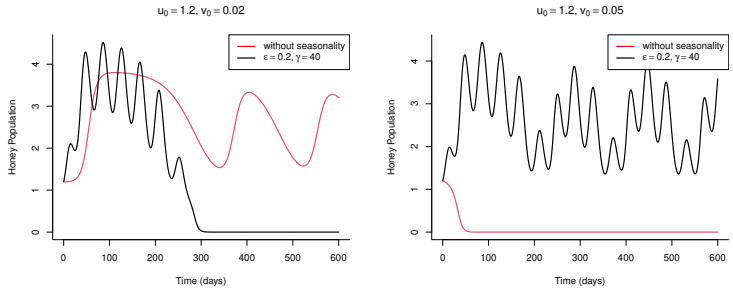

(a) Seasonality promotes honey bee survival

(b) Seasonality leads to the colony collapsing

Figure 4.5: Comparison examples of seasonality having positive or negative effects in the honey bee colony survival with parasitism. Red curves are the honey bee populations without seasonality and black curves are the honey bee population with seasonality.

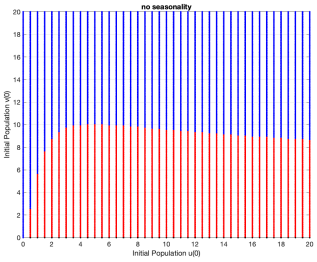

(a) no seasonality

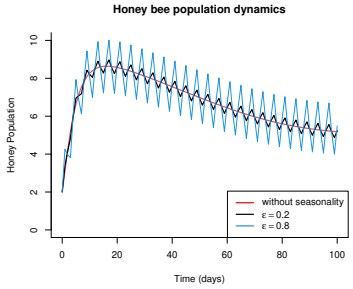

(b) Honey bee Population for those three cases

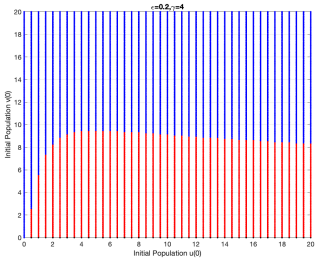

(c) $\gamma = 4, \epsilon = 0.2$

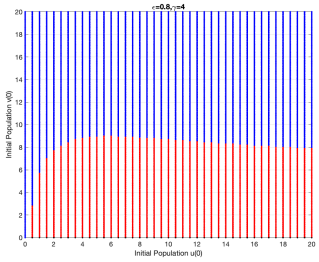

(d) $\gamma = 4, \epsilon = 0.8$

Figure 4.6: Impacts of seasonality on the honey bee colony survival when the period of seasonality γ is large; and $\bar{r}_0 = 2.86$, $\bar{d}_h = \bar{d}_m = 0.25$, $\omega = 0.3$ and $\hat{K} = 2.04$ and $\psi = 0$. Initial population is $u_0 \in [0, 20]$, and $v_0 \in [0, 20]$. The blue area is the basin attraction that leads to colony collapse, while the red area is the basin attraction the colony can survive.

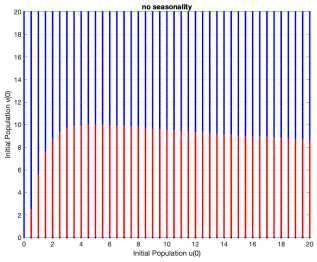

(a) no seasonality

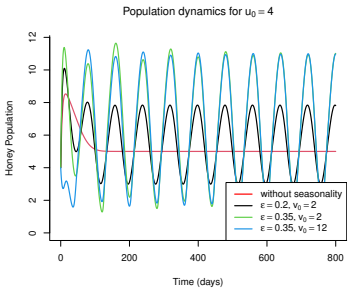

(b) Population Dynamics

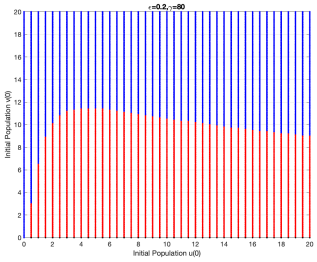

(c) $\gamma = 80, \epsilon = 0.2$

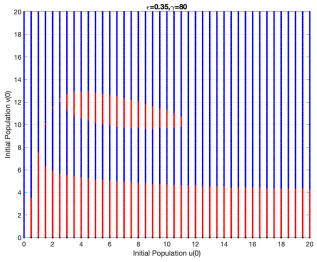

(d) $\gamma = 80, \epsilon = 0.35$

Figure 4.7: Impacts of seasonality on the honey bee colony survival when the period of seasonality γ is intermediate; and $\bar{r}_0 = 2.86$, $\bar{d}_h = \bar{d}_m = 0.25$, $\omega = 0.3$ and $\hat{K} = 2.04$ and $\psi = 0$. Initial population is $u_0 \in [0, 20]$, and $v_0 \in [0, 20]$. The blue area is the basin attraction that leads to colony collapse, while the red area is the basin attraction the colony can survive.

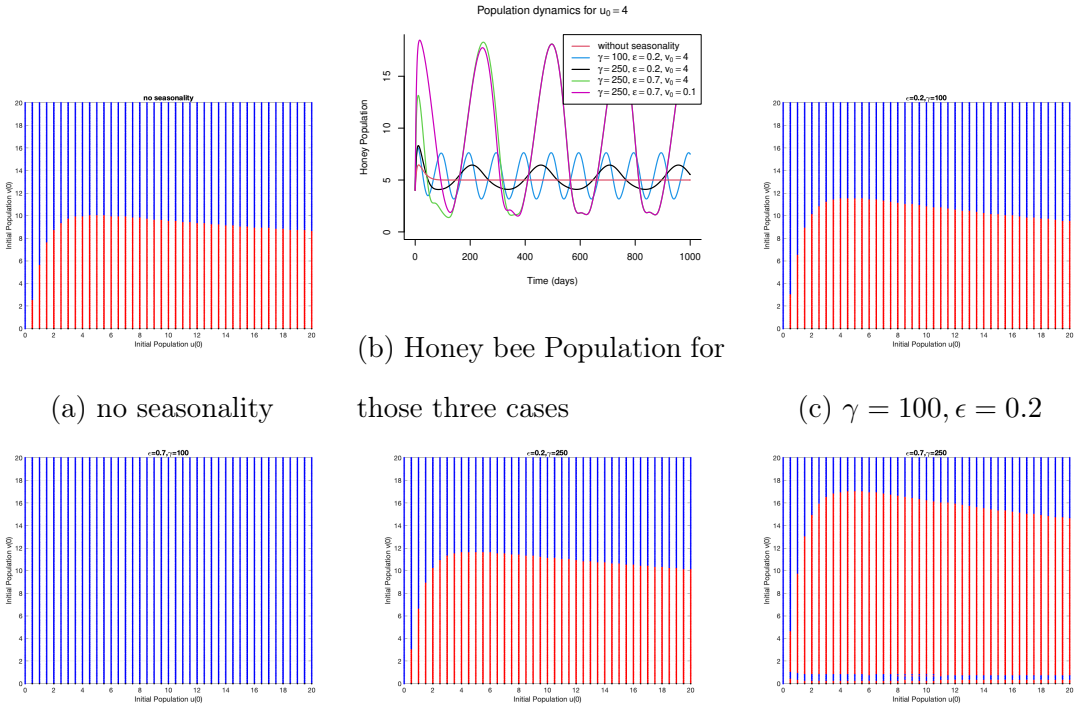

(a) no seasonality

(b) Honey bee Population for those three cases

(c) $\gamma = 100, \epsilon = 0.2$

(d) $\gamma = 100, \epsilon = 0.7$

(e) $\gamma = 250, \epsilon = 0.2$

(f) $\gamma = 250, \epsilon = 0.7$

Figure 4.8: Impacts of seasonality on the honey bee colony survival when the period of seasonality γ is small; and $\bar{r}_0 = 2.86$, $\bar{d}_h = \bar{d}_m = 0.25$, $\omega = 0.3$ and $\hat{K} = 2.04$ and $\psi = 0$. Initial population is $u_0 \in [0, 20]$, and $v_0 \in [0, 20]$. The blue area is the basin attraction that leads to colony collapse, while the red area is the basin attraction the colony can survive.

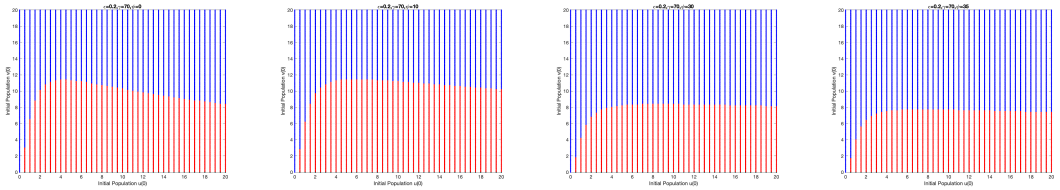

(a) $\epsilon = 0.2, \psi = 0$ (b) $\epsilon = 0.2, \psi = 10$ (c) $\epsilon = 0.2, \psi = 30$ (d) $\epsilon = 0.2, \psi = 35$

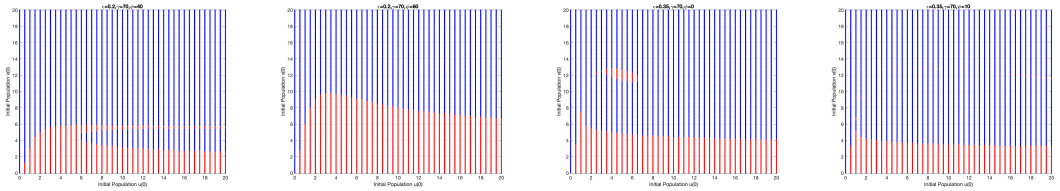

(e) $\epsilon = 0.2, \psi = 40$ (f) $\epsilon = 0.2, \psi = 60$ (g) $\epsilon = 0.35, \psi = 0$ (h) $\epsilon = 0.35, \psi = 10$

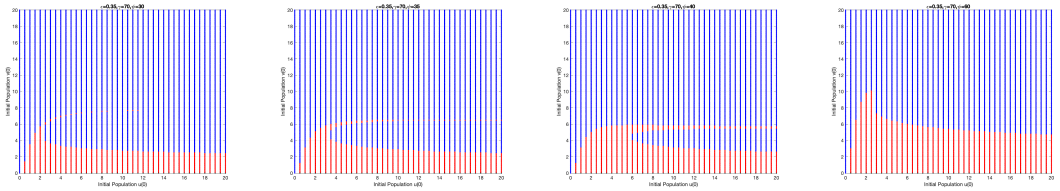

(i) $\epsilon = 0.35, \psi = 30$ (j) $\epsilon = 0.35, \psi = 35$ (k) $\epsilon = 0.35, \psi = 40$ (l) $\epsilon = 0.35, \psi = 60$

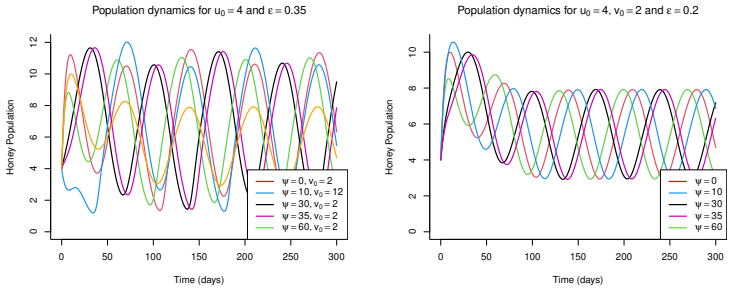

(m) Honey bee population dynamics for $\epsilon = 0.35$ (n) Honey bee population dynamics for $\epsilon = 0.2$

Figure 4.9: Impacts of the timing of the maximum egg-laying rate (ψ). The blue area is colony collapse, and the red area is colony coexistence. $\bar{r}_0 = 2.86$, $\bar{d}_h = \bar{d}_m = 0.25$, $\omega = 0.3$, $\hat{K} = 2.04$, and $\gamma = 70, \epsilon = 0.2\&0.35$ Honey bee initial population is $u_0 \in [0, 20]$, and mite initial population is $v_0 \in [0, 20]$

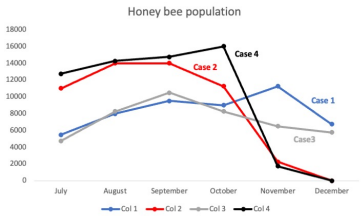

(a) honey bee population

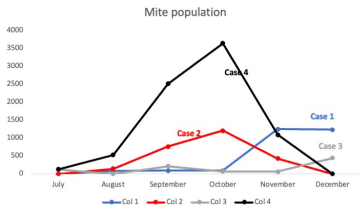

(b) Population Dynamics

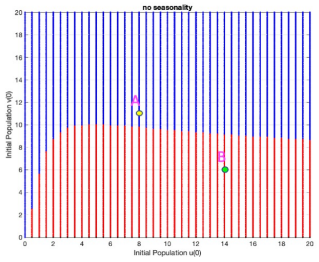

(c) no seasonality

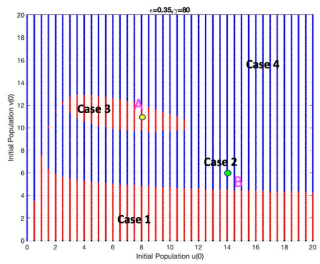

(d) $\gamma = 80, \epsilon = 0.35$

Figure 4.10: Figure 4.10a: the total bee population of four colonies from July to December. Colonies 1 (Case 1, blue) and 3 (Case 3, gray) survive, and Colonies 2 (Case 2, red) and 4 (Case 4, black) collapse. Figure 4.10b: the total mite population in four colonies from July to December. Colonies had different initial populations. Figure 4.10c: the simulation result from Figure 4.7a with two signed points A and B. Figure 4.10d: the simulation result from Figure 4.7d with two signed points A and B and cases. These four cases correspond to Figure 4.10a & 4.10b colonies.

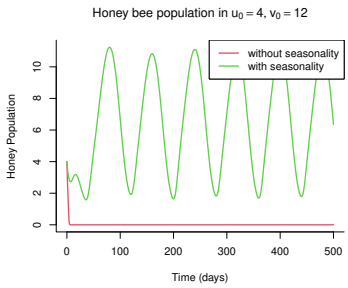

(a) Point A bee population

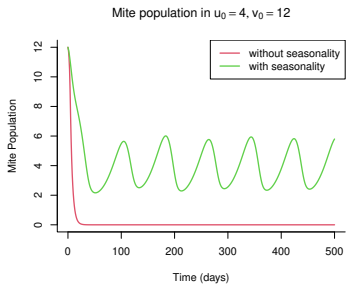

(b) Point A mite population

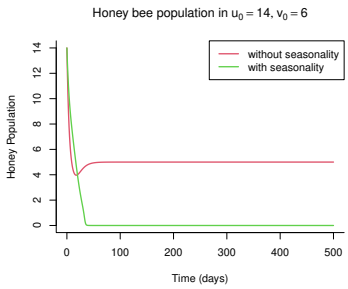

(c) Point B bee population

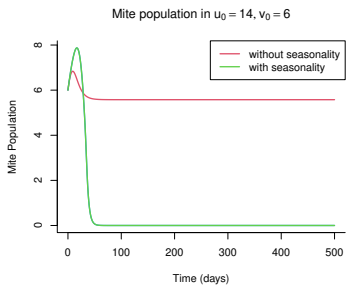

(d) Point B mite population

Figure 4.11: Colony dynamics with time series. These point A and point B correspond with Figure 4.10c & 4.10d. Point A: seasonality leads the colony from collapsing to survive. Point B: seasonality leads the colony from survival to collapse.

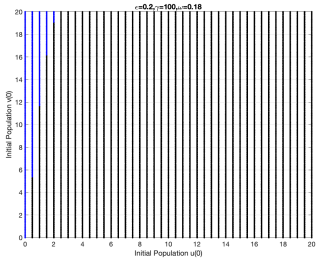

(a) $\omega = 0.18, \epsilon = 0.2$

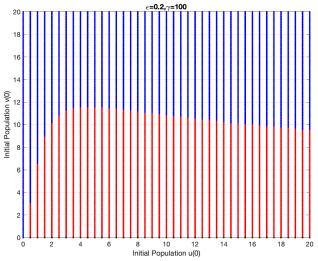

(b) $\omega = 0.3, \epsilon = 0.2$

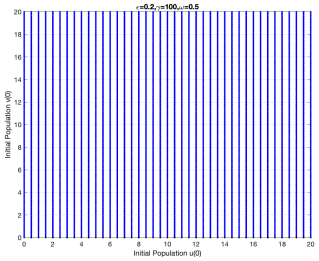

(c) $\omega = 0.5, \epsilon = 0.2$

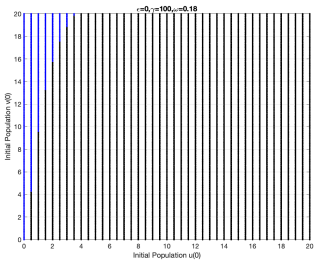

(d) $\omega = 0.18, \epsilon = 0$

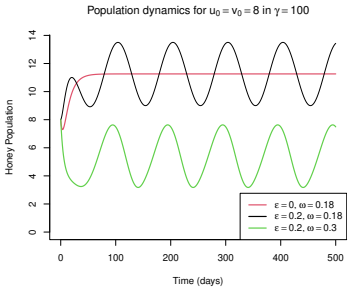

(e) Population Dynamics

Figure 4.12: Impacts of parasitism (ω) on the colony dynamics of honeybee-mite model (4.2). The blue area is colony collapse, the red area is colony coexistence, and the black area is only bee survive with $\bar{r}_0 = 2.86$, $\bar{d}_h = \bar{d}_m = 0.25$, $\gamma = 100$, $\psi = 0$, $\epsilon = 0.2$ and $\hat{K} = 2.04$. Honey bee initial population is $u_0 \in [0, 20]$, and mite initial population is $v_0 \in [0, 20]$

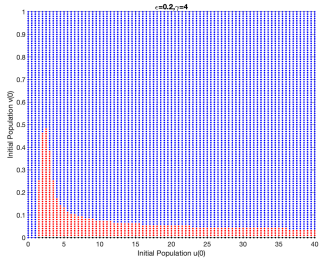

(a) $\gamma = 4, \epsilon = 0.2$

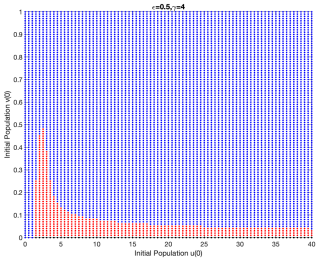

(b) $\gamma = 4, \epsilon = 0.5$

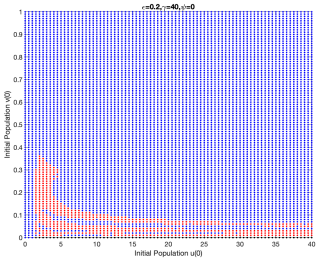

(c) $\gamma = 40, \epsilon = 0.2$

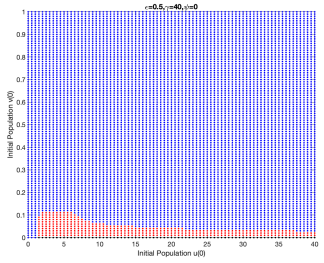

(d) $\gamma = 40, \epsilon = 0.5$

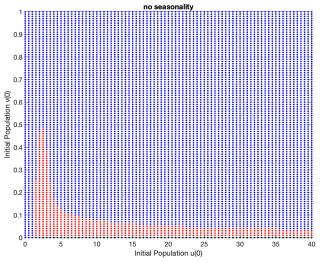

(e) no seasonality

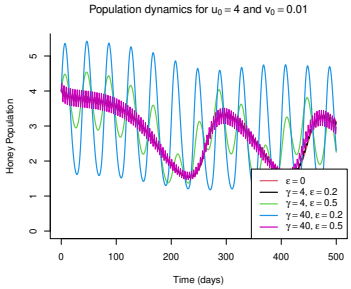

(f) Honey bee population dynamics

Figure 4.13: Impacts of seasonality on the stable limit cycle: the strength of seasonality ϵ and the period of seasonality γ when $\bar{r}_0 = 1$, $\bar{d}_h = 0.2$, $\bar{d}_m = 0.21$, $\omega = 0.3$, $\psi = 0$, and $\hat{K} = 4.49$. Honey bee initial population is $u_0 \in [0, 40]$, and mite initial population is $v_0 \in [0, 1]$. The blue area is colony collapse, and the red area is colony coexistence.

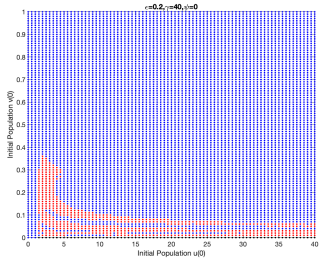

(a) $\gamma = 40, \psi = 0$

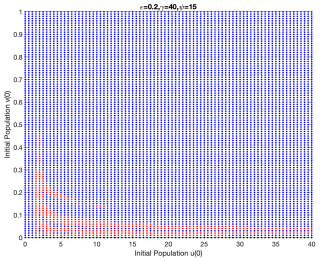

(b) $\gamma = 40, \psi = 15$

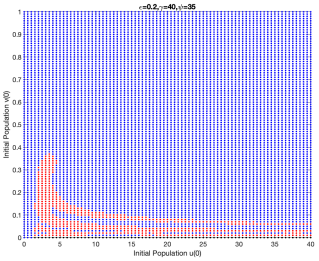

(c) $\gamma = 40, \psi = 35$

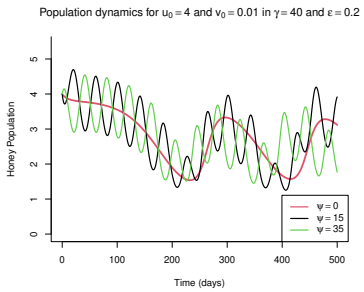

(d) Honey bee population dynamics

Figure 4.14: Impacts of seasonality on the stable limit cycle: the timing of the maximum egg-laying rate ψ when $\bar{r}_0 = 1$, $\bar{d}_h = 0.2$, $\bar{d}_m = 0.21$, $\omega = 0.3$, $\gamma = 40$, $\epsilon = 0.2$, and $\hat{K} = 4.49$. Honey bee initial population is $u_0 \in [0, 40]$, and mite initial population is $v_0 \in [0, 1]$. The blue area is colony collapse, and the red area is colony coexistence.

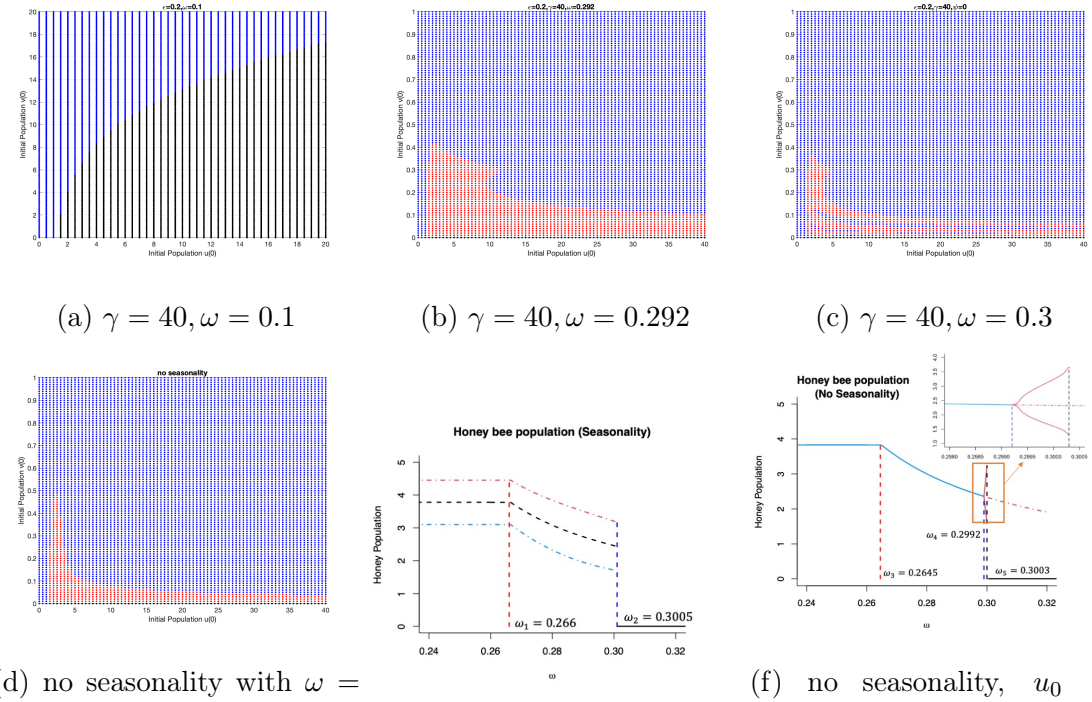

(a) $\gamma = 40, \omega = 0.1$ (b) $\gamma = 40, \omega = 0.292$ (c) $\gamma = 40, \omega = 0.3$

(d) no seasonality with $\omega = 0.3$ (e) $\gamma = 40$, $u_0 = 5$,$v_0 = 0.04$ (f) no seasonality, $u_0 = 5$,$v_0 = 0.04$

Figure 4.15: Impacts of seasonality and parasitism on the stable limit cycle when $\bar{r}_0 = 1$, $\bar{d}_h = 0.2$, $\bar{d}_m = 0.21$, $\gamma = 40$, $\psi = 0$, $\epsilon = 0.2$ and $\hat{K} = 4.49$. Honey bee initial population is $u_0 \in [0, 40]$, and mite initial population is $v_0 \in [0, 1]$. The blue area is colony collapse, the red area is colony coexistence, and the black area is only bee survival. Figure 4.15e: Max and min honey bee population with seasonality. The red dot-dashed curve indicates the maximum bee population of the period, and the blue dot-dashed curve indicates the minimum bee population of the period. The black dashed curve shows the average of the max and min population. Figure 4.15f: Max and min honey bee population without seasonality. The blue solid curve indicates the locally stable equilibrium, the red solid curve indicates the stable limit cycle of the Hopf-bifurcation, and the red dot-dashed curve indicates the source equilibrium. The black dashed line indicates the critical of ω, which makes the colony survive to collapse. The orange square zooms in the Hopf-bifurcation details. Both figures: The black lines indicate collapse. The red and blue indicate critical values of ω.

Chapter 5

IMPACTS OF PESTICIDES ON HONEY BEE DYNAMICS

Abstract

Honey bees (Apis mellifera) are essential pollinators whose health has been impacted by pesticides from crops that are transported into honey bee nests via pollen. We developed a delay differential equation model with age structures to investigate the complex relationship between pesticides and honey bee population dynamics. Our work integrates theoretical analysis, simulation, and experimental data to show that (1) egg-laying rate, death rates, and environmental conditions are pivotal factors influencing colony survival; (2) pesticides impact adult mortality in a linear regression manner; and (3) pesticides have effects on the time of the maximum laying rate, and the adult-larval pollen consumption ratio. The implications of our findings merit further exploration. Overall, our study underscores the significance of applying models to biological systems, offering crucial and new insights for understanding and managing complex interactions between pesticides and honey bees.

Honey bees play a vital role in crop pollination, but their global population is facing a significant decline. In the U.S., their numbers plummeted by approximately 60% from 1947 to 2008, dropping from 5.9 million to 2.3 million Potts *et al.* [2010]; Smith *et al.* [2013]. This decline can be attributed to various factors, with pesticides being a major environmental stressor Fisher *et al.* [2017]; Chmiel *et al.* [2020]. While scientists typically rely on experiments, averages, and statistical methods to understand the impact of pesticides on honey bees, our study takes another approach. We

integrate a dynamic system with experimental data to derive parameter values, allowing us to understand the intricate relationship between pesticides and bee populations.

Bees, crops, and pesticides form a complex interplay that underpins modern agriculture. The economic value of these pollinated crops is staggering, estimated at around $215 billion annually worldwide VanEngelsdorp *et al.* [2008]. Notably, certain crops like almonds, blueberries, and apples heavily rely on honey bee pollination. Pesticides, which encompass a range of formulations, including insecticides, herbicides, acaricides, and fungicides, are indispensable tools in safeguarding crop yields against various pests and diseases. However, bees face pesticide exposure through crucial activities like pollination and nectar collection. For instance, fungicides can induce symptoms similar to malnutrition and weaken colonies, making honey bees more vulnerable to additional stressors such as parasites and pathogens Degrandi-Hoffman *et al.* [2015]. Pesticides can compromise the immunity of developing queens, subsequently reducing the emergence rate DeGrandi-Hoffman *et al.* [2013]. Insecticides, particularly neonicotinoids, pose a significant risk to pollinators. These chemicals can lead to hyperresponsiveness in honey bees from either acute or chronic exposure. Acute exposure can cause increased flight time and distance, causing difficulties in returning to the colony Tosi *et al.* [2017]; Williamson *et al.* [2014]. Chronic exposure can result in neurological damage, manifested as reduced flight speed and duration, along with impaired navigation abilities Chmiel *et al.* [2020]; Tosi *et al.* [2017].

Pesticides affect bees in complex ways. Residues from different pesticides on various crops can combine, leading to a subtler but significant threat for bee colonies

Fisher *et al.* [2023]; Mullin *et al.* [2010]; Traynor *et al.* [2021]; Sánchez-Bayo *et al.* [2016]. This highlights the importance of comprehending the overall impact of pesticide use on bees. Studies have shown that fungicides are the most commonly found agrochemicals in honey bee colonies Johnson *et al.* [2013, 2010]. Fungicides, such as Pristine ®, have been observed to decrease both the lifespan of worker bees and the overall population of the colony. Notably, this detrimental effect was observed at field-relevant concentrations Fisher II *et al.* [2021]. Immature bees exposed to pesticides can experience health effects during their adult stage Tome *et al.* [2020]. The complex effects of pesticides on honey bees, particularly at sublethal exposures, make it challenging to measure in the field. However, using mathematical models can provide insights into short and long-term impacts on colony dynamics and survival.

Research on pesticide exposure of honey bees that have incorporated mathematical models can be divided into two parts: traditional mathematical modeling and computational modeling Chen *et al.* [2021]. Magal et al. consecutively published two papers describing the effects of pesticides on honey bees using traditional mathematical modeling Magal *et al.* [2019, 2020b]. Magal et al. (2019) Magal *et al.* [2019] developed a discrete-time model to describe the effects of homing failure in foraging honey bees from pesticide exposure. They found that the fraction of exposed foragers showing homing failure determined colony survival. Magal et al. (2020) Magal *et al.* [2020b] extended their previous model with the spatial distribution of contaminated and uncontaminated foragers. They found that if foragers were more likely to make multiple visits to pesticide-contaminated food resources, colony collapse would follow. In a computational model examining the effects of pesticides on different life stages of

honey bees, it was shown that adult mortality has a greater impact on colony survival than egg-laying rates or larval mortality Rumkee et al. (2015) Rumkee *et al.* [2015].

In this study, we provide a delay differential equations model and fit it with experimental data to investigate the influence of varying pesticide doses on the population dynamics of honeybee colonies. Our examination approaches this issue from two perspectives: 1) the effect of different pesticide levels on the consumption of pollen by larvae and adult bees, and 2) how various pesticide levels impact the immature and adult bees and colony survival. The structure of the remaining article is as follows: Section 2 provides a comprehensive overview of the dynamic model linking honeybee colonies and pollen consumption established through experimentation. In Section 3, we conduct a mathematical analysis of the model. In Section 4, we fit our model using experimental data to delve into the repercussions of pesticide levels on colony dynamics. Finally, in Section 5, we present the conclusions that can be drawn from our study.

5.1 Model Derivation

This section focuses on modeling the honey bee colony dynamics and pollen consumption based on the cyclic pattern of a honey bee colony. We separate the brood level into three age levels (egg, larvae, and pupae). Let $p(t)$ be the gram of the pollen remaining in the patty, $E(t)$ be the egg population, $L(t)$ be the larvae population, $P(t)$ be the pupae population, $A(t)$ be the adult population. We have the following assumptions:

A1: Each colony receives 150g pollen patty every week Fisher II *et al.* [2021], i.e.

In(t) = 150/7 g/day. We simplified the relationship between pollen intake and the honey bee population by type I functional response: $\alpha * p *$ population, where α is the rate at which honey bees consume pollen patties.

A2: Only larvae and adult bees consume the pollen, the population in the function response is $L(t)$ and $A(t)$ respectively, and α_L and α_A respectively indicate the rate of larva and adult bees consume pollen patties.

A3: The new population term has is $r(t)*\frac{A(t)^2}{K+A(t)^2+\beta E(t)}$ because (1) the queen bee lays egg every day by $r(t)$ rate; (2) the cooperative brood care from adult bees that perform nursing and collecting food for brood and (3) the queen and workers that regulate the actual egg laying/survival based on the currently available egg population Chen *et al.* [2020a]. Therefore, the parameter $\sqrt{K}$ indicates the colony size at which the brood survival rate is half maximum, and β indicates the regulation effects of the brood.

A4: The egg laying rate $r(t)$ is time based. The literature work Chen *et al.* [2021] suggests that food, temperature, weather, and oviposition place would affect the queen Bodenheimer [1937]; Khoury *et al.* [2011]; DeGrandi-Hoffman *et al.* [1989]. From experimental data Fisher II *et al.* [2021] and studies Chen *et al.* [2020a]; Messan *et al.* [2021]; Chen *et al.* [2023], function good applies to the egg-laying rate, which is

$$r(t) = r_0(1 + \epsilon \cos(\frac{2\pi(t-\psi)}{\gamma})), \epsilon \in [0, 1],$$

where r_0 indicates the base line egg-laying rate, ϵ indicates the strength of environment, γ indicates the duration of environmental effect on egg-laying rate and ψ indicates the time of the maximum laying rate.

A5: In the experiment, the r the pollen was replaced immediately after consumption Fisher II *et al.* [2021] so the food source is unlimited. Therefore, colony growth is not affected by food availability.

A6: We assume both brood and adult bees have constant mortality, d_E, d_L, d_P and d_A, respectively. The maturation time from egg E to larvae L is denoted by τ_e. Similarly, τ_l and τ_p are the maturation time from larvae to pupae and from pupae to adults, respectively. After that, the survival rate of eggs during time τ_e is $e^{-d_B\tau}$.

Following our previous work Chen *et al.* [2020a] and our assumptions, we construct the model by three compartmental models, which are pollen remaining (p), egg population (E), larvae population (L), pupae population (P), and adult population (A):

$$
\begin{aligned}
\underbrace{\frac{dp}{dt}}_{\substack{\text{Pollen}\\ \text{remaining}}} &= \underbrace{In(t)}_{\text{Pollen input by day}} - \underbrace{\alpha_L p L}_{\text{Larvae pollen consumption}} - \underbrace{\alpha_A p A}_{\text{Adult pollen consumption}} \\
\underbrace{\frac{dE}{dt}}_{\text{Egg}} &= \underbrace{\frac{r(t)A(t)^2}{K+A(t)^2+\beta E(t)}}_{\text{Newborns}} - \underbrace{d_E E}_{\text{Egg death}} \underbrace{- e^{-d_E\tau_e}\frac{r(t-\tau_e)A(t-\tau_e)^2}{K+A(t-\tau_e)^2+\beta E(t-\tau_e)}}_{\text{Merge to Larvae}} \\
\underbrace{\frac{dL}{dt}}_{\text{Larvae}} &= \underbrace{e^{-d_E\tau_e}\frac{r(t-\tau_e)A(t-\tau_e)^2}{K+A(t-\tau_e)^2+\beta E(t-\tau_e)}}_{\text{Merge from Larvae}} - \underbrace{d_L L}_{\text{Larvae death}} - e^{-d_L\tau_l}e^{-d_E\tau_e}\frac{r(t-\tau_e-\tau_l)A(t-\tau_e-\tau_l)^2}{K+A(t-\tau_e-\tau_l)^2+\beta E(t-\tau_e-\tau_l)} \\
\underbrace{\frac{dP}{dt}}_{\text{Pupae}} &= e^{-d_L\tau_l}e^{-d_E\tau_e}\frac{r(t-\tau_e-\tau_l)A(t-\tau_e-\tau_l)^2}{K+A(t-\tau_e-\tau_l)^2+\beta E(t-\tau_e-\tau_l)} - \underbrace{d_P P}_{\text{Pupae death}} \\
&- e^{-d_P\tau_p}e^{-d_L\tau_l}e^{-d_E\tau_e}\frac{r(t-\tau_e-\tau_l-\tau_p)A(t-\tau_e-\tau_l-\tau_p)^2}{K+A(t-\tau_e-\tau_l-\tau_p)^2+\beta E(t-\tau_e-\tau_l-\tau_p)} \\
\underbrace{\frac{dA}{dt}}_{\text{Adult}} &= e^{-d_P\tau_p}e^{-d_L\tau_l}e^{-d_E\tau_e}\frac{r(t-\tau_e-\tau_l-\tau_p)A(t-\tau_e-\tau_l-\tau_p)^2}{K+A(t-\tau_e-\tau_l-\tau_p)^2+\beta E(t-\tau_e-\tau_l-\tau_p)} - \underbrace{d_A A}_{\text{Adult death}}
\end{aligned}
\tag{5.1}
$$

After that, we perform parameter estimations and model validations based on data. We implement the least-squares statistic parameter sweep method as our fitting

method to the honeybee population data to attain parameter estimates. Essentially, we randomly parameters by Latin hypercube sample with appropriate ranges (see Table 5.1). After that, we performed data fitting on the above model in Tree 5 with different levels of pesticides. The results show in Figure 5.1 and parameters values show in Table 5.2.

Our biologically meaningful parameters align with the value ranges established by previous biologists and mathematicians (refer to Table 5.1)). Our parameters were fitted under these settings and achieved good outcomes (see Figure 5.1). Hence, our model enables us to investigate the impact of pesticides on honey bee dynamics. In the subsequent sections, we will study the colony dynamics through theoretical analysis and explore the influence of pesticides through the outcomes of data fitting of all colonies by statistical methods.

5.2 Mathematical Analysis

Now, we focus on the condition of the colony's survival. Let (p,E,L,P,A) be the equilibrium of Model 5.1, and simplify egg-laying rate to constant $r(t) = r$. Then, it satisfies the following equations:

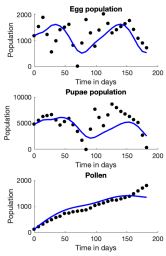

(a) Control group, history population $p(\theta) = 111.16$, $E(\theta) = 1186$, $L(\theta) = 1669$, $P(\theta) = 4801$, $A(\theta) = 7340$, for all $\theta \in [-\tau, 0]$. LSE=0.1973

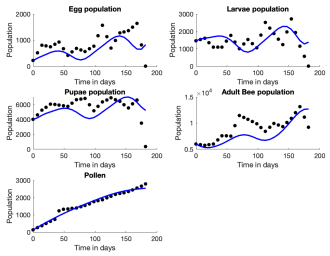

(b) 0.23ppm group, history population $p(\theta) = 139.53$, $E(\theta) = 219$, $L(\theta) = 1462$, $P(\theta) = 4018$, $A(\theta) = 5970$, for all $\theta \in [-\tau, 0]$. LSE=0.2276

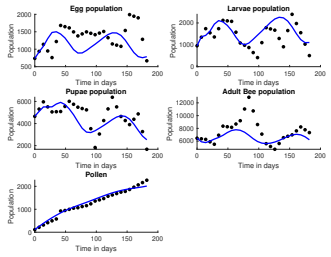

(c) 2.3 ppm group, history population $p(\theta) = 114.75$, $E(\theta) = 737$, $L(\theta) = 956$, $P(\theta) = 4651$, $A(\theta) = 6460$, for all $\theta \in [-\tau, 0]$. LSE=0.2935

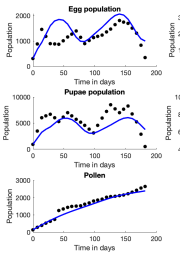

(d) 23 ppm group, history population $p(\theta) = 145.03$, $E(\theta) = 311$, $L(\theta) = 956$, $P(\theta) = 956$, $A(\theta) = 6530$, for all $\theta \in [-\tau, 0]$. LSE=0.2181

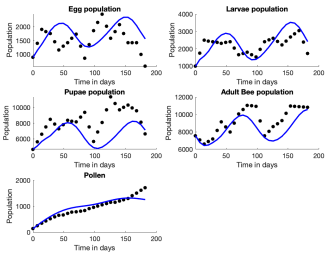

(e) 230 ppm group, history population $p(\theta) = 134.93$, $E(\theta) = 887$, $L(\theta) = 990$, $P(\theta) = 4663$, $A(\theta) = 7555$, for all $\theta \in [-\tau, 0]$. LSE=0.3577

Figure 5.1: The fitting results of 5 single colonies with different concentrations of pesticides around Tree 5. LSE indicates the least square error. Black dots are experimental data, and blue curves are our model fitting.

$$
\begin{aligned}
0 &= In(t) - \alpha_L pL - \alpha_A pA && (5.2)\\
0 &= \frac{rA^2}{K + A^2 + \beta E} - d_E E - e^{-d_E \tau_e} \frac{rA^2}{K + A^2 + \beta E} && (5.3)\\
0 &= e^{-d_E \tau_e} \frac{rA^2}{K + A^2 + \beta E} - d_L L - e^{-d_E \tau_e} e^{-d_L \tau_l} \frac{rA^2}{K + A^2 + \beta E} && (5.4)\\
0 &= e^{-d_E \tau_e} e^{-d_L \tau_l} \frac{rA^2}{K + A^2 + \beta E} - d_P P - e^{-d_E \tau_e} e^{-d_L \tau_l} e^{-d_P \tau_p} \frac{rA^2}{K + A^2 + \beta E} && (5.5)\\
0 &= e^{-d_E \tau_e} e^{-d_L \tau_l} e^{-d_P \tau_p} \frac{rA^2}{K + A^2 + \beta E} - d_A A && (5.6)
\end{aligned}
$$

Eqt.(5.4) and Eqt.(5.6) give

$$d_E E = (1 - e^{-d_E \tau_e}) * \frac{rA^2}{K + A^2 + \beta E}$$

and

$$d_A = e^{-d_E \tau_e} e^{-d_L \tau_l} e^{-d_P \tau_p} \frac{rA}{K + A^2 + \beta E}$$

with

$$\frac{rA^2}{K + A^2 + \beta E} = \frac{d_A A}{e^{-d_E \tau_e - d_L \tau_l - d_P \tau_p}},$$

then solve Eqt.(5.4) to get

$$E = e_1 * \frac{d_A}{d_E} * A \tag{5.7}$$

and solve Eqt.(5.6) by

$$d_A = \frac{e_2 r d_E}{d_E(K + A^2) + \beta e_1 d_A A} * A$$

to get

$$
\begin{aligned}
A_i &= \frac{e_2 r d_E - e_1 d_A^2 \beta \pm \sqrt{-4 d_A^2 d_E^2 K + (e_2 r d_E - e_1 d_A^2 \beta)^2}}{2 d_E d_A} \\
&= \frac{e_2 r}{2 d_A} - \frac{e_1 d_A \beta}{2 d_E} \pm \sqrt{-K + \frac{e_2^2 r^2}{4 d_A^2} + \frac{e_2^2 d_A^2 \beta^2}{4 d_E^2} - \frac{e_1 e_2 r \beta}{2 d_E}}, i = 1, 2
\end{aligned} \tag{5.8}
$$

where $e_1 = e^{d_L\tau_l + d_P\tau_p}(e^{d_E\tau_e} - 1)$ and $e_2 = e^{-d_E\tau_e - d_L\tau_l - d_P\tau_p}$, and $A_1 \leq A_2$. Use E and A_i to solve Eqts.(5.5) and (5.6):

$$L_i = \frac{A_i^2 d_E e^{-d_E\tau_e - d_L\tau_l}(-1 + e^{d_L\tau_l})r}{d_L(A_i^2 d_E + d_E K + A_i e_1 d_A \beta)}, i = 1, 2 \tag{5.9}$$

and

$$P_i = \frac{A_i^2 d_E e_2(-1 + e^{d_P\tau_p})r}{d_P(A_i^2 d_E + d_E K + A_i e_1 d_A \beta)}, i = 1, 2. \tag{5.10}$$

After that, solve Eqt.(5.3):

$$p_i = In * \frac{1}{\alpha_A A_i + \alpha_L L_i}, i = 1, 2.$$

Now we have the following proposition:

Proposition 5.2.1. *[Existence of Interior Equilibria] If* $r > \frac{2d_A d_E\sqrt{K} + e_1 d_A^2 \beta}{e_2 d_E}$, *then Model* (5.1) *has two interior equilibria* E_i^*, $i = 1, 2$*:*

$$\begin{aligned} E_i^* &= (p_i, E_i, L_i, P_i, A_i) \\ &= \left(\frac{In}{\alpha_A A_i + \alpha_L L_i}, \frac{e_1 d_A A_i}{d_E}, \frac{A_i^2 d_E e_3(-1 + e^{d_L\tau_l})r}{d_L\Omega}, \frac{A_i^2 d_E e_2(-1 + e^{d_P\tau_p})r}{d_P\Omega}, A_i\right) \end{aligned}$$

where $e_1 = (e^{d_E\tau_e} - 1)e^{d_L\tau_l + d_P\tau_p}$, $e_2 = e^{-d_E\tau_e - d_L\tau_l - d_P\tau_p}$, $e_3 = e^{-d_E\tau_e - d_L\tau_l}$ *and* $\Omega = A_i^2 d_E + d_E K + A_i e_1 d_A \beta$. *If* $r = \frac{2d_A d_E\sqrt{K} + e_1 d_A^2 \beta}{e_2 d_E}$, *then Model* (5.1) *has an unique interior equilibrium* E^* *with* $A_i = \frac{e_2 r d_E - e_1 d_A^2 \beta}{2 d_E d_A}$.

Note: Proposition 5.2.1 implies the necessary conditions for the honeybee colony survival is $r > \frac{2d_A d_E\sqrt{K} + e_1 d_A^2 \beta}{e_2 d_E}$ which requires the value of the queen egg laying rate r be large, the egg regulation effect β be small, and the death rate of adult d_A be small. In addition, the ratio of egg E to adult population A is determined by their mortality and maturation time through the equation $\frac{e_1 d_A}{d_E}$.

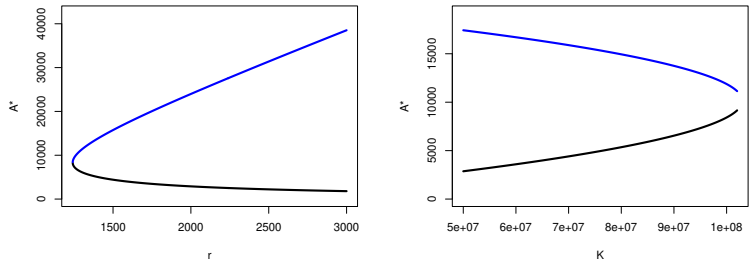

(a) $r \in [1241,\ 3000]$ (b) $K \in [5 * 10^7,\ 1 * 10^8]$

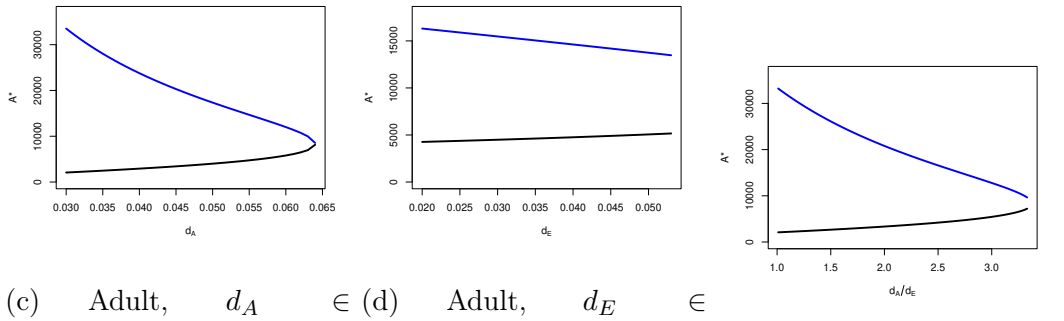

(c) Adult, $d_A \in [0.03,\ 0.0649]$ (d) Adult, $d_E \in [0.02,\ 0.053]$ (e) Adult, $\frac{d_A}{d_E} \in [1.01,\ 3.33]$

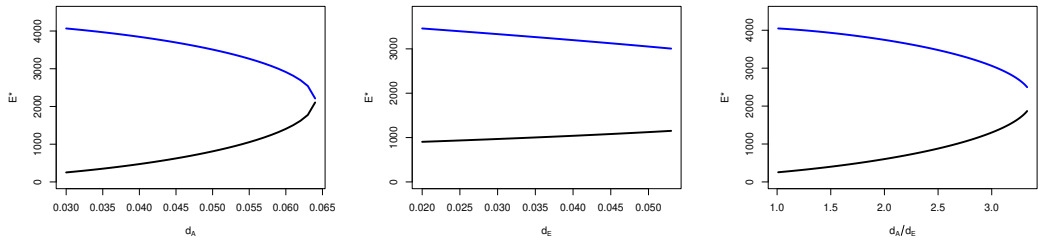

(f) Egg, $d_A \in [0.03,\ 0.0649]$ (g) Egg, $d_E \in [0.02,\ 0.053]$ (h) Egg, $\frac{d_A}{d_E} \in [1.01,\ 3.33]$

Figure 5.2: Bifurcation diagrams of Model (5.1) with constant egg-laying rate. Figure 5.2a-5.2e are for the interior equilibrium A_i^*, $i = 1, 2$ (see Eqt.(5.8)). Figure 5.2f-5.2h are for the interior equilibrium E_i^*, $i = 1, 2$ (see Eqt.(5.7)). Blue curves indicate stable equilibrium, and black curves indicate unstable equilibrium. The fixed parameters' value are $r = 1499$, $K = 69,545,190$, $d_E = 0.027$, $d_L = 0.001$, $d_P = 0.021$, $d_A = 0.053$, $\beta = 15$, $\tau_e = 3$, $\tau_e = 6$ and $\tau_e = 12$.

Figure 5.2 shows bifurcation diagrams of Model (5.1) with constant egg-laying rate regarding: a) Equilibrium (E_1, L_1, P_1, A_1) is an increasing function of K, d_A and d_E, and decreasing function of r. b) Equilibrium (E_2, L_2, P_2, A_2) is decreasing function of K, d_A and d_E, and increasing function of r. Those bifurcation diagrams indicate that: 1) The survival of the colony hinges on a large queen egg-laying rate (r), resulting in a population of eggs and adult individuals with its increase. 2) Changes in the half-saturation coefficient (K) or any mortality rate (d_E or d_A) can potentially trigger colony collapse, resulting in a decline in the adult population relative to these parameter increases.

Our model is based on experimental data. Honey bees can harvest all the pollen and nectar they need, so we assume food resources do not affect colony growth. If we consider bee-only dynamics in our Model (5.1), we will have:

Theorem 5.2.1. *[Stability of Extinction Equilibrium] The extinction equilibrium E_0^* of Model 5.1 without pollen (bee-only model) is always locally asymptotically stable.*

Note: Figure 5.3 emphasizes the significance of the initial conditions, which can determine whether the colony thrives or collapses. Comparing Figure 5.3a and 5.3b, at the beginning of nesting, the number of adult bees is more important than the number of pupae.

The following section will provide our detailed study on how pesticide impacts honey bee population dynamics combined with experimental data.

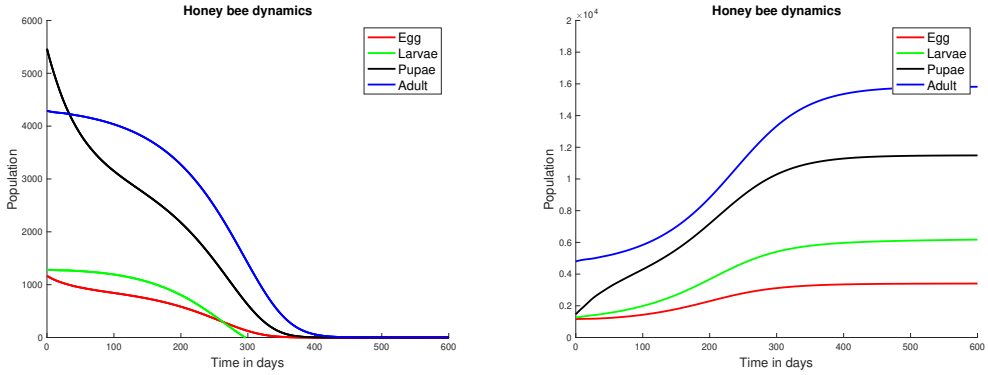

(a) $E_0 = 1166$, $L_0 = 1278$, $P_0 = 5463$ and $A_0 = 4289$ (b) $E_0 = 1166$, $L_0 = 1278$, $P_0 = 1463$ and $A_0 = 4800$

Figure 5.3: Time series of the population of egg (red), larvae (green), pupae (black), and adult (blue) bee for Model (5.1) with constant egg-laying rate $r = 1510$, and other parameters used by $K = 69,545,190$, $\beta = 15$, $d_E = 0.027$, $d_L = 0.001$, $d_P = 0.021$, $d_A = 0.053$, $\alpha_L = 6.48 * 10^{-8}$, and $\alpha_A = 9.77 * 10^{-7}$. Figure 5.3a shows the colony collapses and Figure 5.3b shows the colony survives with the same parameters' value and different initial population.

5.3 Impacts of Pesticide

In the experiment, the maximum pollen consumed by the colony is 150 grams per week. Then we assume to give 150 grams of pollen to one colony every week and weigh the remaining patties to estimate the daily amount of pollen consumed $\frac{150\ g}{7\ days}$. We fit 40 colonies, the range of least square error is [0.1820, 0.6928], and the average of 40 fitting results is 0.2934. Among them, for single colony fitting, 230ppm of tree 2 is the poorest fit, and 2.3 ppm of tree 3 is the best fit; for different concentrations, the control group shows the best fit (average is 0.2479), and the 230 ppm group is worst (average is 0.3785). All fittings are set by constant history functions. In this section, we will categorize our parameters into different groups to demonstrate how we employ mathematical models to examine the impacts of pesticides.

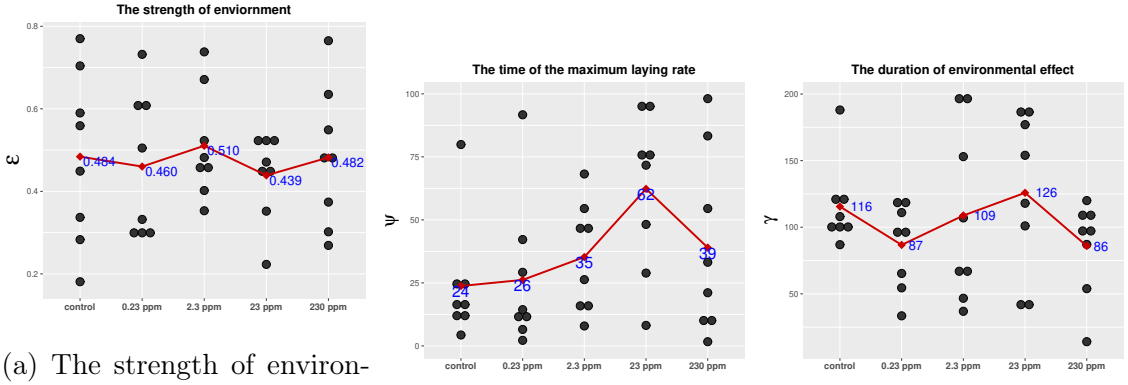

(a) The strength of environment

(b) The time of the max-rate

(c) The length of the period

Figure 5.4: Effects of pesticides on environment factors of egg-laying rate. Black dots are the parameter values for 40 colonies. The red diamond lines present the average value of parameters in the egg-laying rate time base function in different pesticide concentrations (8 colonies per group). There are no significant differences between groups. Only Figure5.4b without outliers is a significant difference between the control and treatment groups, but no significant effect by the level of pesticides.

First, we analyze the value of parameters in the egg-laying rate time-based function (see A4 and Figure 5.4). We used ANOVA to test the five groups by three parameters (ϵ, ψ, and γ). There was no significant dose-dependent effect for the three values (P-value > 0.05). The average of the magnitude of the environmental effect (ϵ) is 0.48, the average of the time of the maximum laying rate (ψ) is 38 days, and the average of the duration of environmental effect on egg-laying rate (γ) is 106 days. However, the three parameters' values have outliers. We also did statistical analyses for the data by removing the outliers. The magnitude of the environmental effect (ϵ) and the duration of the environmental effect (γ) were not significantly affected by pesticides. By ANOVA test, the time of the maximum laying rate (ψ), the mean of groups is unequal, but there is no significant concentration depending. Therefore, the pesticides can affect the time of the maximum laying rate between the

control and treatment groups.

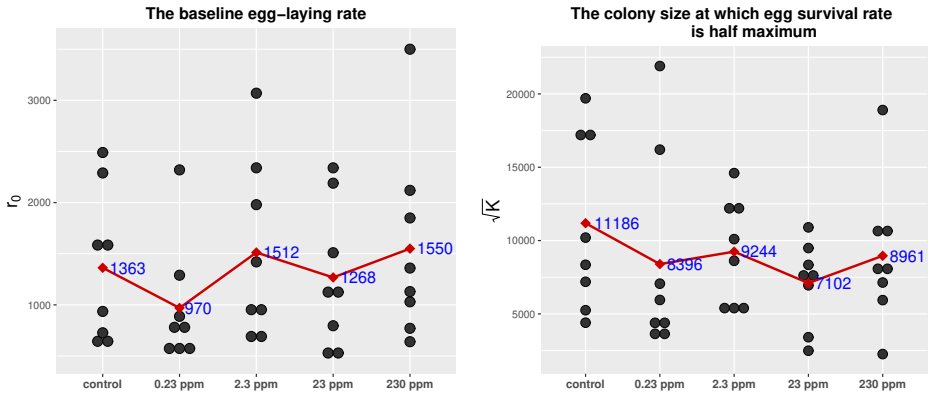

(a) The baseline egg-laying rate (b) The half-saturation coefficient

Figure 5.5: Effects of pesticides on the baseline egg-laying rate (r_0) and the colony size at which egg survival rate is half maximum ($\sqrt{K}$) in different level pesticide concentrations (8 colonies per group). Black dots are the parameter values for 40 colonies. The red diamond lines present the average value of parameters. There are no significant differences between groups.

Then, we determined whether the baseline egg-laying rate is pesticide-related (see Figure 5.5a). The statistical test shows there is no significant difference between the mean values. In addition, we can observe from Figure 5.5b that the $\sqrt{K}$ of the control group is larger than other pesticide groups, but there is no significant dose-dependent effect on the colony size at which egg survival rate is half maximum in the statistical test. When there is no significant difference in egg-laying rate, the reason for the larger control population may be affected by mortality or survival rate.

Our data also suggest a possible mechanism by which fungicides may cause these negative effects on colony demography. Brood mortality fluctuates under different concentrations of pesticides (see Figure 5.6a - 5.6c). Observing the data, the per-

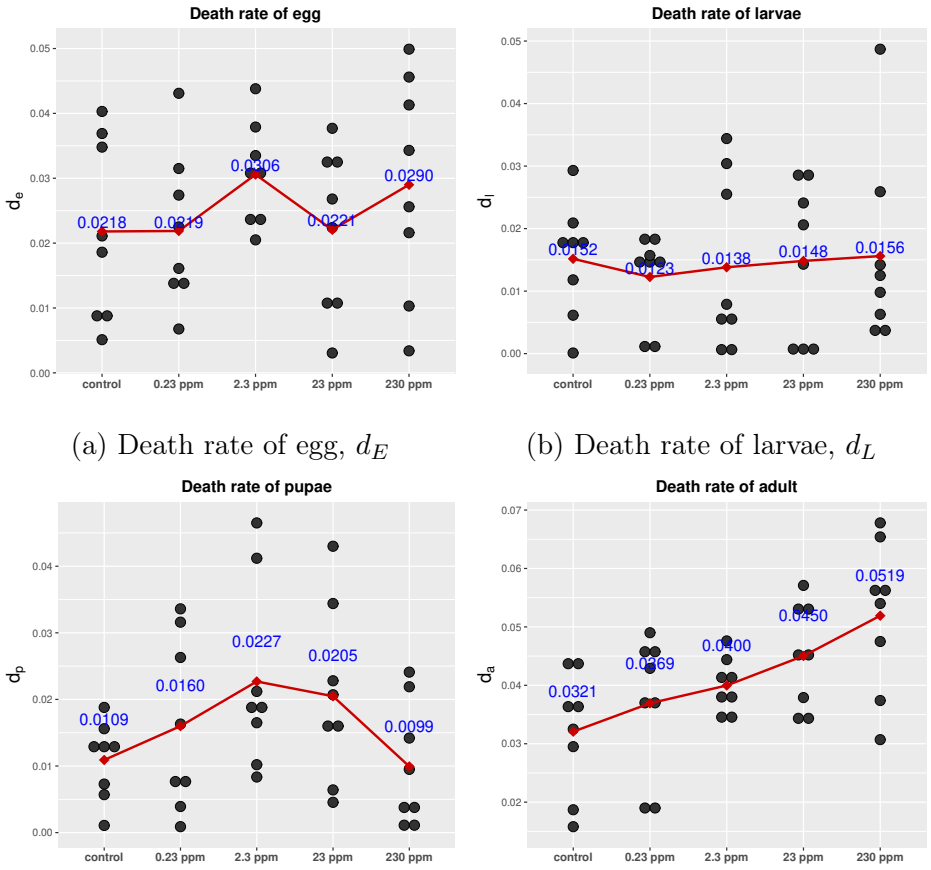

(a) Death rate of egg, d_E

(b) Death rate of larvae, d_L

(c) Death rate of pupae, d_P

(d) Death rate of adult, d_A

Figure 5.6: Effects of pesticides on different death rates. Black dots are the parameter values for 40 colonies. The red diamond lines present the average value of parameters. There are no significant differences between groups in Figure 5.6a - Figure 5.6c. The death rate of adults has significant differences between means of different levels of pesticides.

formance of larvae death in each group is almost the same, and the change range of pupae death is the largest. However, statistical tests show no significant difference among the means (P-value > 0.05). Through the test, there is a significant difference among the means of adult mortality (d_A) (P-value < 0.01). From Figure 5.6d, it can be observed that as the concentration increases, the death rate of adults increases, and the test of linear regression between levels and adult death rate is significant.

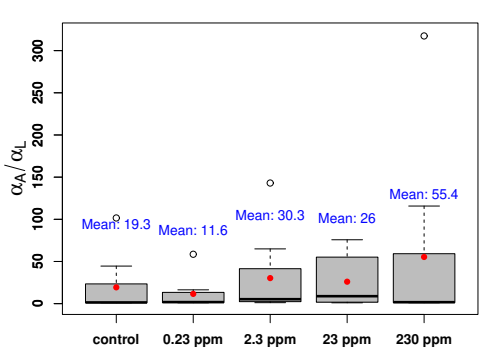

(a) Boxplot by groups with outliers

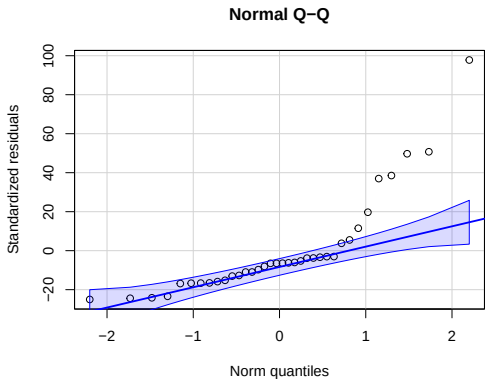

(b) Visually test normality of residuals

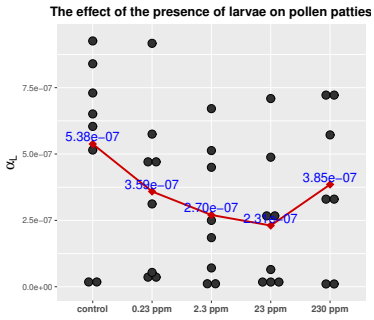

(c) The effect of the presence of larvae on pollen patties, α_L

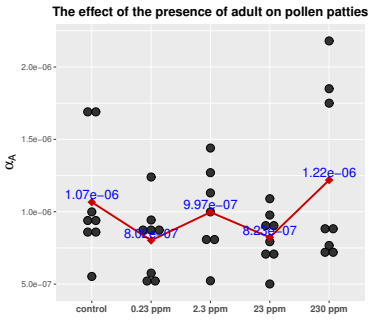

(d) The effect of the presence of adult on pollen patties, α_A

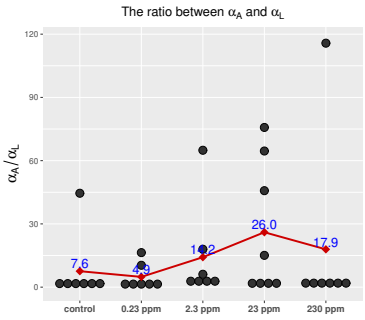

(e) Adults consume pollen in multiples of larvae consume

Figure 5.7: Data visualized for pollen consumption. Fig.5.7a and Fig.5.7b use the values from α_A/α_L to plot boxplot and Q-Qplot. The boxplot shows four outliers, the Q-Qplot shows that data do not come from a normal distribution, and the blue shadow is a confidence band. Fig.5.7c - 5.7e show the result of each colony by dots, and the red diamonds are the mean of each group.

In Model (5.1), the effect on adults feeding on pollen patties with pesticides is greater than larvae Fisher II *et al.* [2021]. The effect of the presence of larvae on pollen patties (α_l) is lower as the pesticide level increases, until 230 ppm, the effect rate grows up (see Figure 5.7c). However, the ANOVA test shows there are no signifi-

cant differences among groups (P-value=0.29), and there are no significant differences (P-value=0.18) in mean between groups of the effect of the presence of adult on pollen patties (α_a). In addition, we also consider the relationship between the ratio of these two variables (α_A/α_L). In Figure 5.7a, treatment groups (2.3 ppm to 230 ppm) have higher ratios than the control group. Removing the outliers (see Figure 5.7e) causes the ratio to increase as the pesticide level increases (from 0.23 ppm to 23 ppm). We test the data as non-normality (P-value < 0.01 in the Shapiro-Wilk test), and apply Kruskal-Wallis tests. The results show that all groups may originate from the same distribution (P-value = 0.27).

Model (5.1) and table 5.1 show effect rates (α_L & α_A, per bee per day). If we remodel pollen remaining equation to $\frac{dp}{dt} = In(t) - \hat{\alpha}_L * L(t) - \hat{\alpha}_A * A(t)$, where $\hat{\alpha}_L$ indicates pollen consumption per larvae per day and $\hat{\alpha}_A$ indicates pollen consumption per adult bee per day. We estimate $\hat{\alpha}_L$ by range $[1*10^{-6}, 2*10^{-2}]$ (unit: $g/(bee*day)$), and $\hat{\alpha}_A$ by range $[1*10^{-5}, 2*10^{-1}]$ (unit: $g/(bee*day)$). Then, the data fitting gives these values in Table 5.3.

The pollen consumption of larvae is [0.002, 1.39] mg/bee, and the pollen consumption of adults is [0.46, 1.84] mg/bee (see Figure 5.8. Figure 5.8a shows the control group and 230 ppm have larger variances of fitting values and significant differences between groups. Figure 5.8b shows the 230 ppm group has larger variances. The pollen patties consumption rates of larvae and adults are not significantly different among groups. The ratio between these two consumption rates has no significant relationship with the level of pesticides. The average ratio of the treatment groups (2.53) is higher than the control groups (see Table 5.3).

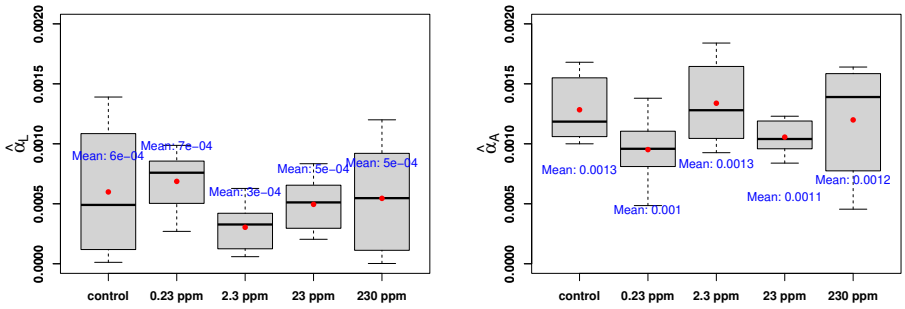

(a) The pollen patties consumption of larvae

(b) The pollen patties consumption of adult

Figure 5.8: Effects of pesticides on the pollen patties consumption of larvae and adult. The red dots present the average value of parameters (8 colonies per group). There are no significant differences between groups.

We used fitting results from 40 colonies to calculate average parameter values for each group. These averages guided our simulations, helping us observe future trends. Our simulations highlight the significant impact of pesticides on colony dynamics. Different initial populations lead to varying outcomes, determining colony survival or collapse. Notably, the 0.23 ppm concentration performed poorly in both simulations, likely due to its lower egg-laying rate (see Figure 5.5a). Additionally, we observed that 230 ppm, under high initial adult population conditions, performed similarly to 23 ppm (see red and green curves in Figure 5.9c & 5.9d). However, as the initial adult population decreased (from 6975 to 4800 in our simulation), 23 ppm colonies still survived, while those exposed to 230 ppm collapsed (see Figure 5.9a & 5.9b). This emphasizes that high pesticide concentrations can lead to colony collapse. When examining the brood population, we found the effect of pesticides was less pronounced,

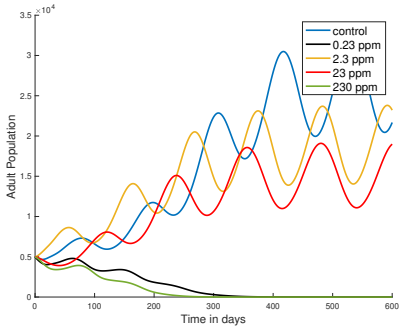

(a) Simulation of adult population

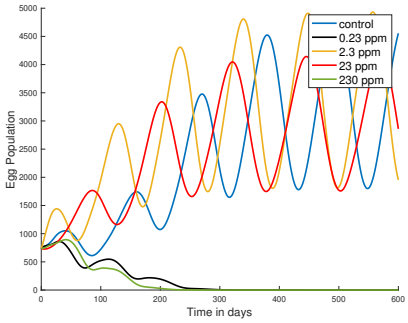

(b) Simulation of egg population

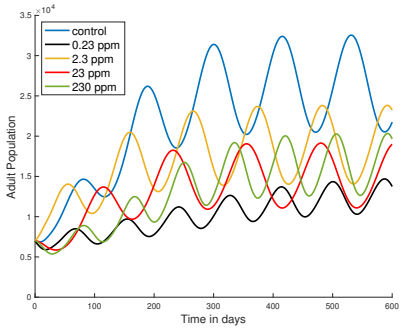

(c) Simulation of adult population

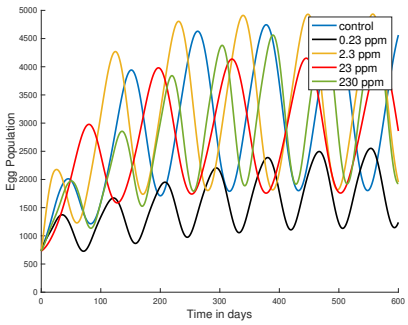

(d) Simulation of egg population

Figure 5.9: Figure 5.9a & 5.9b is a simulation by the average number of parameters in each group. Pesticides can influence colony dynamics, and a high concentration (green curves, 230 ppm) can lead to colony collapse. Figure 5.9a & 5.9b use initial population are: $E_0 = 733$, $L_0 = 1035$, $P_0 = 4798$, $A_0 = 4800$ and $p_0 = 125$. Figure 5.9c & 5.9d use initial population are: $A_0 = 6975$, other initial population is the same with Figure 5.9a & 5.9b.

except in the case of the 0.23 ppm group, where the number of eggs was notably lower, likely due to a lower egg-laying rate. Across other groups, the disparity in adult bee numbers is evident, reinforcing the apparent influence of adult bee mortality on the colony. This Simulation is consistent with our earlier statistical findings.

5.4 Conclusion

We propose a model to analyze and aims to address how pesticides impact honey bee dynamics. We integrate model analysis, data fitting, and simulation to discuss the influence of death rates, egg-laying rates, the half-saturation coefficient, pollen consumption effects, and population from pesticides.

We introduce a model incorporating age structures to characterize the experiment. By integrating theoretical concepts with experimental data, we aim to elucidate the effects of pesticides on honey bee populations. Our theoretical analysis under the constant egg-laying rate suggests that egg-laying rate, adult and egg death rates, the half-saturation coefficient, and the egg regulation effect influence colony survival (see Proposition 5.2.1). Furthermore, our bifurcation diagrams (refer to Figure 5.2 & B.2) confirm diverse dynamic outcomes. Notably, the impact of the egg-laying rate on the population differs from that of the other influencing factors. As the egg-laying rate increases, the population at the equilibrium point also rises, while others are the opposite. Both theoretical and bifurcation results underscore the substantial influence of these factors on bee dynamics.

Given the influence of environmental factors on queen reproduction Bodenheimer [1937]; Khoury *et al.* [2011]; DeGrandi-Hoffman *et al.* [1989] and the resemblance of observed data trends to a cosine function, we incorporated environmental considerations into our bee pesticide model (Model (5.1)) when fitting the data. Using parameter values derived from 40 colonies, we identified a significant correlation between adult mortality and pesticide concentration. We demonstrated an increase

with higher concentrations through linear regression (see Figure 5.6). However, no substantial difference was observed in brood-level mortality. This conclusion aligns with the findings of Fisher et al. (2021) Fisher II *et al.* [2021]. Furthermore, our model introduces a novel focal point. The timing of the maximum laying rate is influenced by pesticides (confirmed through the ANOVA test & Welch's t-test), although it is not dependent on concentration. This timing exerts a crucial and intricate impact on the colony's fate. It intertwines with environmental strength and the duration of environmental effects to shape the dynamic system of the colony Chen *et al.* [2023].

In addition to the findings above, it's worth noting that the average egg-laying rate at 0.23 ppm is lower compared to the other groups (refer to Figure 5.5a). This discrepancy may contribute to nest collapsing or lower population levels (see Figure 5.9). Upon conducting simulations with parameter averages derived from the data, we observed that pesticides reduce the number of workers in the colony Fisher II *et al.* [2021]. However, this effect does not correlate with concentration levels (see Figure 5.9). Our model indicates that the ratio of pollen consumption by adults and larvae in the control group is generally lower compared to the treatment groups, with the exception of the low-concentration group at 0.23 ppm. While this difference may not be statistically significant, it offers valuable insights for consideration. Regarding consumption rate (measured in grams per bee per day), the total consumption by bees falls within the range of 0.003 grams per bee per day Fisher II *et al.* [2021].

The alignment between our model-derived conclusions, simulation and fitting, and actual biological dynamics highlights the significant value of employing models in bio-

logical systems. This not only provides valuable insights for comprehending complex ecological interactions but also uncovers new avenues for exploration. However, it's important to acknowledge the current simplification in our model regarding pollen consumption. Presently, we assume constant consumption rates for all larvae and adults, whereas, in reality, adults consume pollen for a maximum of 8 days Haydak [1970], while larvae engage in this behavior for only half of their development period Owens and Farrar [1967]. Addressing this discrepancy in future iterations of the model will lead to a more accurate representation of bee behavior and dynamics. Moreover, our model holds the potential for extension to incorporate food sources and consider the impact of food reserves on immaturity.

Parameter	Definition	Range	Reference
α_l	the effect of the presence of larvae on pollen patties (per day per bee)	$[3 * 10^{-9}, 2 * 10^{-5}]$ $bee^{-1}day^{-1}$	Estimated by data
α_a	the effect of the presence of adult on pollen patties (per day per bee)	$[3 * 10^{-8}, 2 * 10^{-5}]$ $bee^{-1}day^{-1}$	Estimated by data
β	the regulation effects of egg	[0, 20]	Chen et al. (2020) Chen *et al.* [2020a]
$\sqrt{(K)}$	the colony size at which egg survival rate is half maximum	$K \in [1 * 10^7, 7 * 10^8]$ bees	Chen et al. (2020) Chen *et al.* [2020a], Ratti et al.(2012) Ratti *et al.* [2017]
$r(t)$	the egg laying rate based on time	$r_0 \in$ [500, 3500] bees/day	Chen et al. (2020) Chen *et al.* [2020a], Eberl et al. (2010)Eberl *et al.* [2010], Sumpter and Martin (2004) Sumpter and Martin [2004]
d_E,d_L,d_P,d_A	the death rate of egg, larvae, pupa and adult bees	[0, 0.07] day^{-1}	Chen et al. (2020) Chen *et al.* [2020a], Rueppell et al.(2007) Rueppell *et al.* [2007]
τ_e	time spent in egg	3 days	Winston (1987) Winston [1987]
τ_l	time spent in larvae	6 days	Winston (1987) Winston [1987]
τ_p	time spent in pupae	12 days	Winston (1987) Winston [1987]

Table 5.1: Biological meanings and references of parameters of Model 5.1.

		Value		Value			Value		Value
Control	r_0	2292	ϵ	0.7	0.23 ppm	r_0	2318	ϵ	0.6
	K	306,884,200	ψ	103		K	481,040,200	ψ	96
	d_E	0.0211	γ	25		d_E	0.0132	γ	29
	d_L	0.0176	β	12.71		d_L	0.0157	β	15.9253
	d_P	0.0188	α_l	$1.68 * 10^{-8}$		d_P	0.0009	α_l	$4.64 * 10^{-7}$
	d_A	0.0295	α_a	$1.7 * 10^{-6}$		d_A	0.0193	α_a	$5.15 * 10^{-7}$
2.3 ppm	r_0	3404	ϵ	0.5	23 ppm	r_0	2191	ϵ	0.5
	K	281,464,100	ψ	99		K	118,177,500	ψ	101
	d_E	0.0438	γ	21		d_E	0.0377	γ	29
	d_L	0.0079	β	7.6040		d_L	$4 * 10^{-5}$	β	19.3160
	d_P	0.0212	α_l	$7.08 * 10^{-8}$		d_P	0.0430	α_l	$4.88 * 10^{-7}$
	d_A	0.0444	α_a	$1.27 * 10^{-6}$		d_A	0.0447	α_a	$7.93 * 10^{-7}$
230 ppm	r_0	2191	ϵ	0.4					
	K	118,177,500	ψ	107					
	d_E	0.0456	γ	33					
	d_L	0.0034	β	19.3160					
	d_P	0.0095	α_l	$5.84 * 10^{-9}$					
	d_A	0.0563	α_a	$1.85 * 10^{-6}$					

Table 5.2: Parameters values for Figure 5.1.

Parameter	Control	0.23 ppm	2.3 ppm	23 ppm	230 ppm
$\hat{\alpha}_L$ (mg/[day*bee])	0.60	0.69	0.30	0.50	0.55
$\hat{\alpha}_A$ (mg/[day*bee])	1.28	0.95	1.34	1.06	1.20
Ratio ($\hat{\alpha}_A/\hat{\alpha}_L$)	2.15	1.39	4.40	2.13	2.20

Table 5.3: The average of pollen potties consumption rate in larvae and adult stage.

Chapter 6

FINAL REMARKS AND FUTURE WORK

6.1 Final Remarks

Social insects, such as ants, bees, and termites, form highly organized colonies with specialized roles and cooperative behaviors. The spatial heterogeneity degree demonstrates a linear relationship with contact dynamics, showing no sensitivity to the initial value. The dynamic spatial fidelity mechanism ensures that spatial fidelity and spatial heterogeneity degrees converge to a similar equilibrium regardless of the initial spatial fidelity value. The diverse geometric distributions of task locations significantly influence information transmission. It is evident that mathematical computer simulations offer effective control over variables, allowing for a more precise analysis of internal mechanisms. This method is also extensively utilized in bee research. The model can describe fundamental factors for colony growth [DeGrandi-Hoffman *et al.*, 1989] to study population challenges and expand the model to consider the growth of the varroa population in a colony and its impact on colony dynamics due to reduction in worker longevity [DeGrandi-Hoffman and Curry, 2004]. Models can also be used to simulate the impact of external environmental factors such as pesticides [Becher *et al.*, 2014; Abi-Akar *et al.*, 2020; Thorbek *et al.*, 2017].

Addressing the global crisis of honeybee losses will require an integrated approach to evaluate the combination of factors that culminate in the collapse of a colony population. Mathematical models serve as potent instruments in offering insights into the

contributions of different stressors to colony losses. These theoretical tools are needed to identify mechanisms that can be difficult or costly to quantify in the field and will be an essential component in developing strategies to improve colony health. My models exhibit strong Allee effects generated from the collaborative effects of colony members and colony survival when the egg-laying rate is above a certain threshold. It seems that the model with or without age structure has equilibrium dynamics, and additional age structure components in models may not contribute much to population dynamics. However, age structure may play an important role when additional mortality factors such as parasitism are included in the model.

The period of mite population increase continues through the spring and summer and peaks in the fall when brood rearing is nearly done. This makes the mites very difficult to control, especially in warmer climates where colonies maintain brood year-round DeGrandi-Hoffman and Curry [2004]. Therefore, studying the influence of seasonality and parasitism on honey bees is important. Theoretical and simulation analyses of the model reveal that seasonality exerts intricate effects on mite-infested hives and that seasonal cycles are too large to survive. This underscores the profound influence of climate change and parasites on bee populations.

Pesticides are another environmental stressor causing population reduction. The effects of pesticide exposure include a significant decrease in survival of foragers, reduced flight performance, compromised immunity, difficulty in protein digestion, and bee feeding [Fisher II *et al.*, 2020]. The mathematical modeling with experimental data reaches similar conclusions. The death rate of broods is not affected by pesti-

cides, but the death rate of adults is increasing in a linear relationship with levels of pesticides, and the control group has a higher adult population [Fisher II *et al.*, 2021]. Furthermore, the mathematical model offers novel avenues of exploration, revealing that the timing of the maximum egg-laying rate is influenced by pesticides. This finding is also reflected in chapter4. This calls for further experiments to enhance the depth of analysis. This underscores the valuable role played by mathematical models in scrutinizing experimental data and unraveling the underlying mechanisms of biological dynamic systems.

6.2 Future Work

The behavior of social insects is of great significance to research. The network approach equips us with powerful tools for investigating social insect colonies, such as honeybees, wasps, and ants. The complexity of these colonies primarily arises from local individual interactions influenced by diverse social contexts, inherent preferences, age distribution, and task allocation [Naug, 2008; Richardson and Gorochowski, 2015; Mersch *et al.*, 2013]. Chapter2 can explain a lot of problems, but the model would benefit from additional experimental data to enhance its accuracy. In the future, supplementing the model with more data will lead to more precise results and comprehensive conclusions

The decline of honey bee populations worldwide has gained substantial attention in recent years. My research has confirmed the impact of pesticides on honey bees. However, there are certain influencing relationships are not yet obvious, such as the timing of the peak egg-laying rate and environmental variables. An experimental

study on queen bees laying eggs under varying pesticide levels could shed light on the insights derived from our model. Mathematical modeling proves to be a potent and indispensable tool for elucidating the significance behind the data.

Climate change is an important factor contributing to the ongoing decline of pollinators [Halsch *et al.*, 2021]. Hence, environmental factors hold immense significance and likely serve as the linchpin influencing colony dynamics. Among these factors, temperature emerges as a potential keystone. In the simulation detailed in Chapter 5, it is conceivable that the observed outcomes may be attributed, at least in part, to temperature variations. However, it's important to note that the available data only spans from summer to fall, while the simulation extends over a two-year period, introducing a degree of inaccuracy. Therefore, a more extensive data fitting process is warranted to procure precise parameter values. This could potentially unveil the nuanced impact of temperature on bee dynamics. Furthermore, in the model delineated in Chapter 5, bee population size is unaffected by food availability. Recommendations for rescuing colonies exposed to pesticides by improving nutrition [Crone and Grozinger, 2021] or controlling pests such as varroa might also be generated within the framework of colony dynamics. Therefore, expanding this model to limit food sources to understand how global warming and pesticide exposure affect the intricate bee ecosystem.

In research, determining the population within each hive is crucial for investigating the specific impact of variables on bee populations. Consequently, counting the bees in each hive becomes an indispensable step in the experimental process [Fisher II

et al., 2021; Chen *et al.*, 2020a]. Fisher II *et al.* [2021] used a camera to take photos for each bee frame and estimated the number of individual adult worker bees on the frame using ImageJ (National Institutes of Health, Bethesda, MD). Among these, a colony typically consists of 7-10 frames, each with 2 sides, and harbors approximately 10-1000 bees on each side. With a total of 40 colonies involved in the experiment, the manpower required for counting is substantial. In my dissertation, chapter 3 to chapter 5 also presents the population as important to the dynamics of the colony. But quantifying the number of bee colonies is an estimative process that can potentially influence experimental outcomes [Maucourt *et al.*, 2018], with certain methods demanding a significant investment of time and manpower to execute. Therefore, I hope to study a more accurate and efficient approach to count the population based on the method of Fisher II *et al.* [2021]. Presently, there is a machine learning-based method available for counting objects [Chattopadhyay *et al.*, 2017]. In future work, I can use this method in the experiment to help me obtain better data to improve my model and results.

Furthermore, bees regulate colony temperature through wing flapping and water usage. The model presented in Chapter 3 can be expanded to include a foragers model. This extension allows for a deeper exploration of the influence of temperature on bee behavior and provides insights into how climate change affects bee populations by integrating both pollen foragers and water foragers.

Honey Bee Pathology, 2nd edn (Academic Press, London, UK, 1991).

Abi-Akar, F., A. Schmolke, C. Roy, N. Galic and S. Hinarejos, "Simulating honey bee large-scale colony feeding studies using the beehave model—part ii: Analysis of overwintering outcomes", Environmental toxicology and chemistry **39**, 11, 2286–2297 (2020).

Aeyels, D., "Stability of nonautonomous systems by liapunov's direct method", Banach Center Publications **32**, 1, 9–17 (1995).

Agency, U. E. P., "Seasonality and climate change: A review of observed evidence in the united states", pp. EPA 430–R–21–002, URL `https://www.epa.gov/climate-indicators/seasonality-and-climate-change`. (2021).

Aldridge, G., D. W. Inouye, J. R. Forrest, W. A. Barr and A. J. Miller-Rushing, "Emergence of a mid-season period of low floral resources in a montane meadow ecosystem associated with climate change", Journal of Ecology **99**, 4, 905–913 (2011).

Anderson, C. and D. W. McShea, "Individual versus social complexity, with particular reference to ant colonies", Biological reviews **76**, 2, 211–237 (2001).

Aronstein, K. A., E. Saldivar, R. Vega, S. Westmiller and A. E. Douglas, "How varroa parasitism affects the immunological and nutritional status of the honey bee, apis mellifera", Insects **3**, 3, 601–615 (2012).

Baltiansky, L., E. Sarafian-Tamam, E. Greenwald and O. Feinerman, "Dual-fluorescence imaging and automated trophallaxis detection for studying multi-nutrient regulation in superorganisms", Methods in ecology and evolution **12**, 8, 1441–1457 (2021).

Becher, M. A., V. Grimm, P. Thorbek, J. Horn, P. J. Kennedy and J. L. Osborne, "Beehave: a systems model of honeybee colony dynamics and foraging to explore multifactorial causes of colony failure", Journal of Applied Ecology **51**, 2, 470–482 (2014).

Beshers, S. N. and J. H. Fewell, "Models of division of labor in social insects", Annual review of entomology **46**, 413 (2001).

Betti, M., L. Wahl and M. Zamir, "Age structure is critical to the population dynamics and survival of honeybee colonies", Royal Society open science **3**, 11, 160444 (2016).

Betti, M. I., L. M. Wahl and M. Zamir, "Effects of infection on honey bee population dynamics: a model", PloS one **9**, 10, e110237 (2014).

Bodenheimer, F., "Studies in animal populations. ii. seasonal population-trends of the honey-bee", The Quarterly Review of Biology **12**, 4, 406–425 (1937).

Bourke, A. F., "Colony size, social complexity and reproductive conflict in social insects", Journal of Evolutionary Biology (United Kingdom) (1999).

Brauer, F., "Absolute stability in delay equations", Journal of differential equations **69**, 2, 185–191 (1987).

Camazine, S., J. Sneyd, M. J. Jenkins and J. Murray, "A mathematical model of self-organized pattern formation on the combs of honeybee colonies", Journal of Theoretical Biology **147**, 4, 553–571 (1990).

Campbell, J. B., R. Nath, J. Gadau, T. Fox, G. DeGrandi-Hoffman and J. F. Harrison, "The fungicide pristine® inhibits mitochondrial function in vitro but not flight metabolic rates in honey bees", Journal of insect physiology **86**, 11–16 (2016).

Capinera, J. L., *Encyclopedia of entomology* (Springer Science & Business Media, 2008).

Charbonneau, D. and A. Dornhaus, "When doing nothing is something. how task allocation strategies compromise between flexibility, efficiency, and inactive agents", Journal of Bioeconomics **17**, 3, 217—242 (2015a).

Charbonneau, D. and A. Dornhaus, "Workers 'specialized'on inactivity: behavioral consistency of inactive workers and their role in task allocation", Behavioral ecology and sociobiology **69**, 1459–1472 (2015b).

Charbonneau, D., N. Hillis and A. Dornhaus, "'lazy'in nature: ant colony time budgets show high 'inactivity'in the field as well as in the lab", Insectes sociaux **62**, 31–35 (2015).

Charbonneau, D., T. Sasaki and A. Dornhaus, "Who needs 'lazy'workers? inactive workers act as a 'reserve'labor force replacing active workers, but inactive workers are not replaced when they are removed", PloS one **12**, 9, e0184074 (2017).

Chattopadhyay, P., R. Vedantam, R. R. Selvaraju, D. Batra and D. Parikh, "Counting everyday objects in everyday scenes", in "Proceedings of the IEEE conference on computer vision and pattern recognition", pp. 1135–1144 (2017).

Chen, J., G. DeGrandi-Hoffman, V. Ratti and Y. Kang, "Review on mathematical modeling of honeybee population dynamics", Mathematical Biosciences and Engineering **18**, 6 (2021).

Chen, J., K. Messan, M. R. Messan, G. DeGrandi-Hoffman, D. Bai and Y. Kang, "How to model honeybee population dynamics: stage structure and seasonality", Mathematics in Applied Sciences and Engineering **1**, 2, 91–125 (June 2020a).

Chen, J., J. O. R. Rincon, G. DeGrandi-Hoffman, J. Fewell, J. Harrison and Y. Kang, "Impacts of seasonality and parasitism on honey bee population dynamics", Journal of Mathematical Biology **87**, 1, 19 (2023).

Chen, R., B. Meyer and J. Garcia, "A computational model of task allocation in social insects–ecology and interactions alone can drive specialization", bioRxiv p. 315846 (2018).

Chen, R., B. Meyer and J. García, "A computational model of task allocation in social insects: ecology and interactions alone can drive specialisation", Swarm Intelligence pp. 1–28 (2020b).

Chen, Y. P. and R. Siede, "Honey bee viruses", Advances in virus research **70**, 33–80 (2007).

Chmiel, J. A., B. A. Daisley, A. P. Pitek, G. J. Thompson and G. Reid, "Understanding the effects of sublethal pesticide exposure on honey bees: a role for probiotics as mediators of environmental stress", Frontiers in Ecology and Evolution **8**, 22 (2020).

Class, L., "Sociobiology: The new synthesis", (2000).

Coffey, M. F., *Parasites of the Honeybee* (Teagasc, 2007).

Cowan, G., *Statistical data analysis* (Oxford university press, 1998).

Cox-Foster, D. L., S. Conlan, E. C. Holmes, G. Palacios, J. D. Evans, N. A. Moran, P.-L. Quan, T. Briese, M. Hornig, D. M. Geiser *et al.*, "A metagenomic survey of microbes in honey bee colony collapse disorder", Science **318**, 5848, 283–287 (2007).

Crone, M. K. and C. M. Grozinger, "Pollen protein and lipid content influence resilience to insecticides in honey bees (apis mellifera)", Journal of Experimental Biology **224**, 9, jeb242040 (2021).

De Ridder, D., T. Stöckl, W. T. To, B. Langguth and S. Vanneste, "Noninvasive transcranial magnetic and electrical stimulation: Working mechanisms", in "Rhythmic Stimulation Procedures in Neuromodulation", pp. 193–223 (Elsevier, 2017).

DeGrandi-Hoffman, G., F. Ahumada and H. Graham, "Are dispersal mechanisms changing the host–parasite relationship and increasing the virulence of varroa destructor (mesostigmata: Varroidae) in managed honey bee (hymenoptera: Apidae) colonies?", Environmental entomology **46**, 4, 737–746 (2017).

DeGrandi-Hoffman, G., Y. Chen and R. Simonds, "The effects of pesticides on queen rearing and virus titers in honey bees (apis mellifera l.)", Insects **4**, 1, 71–89 (2013).

Degrandi-Hoffman, G., Y. Chen, E. Watkins Dejong, M. L. Chambers and G. Hidalgo, "Effects of oral exposure to fungicides on honey bee nutrition and virus levels", Journal of economic entomology **108**, 6, 2518–2528 (2015).

DeGrandi-Hoffman, G., V. Corby-Harris, Y. Chen, H. Graham, M. Chambers, E. Watkins deJong, N. Ziolkowski, Y. Kang, S. Gage, M. Deeter *et al.*, "Can supplementary pollen feeding reduce varroa mite and virus levels and improve honey bee colony survival?", Experimental and Applied Acarology **82**, 455–473 (2020).

DeGrandi-Hoffman, G. and R. Curry, "A mathematical model of varroa mite (varroa destructor anderson and trueman) and honeybee (apis mellifera l.) population dynamics", International Journal of Acarology **30**, 3, 259–274 (2004).

Degrandi-Hoffman, G., H. Graham, F. Ahumada, M. Smart and N. Ziolkowski, "The economics of honey bee (hymenoptera: Apidae) management and overwintering strategies for colonies used to pollinate almonds", Journal of economic entomology **112**, 6, 2524–2533 (2019).

DeGrandi-Hoffman, G., S. A. Roth, G. Loper and E. Erickson Jr, "Beepop: a honeybee population dynamics simulation model", Ecological modelling **45**, 2, 133–150 (1989).

Devillers, J. *et al.*, "Acute toxicity of pesticides to honey bees", Honey bees: estimating the environmental impact of chemicals, Taylor and Francis, London pp. 56–66 (2002).

Doeke, M. A., M. Frazier and C. M. Grozinger, "Overwintering honey bees: biology and management", Current Opinion in Insect Science **10**, 185–193 (2015).

Donze, G., M. Herrmann, B. Bachofen and P. R. M. GUERIN, "Effect of mating frequency and brood cell infestation rate on the reproductive success of the honeybee parasite varroa jacobsoni", Ecological entomology **21**, 1, 17–26 (1996).

Eberl, H. J., M. R. Frederick and P. G. Kevan, "Importance of brood maintenance terms in simple models of the honeybee-varroa destructor-acute bee paralysis virus complex", Electronic Journal of Differential Equations **19**, 85–98 (2010).

Eischen, F. A., W. C. Rothenbuhler and J. M. Kulinčević, "Some effects of nursing on nurse bees", Journal of Apicultural Research **23**, 2, 90–93 (1984).

Evans, J. D., C. Saegerman, C. Mullin, E. Haubruge, B. K. Nguyen, M. Frazier, J. Frazier, D. Cox-Foster, Y. Chen, R. Underwood *et al.*, "Colony collapse disorder: a descriptive study", (2009).

Faria, T. and L. T. Magalhaes, "Normal forms for retarded functional differential equations and applications to bogdanov-takens singularity", Journal of differential equations **122**, 2, 201–224 (1995).

Feigenbaum, C. and D. Naug, "The influence of social hunger on food distribution and its implications for disease transmission in a honeybee colony", Insectes sociaux **57**, 2, 217–222 (2010).

Feinerman, O. and A. Korman, "Individual versus collective cognition in social insects", Journal of Experimental Biology **220**, 1, 73–82 (2017).

Feliciano-Cardona, S., M. A. Döke, J. Aleman, J. L. Agosto-Rivera, C. M. Grozinger and T. Giray, "Honey bees in the tropics show winter bee-like longevity in response to seasonal dearth and brood reduction", Frontiers in Ecology and Evolution **8**, 571094 (2020).

Fisher, A., C. Coleman, C. Hoffmann, B. Fritz and J. Rangel, "The synergistic effects of almond protection fungicides on honey bee (hymenoptera: Apidae) forager survival", Journal of economic entomology **110**, 3, 802–808 (2017).

Fisher, A., G. DeGrandi-Hoffman, L.-H. Liao, R. Tadei and J. F. Harrison, "The challenge of balancing fungicide use and pollinator health", PloS one **64**, 117–190 (2023).

Fisher II, A., G. DeGrandi-Hoffman, B. H. Smith, M. Johnson, O. Kaftanoglu, T. Cogley, J. H. Fewell and J. F. Harrison, "Colony field test reveals dramatically higher toxicity of a widely-used mito-toxic fungicide on honey bees (apis mellifera)", Environmental Pollution p. 115964 (2020).

Fisher II, A., G. DeGrandi-Hoffman, B. H. Smith, M. Johnson, O. Kaftanoglu, T. Cogley, J. H. Fewell and J. F. Harrison, "Colony field test reveals dramatically higher toxicity of a widely-used mito-toxic fungicide on honey bees (apis mellifera)", Environmental Pollution **269**, 115964 (2021).

Flores, J. M., S. Gil-Lebrero, V. Gámiz, M. I. Rodríguez, M. A. Ortiz and F. J. Quiles, "Effect of the climate change on honey bee colonies in a temperate mediterranean zone assessed through remote hive weight monitoring system in conjunction with exhaustive colonies assessment", The Science of the Total Environment **653**, 1111–1119 (2019).

Fredrick, C. O., Oldroyd and A. H. Audi, "Reproductive strategies and trophic interactions of honeybees: A review", Biological and Environmental Sciences Journal **14**, 3, 8–13 (2017).

Genersch, E., W. Von Der Ohe, H. Kaatz, A. Schroeder, C. Otten, R. Büchler, S. Berg, W. Ritter, W. Mühlen, S. Gisder *et al.*, "The german bee monitoring project: a long term study to understand periodically high winter losses of honey bee colonies", Apidologie **41**, 3, 332–352 (2010).

Gerkey, B. P. and M. J. Matarić, "A formal analysis and taxonomy of task allocation in multi-robot systems", The International journal of robotics research **23**, 9, 939–954 (2004).

Gordon, D. M., "Dynamics of task switching in harvester ants", Animal Behaviour **38**, 2, 194–204 (1989).

Gordon, D. M., "The organization of work in social insect colonies", Nature **380**, 6570, 121–124 (1996).

Gordon, D. M., B. C. Goodwin and L. E. Trainor, "A parallel distributed model of the behaviour of ant colonies", Journal of theoretical Biology **156**, 3, 293–307 (1992).

Gordon, D. M. and N. J. Mehdiabadi, "Encounter rate and task allocation in harvester ants", Behavioral Ecology and Sociobiology **45**, 5, 370–377 (1999).

Greene, M. J. and D. M. Gordon, "Interaction rate informs harvester ant task decisions", **18**, 2, 451–455, URL `http://beheco.oxfordjournals.org/content/18/2/451.short` (2007).

Guo, X., J. Chen, A. Azizi, J. Fewell and Y. Kang, "Dynamics of social interactions, in the flow of information and disease spreading in social insects colonies: Effects of environmental events and spatial heterogeneity", Journal of Theoretical Biology **492**, 110191 (2020).

Guo, X., M. R. Lin, A. Azizi, L. P. Saldyt, Y. Kang, T. P. Pavlic and J. H. Fewell, "Decoding alarm signal propagation of seed-harvester ants using automated movement tracking and supervised machine learning", Proceedings of the Royal Society B **289**, 1967, 20212176 (2022).

Guzmán-Novoa, E., L. Eccles, Y. Calvete, J. Mcgowan, P. G. Kelly and A. Correa-Benítez, "Varroa destructor is the main culprit for the death and reduced populations of overwintered honey bee (apis mellifera) colonies in ontario, canada", Apidologie **41**, 4, 443–450 (2010).

Halsch, C. A., A. M. Shapiro, J. A. Fordyce, C. C. Nice, J. H. Thorne, D. P. Waetjen and M. L. Forister, "Insects and recent climate change", Proceedings of the national academy of sciences **118**, 2 (2021).

Harris, J. L., "A population model and its application to the study of honey bee colonies", (1980).

Haydak, M. H., "Honey bee nutrition", Annual review of entomology **15**, 1, 143–156 (1970).

Hayes Jr, J., R. M. Underwood, J. Pettis *et al.*, "A survey of honey bee colony losses in the us, fall 2007 to spring 2008", PloS one **3**, 12, e4071 (2008).

Hirsch, W. M., H. Hanisch and J.-P. Gabriel, "Differential equation models of some parasitic infections: methods for the study of asymptotic behavior", Communications on Pure and Applied Mathematics **38**, 6, 733–753 (1985).

Holbrook, C. T., P. M. Barden and J. H. Fewell, "Division of labor increases with colony size in the harvester ant pogonomyrmex californicus", Behavioral Ecology **22**, 5, 960–966 (2011).

Huang, Z.-Y. and G. E. Robinson, "Regulation of honey bee division of labor by colony age demography", Behavioral Ecology and Sociobiology **39**, 3, 147–158 (1996).

Hurlbert, A. H., F. Ballantyne and S. Powell, "Shaking a leg and hot to trot: the effects of body size and temperature on running speed in ants", Ecological Entomology (2008).

Ismail, N. and A. A. Jemain, "Handling overdispersion with negative binomial and generalized poisson regression models", in "Casualty actuarial society forum", pp. 103–158 (Citeseer, 2007).

Jack, C., I. de Bem Oliveira, C. B. Kimmel and J. D. Ellis, "Seasonal differences in varroa destructor population growth in western honey bee (apis mellifera) colonies", Frontiers in Ecology and Evolution **11**, 323 (2023).

Jack, C. J. and J. D. Ellis, "Integrated pest management control of varroa destructor (acari: Varroidae), the most damaging pest of (apis mellifera l.(hymenoptera: Apidae)) colonies", Journal of Insect Science **21**, 5, 6 (2021).

Jack, C. J., E. van Santen and J. D. Ellis, "Evaluating the efficacy of oxalic acid vaporization and brood interruption in controlling the honey bee pest varroa destructor (acari: Varroidae)", Journal of economic entomology **113**, 2, 582–588 (2020).

Jha, S. and J. H. Vandermeer, "Contrasting foraging patterns for africanized honeybees, native bees and native wasps in a tropical agroforestry landscape", Journal of Tropical Ecology **25**, 1, 13–22 (2009).

Johnson, B. R., "Reallocation of labor in honeybee colonies during heat stress: the relative roles of task switching and the activation of reserve labor", Behavioral Ecology and Sociobiology **51**, 2, 188–196 (2002).

Johnson, B. R., "Organization of work in the honeybee: a compromise between division of labour and behavioural flexibility", **270**, 1511, 147–152 (2003).

Johnson, B. R., "A self-organizing model for task allocation via frequent task quitting and random walks in the honeybee", The American Naturalist **174**, 4, 537–547 (2009a).

Johnson, N., *Simply complexity: A clear guide to complexity theory* (Simon and Schuster, 2009b).

Johnson, R., *Honey bee colony collapse disorder* (Congressional Research Service Washington, 2010).

Johnson, R. M., L. Dahlgren, B. D. Siegfried and M. D. Ellis, "Acaricide, fungicide and drug interactions in honey bees (apis mellifera)", PloS one **8**, 1, e54092 (2013).

Johnson, R. M., M. D. Ellis, C. A. Mullin and M. Frazier, "Pesticides and honey bee toxicity–usa", Apidologie **41**, 3, 312–331 (2010).

Jones, J. C., M. R. Myerscough, S. Graham and B. P. Oldroyd, "Honey bee nest thermoregulation: Diversity promotes stability", Science **305**, 5682, 402–404, URL `https://science.sciencemag.org/content/305/5682/402` (2004).

Kang, Y., K. Blanco, T. Davis, Y. Wang and G. DeGrandi-Hoffman, "Disease dynamics of honeybees with varroa destructor as parasite and virus vector", Mathematical biosciences **275**, 71–92 (2016).

Kang, Y., M. Rodriguez-Rodriguez and S. Evilsizor, "Ecological and evolutionary dynamics of two-stage models of social insects with egg cannibalism", Journal of Mathematical Analysis and Applications **430**, 1, 324–353 (2015).

Khoury, D. S., A. B. Barron and M. R. Myerscough, "Modelling food and population dynamics in honey bee colonies", PloS one **8**, 5, e59084 (2013).

Khoury, D. S., M. R. Myerscough and A. B. Barron, "A quantitative model of honey bee colony population dynamics", PloS one **6**, 4, e18491 (2011).

Koleoglu, G., P. H. Goodwin, M. Reyes-Quintana, M. M. Hamiduzzaman and E. Guzman-Novoa, "Effect of varroa destructor, wounding and varroa homogenate on gene expression in brood and adult honey bees", PloS one **12**, 1, e0169669 (2017).

Kribs-Zaleta, C. M. and C. Mitchell, "Modeling colony collapse disorder in honeybees as a contagion.", Mathematical biosciences and engineering: MBE **11**, 6, 1275–1294 (2014).

Kuang, Y., *Delay differential equations: with applications in population dynamics* (Academic press, 1993).

Lawless, J. F., "Negative binomial and mixed poisson regression", Canadian Journal of Statistics **15**, 3, 209–225 (1987).

Leighton, G. M., D. Charbonneau and A. Dornhaus, "Task switching is associated with temporal delays in temnothorax rugatulus ants", Behavioral Ecology **28**, 1, 319–327 (2017).

Leitner, N. and A. Dornhaus, "Dynamic task allocation: how and why do social insect workers take on new tasks?", Animal Behaviour **158**, 47–63 (2019).

Leoncini, I., D. Crauser, G. Robinson and Y. Le Conte, "Worker-worker inhibition of honey bee behavioural development independent of queen and brood", Insectes Sociaux **51**, 4, 392–394 (2004).

Lloyd, M., "Mean crowding"', The Journal of Animal Ecology pp. 1–30 (1967).

Lloyd-Smith, J. O., "Maximum likelihood estimation of the negative binomial dispersion parameter for highly overdispersed data, with applications to infectious diseases", PloS one **2**, 2, e180 (2007).

Magal, P., G. Webb and Y. Wu, "An environmental model of honey bee colony collapse due to pesticide contamination", Bulletin of mathematical biology **81**, 12, 4908–4931 (2019).

Magal, P., G. Webb and Y. Wu, "A spatial model of honey bee colony collapse due to pesticide contamination of foraging bees", Journal of Mathematical Biology (2020a).

Magal, P., G. Webb and Y. Wu, "A spatial model of honey bee colony collapse due to pesticide contamination of foraging bees", Journal of mathematical biology **80**, 7, 2363–2393 (2020b).

Mallon, E., S. Pratt and N. Franks, "Individual and collective decision-making during nest site selection by the ant leptothorax albipennis", **50**, 4, 352–359 (2001).

Martin, S. J., "The role of varroa and viral pathogens in the collapse of honeybee colonies: a modelling approach", Journal of Applied Ecology **38**, 5, 1082–1093 (2001a).

Martin, S. J., "Varroa destructor reproduction during the winter in apis mellifera colonies in uk", Experimental & applied acarology **25**, 4, 321–325 (2001b).

Martin, S. J., A. C. Highfield, L. Brettell, E. M. Villalobos, G. E. Budge, M. Powell, S. Nikaido and D. C. Schroeder, "Global honey bee viral landscape altered by a parasitic mite", Science **336**, 6086, 1304–1306 (2012).

Maucourt, S., V. Fournier and P. Giovenazzo, "Comparison of three methods to multiply honey bee (apis mellifera) colonies", Apidologie **49**, 314–324 (2018).

Meixner, M. D., R. Büchler, C. Costa, R. M. Francis, F. Hatjina, P. Kryger, A. Uzunov and N. L. Carreck, "Honey bee genotypes and the environment", (2014).

Meixner, M. D., C. Costa, P. Kryger, F. Hatjina, M. Bouga, E. Ivanova and R. Büchler, "Conserving diversity and vitality for honey bee breeding", Journal of Apicultural Research **49**, 1, 85–92 (2010).

Mersch, D. P., A. Crespi and L. Keller, "Tracking individuals shows spatial fidelity is a key regulator of ant social organization", Science **340**, 6136, 1090–1093 (2013).

Messan, K., G. DeGrandi-Hoffman, C. Castillo-Chavez and Y. Kang, "Migration effects on population dynamics of the honeybee-mite interactions", Mathematical Modelling of Natural Phenomena **12**, 2, 84–115 (2017).

Messan, K., M. Rodriguez Messan, J. Chen, G. DeGrandi-Hoffman and Y. Kang, "Population dynamics of varroa mite and honeybee: Effects of parasitism with age structure and seasonality", Ecological Modelling **440**, 109359 (2021).

Messan, M. R., *Understanding the Emerging Behaviors and Demands for the Colony Success of Social Insects: A Mathematical Approach* (Arizona State University, 2018).

Messan, M. R., R. E. Page Jr and Y. Kang, "Effects of vitellogenin in age polyethism and population dynamics of honeybees", Ecological Modelling **388**, 88–107 (2018).

Miller, J. H. and S. Page, "Complex adaptive systems", in "Complex Adaptive Systems", (Princeton university press, 2009).

Mullin, C. A., M. Frazier, J. L. Frazier, S. Ashcraft, R. Simonds, D. vanEngelsdorp and J. S. Pettis, "High levels of miticides and agrochemicals in north american apiaries: implications for honey bee health", PLoS one **5**, 3, e9754 (2010).

Myers, J. H., "Selecting a measure of dispersion", Environmental Entomology **7**, 5, 619–621 (1978).

Naug, D., "Structure of the social network and its influence on transmission dynamics in a honeybee colony", Behavioral Ecology and Sociobiology **62**, 11, 1719–1725 (2008).

Naug, D., "Structure and resilience of the social network in an insect colony as a function of colony size", Behavioral Ecology and Sociobiology **63**, 7, 1023–1028 (2009).

Navlakha, S. and Z. Bar-Joseph, "Distributed information processing in biological and computational systems", Communications of the ACM **58**, 1, 94–102 (2014).

Neumann, P., M. Bartholmai, J. H. Schiller, B. Wiggerich and M. Manolov, "Micro-drone for the characterization and self-optimizing search of hazardous gaseous substance sources: A new approach to determine wind speed and direction", in "2010 IEEE International Workshop on Robotic and Sensors Environments", pp. 1–6 (IEEE, 2010).

Neumann, P. and N. L. Carreck, "Honey bee colony losses", (2010).

Ogilvie, J. E. and J. R. Forrest, "Interactions between bee foraging and floral resource phenology shape bee populations and communities", Current opinion in insect science **21**, 75–82 (2017).

Oldroyd, B. P., "Whatâs killing american honey bees", PLoS Biol **5**, 6, e168 (2007).

Oldroyd, B. P. and J. H. Fewell, "Genetic diversity promotes homeostasis in insect colonies", Trends in ecology & evolution **22**, 8, 408–413 (2007).

Olsen, B. D., *Understanding biology through evolution* (Lulu. com, 2009).

Owens, C. D. and C. L. Farrar, *Electric heating of honey bee hives*, no. 1377 (US Agricultural Research Service, 1967).

O'Donnell, S. and S. Bulova, "Worker connectivity: a review of the design of worker communication systems and their effects on task performance in insect societies", Insectes Sociaux **54**, 203–210 (2007).

Pacala, S. W., D. M. Gordon and H. Godfray, "Effects of social group size on information transfer and task allocation", Evolutionary Ecology **10**, 2, 127–165 (1996).

Page Jr, R. E. and S. D. Mitchell, "Self organization and adaptation in insect societies", in "PSA: Proceedings of the biennial meeting of the philosophy of science association", vol. 1990, pp. 289–298 (Philosophy of Science Association, 1990).

Page Jr, R. E. and S. D. Mitchell, "Self-organization and the evolution of division of labor", Apidologie **29**, 1-2, 171–190 (1998).

Paula María Montoya-Pfeiffer, F. C., Daniela Leon and G. N. Parra., *Iniciativa Colombiana de Polinizadores: Abejas ICPA* (Universidad Nacional de Colombia, 2016).

Peng, Y.-S., Y. Fang, S. Xu and L. Ge, "The resistance mechanism of the Asian honey bee, *Apis cerana* Fabr., to an ectoparasitic mite, *Varroa jacobsoni* Oudemans", Journal of Invertebrate Pathology **49**, 1, 54–60 (1987).

Perry, C. J., E. Søvik, M. R. Myerscough and A. B. Barron, "Rapid behavioral maturation accelerates failure of stressed honey bee colonies", Proceedings of the National Academy of Sciences **112**, 11, 3427–3432 (2015).

Piegorsch, W. W., "Maximum likelihood estimation for the negative binomial dispersion parameter", Biometrics pp. 863–867 (1990).

Pinter-Wollman, N., J. Hubler, J.-A. Holley, N. R. Franks and A. Dornhaus, "How is activity distributed among and within tasks in temnothorax ants?", Behavioral Ecology and Sociobiology **66**, 10, 1407–1420 (2012).

Piot, N., O. Schweiger, I. Meeus, O. Yañez, L. Straub, L. Villamar-Bouza, P. De la Rúa, L. Jara, C. Ruiz, M. Malmstrøm *et al.*, "Honey bees and climate explain viral prevalence in wild bee communities on a continental scale", Scientific reports **12**, 1, 1–11 (2022).

Potts, S. G., J. C. Biesmeijer, C. Kremen, P. Neumann, O. Schweiger and W. E. Kunin, "Global pollinator declines: trends, impacts and drivers", Trends in ecology & evolution **25**, 6, 345–353 (2010).

Potts, S. G., V. Imperatriz-Fonseca, H. T. Ngo, M. A. Aizen, J. C. Biesmeijer, T. D. Breeze, L. V. Dicks, L. A. Garibaldi, R. Hill, J. Settele *et al.*, "Safeguarding pollinators and their values to human well-being", Nature **540**, 7632, 220–229 (2016).

Pratt, S. C., E. B. Mallon, D. J. Sumpter and N. R. Franks, "Quorum sensing, recruitment, and collective decision-making during colony emigration by the ant leptothorax albipennis", Behavioral Ecology and Sociobiology **52**, 2, 117–127 (2002a).

Pratt, S. C., E. B. Mallon, D. J. Sumpter and N. R. Franks, "Quorum sensing, recruitment, and collective decision-making during colony emigration by the ant leptothorax albipennis", **52**, 2, 117–127, URL `http://link.springer.com/article/10.1007/s00265-002-0487-x` (2002b).

Quevillon, L. E., E. M. Hanks, S. Bansal and D. P. Hughes, "Social, spatial, and temporal organization in a complex insect society", Scientific reports **5**, 13393 (2015).

Ramsey, S. D., R. Ochoa, G. Bauchan, C. Gulbronson, J. D. Mowery, A. Cohen, D. Lim, J. Joklik, J. M. Cicero, J. D. Ellis *et al.*, "Varroa destructor feeds primarily on honey bee fat body tissue and not hemolymph", Proceedings of the National Academy of Sciences **116**, 5, 1792–1801 (2019).

Randall, B., "U.S. DEPARTMENT OF AGRICULTURE the value of birds and bees", URL `https://www.farmers.gov/connect/blog/conservation/value-birds-and-bees` (2020).

Ratti, V., P. G. Kevan and H. J. Eberl, "A mathematical model of the honeybee–varroa destructor–acute bee paralysis virus system with seasonal effects", Bulletin of mathematical biology **77**, 8, 1493–1520 (2015).

Ratti, V., P. G. Kevan and H. J. Eberl, "A mathematical model of forager loss in honeybee colonies infested with varroa destructor and the acute bee paralysis virus", Bulletin of mathematical biology **79**, 6, 1218–1253 (2017).

Rebelo, C. and C. Soresina, "Coexistence in seasonally varying predator–prey systems with allee effect", Nonlinear Analysis: Real World Applications **55**, 103140 (2020).

Reddy, P., A. Verghese and V. V. Rajan, "Potential impact of climate change on honeybees (apis spp.) and their pollination services", Pest Management in Horticultural Ecosystems **18**, 2, 121–127 (2012).

Regnier, F. and E. O. Wilson, "The alarm-defense system of the ant acanthomyops claviger", Journal of Insect Physiology **14**, 7, 955–970 (1968).

Research, M.-A. A. and M. Extension Consortium, "Basic bee biology for beekeepers", MAAREC **1.4**, URL `https://wasatchwarre.files.wordpress.com/2011/01/basicbeebiology.pdf` (2004).

Richardson, T. O. and T. E. Gorochowski, "Beyond contact-based transmission networks: the role of spatial coincidence", Journal of The Royal Society Interface **12**, 111, 20150705 (2015).

Richardson, T. O., N. Stroeymeyt, A. Crespi and L. Keller, "Two simple movement mechanisms for spatial division of labour in social insects", Nature Communications **13**, 1, 6985 (2022).

Robinson, E. J., O. Feinerman and N. R. Franks, "Flexible task allocation and the organization of work in ants", Proceedings of the Royal Society of London B: Biological Sciences p. rspb20091244 (2009a).

Robinson, E. J., O. Feinerman and N. R. Franks, "Flexible task allocation and the organization of work in ants", Proceedings of the Royal Society B: Biological Sciences **276**, 1677, 4373–4380 (2009b).

Robinson, E. J., O. Feinerman and N. R. Franks, "Flexible task allocation and the organization of work in ants", Proceedings of the Royal Society of London B: Biological Sciences p. rspb20091244 (2009c).

Robinson, G. E., "Regulation of honey bee age polyethism by juvenile hormone", Behavioral ecology and sociobiology **20**, 5, 329–338 (1987).

Robinson, G. E., "Regulation of division of labor in insect societies", Annual review of entomology **37**, 1, 637–665 (1992).

Robinson, G. E., R. E. Page Jr, C. Strambi and A. Strambi, "Colony integration in honey bees: mechanisms of behavioral reversion", Ethology **90**, 4, 336–348 (1992).

Rueppell, O., C. Bachelier, M. K. Fondrk and R. E. Page Jr, "Regulation of life history determines lifespan of worker honey bees (apis mellifera l.)", Experimental gerontology **42**, 10, 1020–1032 (2007).

Rumkee, J. C., M. A. Becher, P. Thorbek, P. J. Kennedy and J. L. Osborne, "Predicting honeybee colony failure: using the beehave model to simulate colony responses to pesticides", Environmental science & technology **49**, 21, 12879–12887 (2015).

Russell, S., A. B. Barron and D. Harris, "Dynamic modelling of honey bee (apis mellifera) colony growth and failure", Ecological Modelling **265**, 158–169 (2013).

Sánchez-Bayo, F., D. Goulson, F. Pennacchio, F. Nazzi, K. Goka and N. Desneux, "Are bee diseases linked to pesticides?—a brief review", Environment international **89**, 7–11 (2016).

Schmickl, T. and K. Crailsheim, "Hopomo: a model of honeybee intracolonial population dynamics and resource management", Ecological modelling **204**, 1, 219–245 (2007).

SEELEY, T. D. and P. K. Visscher, "Survival of honeybees in cold climates: the critical timing of colony growth and reproduction", Ecological Entomology **10**, 1, 81–88 (1985).

Sendova-Franks, A. and N. Franks, "Social resilience in individual worker ants and its role in division of labour", Proceedings of the Royal Society of London B: Biological Sciences **256**, 1347, 305–309 (1994).

Sendova-Franks, A. B. and N. R. Franks, "Spatial relationships within nests of the ant leptothorax unifasciatus (latr.) and their implications for the division of labour", Animal Behaviour **50**, 1, 121–136 (1995).

Sendova-Franks, A. B., R. K. Hayward, B. Wulf, T. Klimek, R. James, R. Planqué, N. F. Britton and N. R. Franks, "Emergency networking: famine relief in ant colonies", Animal Behaviour **79**, 2, 473–485 (2010).

Simpson, J., "Nest climate regulation in honey bee colonies: Honey bees control their domestic environment by methods based on their habit of clustering together.", Science **133**, 3461, 1327–1333 (1961).

Smith, H., *An introduction to delay differential equations with applications to the life sciences*, vol. 57 (Springer Science & Business Media, 2010).

Smith, K. M., E. H. Loh, M. K. Rostal, C. M. Zambrana-Torrelio, L. Mendiola and P. Daszak, "Pathogens, pests, and economics: drivers of honey bee colony declines and losses", EcoHealth **10**, 4, 434–445 (2013).

Smoliński, S., A. Langowska and A. Glazaczow, "Raised seasonal temperatures reinforce autumn varroa destructor infestation in honey bee colonies", Scientific reports **11**, 1, 1–11 (2021).

Stabentheiner, A., H. Pressl, T. Papst, N. Hrassnigg and K. Crailsheim, "Endothermic heat production in honeybee winter clusters", Journal of Experimental Biology **206**, 2, 353–358 (2003).

Stroeymeyt, N., A. V. Grasse, A. Crespi, D. P. Mersch, S. Cremer and L. Keller, "Social network plasticity decreases disease transmission in a eusocial insect", Science **362**, 6417, 941–945 (2018).

Sumpter, D. J. and S. J. Martin, "The dynamics of virus epidemics in varroa-infested honey bee colonies", Journal of Animal Ecology **73**, 1, 51–63 (2004).

Switanek, M., K. Crailsheim, H. Truhetz and R. Brodschneider, "Modelling seasonal effects of temperature and precipitation on honey bee winter mortality in a temperate climate", Science of the Total Environment **579**, 1581–1587 (2017).

Tang, S. and L. Chen, "Density-dependent birth rate, birth pulses and their population dynamic consequences", Journal of Mathematical Biology **44**, 2, 185–199 (2002).

Theraulaz, G., J. Gautrais, S. Camazine and J.-L. Deneubourg, "The formation of spatial patterns in social insects: from simple behaviours to complex structures", Philosophical Transactions of the Royal Society of London. Series A: Mathematical, Physical and Engineering Sciences **361**, 1807, 1263–1282 (2003).

Thieme, H. R., *Mathematics in population biology* (Princeton University Press, 2018).

Thorbek, P., P. J. Campbell, P. J. Sweeney and H. M. Thompson, "Using beehave to explore pesticide protection goals for european honeybee (apis melifera l.) worker losses at different forage qualities", Environmental toxicology and chemistry **36**, 1, 254–264 (2017).

Tome, H. V., D. R. Schmehl, A. E. Wedde, R. S. Godoy, S. V. Ravaiano, R. N. Guedes, G. F. Martins and J. D. Ellis, "Frequently encountered pesticides can cause multiple disorders in developing worker honey bees", Environmental Pollution **256**, 113420 (2020).

Tosi, S., J. C. Nieh, F. Sgolastra, R. Cabbri and P. Medrzycki, "Neonicotinoid pesticides and nutritional stress synergistically reduce survival in honey bees", Proceedings of the Royal Society B: Biological Sciences **284**, 1869, 20171711 (2017).

Tosi, S., C. Sfeir, E. Carnesecchi, M.-P. Chauzat *et al.*, "Lethal, sublethal, and combined effects of pesticides on bees: A meta-analysis and new risk assessment tools", Science of The Total Environment **844**, 156857 (2022).

Traynor, K. S., S. Tosi, K. Rennich, N. Steinhauer, E. Forsgren, R. Rose, G. Kunkel, S. Madella, D. Lopez, H. Eversole *et al.*, "Pesticides in honey bee colonies: Establishing a baseline for real world exposure over seven years in the usa", Environmental Pollution **279**, 116566 (2021).

Tschinkel, W. R. and N. Hanley, "Vertical organization of the division of labor within nests of the florida harvester ant, pogonomyrmex badius", PloS one **12**, 11, e0188630 (2017).

Tuell, J. K. and R. Isaacs, "Weather during bloom affects pollination and yield of highbush blueberry", Journal of economic entomology **103**, 3, 557–562 (2010).

Ullah, A., I. T. Gajger, A. Majoros, S. A. Dar, S. Khan, A. H. Shah, M. N. Khabir, R. Hussain, H. U. Khan, M. Hameed *et al.*, "Viral impacts on honey bee populations: A review", Saudi journal of biological sciences **28**, 1, 523–530 (2021).

USDA, "Honey", USDA (2017).

USDA, "U.S. DEPARTMENT OF AGRICULTURE loss-adjusted food availability data and sugar and sweeteners", URL `www.ers.usda.gov/data-products` (2023).

Vanbergen, A. J., "A cocktail of pesticides, parasites and hunger leaves bees down and out", (2021).

VanEngelsdorp, D., D. Caron, J. Hayes, R. Underwood, M. Henson, K. Rennich, A. Spleen, M. Andree, R. Snyder, K. Lee *et al.*, "A national survey of managed honey bee 2010–11 winter colony losses in the usa: results from the bee informed partnership", Journal of Apicultural Research **51**, 1, 115–124 (2012).

VanEngelsdorp, D., J. Hayes Jr, R. M. Underwood and J. Pettis, "A survey of honey bee colony losses in the us, fall 2007 to spring 2008", PloS one **3**, 12, e4071 (2008).

Vercelli, M., S. Novelli, P. Ferrazzi, G. Lentini and C. Ferracini, "A qualitative analysis of beekeepers' perceptions and farm management adaptations to the impact of climate change on honey bees", Insects **12**, 3, 228 (2021).

Vetharaniam, K. and N. D. Barlow, "Modelling biocontrol of *Varroa destructor* using a benign haplotype as a competitive antagonist", New Zealand Journal of Ecology **30**, 1, 87–102 (2006).

Wang, J., J. Shi and J. Wei, "Predator–prey system with strong allee effect in prey", Journal of Mathematical Biology **62**, 3, 291–331 (2011).

Waters, J. S., A. Ochs, J. H. Fewell and J. F. Harrison, "Differentiating causality and correlation in allometric scaling: ant colony size drives metabolic hypometry", Proceedings of the Royal Society B: Biological Sciences **284**, 1849, 20162582 (2017).

Weidenmuller, A., "The control of nest climate in bumblebee (Bombus terrestris) colonies: interindividual variability and self reinforcement in fanning response", BEHAVIORAL ECOLOGY **15**, 1, 120–128 (2004).

Williamson, S. M., S. J. Willis and G. A. Wright, "Exposure to neonicotinoids influences the motor function of adult worker honeybees", Ecotoxicology **23**, 8, 1409–1418 (2014).

Wilson, E., "0.(1975) sociobiology: The new synthesis", (1978).

Wilson, E. O., "Between-caste aversion as a basis for division of labor in the ant pheidole pubiventris (hymenoptera: Formicidae)", Behavioral ecology and sociobiology **17**, 35–37 (1985).

Wilson, E. O., *Sociobiology: The new synthesis* (Harvard University Press, 2000).

Wilson, E. O. and F. E. Regnier Jr, "The evolution of the alarm-defense system in the formicine ants", The American Naturalist **105**, 943, 279–289 (1971).

Winston, M. L., *The biology of the honey bee* (harvard university press, 1987).

Winston, M. L., *The biology of the honey bee* (harvard university press, 1991).

Yanni, D., S. Jacobeen, P. Márquez-Zacarías, J. S. Weitz, W. C. Ratcliff and P. J. Yunker, "Topological constraints in early multicellularity favor reproductive division of labor", Elife **9**, e54348 (2020).

APPENDIX A

PROOFS

Proofs for Chapter. 3

Proof of Theorem 3.3.1

Proof. First, I look at the following equation that describes the population of adult bees:

$$\frac{dH}{dt} = e^{-d_b\tau}\frac{rH(t-\tau)^2}{K+H(t-\tau)^2+\alpha B(t-\tau)} - d_hH \tag{A.1}$$

Since $H(t)$ is a nonnegative continuous function during the time $t \in [-\tau, 0]$, the equation (A.1) implies that

$$\frac{dH}{dt} \geq -d_hH \text{ for time } t \in [0,\tau] \Rightarrow H(t) \geq H(0)e^{-d_ht} \geq 0 \text{ for time } t \in [0,\tau].$$

By deduction on intervals $[(n-1)\tau, n\tau], n \geq 1]$, I could show that $H(t) \geq 0$.

By integration, I could set

$$B(t) = \int_{t-\tau}^{t}\left[\frac{rH(s)^2}{K+H(s)^2+\alpha B(s)}e^{-d_b(t-s)}\right]ds - B(0)e^{-d_bt} \tag{A.2}$$

which gives $\frac{dB}{dt} = \frac{rH(t)^2}{K+H(t)^2+\alpha B(t)} - d_bB - e^{-d_b\tau}\frac{rH(t-\tau)^2}{K+H(t-\tau)^2+\alpha B(t-\tau)}$,
and $B(0) = \int_{-\tau}^{0}\frac{rH^2(s)e^{d_bs}}{K+H^2(s)+\alpha B(s)}ds$. Thus, the equation (A.2) provides an explicit mathematical expression of $B(t)$ which is nonnegative for all time $t \geq 0$. Thus, the state space $\mathbb{X}$ of the proposed model (3.1) is positive invariant.

To show the boundedness of the model, define $V = B + H$, then I have

$$\begin{aligned}\frac{dV}{dt} = \frac{dB}{dt} + \frac{dH}{dt} &= \frac{rH^2}{K+H^2+\alpha B} - d_bB - d_hH \\ &\leq r - \min\{d_b, d_h\}(B+H) = r - d_{\min}V\end{aligned}$$

with $d_{\min} = \min\{d_b, d_h\}$. Consequently, I have

$$\limsup_{t\to\infty} V(t) = \limsup_{t\to\infty}(B(t)+H(t)) \leq \frac{r}{d_{\min}}$$

which implies that Model (3.1) is bounded in $\mathbb{X}$.

□

Proof of Theorem 3.3.2

Proof. I linearize the Model 3.1:

$$\begin{aligned}D\left(\begin{bmatrix}\dot{B}(t)\\ \dot{H}(t)\end{bmatrix}\right)\Big|_{(B^*,H^*)} &= \begin{bmatrix}-\frac{\alpha H^2 r}{(\alpha B+H^2+K)^2} - d_b & \frac{2Hr(\alpha B+K)}{(\alpha B+H^2+K)^2}\\ 0 & -d_h\end{bmatrix}\begin{bmatrix}B(t)\\ H(t)\end{bmatrix} \\ &+ \begin{bmatrix}\frac{\alpha H^2 re^{-d_b\tau}}{(\alpha B+H^2+K)^2} & -\frac{2Hre^{-d_b\tau}(\alpha B+K)}{(\alpha B+H^2+K)^2}\\ -\frac{\alpha H^2 re^{-d_b\tau}}{(\alpha B+H^2+K)^2} & \frac{2Hre^{-d_b\tau}(\alpha B+K)}{(\alpha B+H^2+K)^2}\end{bmatrix}\begin{bmatrix}B(t-\tau)\\ H(t-\tau)\end{bmatrix}.\end{aligned} \tag{A.3}$$

For extinction equilibrium, the matrix (A.3) gives:

$$D\left(\begin{bmatrix} \dot{B}(t) \\ \dot{H}(t) \end{bmatrix}\right)\Big|_{(0,0)} = \begin{bmatrix} -d_b & 0 \\ 0 & -d_h \end{bmatrix}\begin{bmatrix} B(t) \\ H(t) \end{bmatrix} + \begin{bmatrix} 0 & 0 \\ 0 & 0 \end{bmatrix}\begin{bmatrix} B(t-\tau) \\ H(t-\tau) \end{bmatrix}$$

and from this I obtain the following eigenvalues:

$$\lambda_1 = -d_b < 0, \quad \lambda_2 = -d_h < 0.$$

Thus, I can conclude that E_e is always locally asymptotically stable.

Now I show its global stability as follows. Let $(B(t), H(t))$ be a solution of Model (3.1), then $(B(t), H(t))$ is bounded and positive for all $t > 0$ by Theorem 3.3.1. Define $\limsup_{t\to\infty} H(t) = H^\infty$. By Lemma B in A, there exists sequence $\{t_n\} \uparrow \infty$ such that $\lim_{n\to\infty} H(t_n) = H^\infty$, and $\lim_{n\to\infty} H'(t_n) = 0$, and same for $B(t)$. For any $\epsilon > 0$, there exists N such that for $n > N$, $H(t_n - \tau) \leq H^\infty + \epsilon$ holds. Thus, according to Model (3.1), for $n > N$ I have

$$\begin{aligned} H'(t_n) &= e^{-d_b\tau}\frac{rH(t_n-\tau)^2}{K+H(t_n-\tau)^2+\alpha B(t_n-\tau)} - d_hH(t_n) \\ &\leq e^{-d_b\tau}\frac{rH(t_n-\tau)^2}{K+H(t_n-\tau)^2} - d_hH(t_n) \\ &\leq e^{-d_b\tau}\frac{r(H^\infty+\epsilon)^2}{K+(H^\infty+\epsilon)^2} - d_hH(t_n). \end{aligned}$$

Let $n \to \infty$, I get

$$0 \leq e^{-d_b\tau}\frac{r(H^\infty+\epsilon)^2}{K+(H^\infty+\epsilon)^2} - d_hH^\infty.$$

It follows by the arbitrariness of ϵ that

$$H^\infty\left(-d_h(H^\infty)^2 + e^{-d_b\tau}rH^\infty - d_hK\right) \geq 0.$$

Then $d_h > \frac{re^{-d_b\tau}}{2\sqrt{K}}$, I know that for all $x, y \in \mathbb{R}$, $-d_hx^2 + e^{-d_b\tau}rx - d_hK < 0$. Therefore, $H^\infty = 0$, and hence from the positivity of solution I have $\lim_{t\to\infty} H(t) = 0$. Furthermore, I obtain the following limiting equation

$$\frac{dB}{dt} = -d_bB(t),$$

which implies that $\lim_{t\to\infty} B(t) = 0$. Therefore, $E_e = (0, 0)$ is globally asymptotically stable.

□

Proof of Theorem 3.3.3

Proof. Let (B^*, H^*) be an equilibrium of Model (3.1). Then the linearization of the proposed model (3.1) at the equilibrium (B^*, H^*) is shown as follows:

In the case of the interior equilibrium $(B^*, H^*) = E_i$, from Equation (3.5), I have

$$\frac{2rKH^*}{(K+(H^*)^2)^2} = \frac{rH^*}{(K+(H^*)^2)}\frac{2K}{(K+(H^*)^2)} = \frac{2Kd_he^{d_b\tau}}{(K+(H^*)^2)}.$$

The characteristic equation (3.8) evaluated at the positive interior equilibrium (B^*, H^*) when $\alpha = 0$ gives the following expression:

$$\begin{aligned}
C(\lambda) &= det\left(\begin{bmatrix} -d_b & \frac{2rKH^*}{(K+(H^*)^2)^2} \\ 0 & -d_h \end{bmatrix} + \begin{bmatrix} 0 & -\frac{2rKH^*}{(K+(H^*)^2)^2}e^{-d_b\tau} \\ 0 & \frac{2rKH^*}{(K+(H^*)^2)^2}e^{-d_b\tau} \end{bmatrix} * e^{-\lambda\tau} - \lambda\mathscr{I}\right) \\
&= det\left(\begin{bmatrix} -d_b-\lambda & \frac{2rKH^*}{(K+(H^*)^2)^2}(1-e^{-(\lambda+d_b)\tau}) \\ 0 & -d_h+\frac{2rKH^*}{(K+(H^*)^2)^2}e^{-(\lambda+d_b)\tau}-\lambda \end{bmatrix}\right. \\
&= (-d_b-\lambda)\left(-d_h+\frac{2rKH^*}{(K+(H^*)^2)^2}e^{-(\lambda+d_b)\tau}-\lambda\right) \\
&= (-d_b-\lambda)\left(-d_h+\frac{2Kd_he^{d_b\tau}}{K+(H^*)^2}e^{-(\lambda+d_b)\tau}-\lambda\right)
\end{aligned}$$

where $H^* = \frac{re^{-d_b\tau}\left(1\pm\sqrt{1-\left(\frac{2d_he^{d_b\tau}}{r}\right)^2K}\right)}{2d_h}$. This implies that the stability of the interior equilibrium (B^*, H^*) is determined by the eigenvalues of the following equation evaluated at H^* since $\lambda = -d_b < 0$

$$-d_h+\frac{2Kd_h}{K+(H^*)^2}e^{-\lambda\tau}-\lambda = 0 \Leftrightarrow \lambda = -d_h+\frac{2Kd_h}{K+(H^*)^2}e^{-\lambda\tau}.$$

Let $A = -d_h$ and $B(H) = \frac{2d_hK}{K+H^2}$, then I have $B(H) > 0 > A$. At the mean time, I have

$$0 < H_1^* < H_2^* \text{ and } H_1^*H_2^* = K \Rightarrow (H_1^*)^2 < K \text{ and } (H_2^*)^2 > K.$$

Therefore, I can obtain the following inequalities

$$A+B(H_1^*) = -d_h+\frac{2Kd_h}{K+(H_1^*)^2} > 0 \text{ and } A+B(H_2^*) = -d_h+\frac{2Kd_h}{K+(H_2^*)^2} < 0.$$

By applying Theorem 4.7 from Hal Smith Smith [2010], I can conclude that the interior equilibrium E_1 is always unstable and E_2 is always locally asymptotically stable for any delay $\tau > 0$.

□

Proof of Theorem 3.3.4

Proof. According to Proposition 3.3.1, I know that Model (3.1) has a unique interior $E = (B^*, H^*) = \left(\frac{r\left(1-e^{-d_b\tau}\right)}{2d_b}, \sqrt{K}\right)$ when $d_h = \frac{re^{-d_b\tau}}{2\sqrt{K}}$. In order to study its stability, I define the following matrices:

$$U = \begin{bmatrix} -d_b & \frac{r}{2\sqrt{K}} \\ 0 & -d_h \end{bmatrix} \quad \text{and} \qquad V = \begin{bmatrix} 0 & -d_h \\ 0 & d_h \end{bmatrix}. \tag{A.4}$$

Let $L(\lambda)$ to be represented as follows

$$L(\lambda) = \lambda + d_h - d_h e^{-\lambda\tau} \tag{A.5}$$

which has $\lambda = 0$ as one of its eigenvalues. By applying Lemma A in A to (A.5), except for the root $\lambda = 0$, all roots of (A.5) has negative real parts for all $0 \leq \tau < \infty$. Since (A.5) has a simple zero eigenvalue, I need to use the center manifold and normal form theory in Faria and Magalhaes [1995] to obtain the local stability of $E = \left(\frac{r\left(1-e^{-d_b\tau}\right)}{2d_b}, \sqrt{K}\right)$.

Let $\tilde{B} = B - \frac{r\left(1-e^{-d_b\tau}\right)}{2d_b}$, $\tilde{H} = H - \sqrt{K}$, and still denote $\tilde{B} = B, \tilde{H} = H$, then the system (3.1) becomes

$$\begin{cases} \frac{dB}{dt} &= -d_b B(t) + \frac{r}{2\sqrt{K}} H(t) - d_h H(t-\tau) - \frac{r}{2K} H^2(t) + d_h\sqrt{K} H^2(t-\tau) + O(3), \\ \frac{dH}{dt} &= -d_h H(t) + d_h H(t-\tau) - d_h\sqrt{K} H^2(t-\tau) + O(3). \end{cases} \tag{A.6}$$

Let $\Lambda = \{0\}$. From normal form theory in Faria and Magalhaes [1995], there exists a one-dimension ordinary differential equation which has the same dynamical property as (A.6) near 0. Rewriting (A.6) as

$$\dot{z}(t) = l(z_t) + F(z_t) \tag{A.7}$$

where

$$z_t(\theta) = z(t+\theta) \in \mathcal{C} := ([-\tau, 0], \mathbb{R}^2_+),$$

$\mathcal{C}$ is the phase space with the norm $|\phi| = \max_{-\tau\leq\theta\leq 0} |\phi(\theta)|$, and

$$l(\phi) = U\phi(0) + V\phi(-\tau),$$

where U and V are given in (A.4), and

$$F(\phi) = \begin{bmatrix} -\frac{r}{2K}\phi_2^2(0) + d_h\sqrt{K}\phi_2^2(-\tau) + O(3) \\ -d_h\sqrt{K}\phi_2^2(-\tau) + O(3) \end{bmatrix}.$$

Take $\mu(\theta) = U\delta(\theta) - V\delta(\theta+\tau)$, where

$$\delta(\theta) = \begin{cases} 1, & \theta = 0, \\ 0, & \theta \neq 0. \end{cases}$$

Then I have follows

$$l(\phi) = \int_{-\tau}^{0} d\mu(\theta)\phi(\theta).$$

By the adjoint theory of FDE, the phase space $\mathcal{C}$ can be decomposed as $\mathcal{C} = P \oplus Q$, where $P = span\{\Phi(\theta)\}, \Phi(\theta) = (1,\beta)^T$, $\beta = \frac{d_b}{\frac{\tau}{2\sqrt{K}} - d_h}$. Taking the base Ψ of adjoint space P^* of P satisfies $\langle \Psi, \Phi \rangle = 1$, where $\langle \cdot, \cdot \rangle$ is a bilinear function defined in $\mathcal{C}^* \times \mathcal{C}$ by

$$\langle \psi, \phi \rangle = \psi(0)\phi(0) - \int_{-\tau}^{0}\int_{0}^{s} \psi(\theta - s)d\mu(s)\phi(\theta)d\theta.$$

By a direct computation, I have

$$\Psi(s) = \left(0, (\beta(1+\tau d_h))^{-1}\right).$$

Consider the following expand space

$$\mathcal{BC} = \left\{ \phi |\ \phi : [-\tau, 0] \to \mathcal{C}, \phi \text{ is continuous in } [-\tau, 0) \text{ and } \lim_{\theta \to 0} \phi(\theta) \text{ exists} \right\},$$

then the abstract ODE in $\mathcal{BC}$ associated with FDE (A.7) can be written as the form

$$\frac{d}{dt}u = Au + X_0 F(u), \tag{A.8}$$

where

$$A\phi = \dot{\phi} + X_0(l(\phi) - \dot{\phi}(0)),\ \phi \in C^1([-\tau, 0], \mathbb{R}^2_+),$$

and

$$X_0 = \begin{cases} I, & \theta = 0, \\ 0, & \theta \in [-\tau, 0). \end{cases}$$

The projection mapping $\pi : \mathcal{BC} \to P$:

$$\pi(\phi + X_0\alpha) = \Phi(\langle \Psi, \phi \rangle + \Psi(0)\alpha),$$

leads to the decomposition $\mathcal{BC} = P \oplus \text{Ker}\pi$. Decomposing u in Equation (A.8) in the form of $u = \Phi x + y$ where $x \in \mathbb{R}$ and $y \in Q^1 := \text{Ker}\pi \cap D(A) = Q \cap C^1$. Then (A.8) is equivalent to the system

$$\begin{cases} \dot{x} = \Psi(0)F(\Phi x + y), \\ \dot{y} = A_{Q^1} y + (I - \pi)X_0 F(\Phi x + y). \end{cases}$$

with

$$\Psi(0)F(\Phi x + y) = \frac{-d_h\sqrt{K}}{\beta(1 + \tau d_h)}(\beta x + y_2(-\tau))^2 + O(3).$$

Thus, the local invariable manifold of (A.6) at 0 with the tangency with the space P satisfies $y(\theta) = 0$, the flow on this manifold is given by the following one-dimension ODE

$$\dot{x}(t) = \frac{-\beta d_h\sqrt{K}}{1 + \tau d_h} x^2(t) + O(3). \tag{A.9}$$

This implies that the zero solution of (A.9) is stable. Therefore, the interior equilibrium $E = (B^*, H^*)$ is locally asymptotically stable for all $\tau > 0$. The proof is complete.

□

Proof of Theorem 3.3.5

Proof. I linearize the equations of Model 3.3:

$$D\left(\begin{bmatrix} \dot{B}(t) \\ \dot{H}(t) \end{bmatrix}\right)\Big|_{(B^*,H^*)} = \begin{bmatrix} -d_b & \frac{2rKH^*}{(K+(H^*)^2)^2} \\ 0 & -d_h \end{bmatrix}\begin{bmatrix} B(t) \\ H(t) \end{bmatrix} + \begin{bmatrix} -e^{-d_b\tau} & 0 \\ e^{-d_b\tau} & 0 \end{bmatrix}\begin{bmatrix} B(t-\tau) \\ H(t-\tau) \end{bmatrix}. \tag{A.10}$$

The matrix (A.10) evaluated at the extinction equilibrium E_e gives the characteristic equation

$$\begin{aligned} C(\lambda,\tau) &= det\left(\begin{bmatrix} -d_b & \frac{2rKH^*}{(K+(H^*)^2)^2} \\ 0 & -d_h \end{bmatrix} + \begin{bmatrix} -e^{-d_b\tau} & 0 \\ e^{-d_b\tau} & 0 \end{bmatrix} * e^{-\lambda\tau} - \lambda\mathscr{I}\right) \\ &= det\left(\begin{bmatrix} -d_b - e^{-d_b\tau}e^{-\lambda\tau} - \lambda & \frac{2rKH^*}{(K+(H^*)^2)^2} \\ e^{-d_b\tau}e^{-\lambda\tau} & -d_h - \lambda \end{bmatrix}\right) \\ &= (-d_h - \lambda)(-d_b - e^{-d_b\tau}e^{-\lambda\tau} - \lambda) - \frac{2rKH^*}{(K + (H^*)^2)^2}e^{-(d_b+\lambda)\tau} \end{aligned}$$

At $(0,0)$, $C(\lambda,\tau) = (-d_h - \lambda)(-d_b - e^{-d_b\tau}e^{-\lambda\tau} - \lambda)$. Clearly, one characteristic root is $\lambda = -d_h < 0$, others are the roots of the following equation

$$\lambda + d_b + e^{-d_b\tau}e^{-\lambda\tau} = 0. \tag{A.11}$$

When there is no delay, i.e., $\tau = 0$, (A.11) has only a negative characteristic root $\lambda == -d_b$, Model 3.3 is asymptotically stable at $(0,0)$. Moreover, for every $\tau \geq 0$, (A.11) has no nonnegative real root.

I assume $\lambda = iw$, $w > 0$, is a root of (A.11) for some $\tau > 0$. Then, I have

$$\cos(w\tau) = -d_b e^{d_b\tau}, \quad \sin(w\tau) = we^{d_b\tau}, \tag{A.12}$$

which gives

$$w^2 = e^{-2d_b\tau} - d_b^2. \tag{A.13}$$

It is clear that (A.13) has a positive real root

$$w = (e^{-2d_b\tau} - d_b^2)^{\frac{1}{2}}. \tag{A.14}$$

if and only if $e^{-d_b\tau} > d_b$, i.e., $\tau < \tau^* := \frac{1}{d_b}\ln\left(\frac{1}{d_b}\right)$, and $0 < d_b < 1$.

Notice that $\cos(w\tau) < 0, \sin(w\tau) > 0$, there is a unique θ, $\frac{\pi}{2} < \theta < \pi$, such that $w\tau = \theta$ makes both equation of (A.12) hold. Then, if $e^{-d_b\tau} > d_b$, I get a set of values of τ for which there are imaginary roots:

$$\tau_k = \frac{\theta + k\pi}{w}, \quad k = 0, 1, 2, \cdots, \tag{A.15}$$

where w is given by (A.14) and

$$\theta = \pi - \arctan\left(\frac{w}{d_b}\right). \tag{A.16}$$

From (A.11), I have

$$(1 - \tau e^{-(d_b+\lambda)\tau})\frac{d\lambda}{d\tau} = (\lambda + d_b)e^{-(d_b+\lambda)\tau}, \quad \text{and} \quad \lambda + d_b = -e^{-(d_b+\lambda)\tau}.$$

Thus,

$$\left(\frac{d\lambda}{d\tau}\right)^{-1} = -\frac{\tau}{\lambda + d_b} - \frac{1}{(d_b + \lambda)^2},$$

and

$$\begin{aligned}
S(\tau) :&= \operatorname{sign}\left\{\left(\frac{d(\mathrm{Re}\lambda)}{d\tau}\right)\right\}_{\lambda=iw} = \operatorname{sign}\left\{\mathrm{Re}\left(\frac{d\lambda}{d\tau}\right)^{-1}\right\}_{\lambda=iw} \\
&= \operatorname{sign}\left\{-\mathrm{Re}\frac{\tau}{\lambda+b} - \mathrm{Re}\frac{1}{(b+\lambda)^2}\right\}_{\lambda=iw} \\
&= \operatorname{sign}\{-\tau d_b^3 - d_b^2 + w^2(\tau d_b - 1)\} \\
&= \operatorname{sign}\{-2d_b^2 + (1-\tau d_b)e^{-2d_b\tau}\} \\
&= \operatorname{sign}\{\phi(\tau)\}.
\end{aligned}$$

Here,

$$\phi(\tau) = -2d_b^2 + (1-\tau d_b)e^{-2d_b\tau}. \tag{A.17}$$

Clearly,

$$\phi'(\tau) = e^{-2d_b\tau} d_b(2\tau d_b - 3). \tag{A.18}$$

In order to get the stability of the equilibrium $(0,0)$, I first claim:

- For all $\tau \geq \max\{0, \tau^*\}$, $(0,0)$ is asymptotically stable.

In fact, I rewrite (A.11) as the form $\lambda = A + Be^{-\lambda\tau}$ with $A = -d_b, B = -e^{-d_b\tau}$. For any $\tau \geq \tau^*$, $B \geq -e^{-d_b\tau^*} = -d_b = A$. Thus, by applying Theorem 4.7 from Hal Smith, $(0,0)$ is local asymptotically stable.

Now, I consider the following two cases.

Case 1. $d_b \geq \frac{\sqrt{2}}{2}$.

This case is divided into two subcases: (i) $d_b \geq 1$ and (ii) $\frac{\sqrt{2}}{2} \leq d_b < 1$.

(i) $d_b \geq 1$.

In this subcase, the above claim implies that $(0,0)$ is asymptotically stable for all $\tau \geq 0$. This also can be proved as follows. For all $\tau \geq 0$, $e^{-2d_b\tau} - d_b^2 < 0$ holds, and hence the equation (A.13) has no positive real root. This implies that the equilibrium $(0,0)$ has no stability switch as τ increases in $[0,\infty)$. Since $(0,0)$ is asymptotically stable at $\tau = 0$, then it remains asymptotically stable for all $\tau \geq 0$.

(ii) $\frac{\sqrt{2}}{2} \leq d_b < 1$.

Assume $\tau \in (0, \tau^*)$. Then $e^{-2d_b\tau} - d_b^2 > 0$ and (A.13) has unique positive real root (A.14). In such case, $\tau d_b < 1$ since $\tau d_b < \tau^* d_b = \ln\left(\frac{1}{d_b}\right) \leq \ln\sqrt{2} < 1$, $\phi(\tau) < -2d_b^2 + (1-\tau d_b) \leq -\tau d_b < 0$. It follows that $S(\tau) = -1$ for $\tau \in (0, \tau^*)$, i.e., possible stability switches from unstable to stable may occur. Since $(0,0)$ is asymptotically stable at $\tau = 0$, then it remains asymptotically stable for all $\tau \in (0, \tau^*)$.

When $\tau \geq \tau^*$, our claim shows that $(0,0)$ is asymptotically stable. Therefore, $(0,0)$ is asymptotically stable for all $\tau \geq 0$.

Case 2. $0 < d_b < \frac{\sqrt{2}}{2}$.

This case is also divided into two subcases: (i) $\frac{1}{e} \leq d_b < \frac{\sqrt{2}}{2}$ and (ii) $d_b < \frac{1}{e}$.

(i) $\frac{1}{e} \leq d_b < \frac{\sqrt{2}}{2}$.

For $\tau \geq \tau^*$, I know that $(0,0)$ is asymptotically stable. Now, I assume $\tau \in (0, \tau^*)$, then (A.13) has unique positive real root (A.14). In such case, $\phi(0) = 1 - 2d_b^2 > 0$ and $\phi(\tau^*) = -2d_b^2 + (1 - \tau^* d_b)e^{-2d_b\tau^*} = -2d_b^2 + (1 - \tau^* d_b)d_b^2 < 0$, and, from (A.18), $\phi'(\tau) < 0$ since $\tau d_b < \tau^* d_b = \ln\left(\frac{1}{d_b}\right) \leq 1$. Thus, there exists unique $\tau_c \in (0, \tau^*)$ such that

(a) For $\tau \in (0, \tau_c)$, $\phi(\tau) > 0$ and hence $S(\tau) = 1$. In this case, possible stability switches from stable to unstable may occur as τ increases in $(0, \tau_c)$.

(b) At $\tau = \tau_c$, $\phi(\tau) = 0$ and hence $S(\tau) = 0$;

(c) For $\tau \in (\tau_c, \tau^*)$, $\phi(\tau) < 0$ and hence $S(\tau) = -1$. In this case, possible stability switches from unstable to stable may occur as τ increases in (τ_c, τ^*).

Therefore, by the stability of $(0,0)$ at $\tau = 0$ and $\tau \geq \tau^*$, I can conclude that $(0,0)$ is asymptotically stable for $\tau \in (0, \tau_0)$ or $\tau \geq \tau_1$, while unstable for $\tau \in (\tau_0, \tau_1)$, where τ_0, τ_1 are given by (A.15).

(ii) $d_b < \frac{1}{e}$.

Since $\frac{1}{d_b} > e$, then $\frac{1}{d_b} < \tau^* = \frac{1}{d_b}\ln\left(\frac{1}{d_b}\right)$. Thus, I has the following two scenarios:

(1) $\tau \in \left(\frac{1}{d_b}, \tau^*\right)$. Since $\tau d_b \geq 1$, I have $\phi(\tau) < 0$ and hence $S(\tau) = -1$, which implies that possible stability switches from unstable to stable may occur as τ increases in $\left(\frac{1}{d_b}, \tau^*\right)$.

(2) $\tau \in \left(0, \frac{1}{d_b}\right)$. In such case, $\phi(0) = 1 - 2d_b^2 > 0$ and $\phi\left(\frac{1}{d_b}\right) = -2d_b^2 < 0$, and $\phi'(\tau) < 0$. Thus, there exists unique $\tau_c \in \left(0, \frac{1}{d_b}\right)$

(a) For $\tau \in (0, \tau_c)$, $\phi(\tau) > 0$ and hence $S(\tau) = 1$. .

(b) At $\tau = \tau_c$, $\phi(\tau) = 0$ and hence $S(\tau) = 0$;

(c) For $\tau \in \left(\tau_c, \frac{1}{d_b}\right)$, $\phi(\tau) < 0$ and hence $S(\tau) = -1$. .

Therefore, by the stability of $(0,0)$ at $\tau = 0$ and $\tau \geq \tau^*$, I can conclude that $(0,0)$ is asymptotically stable for $\tau \in (0, \tau_0)$ or $\tau \geq \tau_1$, while unstable for $\tau \in (\tau_0, \tau_1)$.

□

Proof of Theorem 3.3.6

Proof. Consider the positive equilibria of Model 3.3. (B^*, H^*) is a positive equilibrium if and only if $B^* = d_h e^{d_b\tau} H^*$ and H^* is a positive root of

$$\frac{rH}{K+H^2} = d_h(d_b e^{d_b\tau} + 1), \tag{A.19}$$

or, equivalently,

$$d_h(d_b e^{d_b\tau} + 1)H^2 - rH + Kd_h(d_b e^{d_b\tau} + 1) = 0. \tag{A.20}$$

Clearly, if $r < 2\sqrt{K}d_h(d_b e^{d_b\tau}+1)$, there is no positive equilibrium; if $r > 2\sqrt{K}d_h(d_b e^{d_b\tau}+1)$, or, equivalently,

$$\tau < \frac{1}{d_b}\ln\left(\left(\frac{r}{2d_h\sqrt{K}} - 1\right)/d_b\right), \quad \text{and} \quad r > 2d_h\sqrt{K}(1+d_b), \tag{A.21}$$

Model 3.3 has two positive equilibria $E_1 = (B_1^*, H_1^*)$ and $E_2 = (B_2^*, H_2^*)$ $(H_1^* < H_2^*)$, where

$$H_i^* = \frac{r \pm \sqrt{r^2 - 4K\left(d_b d_h e^{d_b\tau} + d_h\right)^2}}{2\left(d_b d_h e^{d_b\tau} + d_h\right)}, \; i = 1, 2.$$

Let

$$\tau^* = \frac{1}{d_b}\ln\left(\left(\frac{r}{2d_h\sqrt{K}} - 1\right)/d_b\right), \quad \text{subject to} \quad r > 2d_h\sqrt{K}(1+d_b). \tag{A.22}$$

The characteristic equation at (B_i^*, H_i^*) is

$$C(\lambda,\tau) = \lambda^2 + (d_b + d_h)\lambda + d_b d_h + (\lambda + d_h - \Phi(H^*)(\tau))e^{-d_b\tau}e^{-\lambda\tau} = 0, \tag{A.23}$$

where

$$\Phi(H^*)(\tau) = \frac{2rKH^*}{(K + (H^*)^2)^2} \tag{A.24}$$

and $H^* = H_1^*$ or H_2^*, depending on τ.

Let

$$P(\lambda,\tau) = \lambda^2 + P_1(\tau)\lambda + P_0(\tau), \quad Q(\lambda,\tau) = Q_1(\tau)\lambda + Q_0(\tau), \tag{A.25}$$

where

$$P_1(\tau) = d_b + d_h, \quad P_0(\tau) = d_b d_h, \tag{A.26}$$

$$Q_1(\tau) = e^{-d_b\tau}, \qquad Q_0(\tau) = (d_h - \Phi(H^*)(\tau))e^{-d_b\tau}. \tag{A.27}$$

Then the characteristic equation (A.28) can be rewritten as follows

$$C(\lambda,\tau) = P(\lambda,\tau) + Q(\lambda,\tau)e^{-\lambda\tau} = 0. \tag{A.28}$$

First, I prove that $\lambda = 0$ cannot be a root of (A.28), i.e., $P(0,\tau) + Q(0,\tau) \neq 0$, for any $\tau \in [0,\tau^*)$. In fact,

$$\begin{aligned} C(0,\tau) &= P(0,\tau) + Q(0,\tau) = P_0(\tau) + Q_0(\tau) \\ &= d_b d_h + (d_h - \Phi(H^*)(\tau))e^{-d_b\tau} \\ &= e^{-d_b\tau}(d_h(d_b e^{d_b\tau} + 1) - \Phi(H^*)(\tau)) \\ &= e^{-d_b\tau}\left(\tfrac{rH^*}{K+(H^*)^2} - \tfrac{2rKH^*}{(K+(H^*)^2)^2}\right) \\ &= e^{-d_b\tau}\Phi(H^*)(\tau)((H^*)^2 - K). \end{aligned} \tag{A.29}$$

Here, (A.19) is used in the third equation. Since $H_1^* H_2^* = K$ and $H_1^* < H_2^*$, I know that $(H_1^*)^2 < K < (H_2^*)^2$. Thus, $C(0,\tau) < 0$ at $E_1 = (B_1^*, H_1^*)$, and $C(0,\tau) > 0$ at $E_2 = (B_2^*, H_2^*)$. It follows that for all $\tau \in [0,\tau^*)$, $\lambda = 0$ cannot be a root of (A.28) at both E_1 and E_2.

Now, I consider the stability of E_1 and E_2 when $\tau = 0$. At $\tau = 0$, the characteristic equation (A.28) becomes $P(0,\tau) + Q(0,\tau) = 0$, i.e.,

$$\lambda^2 + (P_1(0) + Q_1(0))\lambda + P_0(0) + Q_0(0) = 0. \tag{A.30}$$

At $E_1 = (B_1^*, H_1^*)$, since $P_0(\tau)+Q_0(\tau) < 0$ for all $\tau \in [0,\tau^*)$, I have $P_0(0)+Q_0(0) < 0$. At $E_2 = (B_2^*, H_2^*)$, I have $P_0(0)+Q_0(0) > 0$ since $P_0(\tau)+Q_0(\tau) > 0$ for all $\tau \in [0,\tau^*)$. Thus, I can conclude that at $\tau = 0$, E_1 is unstable and E_2 is locally asymptotically stable.

In order to determine the local stability of the interior equilibrium $E_i, i = 1,2$ when $\tau \in (0,\tau^*)$, I proceed as follows Kuang's book Chapter 3 Kuang [1993].

Let $\lambda = iw(\tau), w(\tau) > 0$, be the root of (A.28), then I have

$$\begin{aligned} &P(iw,\tau) = -w^2 + iwP_1(\tau) + P_0(\tau), && Q(iw,\tau) = iwQ_1(\tau) + Q_0(\tau), \\ &P_{\mathrm{R}}(iw,\tau) = P_0(\tau) - w^2, && Q_{\mathrm{R}}(iw,\tau) = Q_0(\tau), \\ &P_{\mathrm{I}}(iw,\tau) = wP_1(\tau), && Q_{\mathrm{I}}(iw,\tau) = wQ_1(\tau). \end{aligned} \tag{A.31}$$

By Theorem 4.1 in Kuang's book Kuang [1993], I look for the positive roots $w(\tau) > 0$ of

$$F(w,\tau) = |P(iw,\tau)|^2 - |Q(iw,\tau)|^2 = 0, \quad \tau \in [0,\tau^*). \tag{A.32}$$

Since

$$F(w,\tau) = w^2 + w^2(-2P_0(\tau) + P_1^2(\tau) - Q_1^2(\tau)) + P_0^2(\tau) - Q_0^2(\tau) \tag{A.33}$$

$$= w^4 + b(\tau)w^2 + c(\tau), \tag{A.34}$$

where

$$b(\tau) = -2P_0(\tau) + P_1^2(\tau) - Q_1^2(\tau), \quad c(\tau) = P_0^2(\tau) - Q_0^2(\tau), \tag{A.35}$$

equation (A.33) may have no positive root, one positive root $w_+(\tau)$ or $w_-(\tau)$, or two positive roots $w_+(\tau)$ and $w_-(\tau)$, depending on $b(\tau)$ and $c(\tau)$. $w_\pm(\tau)$ can be represent as follows:

$$w_\pm(\tau) = \left[\frac{1}{2}(-b(\tau) \pm \sqrt{b^2(\tau) - 4c(\tau)})\right]^{\frac{1}{2}}.$$

In order to determine the occurrence of stability switches, I need to determine the sign of $\frac{d\mathrm{Re}\lambda}{d\tau}$ or $\mathrm{Re}\left(\frac{d\lambda}{d\tau}\right)^{-1}$. From Theorem 3.1 and its proof of KuangKuang [1993], I have

$$\begin{aligned} S(\tau): \ &= \mathrm{sign}\left\{\left(\frac{d(\mathrm{Re}\lambda)}{d\tau}\right)\right\}_{\lambda=iw} = \mathrm{sign}\left\{\mathrm{Re}\left(\frac{d\lambda}{d\tau}\right)^{-1}\right\}_{\lambda=iw} \\ &= \mathrm{sign}\{P_1^2(\tau) - 2P_0(\tau) - Q_1^2(\tau) + 2w^2\} \\ &= \mathrm{sign}\{\pm\sqrt{b^2(\tau) - 4c(\tau)}\}. \end{aligned} \tag{A.36}$$

First, I consider the local stability of the interior equilibrium E_1 when $\tau \in [0, \tau^*)$. Since for all $\tau \in [0, \tau^*)$, $P_0(\tau) + Q_0(\tau) < 0$, and $P_0(\tau) = d_b d_h > 0$, I have $Q_0(\tau) = (d_h - \Phi(H^*)(\tau))e^{-d_b\tau} < 0$. Thus, $P_0(\tau) - Q_0(\tau) > 0$, $\tau \in [0, \tau^*)$. It follows that

$$c(\tau) = P_0^2(\tau) - Q_0^2(\tau) = [P_0(\tau) + Q_0(\tau)][P_0(\tau) - Q_0(\tau)] < 0, \quad \tau \in [0, \tau^*).$$

Therefore, (A.33) has unique positive root $w_+(\tau)$. From (A.36), $S(\tau) = 1$. Since E_1 is unstable at $\tau = 0$, no stability switch occur as τ increases in $[0, \tau^*)$, and E_1 is unstable for all $\tau \in [0, \tau^*)$.

Now, I consider the local stability of the interior equilibrium E_2 when $\tau \in [0, \tau^*)$. I have know that for all $\tau \in [0, \tau^*)$, $P_0(\tau)+Q_0(\tau) > 0$ and $c(\tau) = [P_0(\tau)+Q_0(\tau)][P_0(\tau)-Q_0(\tau)]$. Thus, I consider the sign of $P_0(\tau) - Q_0(\tau)$. By a careful computation, I get

$$P_0(\tau) - Q_0(\tau) = d_h e^{-d_b\tau}\varphi(\tau), \tag{A.37}$$

where

$$\varphi(\tau) = (d_b e^{d_b\tau} + 1)\left[2 - \sqrt{1 - \frac{4Kd_h^2(d_b e^{d_b\tau} + 1)^2}{r^2}}\right] - 2. \tag{A.38}$$

It is clear that $\varphi(\tau)$ is strictly increasing with respect to $\tau \in [0, \tau^*)$, $f(\tau^*) = 2d_b e^{d_b\tau^*}$, and

$$\varphi(0) = (d_b + 1)\left[2 - \sqrt{1 - \frac{4Kd_h^2(d_b + 1)^2}{r^2}}\right] - 2.$$

Now, I consider the following two cases.

Case 1. $d_b \geq 1$. Then clearly $\varphi(0) > 0$ and hence $\varphi(\tau) > 0$ for all $\tau \in [0, \tau^*)$. Thus, $c(\tau) > 0$. In addition, $b(\tau) = d_b^2 + d_h^2 - e^{-2d_b\tau} > 0$. Therefore, for all $\tau \in [0, \tau^*)$, $F(w, \tau) \neq 0$. This implies that in such case no stability switch occur with τ increasing in $[0, \tau^*)$. Since E_2 is is locally asymptotically stable at $\tau = 0$, I can conclude that E_2 is is locally asymptotically stable for all $\tau \in [0, \tau^*)$ if $d_b \geq 1$.

Case 2. $0 < d_b < 1$. Then, $(1 + d_b)^2 - 4d_b^2 > 0$. When $r > 2d_h\sqrt{K}(1 + d_b)$, I have

$$\begin{aligned} \varphi(0) > 0 \quad &\Leftrightarrow \sqrt{1 - \tfrac{4Kd_h^2(d_b+1)^2}{r^2}} < \tfrac{2d_b}{1+d_b} \\ &\Leftrightarrow r < \tfrac{2d_h\sqrt{K}(1+d_b)^2}{\sqrt{(1+d_b)^2-4d_b^2}}. \end{aligned} \tag{A.39}$$

Thus, when $2d_h\sqrt{K}(1+d_b) < r < \frac{2d_h\sqrt{K}(1+d_b)^2}{\sqrt{(1+d_b)^2-4d_b^2}}$, $\varphi(0) > 0$ and hence for all $\tau \in [0, \tau^*)$, $c(\tau) > 0$.

This case is also divided into two subcases: (i) $d_b^2 + d_h^2 \geq 1$, (ii) $d_b^2 + d_h^2 < 1$.

(i) $d_b^2 + d_h^2 \geq 1$. It follows $b(\tau) = d_b^2 + d_h^2 - e^{-2d_b\tau} > 0$. Thus, in such case, $F(w, \tau) \neq 0$ holds for all $\tau \in [0, \tau^*)$. This implies that in such case no stability switch occur with τ increasing in $[0, \tau^*)$. Since E_2 is locally asymptotically stable at $\tau = 0$, I can conclude that E_2 is is locally asymptotically stable for all $\tau \in [0, \tau^*)$ if $2d_h\sqrt{K}(1 + d_b) < r \leq \frac{2d_h\sqrt{K}(1+d_b)^2}{\sqrt{(1+d_b)^2-4d_b^2}}$.

If $r > \frac{2d_h\sqrt{K}(1+d_b)^2}{\sqrt{(1+d_b)^2-4d_b^2}}$, then $\varphi(0) < 0$ and there exists unique $\tau_c \in (0, \tau^*)$ such that $c(\tau) < 0$ for $\tau \in (0, \tau_c)$ and $c(\tau) > 0$ for $\tau \in (\tau_c, \tau^*)$. Thus, if $\tau \in (\tau_c, \tau^*)$, then $F(w, \tau) = 0$ has no positive root; if $\tau \in (0, \tau_c)$, then $F(w, \tau) = 0$ has a unique positive root w_+ and $S(\tau) = 1$. Since E_2 is stable at $\tau = 0$, from Theorem 3.1 of Kuang Kuang [1993], I know that the stability of E_2 switches just once in $[0, \tau_c)$ from stable to unstable.

(ii) $d_b^2 + d_h^2 < 1$. I divide this subcase into the following two scenarios:

(a) $\frac{d_b^2}{\left(\frac{(1+d_b)^2}{\sqrt{(1+d_b)^2-4d_b^2}}-1\right)^2} < d_b^2 + d_h^2 < 1$, which implies that

$$2d_h\sqrt{K}\left(1 + \sqrt{\frac{d_b^2}{d_b^2 + d_h^2}}\right) < 2d_h\sqrt{K}\frac{(1 + d_b)^2}{\sqrt{(1 + d_b)^2 - 4d_b^2}}.$$

This scenario is again divided into following three cases:

(1) $2d_h\sqrt{K}\left(1 + \sqrt{\frac{d_b^2}{d_b^2+d_h^2}}\right) < r \leq 2d_h\sqrt{K}\frac{(1+d_b)^2}{\sqrt{(1+d_b)^2-4d_b^2}}$.

Since $2d_h\sqrt{K}\left(1+\sqrt{\frac{d_b^2}{d_b^2+d_h^2}}\right) > 2d_h\sqrt{K}(1+d_b)$, from (A.39), $\varphi(0) \geq 0$ and hence for all $\tau \in [0, \tau^*)$, $c(\tau) \geq 0$.

When $\frac{1}{2d_b}\ln\left(\frac{1}{d_b^2+d_h^2}\right) \leq \tau < \tau^*$, $b(\tau) \geq 0$. Thus, for all $\tau \in [0, \tau^*)$, $F(w, \tau) \neq 0$.

When $0 < \tau < \frac{1}{2d_b}\ln\left(\frac{1}{d_b^2+d_h^2}\right)$, I have $b(\tau) < 0$. Thus, I consider $b^2(\tau) - 4c(\tau)$. By a simple computation, I have

$$\begin{aligned} b^2(\tau) - 4c(\tau) &= (P_1^2(\tau) - Q_1^2(\tau))(P_1^2(\tau) - Q_1^2(\tau) - 4P_0(\tau)) + 4Q_0^2(\tau) \\ &= \phi(\tau) + 4Q_0^2(\tau). \end{aligned}$$

Here, $\phi(\tau) = \left((d_b+d_h)^2 - e^{-2d_b\tau}\right)\left((d_b+d_h)^2 - e^{-2d_b\tau} - 4d_bd_h\right)$. It is clear that

$$\phi(\tau) \geq 0 \Leftrightarrow \tau \leq \frac{1}{2d_b}\ln\left(\frac{1}{(d_b+d_h)^2}\right) \quad \text{or} \quad \tau \geq \frac{1}{2d_b}\ln\left(\frac{1}{(d_b-d_h)^2}\right).$$

Thus, if $\frac{1}{2d_b}\ln\left(\frac{1}{(d_b+d_h)^2}\right) < \tau < \frac{1}{2d_b}\ln\left(\frac{1}{d_b^2+d_h^2}\right)$, then $\phi(\tau) < 0$.
If $0 < \tau \leq \frac{1}{2d_b}\ln\left(\frac{1}{(d_b+d_h)^2}\right)$, then $\phi(\tau) \geq 0$ and hence $b^2(\tau) - 4c(\tau) > 0$, which implies that $F(w, \tau) = 0$ have two positive roots $0 < w_- < w_+$. Thus, from Theorem 3.1 of KuangKuang [1993], the stability of E_2 can change a finite number of times at most as τ is increased $\tau \in [0, \tau^*)$, and eventually it becomes unstable.

(2) $2d_h\sqrt{K}(1+d_b) < r \leq 2d_h\sqrt{K}\left(1+\sqrt{\frac{d_b^2}{d_b^2+d_h^2}}\right)$.

From (A.39), $\varphi(0) > 0$ and hence for all $\tau \in [0, \tau^*)$, $c(\tau) > 0$. In this case,

$$\tau^* = \frac{1}{d_b}\ln\left(\left(\frac{r}{2d_h\sqrt{K}} - 1\right)/d_b\right) \leq \frac{1}{2d_b}\ln\left(\frac{1}{d_b^2+d_h^2}\right).$$

It follows $b(\tau) = d_b^2 + d_h^2 - e^{-2d_b\tau} < 0$ for all $\tau \in (0, \tau^*)$. Note that

$$\begin{aligned} \tau^* = \frac{1}{d_b}\ln\left(\left(\frac{r}{2d_h\sqrt{K}} - 1\right)/d_b\right) \leq \frac{1}{2d_b}\ln\left(\frac{1}{(d_b+d_h)^2}\right) \\ \Leftrightarrow r \leq 2d_h\sqrt{K}\left(\frac{d_b}{d_b+d_h} + 1\right). \end{aligned}$$

Thus,

- when $2d_h\sqrt{K}(1+d_b) < r \leq 2d_h\sqrt{K}\left(\frac{d_b}{d_b+d_h}+1\right)$, $\phi(\tau) \geq 0$ and hence $b^2(\tau) - 4c(\tau) > 0$ for all $\tau \in [0, \tau^*)$. It yields that $F(w, \tau) = 0$ have two positive roots $0 < w_- < w_+$. Thus, from Theorem 3.1 of Kuang Kuang [1993], the stability of E_2 can change a finite number of times at most as τ is increased in $[0, \tau^*)$, and eventually it becomes unstable.

- when $2d_h\sqrt{K}\left(\frac{d_b}{d_b+d_h}+1\right) < r \le 2d_h\sqrt{K}\left(1+\sqrt{\frac{d_b^2}{d_b^2+d_h^2}}\right)$,
  I have $\tau^* > \frac{1}{2d_b}\ln\left(\frac{1}{(d_b+d_h)^2}\right)$. If $\frac{1}{2d_b}\ln\left(\frac{1}{(d_b+d_h)^2}\right) < \tau < \tau^*$, then $\phi(\tau) < 0$. If $0 < \tau \le \frac{1}{2d_b}\ln\left(\frac{1}{(d_b+d_h)^2}\right)$, $\phi(\tau) \ge 0$ and hence $b^2(\tau) - 4c(\tau) > 0$. Thus, in such case, from Theorem 3.1 of Kuang Kuang [1993] the stability of E_2 can change a finite number of times at most as τ is increased in $[0, \tau^*)$.

(3) $r > \frac{2d_h\sqrt{K}(1+d_b)^2}{\sqrt{(1+d_b)^2-4d_b^2}}$.

In this case, $\varphi(0) < 0$ and there exists unique $\tau_c \in (0, \tau^*)$ such that $c(\tau) < 0$ for $\tau \in (0, \tau_c)$ and $c(\tau) > 0$ for $\tau \in (\tau_c, \tau^*)$. Thus, if $\tau \in (0, \tau_c)$, then $F(w, \tau) = 0$ has a unique positive root w_+ and $S(\tau) = 1$. Since E_2 is stable at $\tau = 0$, from Theorem 3.1 of Kuang Kuang [1993], I know that the stability of E_2 switches once in $[0, \tau_c)$ from stable to unstable.

(b) $d_b^2 + d_h^2 \le \frac{d_b^2}{\left(\frac{(1+d_b)^2}{\sqrt{(1+d_b)^2-4d_b^2}}-1\right)^2}$, which implies that

$$2d_h\sqrt{K}\left(1+\sqrt{\frac{d_b^2}{d_b^2+d_h^2}}\right) \ge 2d_h\sqrt{K}\frac{(1+d_b)^2}{\sqrt{(1+d_b)^2-4d_b^2}}.$$

This scenario is again divided into following two cases:

(1) $2d_h\sqrt{K}(1+d_b) < r \le \frac{2d_h\sqrt{K}(1+d_b)^2}{\sqrt{(1+d_b)^2-4d_b^2}}$.

From (A.39), $\varphi(0) > 0$ and hence for all $\tau \in [0, \tau^*)$, $c(\tau) > 0$. In this case, I also have $\tau^* \le \frac{1}{2d_b}\ln\left(\frac{1}{d_b^2+d_h^2}\right)$. It follows $b(\tau) = d_b^2 + d_h^2 - e^{-2d_b\tau} < 0$ for all $\tau \in (0, \tau^*)$.

If $2d_h\sqrt{K}\left(\frac{d_b}{d_b+d_h}+1\right) < \frac{2d_h\sqrt{K}(1+d_b)^2}{\sqrt{(1+d_b)^2-4d_b^2}}$, similar to the arguments above, I get that no matter $2d_h\sqrt{K}(1+d_b) < r \le 2d_h\sqrt{K}\left(\frac{d_b}{d_b+d_h}+1\right)$ or $2d_h\sqrt{K}\left(\frac{d_b}{d_b+d_h}+1\right) < r \le 2d_h\sqrt{K}\frac{(1+d_b)^2}{\sqrt{(1+d_b)^2-4d_b^2}}$ the stability of E_2 can change a finite number of times at most as τ is increased in $[0, \tau^*)$.

If $\frac{2d_h\sqrt{K}(1+d_b)^2}{\sqrt{(1+d_b)^2-4d_b^2}} < 2d_h\sqrt{K}\left(\frac{d_b}{d_b+d_h}+1\right)$, then when $2d_h\sqrt{K}(1+d_b) < r \le \frac{2d_h\sqrt{K}(1+d_b)^2}{\sqrt{(1+d_b)^2-4d_b^2}}$, $\phi(\tau) \ge 0$ for all $[0, \tau^*)$ and hence $b^2(\tau) - 4c(\tau) > 0$ for all $\tau \in [0, \tau^*)$. It yields that $F(w, \tau) = 0$ have two positive roots $0 < w_- < w_+$. Thus, from Theorem 3.1 of Kuang Kuang [1993], the stability of E_2 can change a finite number of times at most as τ is increased in $[0, \tau^*)$, and eventually it becomes unstable.

(2) $r > \frac{2d_h\sqrt{K}(1+d_b)^2}{\sqrt{(1+d_b)^2-4d_b^2}}$.

Similar to the arguments above, $\varphi(0) < 0$ and there exists unique $\tau_c \in (0, \tau^*)$ such that the stability of E_2 switches once in $[0, \tau_c)$ from stable to unstable.

The proof is completed.

□

Some Important Lemmas

Consider the characteristic equation of the form

$$p(z) + e^{-z\tau}q(z) = 0 \tag{A.40}$$

where p and q are polynomials with real coefficients and $\tau > 0$ is the delay. The following result was given by Brauer Brauer [1987].

Lemma A. *Suppose that $p(z)$ and $q(z)$ are analytic in some open set containing $z \geq 0$, and satisfying the following conditions:*
(i) $p(z) \neq 0$, $Rez \geq 0$,
(ii) $\overline{p(-iy)} = p(iy), \overline{q(-iy)} = q(iy), 0 \leq y < \infty$,
(iii) $p(0) + q(0) = 0$,
(iv) $|q(iy)| < |p(iy)|$ *for* $0 < y < \infty$,
(v) $\lim_{|z|\to\infty, Rez\geq 0} |q(z)/p(z)| = 0$.
Then except for the roots $z = 0$, all roots of (A.40) *are in $Rez < 0$ for all $0 \leq \tau < \infty$.*

I need the fluctuation lemma due to Hirsh, Hanisch, and GabrielHirsch *et al.* [1985].

Lemma B (Fluctuation Lemma)**.** *Let $f : \mathbb{R}_+ \to \mathbb{R}$ be a differentiable function. If $\liminf_{t\to\infty} f(t) < \limsup_{t\to\infty} f(t)$, then there are sequences $\{t_m\} \uparrow \infty$ and $\{s_m\} \uparrow \infty$ such that*

$$f(t_m) \to \limsup_{t\to\infty} f(t), \quad f'(t_m) \to 0 \quad as \quad m \to \infty,$$
$$f(s_m) \to \liminf_{t\to\infty} f(t), \quad f'(s_m) \to 0 \quad as \quad m \to \infty.$$

Proof of Proposition 3.3.1

Proof. Let $m = d_b r$, $n = d_h^2 e^{d_b\tau}(e^{d_b\tau} - 1)$, and $c = 4d_b^2 d_h^2 K e^{2d_b\tau}$, then:

$$H_1^* = \frac{e^{-d_b\tau}}{2d_b d_h}(m - \alpha n - \sqrt{(m - \alpha n)^2 - c}),$$

and

$$H_2^* = \frac{e^{-d_b\tau}}{2d_b d_h}(m - \alpha n + \sqrt{(m - \alpha n)^2 - c}).$$

So, function $g = m - \alpha n - \sqrt{(m - \alpha n)^2 - c}$ and function $f = m - \alpha n + \sqrt{(m - \alpha n)^2 - c}$ will decide two equilibrium functions are increasing or decreasing functions of α. After that,

$$g'(\alpha) = n(-1 + \frac{m - n\alpha}{\sqrt{(m - n\alpha)^2 - c}}),$$

and

$$f'(\alpha) = n(-1 + \frac{n\alpha - m}{\sqrt{(m - n\alpha)^2 - c}}).$$

Since $H_1^* > 0$, $m > n\alpha$ and $m - n\alpha > \sqrt{(m - \alpha n)^2 - c}$, therefore $g'(\alpha) > 0$ and $f'(\alpha) < 0$, i.e. H_1^* is monotonically increasing, and H_2^* is monotonically decreasing.

Next, I consider parameter r. Then

$$g'(r) = d_b(1 - \frac{d_b r - n\alpha}{\sqrt{(d_b r - n\alpha)^2 - c}}) < 0,$$

and

$$f'(r) = d_b(1 + \frac{d_b r - n\alpha}{\sqrt{(d_b r - n\alpha)^2 - c}}) > 0.$$

Therefore, H_1^* is monotonically decreasing by r, and H_2^* is monotonically increasing by r.

Afterwards, if K increases, only c will increase. Then $\sqrt{(m - n\alpha)^2 - c}$ will decrease. Therefore, H_1^* is monotonically increasing by K, and H_2^* is monotonically decreasing by K.

When I consider d_b and d_h, I can simplified the model to Model (3.2), i.e. $\alpha = 0$. Then I let H_1^* be the function $p = \frac{e^{-d_b\tau}\left(r - \sqrt{r^2 - 4d_h^2 K e^{2d_b\tau}}\right)}{2d_h}$, and H_2^* be the function $q = \frac{e^{-d_b\tau}\left(r + \sqrt{r^2 - 4d_h^2 K e^{2d_b\tau}}\right)}{2d_h}$. So,

$$p'(d_h) = \frac{re^{-d_b\tau}\left(\frac{r}{\sqrt{r^2 - 4d_h^2 K e^{2d_b\tau}}} - 1\right)}{2d_h^2} > 0,$$

and

$$q'(d_h) = \frac{re^{-d_b\tau}\left(-\frac{r}{\sqrt{r^2 - 4d_h^2 K e^{2d_b\tau}}} - 1\right)}{2d_h^2} < 0.$$

Therefore, H_1^* is monotonically increasing by d_h, and H_2^* is monotonically decreasing by d_h.

Finally, let us see d_b. Then

$$p'(d_b) = \frac{re^{-d_b\tau}\left(\frac{r}{\sqrt{r^2 - 4d_h^2 K e^{2d_b\tau}}} - 1\right)\tau}{2d_h} > 0,$$

and

$$q'(d_b) = \frac{re^{-d_b\tau}\left(-\frac{r}{\sqrt{r^2-4d_h^2Ke^{2d_b\tau}}}-1\right)\tau}{2d_h} < 0.$$

Therefore, H_1^* is monotonically increasing by d_b, and H_2^* is monotonically decreasing by d_b. □

Proofs for Chapter. 4

Proof of Theorem 4.3.1

Proof. Let

$$f_1(u,v) = \bar{r}(t)\frac{u^2}{\hat{K}+u^2} - \bar{d}_h u - \frac{\omega u}{1+u}v$$

and

$$f_2(u,v) = \frac{\omega u}{1+u}v - \bar{d}_m v.$$

Assume each point $(u_1, v_1) \in \mathbb{X}$ in functions f_1 and f_2 has a neighbour $(u_2, v_2) \in \mathbb{X}_0$, and $u_1 > u_2$. As I know, $r(t) = r_0(1 + \epsilon\cos(\frac{2\pi(t-\psi)}{\gamma}))$, the maximum of $r(t)$ is $r_{max} = r_0(1+\epsilon)$, and the minimum of $r(t)$ is $r_{min} = r_0(1-\epsilon)$. Then $\bar{r}_{max} = \frac{r_{max}*c}{R*b}$ and $\bar{r}_{min} = \frac{r_{min}*c}{R*b}$. Then I can get:

$$\begin{aligned}
|f_1(u_1,v_1) - f_1(u_2,v_2)| &= |\bar{r}(t)(\frac{u_1^2}{\hat{K}+u_1^2} - \frac{u_2^2}{\hat{K}+u_2^2}) + \bar{d}_h(u_2-u_1) + (\frac{\omega u_2}{1+u_2}v_2 - \frac{\omega u_1}{1+u_1}v_1)| \\
&< |\bar{r}_{max}(\frac{u_1^2-u_2^2}{\hat{K}+u_2^2}) + \bar{d}_h(u_2-u_1) + \omega(v_2-v_1)| \\
&= |\bar{r}_{max}(\frac{(u_1+u_2)(u_1-u_2)}{\hat{K}+u_2^2}) + \bar{d}_h(u_2-u_1) + \omega(v_2-v_1)| \\
&< (\bar{r}_{max}+\bar{d}_h)|u_2-u_1| + \omega|v_2-v_1|
\end{aligned}$$

Therefore, there exists two real constants $M_1 = \bar{r}_{max} + \bar{d}_h$ and $M_2 = \omega$ for $|f_1(u_1,v_1) - f_1(u_2,v_2)| \leq M_1|u_1-u_2| + M_2|v_1-v_2|$. Similarly, function $f_2(u,v)$ has:

$$\begin{aligned}
|f_2(u_1,v_1) - f_2(u_2,v_2)| &= |\frac{\omega u_1}{1+u_1}v_1 - \frac{\omega u_2}{1+u_2}v_2 + \bar{d}_m(v_2-v_1)| \\
&< \omega|v_2-v_1| + \bar{d}_m|v_2-v_1|
\end{aligned}$$

Therefore, there exists a real constant $L = \omega + \bar{d}_m$ for $|f_2(u_1,v_1) - f_2(u_2,v_2)| \leq L|v_1-v_2|$. Since eqts.(4.3) are Lipschitz continuous, following the Lipschitz condition,

the system (4.3) has local existence and uniqueness solution.

According to Theorem A.4 (p.423) of Thieme (2003) Thieme [2018], I can conclude that Model (4.3) is positive invariant in $\mathbb{X}$. Let $g(u) = \frac{u^2}{\hat{K}+u^2} < 1$ and $h(u) = \frac{\omega u}{1+u}$, then model (4.3) follows:

$$u' = \bar{r}(t)g(u) - \bar{d}_h u - h(u)v$$

and

$$v' = (h(u) - \bar{d}_m)v.$$

From above,

$$\begin{aligned} u' &< \bar{r} - \bar{d}_h u < \bar{r}_{max} - \bar{d}_h u \\ &\Rightarrow u(t) < \tfrac{\bar{r}_{max}}{\bar{d}_h} - (\tfrac{\bar{r}_{max}}{\bar{d}_h} - u_0)e^{-\bar{d}_h t} \\ &\Rightarrow u(t) < max\{u_0, \tfrac{\bar{r}_{max}}{\bar{d}_h}\}. \end{aligned}$$

Therefore, u is boundedness.

Now, to show the boundedness of v, define $H = u + v$, then

$$\begin{aligned} H' &= u' + v' = \bar{r}(t)g(u) - \bar{d}_h u - \bar{d}_m v \\ H' &< \bar{r}(t) - \max\{\bar{d}_h, \bar{d}_m\}H \end{aligned}$$

Therefore, H is boundedness. Since u is boundedness, v is boundedness. □

Proof of Proposition 4.3.1

Proof. Let

$$f(u) = \frac{r_0 u^2}{\hat{K} + u^2} - \bar{d}_h u = u[\frac{r_0 u - d_h(\hat{K} + u^2)}{\hat{K} + u^2}],$$

Then if $r_0 > 2\bar{d}_h\sqrt{\hat{K}}$, there exists u_1^* and u_2^* such that $f(u_i^*) = 0, i = 1, 2$ and

$$u_1^* = \frac{r_0 - \sqrt{r_0^2 - 4\bar{d}_h^2\hat{K}}}{2\bar{d}_h} \leq u_2^* = \frac{r_0 + \sqrt{r_0^2 - 4\bar{d}_h^2\hat{K}}}{2\bar{d}_h}$$

with

$$u_2^* = \frac{r_0 + \sqrt{r_0^2 - 4\bar{d}_h^2\hat{K}}}{2\bar{d}_h} > \frac{r_0}{2\bar{d}_h} > \sqrt{\hat{K}}.$$

Notice that

$$f'(u) = \frac{-\bar{d}_h\hat{K}^2 - 2\bar{d}_h\hat{K}u^2 - \bar{d}_h u^4 + 2\hat{K}r_0 u}{\left(\hat{K} + u^2\right)^2} = \frac{-\bar{d}_h\left(\hat{K} + u^2\right)^2 + 2\hat{K}r_0 u}{\left(\hat{K} + u^2\right)^2},$$

then I have

$$f'(0) = -d < 0, f'(u_i^*) = -d_h + \frac{2\hat{K}d_h^2}{r_0 u_i^*}$$

which implies that $u^* = 0$ is a locally stable equilibrium, and $f'(u_1^*) > 0$ and $f'(u_2^*) < 0$. Therefore u_2^* is locally stable equilibrium while u_1^* is locally unstable.

Note that

$$u' = f(u) = u[\frac{r_0 u - d_h(\hat{K} + u^2)}{\hat{K} + u^2}] = d_h u[\frac{(u - u_1^*)(u_2^* - u)}{\hat{K} + u^2}].$$

For any initial condition $u(0) \in (u_1^*, u_2^*)$, I have $u' > 0$ for all future $t > 0$, thus $u(t)$ increases and approaches to u_2^*. For any initial condition $u(0) > u_2^*$, I have $u' < 0$ for all future $t > 0$, thus $u(t)$ decreases and approaches to u_2^*.

If $r_0 < 2\bar{d}_h\sqrt{\hat{K}}$, then I have

$$u' = f(u) = u[\frac{r_0 u - d_h(\hat{K} + u^2)}{\hat{K} + u^2}] = d_h u\left[\frac{-(u - \frac{r_0}{2d_h})^2 + ((r_0/2\bar{d}_h)^2 - \hat{K})}{\hat{K} + u^2}\right] < 0.$$

Therefore $u(t)$ converges to 0 if $r_0 < 2\bar{d}_h\sqrt{\hat{K}}$ holds.

□

Proof of Theorem 4.3.3

Proof. Notice that $u = 0$ is an equilibrium of

$$u' = \frac{\bar{r}(t)u^2}{\hat{K} + u^2} - \bar{d}_h u = u\left[\frac{\bar{r}(t)u}{\hat{K} + u^2} - \bar{d}_h\right].$$

From Theorem 4.3.1, I know that $u \geq 0$ for any initial $u(0) \geq 0$. Define $\mathcal{D} = \{u \in [0, \frac{\bar{d}_h\hat{K}}{r_M})\}$. Applying for Lyapunov Stability Theorem Aeyels [1995] and I define $V(u) = u^2 \geq 0\ \forall u \in \mathcal{D}$.
Notice that

$$\dot{V}(t,u) = u' = u\left[\frac{\bar{r}(t)u - \bar{d}_h(\hat{K} + u^2)}{\hat{K} + u^2}\right] < \frac{r_M u}{\hat{K}} - \bar{d}_h.$$

Thus,

$$\dot{V}(t,u) \leq 0, \forall u \in \mathcal{D} \text{and} t \geq 0$$

which the $\mathcal{D}$ is a neighborhood of the origin, and $t \geq 0$. Thus I can conclude that $u = 0$ is locally stable.

Define $f(u,t) = \frac{\bar{r}(t)u^2}{\hat{K}+u^2} - \bar{d}_h u$, then I have

$$f(u,t) = u\left[\frac{\bar{r}(t)u - d_h(\hat{K}+u^2)}{\hat{K}+u^2}\right].$$

If $r_{max} = r_M = r_0(1+\epsilon) < 2\bar{d}_h\sqrt{\hat{K}}$, then I have

$$\bar{r}(t) \le r_M < 2\bar{d}_h\sqrt{\hat{K}}.$$

Thus,

$$u' = f(u,t) \le u\left[\frac{r_M u - d_h(\hat{K}+u^2)}{\hat{K}+u^2}\right] = d_h u\left[\frac{-(u-\frac{r_M}{2\bar{d}_h})^2 + ((r_M/2\bar{d}_h)^2 - \hat{K})}{\hat{K}+u^2}\right] < 0.$$

This implies that $u=0$ is globally stable when $r_M = r_0(1+\epsilon) < 2\bar{d}_h\sqrt{\hat{K}}$.

If $r_{min} = r_m = r_0(1-\epsilon) > 2\bar{d}_h\sqrt{\hat{K}}$ holds, then $r_m \le \bar{r}(t) \le r_M = r_0(1+\epsilon)$ and

$$u' = f(u,t) \ge u\left[\frac{r_m u - d_h(\hat{K}+u^2)}{\hat{K}+u^2}\right] = u[\frac{r_m u - d_h(\hat{K}+u^2)}{\hat{K}+u^2}] = d_h u[\frac{(u-u_1^*)(u_2^*-u)}{\hat{K}+u^2}]$$

with

$$u_1^* = \frac{r_m - \sqrt{r_m^2 - 4\bar{d}_h^2\hat{K}}}{2\bar{d}_h} \le u_2^* = \frac{r_m + \sqrt{r_m^2 - 4\bar{d}_h^2\hat{K}}}{2\bar{d}_h}.$$

Similar, I have

$$u' = f(u,t) \le u\left[\frac{r_M u - d_h(\hat{K}+u^2)}{\hat{K}+u^2}\right] = u[\frac{r_M u - d_h(\hat{K}+u^2)}{\hat{K}+u^2}] = d_h u[\frac{(u-h_1^*)(h_2^*-u)}{\hat{K}+u^2}]$$

with

$$h_1^* = \frac{r_M - \sqrt{r_M^2 - 4\bar{d}_h^2\hat{K}}}{2\bar{d}_h} \le h_2^* = \frac{r_M + \sqrt{r_M^2 - 4\bar{d}_h^2\hat{K}}}{2\bar{d}_h}.$$

Therefore, I have u being a positive invariant in $[u_1^*, h_2^*]$. Note that for any $u > h_2^*$ I have $u' < 0$, thus I have

$$\liminf_{t\to\infty} u(t) \le u_1^* \le \limsup_{t\to\infty} u(t) < h_2^*$$

if $r_m \ge 2\bar{d}_h\sqrt{\hat{K}}$ and $u(0) > u_1^*$.

□

Proof of Theorem 4.3.4

Proof. Let $f(u) = \frac{u^2}{\hat{K}+u^2}$, then Eq. 4.4 rewrites to

$$u' = L(u) = \bar{r}(t) * f(u) - \bar{d}_h u. \tag{A.41}$$

Linearizing Eqt.A.41 about $u = u^*$ gives,

$$L(u) \approx L(u^*) + \left[\bar{r}(t) * f'(u^*) - \bar{d}_h\right] * (u - u^*).$$

Then, this linear equation can be

$$h' = \left[\bar{r}(t) * f'(u^*) - \bar{d}_h\right] * h$$

where $h = u - u^*$. After that, I can solve the differential equation by integrating factors:

$$h(t) = C_0 e^{\int_0^t \left[\bar{r}(z) * f'(u^*) - \bar{d}_h\right] dz} = C_0 e^{\lambda}$$

Therefore, if $\lambda < 0$, the stability of the periodic solution $u = u^*$ is stable; if $\lambda > 0$, then the solution is unstable. □

Proof of Theorem 4.3.5

Proof. 1. For $E_1^* = (0, 0)$,

$$J_{E_1^*} = \begin{Bmatrix} -\bar{d}_h & 0 \\ 0 & -\bar{d}_m \end{Bmatrix}.$$

Eigenvalues are $\lambda_1 = -\bar{d}_h < 0$ and $\lambda_2 = -\bar{d}_m < 0$, therefore E_1^* always stable.

2. For $E_{b1} = (\frac{\bar{r} - \sqrt{\bar{r}^2 - 4\hat{K}\bar{d}_h^2}}{2\bar{d}_h}, 0)$, eigenvalues are

$$\lambda_1 = \frac{\left(\omega - \bar{d}_m\right)\left(-\bar{r} + \sqrt{\bar{r}^2 - 4\hat{K}\bar{d}_h^2}\right) + 2\bar{d}_h\bar{d}_m}{2\bar{d}_h + \sqrt{\bar{r}^2 - 4\hat{K}\bar{d}_h^2} + \bar{r}}$$

and

$$\lambda_2 = \frac{\bar{r}\bar{d}_h\left(\bar{r} - \sqrt{\bar{r}^2 - 4\hat{K}\bar{d}_h^2}\right) - 4\hat{K}\bar{d}_h^3}{\bar{r}\left(\sqrt{\bar{r}^2 - 4\hat{K}\bar{d}_h^2} - \bar{r}\right)}.$$

Since $\frac{\bar{r}}{2\sqrt{\hat{K}}\bar{d}_h} > 1$, $\lambda_2 > 0$. If $\bar{d}_m > \omega$, $\lambda_1 > 0$, then E_{b1} is source. If $\bar{d}_m < \omega$, $u^* = \frac{\bar{d}_m}{\omega - \bar{d}_m} > \bar{N}_h^c = \frac{\bar{r} - \sqrt{\bar{r}^2 - 4\hat{K}\bar{d}_h^2}}{2\bar{d}_h}$, then $\frac{2\bar{d}_h\bar{d}_m}{\omega - \bar{d}_m} > \bar{r} - \sqrt{\bar{r}^2 - 4\hat{K}\bar{d}_h^2}$, i.e. $\lambda_1 < 0$, therefore E_{b1} is saddle.

For $E_{b2} = (\frac{\bar{r} + \sqrt{\bar{r}^2 - 4\hat{K}\bar{d}_h^2}}{2\bar{d}_h}, 0)$, eigenvalues are

$$\lambda_1 = \frac{\left(\omega - \bar{d}_m\right)\left(\bar{r} + \sqrt{\bar{r}^2 - 4\hat{K}\bar{d}_h^2}\right) - 2\bar{d}_h\bar{d}_m}{2\bar{d}_h + \sqrt{\bar{r}^2 - 4\hat{K}\bar{d}_h^2} + \bar{r}}$$

and

$$\lambda_2 = \frac{\sqrt{\bar{r}^2 - 4\hat{K}\bar{d}_h^2}\left(4\hat{K}\bar{d}_h^3 - 2\bar{r}^2\bar{d}_h\right) + r\left(8\hat{K}\bar{d}_h^3 - 2\bar{r}^2\bar{d}_h\right)}{\bar{r}\left(\sqrt{\bar{r}^2 - 4\hat{K}\bar{d}_h^2} + \bar{r}\right)^2}.$$

Since $\bar{r}^2 > 4\hat{K}\bar{d}_h^2 > 2\hat{K}\bar{d}_h^2$, $2\bar{r}^2\bar{d}_h > 8\hat{K}\bar{d}_h^3 > 4\hat{K}\bar{d}_h^3$, then $8\hat{K}\bar{d}_h^3 - 2\bar{r}^2\bar{d}_h < 0$ and $4\hat{K}\bar{d}_h^3 - 2\bar{r}^2\bar{d}_h < 0$, i.e. $\lambda_2 < 0$. If $\bar{d}_m > \omega$, $\lambda_1 < 0$, then E_{b2} is sink. If $\bar{d}_m < \omega$, $\bar{N}_h^* = \frac{\bar{r} + \sqrt{\bar{r}^2 - 4\hat{K}\bar{d}_h^2}}{2\bar{d}_h} > u^* = \frac{\bar{d}_m}{\omega - \bar{d}_m}$, then $\left(\omega - \bar{d}_m\right)\left(\sqrt{\bar{r}^2 - 4\hat{K}\bar{d}_h^2} + \bar{r}\right) > 2\bar{d}_h\bar{d}_m$, i.e. $\lambda_1 > 0$. Therefore E_{b2} is saddle.

3. For $E^* = (\frac{\bar{d}_m}{\omega - \bar{d}_m}, \frac{\left[\bar{r}u^* - \bar{d}_h\left((u^*)^2 + \hat{K}\right)\right](u^*+1)}{\omega((u^*)^2 + \hat{K})})$, I simplified the matrix J to

$$J_{E^*} = \begin{Bmatrix} -\frac{u^*\left(d_h\left(\hat{K} + (u^*)^2\right)^2 + r\left((u^*)^2 - \hat{K}(2u^*+1)\right)\right)}{(u^*+1)\left(\hat{K} + (u^*)^2\right)^2} & -\frac{\omega u^*}{u^*+1} \\ \frac{\omega v^*}{(u^*+1)^2} & 0 \end{Bmatrix}.$$

which gives the following two equations:

$$\begin{aligned} \lambda_1 + \lambda_2 &= -\frac{u^*\left(d_h\left(\hat{K} + (u^*)^2\right)^2 + \bar{r}\left((u^*)^2 - \hat{K}(2u^*+1)\right)\right)}{(u^*+1)\left(\hat{K} + (u^*)^2\right)^2} \\ &= \frac{u^*(-\bar{d}_h\hat{K}^2 + (\bar{r} + 2u^*\bar{r} - 2\bar{d}_h(u^*)^2)\hat{K} - \bar{r}(u^*)^2 - \bar{d}_h(u^*)^4)}{(u^*+1)\left(\hat{K} + (u^*)^2\right)^2} \qquad \text{(A.42)} \\ \lambda_1\lambda_2 &= \frac{\omega^2 u^* v^*}{(u^*+1)^3} > 0 \end{aligned}$$

-rEqt. A.42 gets two $\hat{K}_{1,2}$ to make the $\lambda_1 + \lambda_2 = 0$, where $\hat{K}_2 = \frac{\bar{r}u^*}{\bar{d}_h} - (u^*)^2 + \frac{\bar{r}}{2\bar{d}_h} + \frac{\sqrt{\bar{r}}\sqrt{\bar{r}(2u^*+1)^2 - 8\bar{d}_h(u^*)^2(u^*+1)}}{2\bar{d}_h}$ and the condition of E^* is $\hat{K} < \frac{\bar{r}u^*}{\bar{d}_h} - (u^*)^2$, therefore

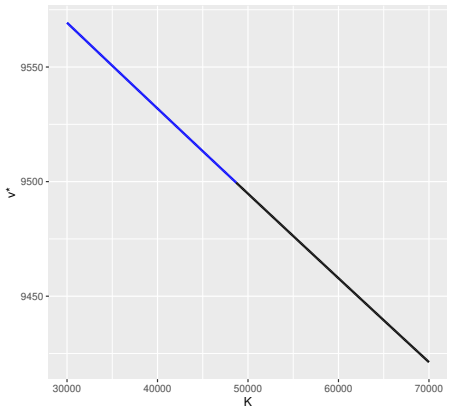

Figure A.1: Simulation for the trace $(\lambda_1 + \lambda_2)$ of J_{E^*} . The black curve indicates the trace is positive, i.e. the stability of E^* is source, and the blue curve indicates the trace is negative, i.e. the stability of E^* is sink. $\bar{r} = 500$, $\omega = 0.05$, $\bar{d}_h = 0.01$, $\bar{d}_m = 0.049969$, and $\hat{K} \in [30000, 70000]$.

only $\hat{K}_1 = \frac{\bar{r}u^*}{\bar{d}_h} - (u^*)^2 + \frac{\bar{r}}{2\bar{d}_h} - \frac{\sqrt{\bar{r}}\sqrt{\bar{r}(2u^*+1)^2 - 8\bar{d}_h(u^*)^2(u^*+1)}}{2\bar{d}_h}$ exists E^* where is the trace equals 0. Because of $\lambda_1\lambda_2 > 0$, $\lambda_1 + \lambda_2 > 0$ as $\hat{K} \in (\hat{K}_1, \frac{\bar{r}u^*}{\bar{d}_h} - (u^*)^2)$, i.e. E^* is source, whereas, $\lambda_1 + \lambda_2 < 0$ as $\hat{K} \in (-\infty, \hat{K}_1)$, i.e. E^* is sink. From Fig. A.1, there exists a $\hat{K}$ that makes interior equilibrium (E^*) from sink to source. □

Proof of Theorem 4.3.6

Proof. I re-scaled the system 4.3 to the following model:

$$\begin{aligned} u' &= g(u)(f(u) - v) \\ v' &= v(g(u) - \bar{d}_m), \end{aligned} \tag{A.43}$$

where $g(u) = \frac{\omega u}{1+u}$ and $f(u) = \frac{\bar{r}}{g(u)} \cdot \frac{u^2}{\hat{K}+u^2} - \frac{\bar{d}_h}{g(u)} \cdot u$.

I would apply Theorem 3.1 in Wei et al. (2011) Wang *et al.* [2011] into system A.43, then our system must have:

(a1) $f \in C^1(\bar{\mathbb{R}}), f(a) = f(b) = 0$, where $0 < a < b$; $f(u)$ is positive for $a < u < b$, and $f(u)$ is negative otherwise; there exists $\bar{\lambda} \in (a, b)$ such that $f'(u) > 0$ on $[a, \bar{\lambda})$, $f'(u) < 0$ on $(\bar{\lambda}, b]$;

(a2) $g \in C^1(\bar{\mathbb{R}}), g(0) = 0$; $g(u) > 0$ for $u > 0$ and $g'(u) > 0$ for $u > 0$, and there exists $\lambda > 0$ such that $g(\lambda) = d$.

(a3) $f(u)$ and $g(u)$ are C^3 near $\lambda = \bar{\lambda}$ and $f''(\bar{\lambda}) < 0$.

Then the Jacobean matrix of Model (A.43) is

$$J = \begin{Bmatrix} f'(u)g(u) & -g(u) \\ vg'(u) & 0 \end{Bmatrix}$$

$$g'(u) = \frac{\omega}{(u+1)^2} > 0$$

and I set $h(u) = \frac{ru^2}{K+u^2} - u\bar{d}_h$,$f(u) = \frac{h(u)}{g(u)}$,then

$$\begin{aligned} f'(u) &= \frac{h'(u)g(u) - h(u)g'(u)}{g^2(u)} \\ &= \frac{h'(u)}{g(u)} - \frac{f(u)g'(u)}{g(u)} \\ &= \frac{\frac{\bar{r}\left(2\hat{K}u + \hat{K} - u^2\right)}{\left(\hat{K}+u^2\right)^2} - \bar{d}_h}{\omega} \end{aligned} \tag{A.44}$$

(a1) $f \in C^1(\bar{\mathbb{R}}), f(a) = f(b) = 0$, where $0 < a < b$; $f(u)$ is positive for $a < u < b$, and $f(u)$ is negative otherwise; there exists $\bar{\lambda} \in (a, b)$ such that $f'(u) > 0$ on $[a, \bar{\lambda})$, $f'(u) < 0$ on $(\bar{\lambda}, b]$;

$f(u) = \frac{h(u)}{g(u)}$ where $h(u) = \frac{ru^2}{K+u^2} - u\bar{d}_h$ and the solution of $h(u) = 0$ being $u_1 = \frac{\bar{r} - \sqrt{\bar{r}^2 - 4\bar{d}_h^2\hat{K}}}{2\bar{d}_h}$ and $u_2 = \frac{\bar{r} + \sqrt{\bar{r}^2 - 4\bar{d}_h^2\hat{K}}}{2\bar{d}_h}$. Let $a = u_1$ and $b = u_2$,then you have $f(a) = f(b) = 0$.

Then,

$$h'(u_1) = -\frac{2\bar{d}_h\left(\bar{r}^2\left(\bar{r} - \sqrt{\bar{r}^2 - 4\hat{K}\bar{d}_h^2}\right) + 2\hat{K}\bar{d}_h^2\left(\sqrt{\bar{r}^2 - 4\hat{K}\bar{d}_h^2} - 2\bar{r}\right)\right)}{\bar{r}\left(\bar{r} - \sqrt{\bar{r}^2 - 4\hat{K}\bar{d}_h^2}\right)^2}$$

and

$$h'(u_2) = -\frac{2\bar{d}_h\left(\bar{r}^2\left(\sqrt{\bar{r}^2 - 4\hat{K}\bar{d}_h^2} + \bar{r}\right) + 2\hat{K}\bar{d}_h^2\sqrt{\bar{r}^2 - 4\hat{K}\bar{d}_h^2}\right)}{\bar{r}\left(\sqrt{\bar{r}^2 - 4\hat{K}\bar{d}_h^2} + \bar{r}\right)^2}$$

Since $\bar{r}^2 > 4\hat{K}\bar{d}_h^2$, $h'(u_1) > 0$ and $h'(u_2) < 0$, then I have

$$f'(u_1) = \frac{h'(u_1)}{g(u_1)} > 0 \text{ and } f'(u_2) = \frac{h'(u_2)}{g(u_2)} < 0$$

Therefore, there exists a $\bar{\lambda} \in (a, b)$ make the sign of $f'(u)$ from positive to negative.

(a2) $g \in C^1(\bar{\mathbb{R}}), g(0) = 0$; $g(u) > 0$ for $u > 0$ and $g'(u) > 0$ for $u > 0$, and there exists $\lambda > 0$ such that $g(\lambda) = d$.

$g(u) = \frac{\omega u}{1+u}$, if $u = 0$ then $g(0) = 0$, if $u > 0$ then $g(u) > 0$. $g'(u) = \frac{\omega}{(1+u)^2} > 0$. I assume there exist $\lambda > 0$ such that $g(\lambda) = \frac{\omega\lambda}{1+\lambda} = d > 0$, i.e $\lambda = \frac{d}{\omega - d}$.

(a3) $f(u)$ and $g(u)$ are C^3 near $\lambda = \bar{\lambda}$ and $f''(\bar{\lambda}) < 0$.

$$\begin{aligned} f''(\lambda) &= f''(\bar{\lambda}) \\ &= -\frac{4\bar{r}\bar{\lambda}^2}{\omega\left(\hat{K}+\bar{\lambda}^2\right)^2} - \frac{6\bar{r}(\bar{\lambda}+1)\bar{\lambda}}{\omega\left(\hat{K}+\bar{\lambda}^2\right)^2} + \frac{2\bar{r}}{\omega\left(\hat{K}+\bar{\lambda}^2\right)} + \frac{8\bar{r}(\bar{\lambda}+1)\bar{\lambda}^3}{\omega\left(\hat{K}+\bar{\lambda}^2\right)^3} \\ &= \frac{2\bar{r}\left(\hat{K}^2 - 3\hat{K}(\bar{\lambda}+1)\bar{\lambda} + \bar{\lambda}^3\right)}{\omega\left(\hat{K}+\bar{\lambda}^2\right)^3} \end{aligned} \tag{A.45}$$

From (A.44), since $f'(\bar{\lambda}) = 0$,

$$\frac{\bar{r}\left(2\hat{K}\bar{\lambda} + \hat{K} - \bar{\lambda}^2\right)}{\left(\hat{K} + \bar{\lambda}^2\right)^2} = \bar{d}_h \Rightarrow \bar{r}(\hat{K} + 2\hat{K}\bar{\lambda} - \bar{\lambda}^2) = \bar{d}_h(\hat{K} + \bar{\lambda}^2)^2$$

Therefore, it must has $\hat{K} + 2\hat{K}\bar{\lambda} > \bar{\lambda}^2$.

In addition to this, $f'(u)$ also is following

$$\begin{aligned} f'(u) &= -\frac{\bar{d}_h}{\omega} - \frac{2\bar{r}(u+1)u^2}{\omega\left(\hat{K}+u^2\right)^2} + \frac{\bar{r}u}{\omega\left(\hat{K}+u^2\right)} + \frac{\bar{r}(u+1)}{\omega\left(\hat{K}+u^2\right)} \\ &= -\frac{2\bar{r}(u+1)u^2}{\omega\left(\hat{K}+u^2\right)^2} + \frac{\bar{r}(u+1)}{\omega\left(\hat{K}+u^2\right)} + v^* \\ &= v^* + \frac{\bar{r}(1+u)}{(\hat{K}+u^2)\omega}\left(1 - \frac{2u^2}{\hat{K}+u^2}\right) \end{aligned} \tag{A.46}$$

From (A.46), $v* > 0$ and $f'(u) = 0$, if $u{=}\bar{\lambda}$, then $\bar{\lambda}$ and $\hat{K}$ must be $\bar{\lambda}^2 > \hat{K}$. Then

$$\hat{K}^2 - 3\hat{K}\bar{\lambda}^2 - 3\hat{K}\bar{\lambda} + \bar{\lambda}^3 = (\hat{K}^2 - 2\bar{\lambda}\hat{K} - \bar{\lambda}^2\hat{K}) + (\bar{\lambda}^3 - \bar{\lambda}\hat{K} - 2\bar{\lambda}^2\hat{K}) < 0.$$

In summary, $f''(\bar{\lambda}) < 0$.

Corollary A.0.0.1. *(Theorem 3.1 in Wei et al. (2011)) Assume that f,g satisfy (a1)-(a3). Then the system* (A.43) *undergoes a Hopf bifurcation at $(\bar{\lambda}, v_\lambda)$; the Hopf bifurcation is supercritical and backward (respectively, subcritical and forward) if $a(\bar{\lambda}) < 0$ ($a(\bar{\lambda}) > 0$), where $a(\bar{\lambda})$ is defined in A.47.*

According to the Corollary (A.0.0.1), the direction of the Hopf bifurcation and the stability of bifurcating periodic orbits are determined by the first Lyapunov coefficient

$$
\begin{aligned}
a(\bar{\lambda}) &= \frac{f'''(\bar{\lambda})g(\bar{\lambda})g'(\bar{\lambda})+2f''(\bar{\lambda})[g'(\bar{\lambda})]^2-f''(\bar{\lambda})g(\bar{\lambda})g''(\bar{\lambda})}{16g'(\bar{\lambda})} \\
&= \frac{\omega}{16(1+\bar{\lambda})}(2f''(\bar{\lambda})+\bar{\lambda}f'''(\bar{\lambda}))
\end{aligned} \tag{A.47}
$$

From Eqt.(A.47), since $\bar{\lambda} > 0$, $\frac{\omega}{16(1+\bar{\lambda})} > 0$, and

$$
2f''(\bar{\lambda})+\bar{\lambda}f'''(\bar{\lambda}) = \frac{2\bar{r}\left(2\hat{K}^3-\hat{K}^2(2\bar{\lambda}(2\bar{\lambda}+9)+3)+2\hat{K}(\bar{\lambda}(4-3\bar{\lambda})+9)\bar{\lambda}^2+(2\bar{\lambda}-3)\bar{\lambda}^4\right)}{\omega\left(\hat{K}+\bar{\lambda}^2\right)^4}
$$

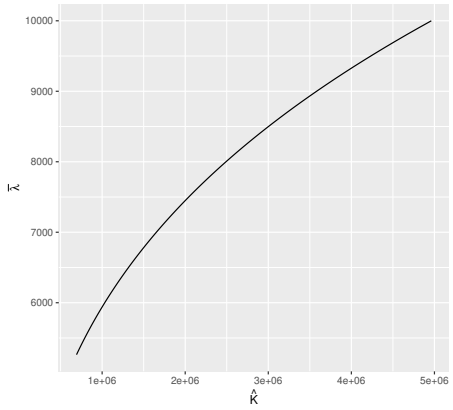

Figure A.2: Simulation for the sign of $a(\bar{\lambda})$. All $a(\bar{\lambda})$ is positive. From Theorem A.0.0.1, the bifurcation is subcritical and forward. The black curve indicates positive and red curve indicates negative. $\bar{r} = 100$, $\omega = \in [0.000010001, 0.0010002]$, $\bar{d}_h = 0.0009$, $\bar{d}_m = 0.001$, and $\hat{K} = \hat{K}_1 \in [6.9 * 10^5, 5.0 * 10^6]$.

From Figure A.2 and Eqt.A.47, I got $a(\bar{\lambda}) > 0$. According to Corollary A.0.0.1, the system 4.3 undergoes a Hopf bifurcation at $\hat{K} = \hat{K}_1$; the Hopf bifurcation is subcritical and forward. From Figure A.3 and Eqt.A.47, I can got $a(\bar{\lambda}) < 0$. According to Corollary A.0.0.1, the system 4.3 undergoes a Hopf bifurcation at $\hat{K} = \hat{K}_1$; the Hopf bifurcation is supercritical and backward .

From Figure A.3, $\hat{K} > \hat{K}_1$, there exists a stable limit cycle.

□

Proof of Theorem 4.4.1

Proof. Let $f(u) = \frac{u^2}{\hat{K}+u^2}$, then the Jacobian of the system is obtained as:

$$
J = \begin{Bmatrix} -\bar{d}_h + \bar{r}(t)f'(u) - \frac{\omega v}{(1+u)^2} & -\frac{\omega u}{1+u} \\ \frac{\omega v}{(u+1)^2} & \frac{\omega u}{u+1} - \bar{d}_m \end{Bmatrix}.
$$

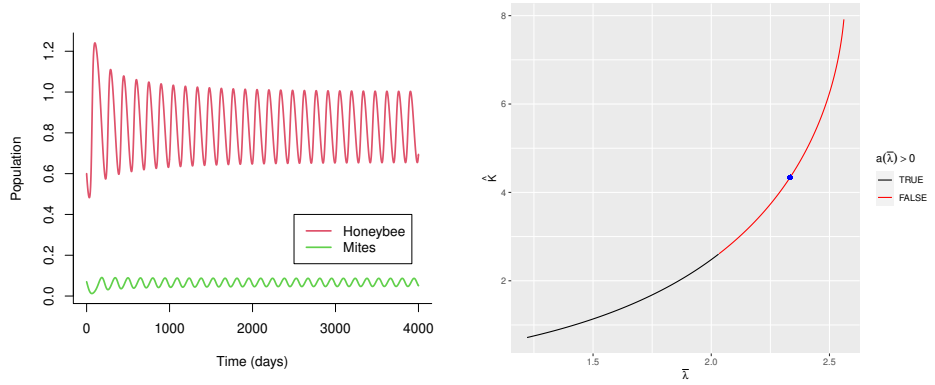

(a) (b)

Figure A.3: Simulation for a stable limit cycle around whenever $\hat{K} > \hat{K}_1$. Figure A.3b: the conditions for subcritical or supcritical of hopf-bifurcation when $\hat{K} = \hat{K}_1$. The black indicates supcritical i.e. $a(\bar{\lambda}) > 0$; the blue indicates subcritical i.e. $a(\bar{\lambda}) > 0$. Choose values at blue dot conditions to get Figure A.3a: $\hat{K} = 4.6$, $\hat{K}_1 = 4.34$, $\bar{r} = 1$, $\omega = 0.3$, $\bar{d}_h = 0.2$, $\bar{d}_m = 0.21$, $u^* = 2.33$, $\frac{\bar{r}u^*}{\bar{d}_h} - (u^*)^2 = 6.22$.

After that, the linearized system at $(u^*, 0)$ is

$$\begin{bmatrix} h' \\ g' \end{bmatrix} = \begin{bmatrix} -\bar{d}_h + \bar{r}(t)f'(u^*) & -\frac{\omega u^*}{1+u^*} \\ 0 & \frac{\omega u^*}{u^*+1} - \bar{d}_m \end{bmatrix} * \begin{bmatrix} h \\ g \end{bmatrix}.$$

Assume the linearly independent set of initial conditions:

$$h_1(0) = 1, g_1(0) = 0$$

and

$$h_2(0) = 0, g_2(0) = 1$$

to find linearly independent solutions $(h_1(t), g_1(t))$ and $(h_2(t), g_2(t))$ of linear system. Then the solutions are:

$$h_1(t) = e^{\int_0^t \left[\bar{r}(z) * f'(u^*) - \bar{d}_h\right] dz} \quad \text{and} \quad g_1(t) = 0,$$

$$h_2(t) = e^{\int_0^t \left[\bar{r}(z) * f'(u^*) - \bar{d}_h\right] dz} * \int_0^t \left[-\frac{\omega u^*}{u^* + 1} e^{\int_0^s \left[\frac{\omega u^*}{1+u^*} - \bar{d}_m + \bar{d}_h - \bar{r}(s) * f'(u^*)\right] ds} \right] dz$$

and

$$g_2(t) = e^{\int_0^t \left[\frac{\omega u^*}{1+u^*} - \bar{d}_m\right] dz}.$$

Hence, I can obtain the fundamental matrix $\mathcal{F}(t)$ of the linearized system over the interval $0 \leq t \leq T$, where T is the period, which is following:

$$\mathcal{F}(T) = \begin{bmatrix} h_1(T) & h_2(T) \\ g_1(T) & g_2(T) \end{bmatrix},$$

and the eigenvalues of the transition matrix are

$$\lambda_1 = e^{\int_0^T \left[\bar{r}(t) * f'(u^*) - \bar{d}_h\right] dt} \quad \text{and} \quad \lambda_2 = e^{\int_0^T \left[\frac{\omega u^*}{1+u^*} - \bar{d}_m\right] dt}.$$

Therefore, if $\lambda_1 < 0$ and $\lambda_2 < 0$, the $(u^*, 0)$ is stable, otherwise, it is unstable. □

Proof for Chapter. 5

Proof of Theorem 5.2.1

Proof. I linearize the bee-only model:

$$\begin{aligned}
D\left(\begin{bmatrix} \dot{E}(t) \\ \dot{L}(t) \\ \dot{P}(t) \\ \dot{A}(t) \end{bmatrix}\right)\Big|_{E_i^*} = &\begin{bmatrix} -\frac{\beta A^2 r}{\left(\beta E + A^2 + K\right)^2} - d_E & 0 & 0 & \frac{2Ar(\beta E+K)}{\left(\beta E + A^2 + K\right)^2} \\ 0 & -d_L & 0 & 0 \\ 0 & 0 & -d_P & 0 \\ 0 & 0 & 0 & -d_A \end{bmatrix} \begin{bmatrix} E(t) \\ L(t) \\ P(t) \\ A(t) \end{bmatrix} \\
&+ \begin{bmatrix} \frac{\beta A^2 r e^{-d_E \tau_e}}{\left(\beta E + A^2 + K\right)^2} & 0 & 0 & -\frac{2Are^{-d_E\tau_e}(\beta E+K)}{\left(\beta E + A^2 + K\right)^2} \\ -\frac{\beta A^2 r e^{-d_E \tau_e}}{\left(\beta E + A^2 + K\right)^2} & 0 & 0 & \frac{2Are^{-d_E\tau_e}(\beta E+K)}{\left(\beta E + A^2 + K\right)^2} \\ 0 & 0 & 0 & 0 \\ 0 & 0 & 0 & 0 \end{bmatrix} \begin{bmatrix} E(t-\tau_e) \\ L(t-\tau_e) \\ P(t-\tau_e) \\ A(t-\tau_e) \end{bmatrix} \\
&+ \begin{bmatrix} 0 & 0 & 0 & 0 \\ \frac{\beta A^2 r e^{-d_E \tau_e - d_L \tau_l}}{\left(\beta E + A^2 + K\right)^2} & 0 & 0 & -\frac{2Are^{-d_E\tau_e - d_L\tau_l}(\beta E+K)}{\left(\beta E + A^2 + K\right)^2} \\ -\frac{\beta A^2 r e^{-d_E \tau_e - d_L \tau_l}}{\left(\beta E + A^2 + K\right)^2} & 0 & 0 & \frac{2Are^{-d_E\tau_e - d_L\tau_l}(\beta E+K)}{\left(\beta E + A^2 + K\right)^2} \\ 0 & 0 & 0 & 0 \end{bmatrix} \begin{bmatrix} E(t-\tau_e-\tau_l) \\ L(t-\tau_e-\tau_l) \\ P(t-\tau_e-\tau_l) \\ A(t-\tau_e-\tau_l) \end{bmatrix} \\
&+ \begin{bmatrix} 0 & 0 & 0 & 0 \\ 0 & 0 & 0 & 0 \\ \frac{\beta A^2 r e^{-d_E \tau_e - d_L \tau_l - d_A \tau_a}}{\left(\beta E + A^2 + K\right)^2} & 0 & 0 & -\frac{2Are^{-d_E\tau_e - d_L\tau_l - d_A\tau_a}(\beta E+K)}{\left(\beta E + A^2 + K\right)^2} \\ -\frac{\beta A^2 r e^{-d_E \tau_e - d_L \tau_l - d_A \tau_a}}{\left(\beta E + A^2 + K\right)^2} & 0 & 0 & \frac{2Are^{-d_E\tau_e - d_L\tau_l - d_A\tau_a}(\beta E+K)}{\left(\beta E + A^2 + K\right)^2} \end{bmatrix} \begin{bmatrix} E(t-\tau_e-\tau_l-\tau_p) \\ L(t-\tau_e-\tau_l-\tau_p) \\ P(t-\tau_e-\tau_l-\tau_p) \\ A(t-\tau_e-\tau_l-\tau_p) \end{bmatrix}
\end{aligned} \tag{A.48}$$

For extinction equilibrium, the matrix (A.48) gives:

$$D\left(\begin{bmatrix} \dot{E}(t) \\ \dot{L}(t) \\ \dot{P}(t) \\ \dot{A}(t) \end{bmatrix}\right)\Big|_{(0,0,0,0)} = \begin{bmatrix} -d_E & 0 & 0 & 0 \\ 0 & -d_L & 0 & 0 \\ 0 & 0 & -d_P & 0 \\ 0 & 0 & 0 & -d_A \end{bmatrix} \begin{bmatrix} E(t) \\ L(t) \\ P(t) \\ A(t) \end{bmatrix} + 0$$

and from the matrix, I obtain the following eigenvalues:

$$\lambda_1 = -d_E < 0, \quad \lambda_2 = -d_L < 0, \quad \lambda_3 = -d_P < 0, \quad \lambda_4 = -d_A < 0$$

Thus, I can conclude that E_0^* is always locally asymptotically stable.

□

APPENDIX B

OTHER FIGURES & TABLE

Figure and table for Chapter. 2

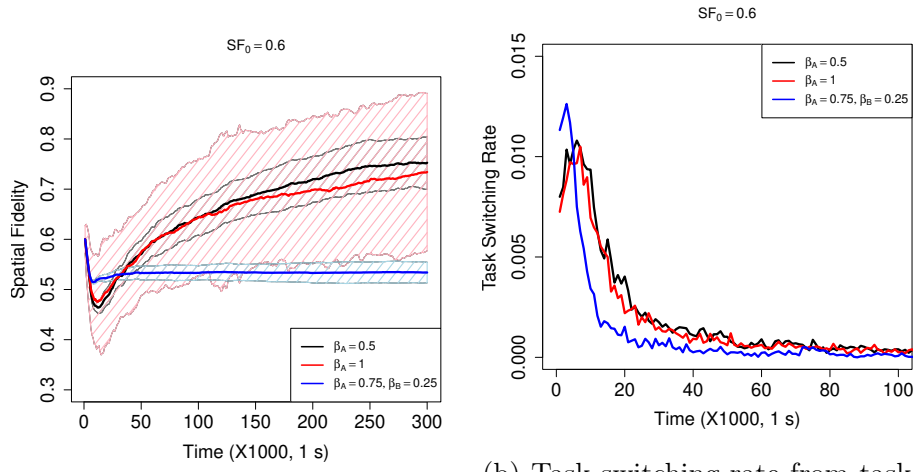

(a) Spatial fidelity dynamics with different task switching probability.

(b) Task switching rate from task B to task A with different task switching probability.

Figure B.1: Black and red curves which are $\beta_A = \beta_B = 0.5$ and $\beta_A = \beta_B = 1$, separately. The blue curve is task switching probability to task A is $\beta_A = 0.75$; however, to task B is $\beta_A = 0.25$. Figure B.1a: Black, red, and blue shadows are standard deviations.

Test	P-value	Test	P-value
ANOVA for all groups *	<2.2e-16	3 groups vs 4 groups *	0.1409
2 groups vs 3 groups *	<2.2e-16	3 groups vs 5 groups	0.0051
2 groups vs 4 groups *	<2.2e-16	4 groups vs 5 groups	0.2512
2 groups vs 5 groups *	<2.2e-16		

Table B.1: P-values of the Welch ANOVA test and T-test. Star * means they have different variances.

Figure for Chapter. 5

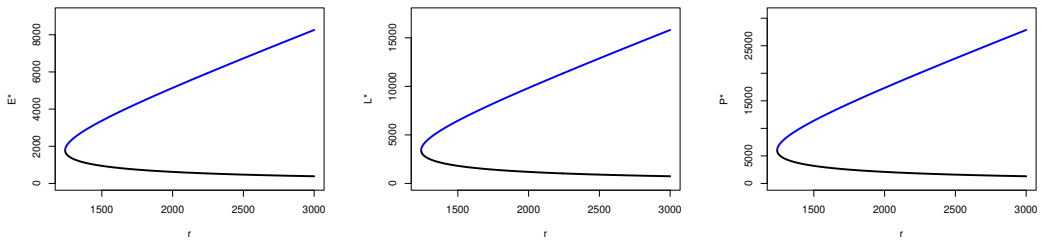

(a) Egg

(b) Larvae

(c) Pupae

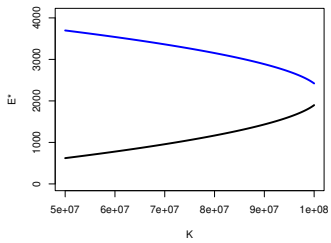

(d) Egg

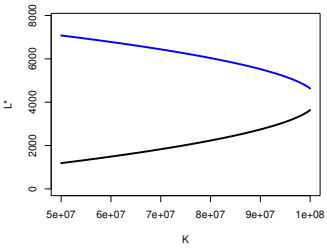

(e) Larvae

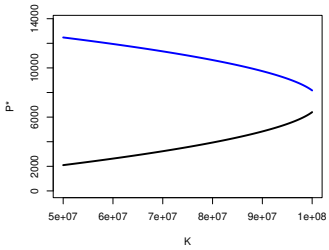

(f) Pupae

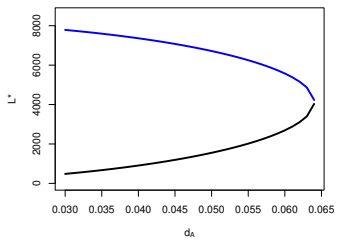

(g) Larvae

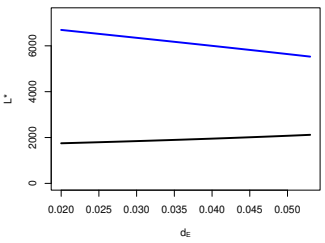

(h) Larvae

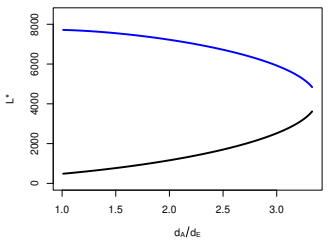

(i) Larvae

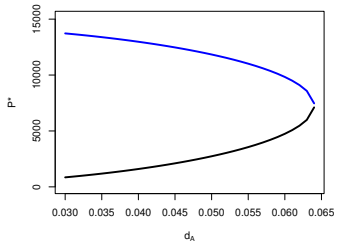

(j) Pupae

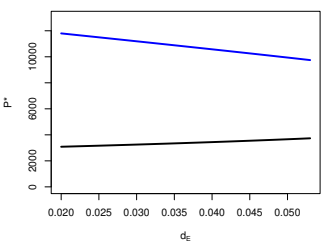

(k) Pupae

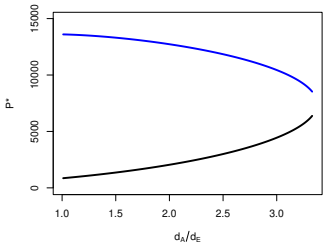

(l) Pupae

Figure B.2: Bifurcation diagrams of Model (5.1) with constant egg-laying rate for death rates. Figure B.2g-B.2i are for the interior equilibrium L_i^*, $i = 1, 2$ (see Eqt.(5.9)). Figure B.2j-B.2l are for the interior equilibrium P_i^*, $i = 1, 2$ (see Eqt.(5.10)). Blue curves indicate stable equilibrium, and black curves indicate unstable equilibrium. The fixed parameters' value are $r = 1499$, $K = 69,545,190$, $d_E = 0.027$, $d_L = 0.001$, $d_P = 0.021$, $d_A = 0.053$, $\beta = 15$, $\tau_e = 3$, $\tau_e = 6$ and $\tau_e = 12$.

APPENDIX C

STATEMENT OF AUTHORIZATION

The project "How to model honey bee population dynamics: stage-structure and seasonality" (where I am the first author), published in the Mathematics in Applied Sciences and Engineering (2020), is elaborated in Chapter3 of the dissertation.

The project "Impacts of seasonality and parasitism on honey bee population dynamics" (where I am the first author) under the Journal of Mathematical Biology (2023) is elaborated in Chapter4 of the dissertation.

The project "Review on mathematical modeling of honey bee population dynamics" (where I am the first author) under the Mathematical Biosciences and Engineering (2021) is used in Chapter 1 and Chapter6 of the dissertation.

The project "Dynamics of information flow and task allocation of social insect colonies: impacts of spatial interactions and task switching" (where I am the first author) that has been submitted for review is used in Chapter 2 of the dissertation.

The project "Impacts of pesticides on honey bee dynamics" (where I am the first author) that will be submitted is used in Chapter 5 of the dissertation.

I am profoundly grateful to my co-authors for their substantial contributions and for granting permission to incorporate this collaborative work into this dissertation.